

Formability assessment of press forming process for uncured metal-composite laminates

Liu, S.

DOI

[10.4233/uuid:161b044c-a2a2-435b-89ca-655ced4f321c](https://doi.org/10.4233/uuid:161b044c-a2a2-435b-89ca-655ced4f321c)

Publication date

2024

Document Version

Final published version

Citation (APA)

Liu, S. (2024). *Formability assessment of press forming process for uncured metal-composite laminates*. [Dissertation (TU Delft), Delft University of Technology]. <https://doi.org/10.4233/uuid:161b044c-a2a2-435b-89ca-655ced4f321c>

Important note

To cite this publication, please use the final published version (if applicable). Please check the document version above.

Copyright

Other than for strictly personal use, it is not permitted to download, forward or distribute the text or part of it, without the consent of the author(s) and/or copyright holder(s), unless the work is under an open content license such as Creative Commons.

Takedown policy

Please contact us and provide details if you believe this document breaches copyrights. We will remove access to the work immediately and investigate your claim.

**FORMABILITY ASSESSMENT OF PRESS FORMING
PROCESS FOR UNCURED METAL-COMPOSITE
LAMINATES**

FORMABILITY ASSESSMENT OF PRESS FORMING PROCESS FOR UNCURED METAL-COMPOSITE LAMINATES

Dissertation

for the purpose of obtaining the degree of doctor
at Delft University of Technology
by the authority of the Rector Magnificus Prof.dr.ir. T.H.J.J. van der Hagen
chair of the Board for Doctorates
to be defended publicly on
Monday 16th September 2024 at 15:00 pm

by

Shichen LIU

Master of Engineering in Aerospace Manufacturing,
Beijing University of Aeronautics and Astronautics, China
born in Ji'an, China.

This dissertation has been approved by the promotor.

Prof. C. A. Dransfeld,	Delft University of Technology, promotor
Ir. J. Sinke,	Delft University of Technology, copromotor

Composition of the doctoral committee:

Rector Magnificus,	Chairperson
Prof. C. A. Dransfeld,	Delft University of Technology, promotor
Ir. J. Sinke,	Delft University of Technology, copromotor

Independent members:

Prof. dr. ir. R. Benedictus,	Delft University of Technology, Netherlands
Prof. dr. ir. K. B. M. Jansen,	Delft University of Technology, Netherlands
Dr. ir. W. J. B. Grouve,	University of Twente, Netherlands
Prof. Dr.-Ing. W. Homberg,	University of Paderborn, Germany
Prof. dr. ir. J. M. C. Mol,	Delft University of Technology, Reserve member



Keywords: Metal-composite laminates; Inter-ply friction; Intra-ply shear; Flexural behaviour; Cure-dependent spring-back; Simultaneous deformation; Finite element modelling;

Printed by: Ipskamp printing

Front & Back: Beautiful cover that captures the entire content of this thesis.

Copyright © 2024 by Shichen Liu

All right reserved. No part of this publication may be reproduced, stored in a retrieval system or transmitted in any form or by any means, electronic, mechanical, photocopying, recording or otherwise, without the prior written permission of the author.

ISBN 978-94-6384-609-7

An electronic version of this dissertation is available at
<http://repository.tudelft.nl/>.

To my family

Shichen Liu

CONTENTS

Summary	xi
Samenvatting	xiii
List of Figures	xv
List of Tables	xxi
1 Introduction	1
1.1 Metal-composite laminates	2
1.2 Literature on forming techniques	4
1.3 Deformation mechanisms	7
1.4 Deformation defects	8
1.5 press forming of uncured laminates.	9
1.6 Research goal and scope	10
1.7 Thesis outline	11
References	12
2 A double-lap sliding test method for an inter-ply friction model	19
2.1 Introduction	20
2.2 Literature on inter-ply friction	20
2.3 Theory of friction models	21
2.4 Inter-ply friction experiment	24
2.4.1 Materials.	24
2.4.2 Setups	25
2.5 Results and discussion	29
2.5.1 Effect of normal force and sliding velocity	30
2.5.2 Effect of fibre orientation	32
2.5.3 Effect of resin viscosity and temperature	35
2.6 Development of inter-ply friction model	37
2.7 Finite element model validation	39
2.8 Conclusions.	40
References	41
3 A modified bias-extension test method for intra-ply shear characterisation	45
3.1 Introduction	46
3.2 Literature on intra-ply shear	46
3.3 Materials and methods	48
3.3.1 Material constituents	48
3.3.2 Modified bias-extension test	50

3.4	Experimental setups	51
3.4.1	Test conditions.	51
3.4.2	Shear angle measurement	52
3.5	Results and discussion	53
3.5.1	Effect of failure mode	53
3.5.2	Effect of material constituent	55
3.5.3	Effect of clamp displacement rate	57
3.5.4	Effect of preheat temperature	60
3.5.5	Effect of normal pressure	63
3.6	Conclusions.	64
	References	65
4	A clamped-beam bending test method for laminate flexural behaviour	71
4.1	Introduction	72
4.2	Literature on laminate bending	72
4.3	Materials and methods	75
4.3.1	Material preparation	75
4.3.2	Concept design	75
4.3.3	Experimental procedure	77
4.4	Finite element model	78
4.5	Results and discussion	80
4.5.1	Bending load-displacement response	80
4.5.2	Laminate bendability characterisation.	86
4.6	Conclusions.	93
	References	94
5	A cure-dependent spring-back investigation in a press forming cycle	97
5.1	Introduction	98
5.2	Literature on spring-back	98
5.3	Materials and methods	100
5.3.1	Material constituents	100
5.3.2	Rheological analysis	101
5.3.3	Experimental setup	104
5.3.4	Spring-back characterisation	105
5.4	Results and discussion	107
5.4.1	Effect of measure length	107
5.4.2	Effect of laminate design.	108
5.4.3	Effect of degree of cure.	112
5.4.4	Effect of forming pressure	115
5.5	Conclusions.	116
	References	117
6	A numerical study on simultaneous deformation for a dome part	123
6.1	Introduction	124
6.2	Literature on simultaneous deformation	124
6.3	Materials and method.	125
6.3.1	Materials.	125

6.3.2	Concept design	126
6.3.3	Finite element model	127
6.4	Results and discussion	128
6.4.1	Effect of material composition	128
6.4.2	Effect of clamping force	129
6.4.3	Effect of fibre orientation	130
6.4.4	Effect of inter-ply friction	132
6.4.5	Discussion of other effects	132
6.5	Conclusion	133
	References	134
7	Conclusions and recommendations	137
7.1	Main Conclusions.	138
7.1.1	Characterisation of deformation mechanisms and defects	138
7.1.2	Roles on individual layers of metal sheet and fibre prepreg	139
7.1.3	Influencing Factors on uncured laminate deformation	140
7.2	Recommendations for future work	141
	Acknowledgements	143
	Curriculum Vitae	145
	List of Publications	147

SUMMARY

METAL-composite laminates, also known as fibre metal laminates (FMLs), which are made by alternating thin sheets of metal alloys and layers of fibre reinforced polymers, have attracted the interest of many scholars and researchers in the field of aerospace applications, including manufacturing. These hybrid materials are widely applied owing to their significant advantages of weight reduction, superior specific strength, higher stiffness, and more fatigue resistance than monolithic metal sheets as well as the better impact strength and damage tolerance compared with the full composites. However, the manufacturing process of such laminates is difficult as various forming and curing stages are required in combination with the complex deformation and failure mechanisms. Hence to improve the manufacturability of these structures, it is crucial to develop a material forming method with optimized material compositions and process parameters.

The proposed press forming process, consists of an integral forming and curing cycle, is an innovative method for manufacturing small-to-medium sized components. The cycle involves a laminate preparing and preheating process, forming of the uncured laminate, consolidation and (partial) curing in a same mould as well as cooling and removal of the component. The most critical aspect of the cycle is a proper control of the different deformation mechanisms in different layers. For that, during the preheating stage, temperature and time needs to be carefully controlled so that the inter-ply sliding at the metal-prepreg interfaces and the intra-ply shear within the prepregs can be greatly enhanced when the resin viscosity decreases. Then, the still uncured laminate is formed and subsequently cured under pressure, avoiding a separate curing system with pressure, which is time and cost-saving.

The research presented in this thesis started with the investigation of the inter-ply slip deformation for uncured metal-composite laminates. An inter-ply friction model for the metal-prepreg interfaces was developed using a double-lap sliding test method. The static and kinetic coefficients of friction were quantified considering the effect of various process parameters. Then, the friction coefficients obtained from experimental results were analysed to fit the current friction models and by using those models, optimised conditions for proper sliding can be determined. Finally, the inter-ply friction model was incorporated into a finite element simulation which can be applied in the press forming process.

Secondly, the intra-ply shear properties of uncured metal-composite laminates were characterised through a modified bias-extension test. The hybrid material system consisting of different metal sheets as well as carbon fibre reinforced prepregs of woven fabric and cross-ply UD, was used to understand the role of metal sheet layers on the shear deformability of the prepreg layer. In addition, different shearing mechanisms for the two prepregs were observed and the results were compared with the theoretical pin-jointed net (PJN) method. Finally, the shear angle evolution of each prepreg system and

its corresponding metal-composite laminates can be analysed.

Thirdly, the flexural behaviour of uncured metal-CFRP laminates was studied by a clamped-beam bending test method. The role of local clamping pressure on the bending properties was illustrated in terms of plastic strain in the metal sheet for the hybrid materials. Experimental test and numerical simulation methods were performed to compare and validate the results of load-displacement response and laminate bendability characterisation. Besides, the radius and angle of the bent materials can be evaluated and the optimisations for material as well as process parameters can be achieved for the press forming of the uncured metal-CFRP laminates.

The previous chapters focused on separate deformation mechanisms occur during forming. However, the combined effects after forming and during curing were also important. Therefore, the research presented an investigation on the effect of spring-back on the final quality of the formed component after the curing stage. A series of experimental tests were performed to compare the impact of two processing conditions of full-cured and partially-cured after the press forming process on the calculated spring-back ratio. The factors affecting the cure-dependent spring-back of uncured metal-composite laminates were evaluated.

Lastly, the simultaneous deformability during the forming stage of dome component was validated through numerical simulations. The results from the previous studies were incorporated into the simulation model. The failure modes during the press forming simulation were analysed and compared. The effect of material constituent, fibre orientation, clamping force as well as inter-ply friction were analysed and combined to explore which factors are the most important and how they affect the final quality of the component.

In conclusion, the thesis has proposed and developed a press forming process integrated with forming and curing for the manufacturing of uncured metal-composite laminates. The deformation mechanisms including inter-ply friction, intra-ply shear, flexural bending, cure-dependent spring-back were studied and a numerical simulation on the simultaneous deformation was validated. This thesis contributes to a better understanding of the deformability, and opens opportunities for material and process optimisations for the press forming of uncured metal-composite laminates.

SAMENVATTING

METAAL-composiet laminaten, ook wel vezelmetaallaminaten (FMLs) genoemd, die worden gemaakt door dunne platen van metaallegeringen en lagen vezelversterkte polymeren af te wisselen, hebben de belangstelling getrokken van veel wetenschappers en onderzoekers op het gebied van de luchtvaart- en ruimtevaart(productie). Deze hybride materialen worden op grote schaal toegepast vanwege aanzienlijke voordelen op het gebied van gewichtsvermindering, en superieure specifieke sterkte, hogere stijfheid en meer weerstand tegen vermoeiing dan voor de monolithische metalen platen, evenals de betere impactsterkte en schadetolerantie vergeleken met de pure composieten. Het vervaardigingsproces van dergelijke laminaten is echter moeilijk omdat er verschillende vormings- en uithardingsfasen nodig zijn in combinatie met complexe vervormings- en bezwijkmechanismen. Om de maakbaarheid van deze constructies te verbeteren, is het daarom van cruciaal belang om een materiaalvormingsmethode te ontwikkelen met geoptimaliseerde materiaalstukken en procesparameters.

Het persvormproces, dat bestaat uit een integrale vormings- en uithardingscyclus en, is een innovatieve methode voor het vervaardigen van kleine tot middelgrote componenten. De cyclus omvat een voorbereidings- en voorverwarmingsproces van het laminaat, het vervormen van het niet-uitgeharde laminaat, het consolideren en (gedeeltelijk) uitharden in dezelfde mal, evenals het afkoelen en verwijderen van het onderdeel. Het meest kritische aspect van de cyclus is een goede beheersing van de verschillende vervormingsmechanismen in verschillende lagen. Daarom moeten tijdens de voorverwarmingsfase de temperatuur en de tijd zorgvuldig worden gecontroleerd, zodat het glijden tussen de lagen op de grensvlakken van metaal en prepreg en de afschuivings in de prepregs aanzienlijk kunnen worden verbeterd wanneer de viscositeit van de hars afneemt. Vervolgens wordt het nog niet uitgeharde laminaat gevormd en vervolgens onder druk uitgehard, waardoor een apart uithardingsstelsel met druk wordt vermeden, wat tijd- en kostenbesparend is.

Het onderzoek dat in dit proefschrift wordt gepresenteerd, begint met onderzoek naar de afschuifvervorming tussen de lagen bij niet-uitgeharde metaal-composiet laminaten. Een model voor de wrijving tussen de lagen op de metaal-prepreg-grensvlakken werd ontwikkeld met behulp van een dubbele-lap-afschuiftest. De statische en kinetische wrijvingscoëfficiënten werden gekwantificeerd rekening houdend met het effect van verschillende procesparameters. Vervolgens werden de wrijvingscoëfficiënten verkregen uit experimentele resultaten om toe te passen in wrijvingsmodellen om door die modellen geoptimaliseerde omstandigheden voor afschuiving te kunnen bepalen. Ten slotte werd het wrijvingsmodel geïntegreerd in een eindige-element model dat kan worden toegepast in het persvormproces.

Ten tweede werden de afschuifeigenschappen persvormproces van niet-uitgeharde metaal-composietlaminaten gekarakteriseerd door middel van een aangepaste bias-trek test. Het hybride materiaalsysteem bestaande uit verschillende metaalagen en koolstof-

vezel versterkte prepregs van weefsel en kruislings gelegd UD, werd gebruikt om het effect van de metaallagen op de afschuifvervorming van de prepreglaag te analyseren. Daarnaast werden verschillende afschuifmechanismen voor de twee prepregs waargenomen en werden de resultaten vergeleken met de theoretische pin-jointed net (PJN)-methode. Ten slotte kan de evolutie van de afschuifhoek van elk prepreg-systeem en de bijbehorende metaal-composietlaminaten worden geanalyseerd.

In de derde plaats werd het buiggedrag van niet-uitgeharde metaal-CFRP-laminaten bestudeerd met behulp van een buigtestmethode met ingeklemde uiteinden. De invloed van lokale klemdruk op de buigeigenschappen werd zichtbaar in de plastische vervormingen in de metaalplaat van de hybride materialen. Experimentele tests en numerieke simulatiemethodens werden uitgevoerd om de resultaten van de kracht-verplaatsings krommen en de karakterisering van de buigbaarheid van laminaten te vergelijken en te valideren. Bovendien kan de radius en buighoek van de gebogen materialen worden geëvalueerd en kunnen optimalisaties voor zowel materiaal als procesparameters worden bereikt voor het persvormen van de niet-uitgeharde metaal-CFRP-laminaten.

De voorgaande hoofdstukken concentreerden zich op afzonderlijke vervormingsmechanismen die optreden tijdens het vervormen. De tijdens het vervormen effecten op het stadium van vervorming en uitharding zijn echter ook belangrijk. Daarom presenteerde het onderzoek een onderzoek naar het effect van terugveren op de uiteindelijke kwaliteit van het gevormde onderdeel na de uithardingsfase. Er werd een reeks experimentele tests uitgevoerd om de effecten van twee verwerkingsomstandigheden van volledig uitgehard en gedeeltelijk uitgehard na het heetpersproces te vergelijken door de variatie van de berekende terugveringsverhouding. De factoren die de uithardingsafhankelijke terugvering van niet-uitgehard materiaal beïnvloeden metaal-composietlaminaten werden geëvalueerd.

Ten slotte werd de gelijktijdige vervormbaarheid tijdens de vormingsfase van een halve bolvorm gevalideerd door middel van numerieke simulaties. De resultaten uit de eerdere onderzoeken zijn verwerkt in het simulatiemodel. De bezwijkvormen tijdens de simulatie van het persen werden geanalyseerd en vergeleken. Het effect van het type materiaal, de vezeloriëntatie, de klemkracht en de wrijving tussen de lagen werden geanalyseerd en gecombineerd om te onderzoeken welke factoren het belangrijkst zijn en hoe deze de uiteindelijke kwaliteit van het onderdeel beïnvloeden.

Concluderend is in het proefschrift een persvormproces voorgesteld en ontwikkeld, waarin vervormen en uitharden geïntegreerd worden, voor het vervaardigen van niet-uitgeharde metaal-composietlaminaten. De vervormingsmechanismen, waaronder wrijving tussen de lagen, afschuiving binnen de composiet lagen, buiging en uithardingsafhankelijke terugvering, werden bestudeerd en een numerieke simulatie van de gelijktijdige vervorming werd gevalideerd. Dit proefschrift draagt bij aan een beter begrip van de vervormbaarheid en opent mogelijkheden voor materiaal- en procesoptimalisaties voor het persvormen van niet-uitgeharde metaal-composietlaminaten.

LIST OF FIGURES

1.1 Schematic graph of the standard GLARE grades [7]	2
1.2 Typical classification of metal-composite laminates	3
1.3 Autoclave curing process for forming metal-composite laminates [22] . .	4
1.4 Three categories of the press forming techniques for metal-composite lam- inates	4
1.5 Processing strategies for the forming of metal-composite laminates [17] .	5
1.6 Primary deformation mechanisms for metal-composite laminates during forming	7
1.7 Primary deformation defects for metal-composite laminates during forming	9
1.8 Processing temperature and time profile of the tool surface and uncured hybrid laminate in a press forming cycle	10
1.9 Schematic description of the research outline of the PhD thesis	12
2.1 Stribeck curve on friction coefficient versus Hersey number, indicating the range of Chow’s research [23]	23
2.2 Preheat temperature and time cycles for the pre-stacked GLARE materials	24
2.3 (a) Schematic graph and (b) Dimension for the friction test, (c) Details of the clamping loadcell	26
2.4 Experimental setup and apparatus: (a) Calibration test of normal force; (b) Inter-ply friction test	26
2.5 Normal force and strain voltage curve under various temperatures for the clamping loadcell	27
2.6 Predicted cure evolution of FM-94 epoxy at various temperatures: (a) De- gree of cure; (b) Viscosity	29
2.7 Schematic curve of pull-out force and displacement relation for the friction test	29
2.8 Friction coefficients as a function of normal force and sliding velocity at room temperature (23°C): (a) Static; (b) Kinetic	30
2.9 Sketch for illustrating the effect of normal force and temperature after the friction test	30
2.10 Sketch of the laminate sample after the friction test: (a) Cut-outs; (b) Slid- ing surfaces	31
2.11 Cross-section micrographs after friction test performed with a normal force of (a): 200N and (b)1000N at the temperature of 80°C – (×80)	31
2.12 Hersey number versus test friction coefficient at room temperature: (a) Ki- netic; (b) Static	32
2.13 Kinetic friction coefficients of (a) different normal forces at room temper- ature of 23°C and (b) different temperatures at normal force of 500N	33

2.14 Sliding surfaces after the friction test performed with different fibre orientations – ($\times 12$)	33
2.15 Cross-section micrographs after friction test performed with a fibre orientation of (a) $45^\circ/45^\circ$ and (b) $90^\circ/90^\circ$ at the temperature of 80°C and 500N – ($\times 80$)	34
2.16 Experimental Friction coefficients under different temperatures: (a) Static; (b) Kinetic	35
2.17 Sliding surfaces after the friction test performed with different temperatures for $0^\circ/0^\circ$ interfaces at 500N and $10\text{mm}/\text{min}$ – ($\times 12$)	36
2.18 Cross-section micrographs after friction test performed with a temperature of (a) 40°C and (b) 120°C – ($\times 80$)	36
2.19 Effect of temperature on test friction coefficient and Hersey number: (a) Kinetic; (b) Static	37
2.20 Finite element model of the inter-ply friction test of the pre-stacked laminates	39
2.21 Comparison between numerical and experimental results for inter-ply friction of uncured hybrid laminates: (a) At room temperature of 23°C ; (b) At sliding velocity of $10\text{mm}/\text{min}$	40
3.1 Typical intra-ply shear deformation behaviour of textile reinforcement materials	47
3.2 Two types of fibre reinforced prepregs used for the intra-ply shear tests	49
3.3 Viscosity profile for MTC510 matrix system used for SHD-TW and SHD-UD prepreg as a function of temperature	49
3.4 Schematic graph and dimension for the modified bias-extension test of metal-composite laminate	50
3.5 Experimental setups and apparatus for modified BE test used under various normal pressure conditions: (a) Standard condition; (b) Vacuum condition of 0.1MPa ; (c) Autoclave condition of 0.6MPa	51
3.6 Whole process for the shear angle measurement of metal-composite laminates	53
3.7 Stress and strain curves for different combination of hybrid as well as composite materials under the condition of room temperature and $10\text{mm}/\text{min}$ clamp displacement rate: (a) Based on woven fabric reinforced laminates; (b) Based on cross-plyed UD fibre reinforced laminates	54
3.8 Microscopic measurements of the rotation angle (α) evolution for aluminium-fibre reinforced laminate under the condition of room temperature and $10\text{mm}/\text{min}$ clamp displacement rate: (a) Cross-plyed UD structure; (b) Woven fabric structure	55
3.9 Shear deformation mechanism schematic of two different fibre prepregs: (a) Woven fabric; (b) Cross-plyed UD fibres	56
3.10 Shear angle and strain curves for different combinations of metal-composite laminates under the condition of room temperature and $10\text{mm}/\text{min}$ clamp displacement rate	57

3.11 Shear angle and strain curves of aluminium-fibre reinforced laminate and its pure prepreg under different clamp displacement rates without normal pressure: (a) Woven fabric structure; (b) Cross-ply UD structure	58
3.12 Shear angle and strain curves of stainless steel-fibre reinforced laminate and its pure prepreg under different clamp displacement rates without normal pressure: (a) Woven fabric structure; (b) Cross-ply UD structure	58
3.13 Schematic of the force transmitting and contact surfaces: (a) Woven fabric prepreg; (b) Metal-composite laminate	58
3.14 Picture of test-specimens to the shear strain of 30% at room temperature for different material combinations without normal pressure (UD-Cross-ply unidirectional fibre prepreg, WF-Woven fabric prepreg, Ss-Stainless steel)	59
3.15 Shear angle and strain curves of woven fabric reinforced-metal laminate and its pure prepreg under different preheat temperatures without normal pressure: (a) Aluminium alloy structure; (b) Stainless steel structure	60
3.16 Shear deformation of two different prepregs at higher temperature:(a) Woven fabric; (b) Cross-ply UD	61
3.17 Picture of test-specimens to the shear strain of 30% at room temperature and 80°C for pure composite prepregs (UD-Cross-ply unidirectional fibre prepreg, WF-Woven fabric prepreg)	61
3.18 Shear angle and strain curves of cross-ply UD reinforced-metal laminate and its pure prepreg under different preheat temperatures without normal pressure: (a) Aluminium alloy structure; (b) Stainless steel structure	62
3.19 Shear angle values at two strains for aluminium alloy-fibre reinforced laminate and its pure prepreg under different normal pressures: (a) Woven fabric structure; (b) Cross-ply UD structure	63
3.20 Shear angle values at two strains for stainless steel-fibre reinforced laminate and its pure prepreg under different normal pressures: (a) Woven fabric structure; (b) Cross-ply UD structure	63
3.21 Picture of test-specimens to the shear strain of 45% at RT under two normal pressures for hybrid laminates (UD-Cross-ply unidirectional fibre prepreg, WF-Woven fabric prepreg, Ss-Stainless steel)	64
4.1 Setups for the characterisation of bending behaviour for fibre reinforced composites: (a) Cantilever test based, (b) Kawabata test based and (c)-(e) Vee-bending test based methods	73
4.2 Schematic graph and specimen dimensions for the laminate clamped-beam bending concept	76
4.3 Double-acting pneumatic cylinder and the schematic graph of the pressure loading concept	76
4.4 Bending tool system with two pneumatic cylinders for the clamped-beam bending concept	77
4.5 Experimental procedure and apparatus of the laminate bending: (a) Clamped-beam bending setup; (b) Real-time pressure gauge tank; (c) Manual pressure controller	78

4.6	Finite element model of the clamped-beam bending test for the uncured metal-CFRP laminates	79
4.7	Stress-strain curve of the metal sheets applied for the clamped-beam bending test simulations	79
4.8	Experimental and numerical results on the bending force evolution of the metal sheet and the corresponding metal-CFRP laminate at room temperature (RT) with the clamping pressure of 0 bar	80
4.9	Schematic graph of the stress distribution after bending process for different test materials: (a) Single-layer metal sheet; (b) uncured metal-composite laminate with 2/1 layups	81
4.10	Experimental bending force and displacement curves under various clamping pressures for clamped-beam bending test: (a) Single-layer aluminium alloy 2024-T3; (b) 2/1, 0°/90° Al/CFRP at room temperature of 23°C	82
4.11	Experimental bending force and displacement curves of the single-layer stainless steel and its corresponding hybrid laminates at room temperature (23°C) for clamped-beam bending with two clamping pressures: (a) 0 bar; (b) 3 bar	83
4.12	Experimental results for the maximum bending force of different laminate structures under three clamping pressures	84
4.13	Schematic graph of the deformation mechanisms during bending for two typical fibre orientations of cross-ply UD prepregs: (a) 0°/90°; (b) 45°/-45°	84
4.14	Experimental results on the maximum bending force and a displacement of 40mm for various processing temperature and pressure conditions for the hybrid laminate of 2/1 layups: (a) 0 bar; (b) 3 bar	85
4.15	Microscopic measurements of the rotation angle on the centre region of the 2/1, Al/CFRP laminate with the fibre orientation of 45°/-45° under various bending conditions: (a) Initial state; (b) RT, 0 bar; (c) 80°C, 0 bar; (d) 80°C, 3 bar	86
4.16	Schematic graph and dimension of three different stages during the laminate bending process	87
4.17	Experimental and numerical comparisons on the spring-back depth for different material configurations	87
4.18	Numerical results of the vertical displacement (U_3) before and after spring-back of bending for different materials under the conditions of no clamping pressure and room temperature (23°C): (a) Single-layer aluminium alloy 2024-T3; (b) Single-layer stainless steel 304L; (c) 2/1, 0°/90°, Al/CFRP; (d) 2/1, 0°/90°, Ss/CFRP; (e) 3/2, 0°/90°, Al/CFRP; (f) 3/2, 0°/90°, Ss/CFRP	88
4.19	Test specimens after spring-back for different laminate configurations and test conditions at room temperature: (a) 2/1, 0°/90°, Al/CFRP laminates; (b) 0°/90°, Ss/CFRP laminates	89
4.20	Experimental results on the spring-back depth and length reduction after unloading under various pressure conditions: (a) Aluminium alloy based materials; (b) Stainless steel based materials	89

4.21	Test specimens under two clamping pressure conditions at room temperature for different materials after spring-back: (a) Single-layer metal sheets; (b) 2/1, 0°/90°, hybrid metal-CFRP laminates	90
4.22	Numerical results on the equivalent plastic strain at room temperature (23°C) for hybrid laminates after the bending process	92
4.23	Numerical results on the relationship of maximum plastic strain and clamping pressure for different materials	92
5.1	Stress-strain curve until fracture of two different metal sheets used for the spring-back analysis	100
5.2	Predicted degree of cure evolution of the epoxy under specific temperatures: Solid line-FM94 and Dashed line-MTC510	102
5.3	Rheological data of the FM94 and MTC510 epoxy at the ramp of 2°C/min	103
5.4	Single-curved mould design for the laminate press forming process: (a) mould dimension; (b) mould manufacture	103
5.5	Experimental setup and apparatus for the hybrid laminate press forming process	103
5.6	Schematic graph of the laminate forming process on cure-dependent spring-back	105
5.7	Definition of the spring-back angle and radius for the metal sheet forming process	106
5.8	Geometric analysis of the laminate spring-back radius after removal of the forming loads	107
5.9	Single-curved parts and their profiles after spring-back for various material combinations	108
5.10	Two spring-back parameters under various measure lengths for different material combinations: (a) Forming depth; (b) Forming radius	108
5.11	Single-curved part after full-cured process with different metal-composite combinations: (a) Al/GFRP; (b) Ss/GFRP; (c) Al/CFRP; (d) Ss/CFRP	109
5.12	Schematic diagram of stress distribution after bending for metal-composite laminates: (a) Bent with an uncured prepreg and subsequently cured; (b) Bent with a full-cured prepreg	109
5.13	Cross-sectional micrographs of the central region in hybrid laminates after full-cured : (a) Al/GFRP with the layup of 2/1 and fibre orientation of 0°/0°; (b) Al/GFRP with the layup of 3/2 and fibre orientation of 0°/0°; (c) Al/CFRP with the layup of 2/1 and fibre orientation of 0°/0°; (d) Al/GFRP with the layup of 3/2 and fibre orientation of 90°/90°.	110
5.14	Spring-back ratio K_2 under different layup and fibre orientation conditions for hybrid laminates	111
5.15	Single-curved parts after spring-back for two metal-composite combinations under various temperatures at the holding time of 20 min: (a) 2/1, 0°/0°, Al/GFRP; (b) 2/1, 0°/0°, Ss/CFRP	113
5.16	Cross-section micrographs of the central region in 2/1, 0°/0°, Al/CFRP laminate under three temperature conditions	114

5.17	Spring-back ratio K_1 under various temperature and time conditions after partially-cured process: (a) 2/1, 0°/0°, Al/GFRP; (b) 2/1, 0°/0°, Ss/CFRP . . .	115
5.18	Evolution of spring-back ratio K as a function of degree of cure α for metal-composite laminates	115
5.19	Spring-back ratio K_2 after full-cured under different forming pressures for hybrid laminates	116
6.1	(a) Schematic graph of the double-curved dome forming tool design and dimensions; (b) Deformation mechanisms and initial shapes of the individual metal sheet and uncured fibre prepreg	126
6.2	Finite element model of the press forming process for uncured hybrid laminates	127
6.3	Numerical simulation on vertical displacement (U3,mm) before failure at room temperature and zero clamping force for Al/GFRP laminate: (a) XY plane-Al; (b) XZ plane-Al	128
6.4	Numerical simulation on vertical displacement (U3,mm) before failure at room temperature and zero clamping force for stainless steel (Ss)-based hybrid materials: (a) CFRP layer; (b) GFRP layer	129
6.5	Numerical simulation on maximum draw depths and failure modes at room temperature under different clamping force for metal-composite laminates	130
6.6	Numerical simulation on vertical displacement (U3,mm) at the maximum value at room temperature for Ss/CFRP laminates under two clamping forces: (a) 1kN; (b) 2kN	130
6.7	Comparison between two clamping forces against the initial and final prepreg shapes from the numerical simulation for Ss/CFRP laminates (Draw depth=40mm)	131
6.8	Numerical comparison on the shear strain distributions of the prepreg layer for Ss/CFRP laminates at room temperature (Draw depth=40mm): (a) 0kN, 0°/90°; (b) 2kN, 0°/90°; (c) 0kN, 45°/-45°; (d) 2kN, 45°/-45°	131
6.9	Comparison between different inter-ply frictions against the initial and final laminate shapes from the numerical simulation for Ss/CFRP laminates under the clamping force of 1kN (Draw depth=40mm)	131
6.10	Numerical simulation on vertical displacement (U3,mm) before failure for Ss/CFRP laminates under the clamping force of 1kN and two inter-ply friction coefficients: (a) $\mu = \infty$; (b) $\mu = 0.2$	132
7.1	Summary on the main topics of the thesis	138

LIST OF TABLES

2.1	Details of layup configuration and thickness of pre-stacked laminates . . .	25
2.2	Test parameters used for inter-ply friction experiments	27
2.3	Test conditions for Hersey number studied at room temperature of 23°C ($\eta_0 \approx 10^4$ Pa-s)	28
2.4	The constants used in the viscosity model (Equation 2.7) for FM-94 epoxy [35, 36]	28
2.5	Computed viscosity used in the friction models with a constant preheat time of 20 minutes	28
3.1	Material configurations used for modified bias-extension test	52
3.2	Test conditions used for modified bias-extension test	52
4.1	Mechanical properties of the material constituents in bending test [33–35]	75
4.2	Material configurations and test parameters used for clamped-beam bend- ing test	77
5.1	Mechanical properties of the material constituents in spring-back analysis [42, 43]	101
5.2	Cure kinetic parameters for epoxy FM94 and MTC510 [45–47]	102
5.3	Material configurations used for press forming process	104
5.4	Test conditions used for laminate press forming process	104
5.5	Computed degree of cure used for various holding time and temperature	105
6.1	Mechanical properties of the material in the forming simulation [25, 26] .	126
6.2	Test parameters used for the hybrid laminate press forming concept . . .	126

1

INTRODUCTION

1.1. METAL-COMPOSITE LAMINATES

IN recent years, lightweight composite materials with excellent mechanical and physical properties have become a trend for aircraft manufacturing. Metal-composite laminates, also known as fibre metal laminates (FMLs), are one of those materials consist of thin, high-strength metal sheets alternatively bonded to plies of fibre-reinforced polymers [1, 2]. This hybrid combination provides substantial weight reductions, superior fatigue behaviour and damage tolerant properties, inherent resistance to corrosion, good fire resistance for safety improvement, which makes the metal-composite laminates very attractive candiate materials for aircraft structures [3, 4].

A wide range of combinations are available according to the type of metal sheets, the choice of fibres and resins, the number and thickness of layers, etc [5, 6]. The metal alloy sheets currently being used are aluminium, titanium, stainless steel or magnesium, and the fibre reinforced polymers (FRPs) can be made from dry fibres such as aramid, carbon or glass fibres with the infusion of resin or preregs made by pre-impregnated fibres and a partially cured polymer matrix. Among the family of metal-composite laminates, GLARE is the most well-known member, which consists of thin aluminium sheets (usually 0.3-0.5 mm thick) and unidirectional S-2 glass fibre reinforced prepreg layers. A schematic graph of the standard GLARE grades is shown in Figure 1.1 where GLARE 4B 3/2-0.4 denotes that the GLARE material consists of 3 layers of metal sheet of 0.4 mm thickness and 2 layers of prepreg with the fibre orientation of $90^\circ/0^\circ/90^\circ$ (coded as 4B). The fibre orientation of 0° is parallel to the rolling direction of the metal sheet. The most widely application of GLARE for aerospace thus far is the fuselage skin of the Airbus A-380 (total surface area of about 470 m^2) where single-curved and double-curved GLARE panels are applied [7]. Other combinations of the metal-composite laminates include aramid-reinforced aluminium laminate (ARALL), carbon-reinforced aluminium laminate (CARALL) and graphite-reinforced titanium laminate (TIGR). These combinations have their respective benefits and drawbacks despite that most of them have been successfully applied for aircraft structures [8–10].

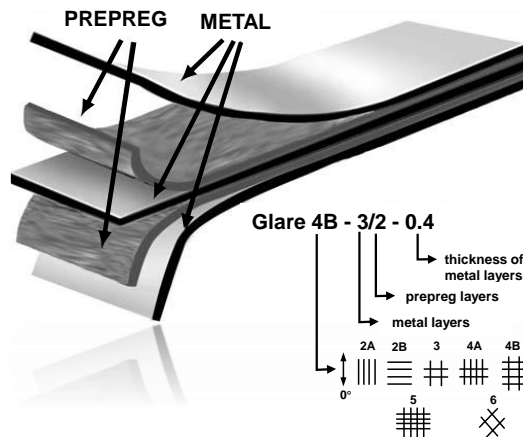


Figure 1.1: Schematic graph of the standard GLARE grades [7]

In addition to the traditional classification of metal-composite laminates, the composition of composite layers can also consist of woven fabrics and thermoplastic resins instead of the unidirectional (UD) reinforcements and thermoset epoxies. The hybrid laminate with UD fibre reinforced composites have higher mechanical performance, while the anisotropic properties as all the fibres running in one parallel direction make it easier to crack and induce wrinkles during the forming process. Another advantage for the choice of UD-fibre prepreg is that all variants (2A to 6) can be made by one type of prepreg just by changing orientations and number of layers. The woven fabric reinforced metal laminates like the plain, twill and satin types are more favourable for forming due to the symmetric properties, while the deformation and failure mechanisms are more complex [11, 12]. The thermoset epoxies are most commonly applied due to the low shrinkage during curing, high-strength and excellent durability in hot and moist environment. The advantages include the drapability at room temperature, the low processing temperatures as well as the easier impregnation with low viscosities [13]. However, the long curing cycle of such matrix system increases the production time and consequently restricts the fabrication volume. The thermoplastic based metal-composite laminates have received increasing interest because of their potential advantages including superior toughness and chemical resistance in service, better recyclability, as well as their decreased processing time. While the disadvantages for such hybrid thermoplastic materials include the higher processing temperatures which may result in problems with the temperature of metal alloys as well as the increase in residual stress, and the reduced bonding capability between composite and metal sheets [14–16]. The typical classification of metal-composite laminates based on the material constituents, laminate layups as well as fibre architectures is presented in Figure 1.2.

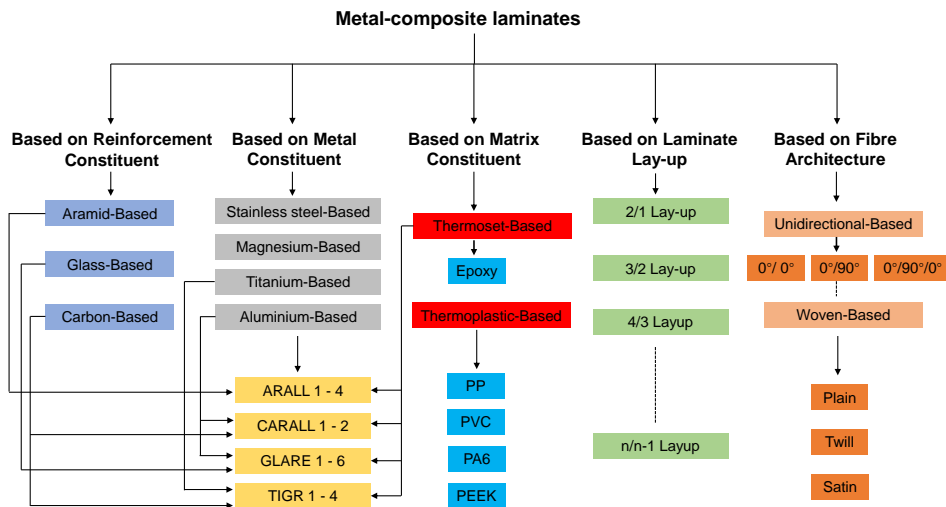


Figure 1.2: Typical classification of metal-composite laminates

1.2. LITERATURE ON FORMING TECHNIQUES

THE most common and simplest approach for forming metal-composite laminates is through lay-up techniques followed by autoclave curing (Figure 1.3), which is applicable for large components like fuselage and wing panels. The forming quality and mechanical properties are excellent for single-curved components while this technique is significantly limited for double-curved components [5] [17]. As the metal sheet is not deformed plastically at these processing temperature, the waviness generated at the edges during layup is suppressed at high curing pressure, leaving acceptable residual stresses remain in the panels. Other forming methods for large components by metal-composite laminates such as press brake bending [18], stretch forming [19], shot peening or incremental sheet forming [20] and laser forming [21] are described in the literature including their benefits and drawbacks.

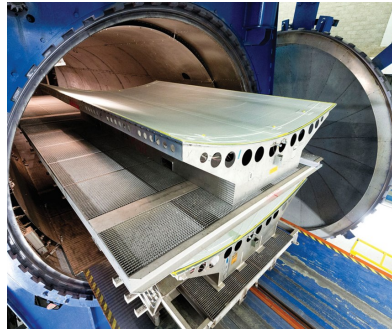


Figure 1.3: Autoclave curing process for forming metal-composite laminates [22]

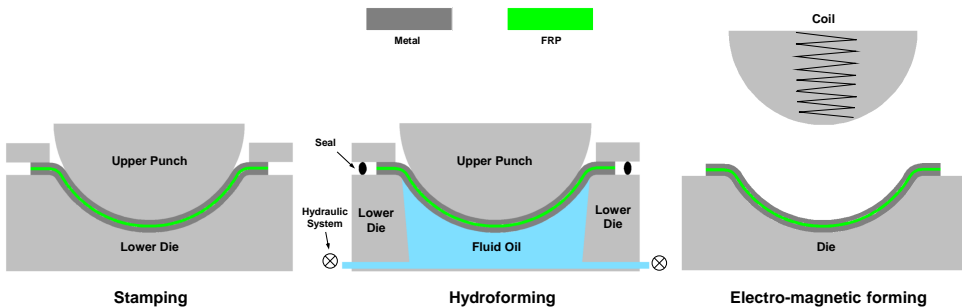


Figure 1.4: Three categories of the press forming techniques for metal-composite laminates

As for the forming of small and medium sized components with relatively small radii and complex shapes, the concept of press forming is introduced where the sheets are forced by solid dies which are shaped in the required geometry. This concept has proven to be a well-developed mass-production technology for forming metal sheet components, and fibre-reinforced polymer (FRP) components in recent years [23, 24]. Therefore, the method of press forming can be utilized to form metal-composite laminates for the hybrid material with thermoplastic matrix because of the short processing time and

the improved formability of FRP layers at elevated temperatures. However, the higher processing temperature which may affect the heat treatments of the metal sheet and induce higher residual stresses hinders its development [25]. There are three main categories of the press forming techniques feasible for the forming of metal-composite laminates, and the schematic graphs are shown in Figure 1.4. Stamping is the most widely applied press forming method which consists of an upper and lower die and a blank holder. The tools and hybrid sheets are usually preheated before the stamping process and the cycle time can be short for both thermoplastic-based and thermoset-based metal-composite laminates [26, 27]. Hydroforming, which uses pressurized liquid replacing the lower rigid dies, is a widely applied press forming process for metal sheet and tubular components. The benefits of the hydroforming process are its uniform load distribution and better surface quality, which is applicable to form metal-composite laminates [28, 29]. Electro-magnetic forming, which utilizes a pulsed magnetic field to apply loads on the workpiece, is a high speed and non-contact forming technology for metal sheet and tubular components. One of the studies investigated the feasibility for the forming of metal-composite laminate components using this method and it has shown the possibility of formability increasing due to change of strain state [30].

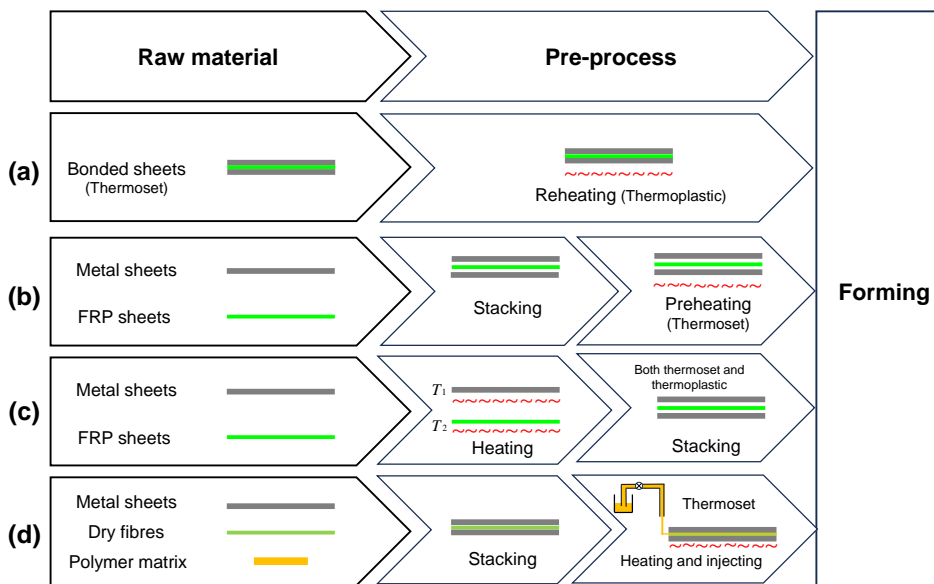


Figure 1.5: Processing strategies for the forming of metal-composite laminates [17]

The metal-composite laminate parts can be manufactured by forming metal sheets and shaping FRP sheets into designed shapes separately and then bonding them together with adhesives [31]. Zafar et al. [32] developed a “3A” method which is based on simultaneous forming of multi-layer metal sheet through hydroforming technology. This method helps to make the part with any type of dry fibre/polymer matrix systems as well as any layup and thickness of the hybrid laminates. However, the long cycle time, the

required heat and pressure, the as-formed geometric accuracy and final product quality it achieved all limit its development. Therefore, the direct forming methods of metal-composite laminate might offer a better solution. The methods can be categorised into four processing strategies with various raw materials and pre-process steps before forming as schematically illustrated in Figure 1.5.

The first strategy is to have bonded hybrid laminates as raw materials, which might undergo the reheating and a subsequent forming process for the sheet. For thermoset-based metal-composite laminates, such laminates go (without heating) directly through a cold forming process as the epoxy matrix cannot be remelted. Therefore, this method is typically applied for the thermoplastic-based metal-composite laminates as the deformability is poor at low temperatures. Mosse and Kalyanasundaram et al. [26][33] applied the stamp forming process of aluminium alloy based polypropylene (PP) laminates after heating the bonded blanks and studied the effect of process parameters. They found that these hybrid laminates have potential for high formability characteristics and significant reductions in shape errors can be achieved. Nam et al. [34] and Zal et al. [35] extended this strategy to the steel/PP-based and Al/PVC-based metal-composite laminates, respectively, and similar conclusions can be obtained from their studies.

The second strategy aims to achieve the forming of thermoset-based hybrid laminates where the metal sheets and FRP sheets (uncured prepregs) are stacked and preheated prior to forming. The preheating temperature is always below the curing temperature of the prepreg which reduces the resin viscosity. Lee et al. [36] preheated semi-finished stacks consisting of steel and carbon fibre-reinforced epoxy prepregs before deep drawing. He concluded that the forming depth increases with lower blank holder force while the influence of punch velocity is limited. Liu et al. [37] applied the method to semi-finished GLARE laminates stacked at room temperature to validate the formability under different fibre orientations in a stamp forming process. He believed that multi-directional fibre layers are a good alternative compared to the unidirectional fibre layers especially when a better formability is the main goal. In the study of Behrens et al. [38], the aluminium alloy sheets and carbon fibre-reinforced PA6 sheets were stacked at room temperature and heated in a forming tool system with heating concepts. Here, the forming and adhering of thermoplastics and metal sheet in one step can be achieved following this method. The resulting hat profiles can be produced successfully with a tool temperature of 250°C and the application results in economic benefits.

The third strategy is the method where metal sheets and FRP sheets are separately heated to different temperatures and subsequently stacked before forming. Guo et al. [39] formed the steel/CFRP U-shaped and box-shaped structures when heating the CFRP sheets at the melting temperature of the resin matrix (120°C) and steel sheets at the warm forming temperature (550°C), respectively. He discovered that the formed components have a higher forming precision and much higher load-carrying capability as well as better energy absorption than their pure steel counterparts. However, one of the drawbacks may be the damage of the composite parts when two sheets come into contact at this high temperature, which hinders its development.

Compression moulding and resin transfer moulding (RTM) are techniques developed to fabricate composite components where the bottom metal sheet is placed on a heated tool with the dry fibres on top, and the polymer matrix is injected onto the sheet

before the top steel layer is being stacked. Mennecart et al. [40] proposed two innovative methods applying such techniques to form the metal-composite laminates. One is the combination process of deep drawing and wet compression moulding, and the other is the deep drawing process coupled with resin transfer moulding. He mentioned that these processes have better forming behaviour due to the application of the epoxy resin which polymerizes directly between the metal sheets. The used polymer matrix is usually low-viscosity thermoset in the laminates, while the forming of thermoplastic-based hybrid laminates can be achieved once the polymer has a suitable viscosity.

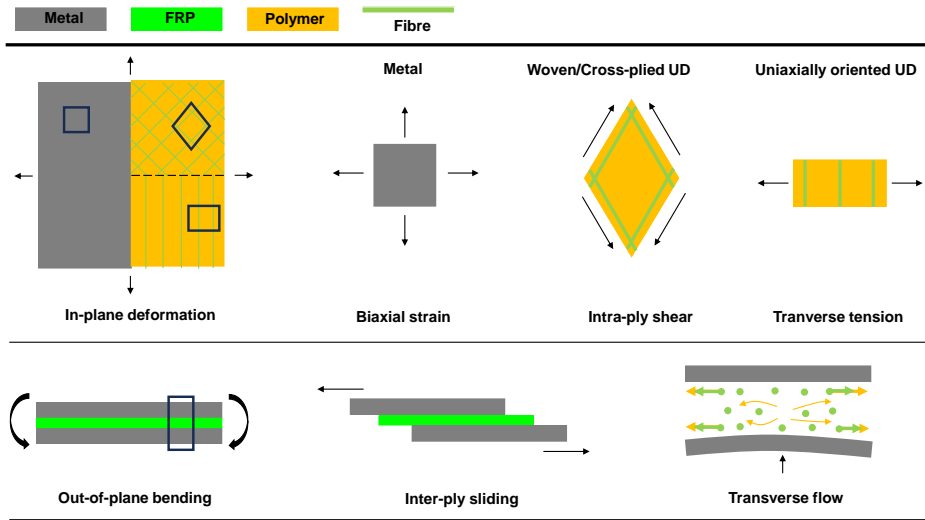


Figure 1.6: Primary deformation mechanisms for metal-composite laminates during forming

1.3. DEFORMATION MECHANISMS

DURING the forming process of metal-composite laminates, the material properties and layer interactions are the key indexes for evaluating the deformability of the hybrid materials. The primary deformation mechanisms shown in Figure 1.6 reveal that the forming behaviour of metal-composite laminates is determined by the deformation mechanisms of metal and FRP sheets, and the movements between the sheets. As for the deformation modes involved in sheet metal forming, the in-plane deformations like biaxial straining dominate the forming of three-dimensional (3D) shapes. The mechanical responses of the metal sheets can be either obtained from the uniaxial tensile tests [41], or characterised through the forming limit diagram (FLD) created by different test methods [42–44]. The deformation mode for FRP sheets varies with different types of fibre reinforcement, including woven and unidirectional (UD), with the UD being available in cross-ply UD and uniaxially oriented UD. The dominating deformation mechanism for woven fabrics or cross-ply UD fibres is intra-ply shear, which denotes the rotation of the inextensible fibres. The intra-ply shear mechanism, also known as Trelis effect, is mainly responsible for FRP sheet to be formed into three-dimensional (3D)

shapes [45, 46]. Transverse tension is the deformation mechanism in the UD polymers oriented parallel to the tension line during forming since the tension force in transverse direction is much lower than the shear force. The influence of tension along the longitudinal direction for the FRP sheets can be neglected due to the limited failure strain of the UD fibres [47, 48].

The movements between metal sheets and FRP sheets should also be noted as significant factors affecting the laminate deformability. Out-of-plane bending is one of the deformation mechanisms in forming metal-composite laminates and the bending performance depends on the types of metal and FRP materials, as well as on the inter-ply interaction of sliding and through-the-thickness behaviour like transverse flow.

The bending behaviour for sheet metal forming has been well illustrated in the literature [49, 50], but the bending of a FRP sheet seems to be less important due to the fact that the bending resistance is usually orders of magnitude lower than the intra-ply shear resistance for uncured polymers [51]. Inter-ply sliding is also one of the deformation mechanisms for the bending of metal-composite laminates, especially for the forming of single-curved parts. The relative movement at the metal-composite interfaces contributes to the reduction of wrinkles at the inner metal layer and cracks at the outer metal layer of a laminate [52, 53]. Transverse flow is another important factor affecting the deformation during bending, particularly for hybrid laminates with UD fibre reinforced polymers oriented parallel to the bend line at elevated temperatures. The uneven pressure applied on the metal surface induces thickness variations by allowing the polymers to flow in transverse direction. Furthermore, the resin flow parallel to the fibre direction is hindered by high friction force (large contact areas), which makes transverse flow become much easier. Therefore, the fibres tend to move sideways with the polymer when flow occurs in a direction off-axis to the fibre orientation [54].

1.4. DEFORMATION DEFECTS

As the above-mentioned deformation mechanisms affect the deformability of metal-composite laminates, there are some deformation defects like spring-back, wrinkling, cracking, thickness variation as well as delamination, that limit the formability of the hybrid materials. These defects are the results of interaction of factors including laminate structure, component geometry and process parameters like speed, pressure, temperature, etc. Schematic graphs of some deformation defects are presented in Figure 1.7.

The concept of spring-back comes as a consequence of elastic strain recovery after the removal of forming loads. During sheet metal forming, the spring-back is inevitable and common in each stage where the metal sheet undergoes plastic deformation. The spring-back behaviour of metal-composite laminates is complex where the anisotropic elastic recovery of FRP should be taken into account at the same time [55, 56].

Wrinkling is another common defect that occurs in sheet metal forming process, especially in the wall or flange regions of the component. The wrinkles are caused by compressive stresses, and can be prevented if the forming strategy and formed components are designed properly [57]. Wrinkling is related to metal sheet where a thickness increase helps to postpone such phenomenon, which is also true for cured hybrid laminates. However, the FRP layers have limited influences on the wrinkling of the thin metal

layers in case of uncured hybrid laminates. For the FRP layers with woven fabrics, angle locking with rapid increase of shear stress results in (fibre) wrinkling [58, 59]. Besides, also the lack of inter-ply sliding will induce wrinkles and cracks at the inner and outer layers of a laminate, respectively [60].

Despite the fact that the metal sheets usually have a higher failure limit than the composite layers, the cracks of metal sheets often occur due to the high local strains induced by delamination, fibre failure, etc. When the laminate or some layers are cracked, the material has failed and the mechanical performance is jeopardised [61, 62].

Moreover, the hybrid laminated structure has a complex multi-interface system with fibre-matrix and metal-matrix interface. Delamination is usually one of the failure modes for the cured laminates, and it may occur at different interfaces coupled with thickness variation and matrix percolation for the uncured laminates. The resistance of delamination can be measured using the interlaminar fracture toughness testing [63], and the damage caused due to the growth of delamination results in the decrease of strength, toughness and fatigue [64, 65].

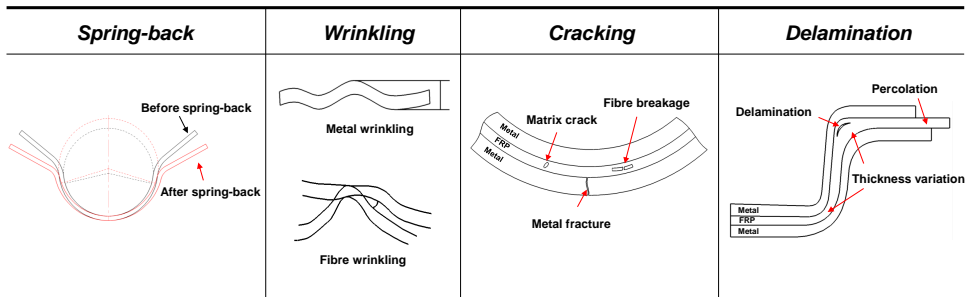


Figure 1.7: Primary deformation defects for metal-composite laminates during forming

1.5. PRESS FORMING OF UNCURED LAMINATES

The forming process of metal-composite laminates focuses on the epoxy-based hybrid materials under low temperature conditions. In order to improve the formability of such laminates, a press forming cycle is proposed and the processing temperature-time profile of the cycle is shown in Figure 1.8. The press forming cycle consists of a laminate preparing and preheating process, forming of uncured laminate, consolidation and (partial) curing under pressure in a same mould and the cooling and removal of the component. The most critical stage is in the forming cycle which requires a proper control of the different deformation mechanisms in different layers. During the preheating stage, temperature and time needs to be carefully controlled so that the inter-ply sliding at the metal-prepreg interfaces and the intra-ply shear within the prepregs are greatly enhanced when the resin viscosity decreases [66, 67]. Then, the still uncured laminate is formed and cured in subsequent stages, avoiding a separate curing process and an extra curing, which can be time-saving and cost-saving [68]. This method contributes to a better formability of metal-composite laminates based on the utilisation of deformation mechanisms for both material layers and the optimisation of processing parameters in a press forming cycle. For example, the metal sheets are usually deformed into three-

dimensional shapes by bending and in-plane plastic deformation, while the deformation of fibre reinforced prepreg is always achieved by inter-ply sliding in-between the layers and intra-ply shear within the layers. All these mechanisms need to be combined and considered in the proposed press forming cycle. In addition, the processing parameters such as preheating temperature and time, curing pressure and time, etc should also be studied and optimised for the press forming of uncured laminates.

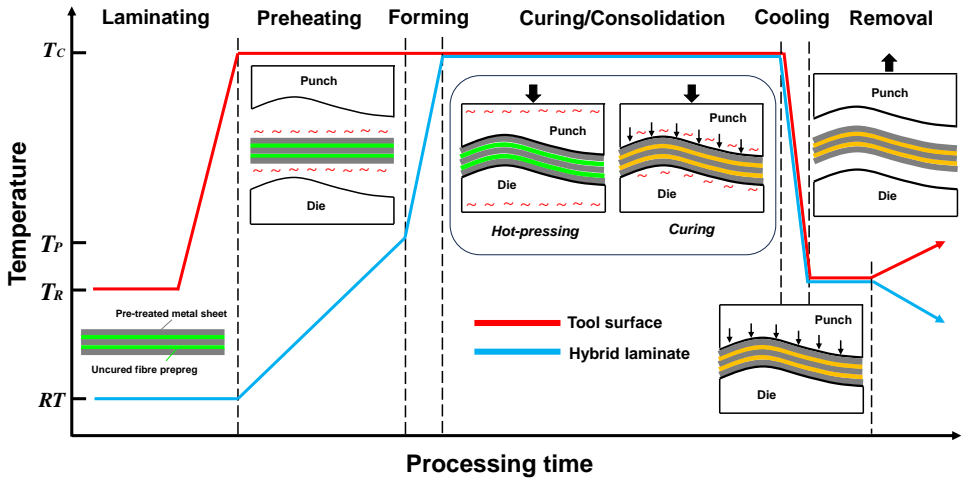


Figure 1.8: Processing temperature and time profile of the tool surface and uncured hybrid laminate in a press forming cycle

1.6. RESEARCH GOAL AND SCOPE

During press forming process of the uncured metal-composite laminates as shown in Figure 1.8, the goal is a high-quality deformation of the component into a desired shape without defects and failures. The uncured laminate deformation occurs in a narrow timeslot between the preheating stage and the curing/consolidation stage, and it is expected that multiple deformation mechanisms play a significant role during forming. Therefore, it should become clear how the application of preheating, subsequent forming and curing affect the deformability of the uncured laminate. In addition, the role of individual layers in a complex multi-interface system in an uncured hybrid laminate remains to be explored. To this end, the material constituents, laminate structures and process parameters need to be selected and optimised.

Therefore, the thesis aims at evaluating the deformation mechanisms and defects for the uncured epoxy-based metal-composite laminates applying corresponding testing methods. The research gaps are covered by the following research questions:

- How to analyse and characterise the mechanisms and defects in non-coherent deformations ?
- What roles have the individual layers of metal sheet and uncured fibre prepreg play

during forming?

- Which factors influence the simultaneous deformation of uncured laminates and how do they correlate?

By answering the above questions, we can have a clear formability assessment of the uncured metal-composite laminate during the proposed press forming process. These achievements enhance the understanding of material selection, process design and parameter optimisation for the hybrid laminates. As mentioned in the previous literature, forming behaviour for such materials is quite complex and most studies focus on the forming process of the cured laminates. Therefore, it is meaningful to contribute this effort in the forming of uncured laminates.

The method to address these questions is based on the experimental analysis and characterisation with the measurement and digital microscopy techniques to study the evolution of the sliding surface, fibre orientation and cross-section thickness. Then, the numerical modelling method is proposed to validate the test results and help to support the understanding of the deformation behaviour of uncured hybrid laminates.

1.7. THESIS OUTLINE

The outline of the thesis is planned as a series of investigations following the deformation mechanisms of the proposed press forming cycle (Figure 1.8), which is schematically described in Figure 1.9. The stages of the process which are relevant to each chapter are indicated in this figure.

The inter-ply sliding behaviour of uncured metal-composite laminates is investigated in Chapter 2. An inter-ply friction model at the metal-prepreg interfaces is developed and by using the model, the optimised conditions for proper sliding can be determined. Such model involving the influence of various process parameters can be incorporated into a finite element simulation.

In Chapter 3, the intra-ply shear properties of uncured hybrid laminates are characterised and the effect of metal sheet layers on the shear deformability of the prepreg layer is investigated. The results are compared with theoretical pin-jointed net (PjN) method and the shear angle evolution of the prepreg system coupled with the corresponding uncured metal-composite laminates are analysed.

In Chapter 4, the flexural behaviour of uncured metal-CFRP laminates is investigated and the role of clamping pressure on the bending properties is discussed. Experimental tests and finite element simulations are proposed to compare and validate the results. In addition, the final shape of the bent materials is evaluated.

The previous chapters focused on deformation mechanisms which may encounter after the preheating stage on two-dimensional levels. In Chapter 5, a valuable complementary study on the effect of spring-back for the final shape of the formed component after curing stage is outlined. Two processing conditions of full-cured and partially-cured after press forming are performed and the spring-back ratio is calculated. The parameters including laminate structure, temperature, time and pressure are evaluated on their effect of cure-dependent spring-back as those effects are interrelated.

In Chapter 6, the simultaneous deformation during the forming stage of a dome part

is analysed and validated through numerical simulation. The effect of material constituent, fibre orientation, clamping force as well as inter-ply friction are investigated and combined to explore which factors are the most important and how they affect the final shape of the component.

Finally, Chapter 7 summarizes the main conclusions of the thesis and offers some suggestions for future work.

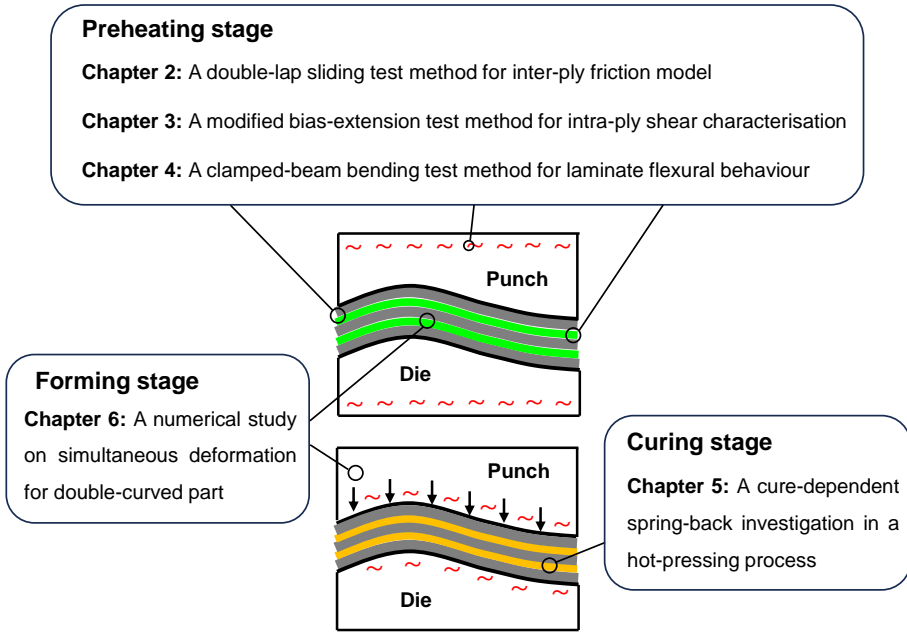


Figure 1.9: Schematic description of the research outline of the PhD thesis

REFERENCES

- [1] A. Asundi and A. Y. Choi, "fibre metal laminates: An advanced material for future aircraft," *Journal of Materials Processing Technology*, vol. 63, no. 1, pp. 384–394, 1997.
- [2] L. Vogelesang and A. Vlot, "Development of fibre metal laminates for advanced aerospace structures," *Journal of Materials Processing Technology*, vol. 103, no. 1, pp. 1–5, 2000.
- [3] E. C. Botelho, R. A. Silva, L. C. Pardini, and M. C. Rezende, "A review on the development and properties of continuous fibre/epoxy/aluminum hybrid composites for aircraft structures," *Materials Research*, vol. 9, pp. 247–256, 2006.
- [4] T. Sinmazçelik, E. Avcu, M. Özgür Bora, and O. Çoban, "A review: Fibre metal laminates, background, bonding types and applied test methods," *Materials & Design*, vol. 32, no. 7, pp. 3671–3685, 2011.

- [5] J. Sinke, "Manufacturing of glare parts and structures," *Applied composite materials*, vol. 10, pp. 293–305, 2003.
- [6] D. Nardi, M. Abouhamzeh, R. Leonard, and J. Sinke, "Investigation of kink induced defect in aluminium sheets for glare manufacturing," *Composites Part A: Applied Science and Manufacturing*, vol. 125, p. 105531, 2019.
- [7] T. de Jong, *Forming of Laminates*. PhD thesis, Delft University of Technology, 2006.
- [8] L. Vogelesang and J. Gunnink, "Arall: A materials challenge for the next generation of aircraft," *Materials & Design*, vol. 7, no. 6, pp. 287–300, 1986.
- [9] M. Sasso, E. Mancini, G. Dhaliwal, G. Newaz, and D. Amodio, "Investigation of the mechanical behaviour of carall fml at high strain rate," *Composite Structures*, vol. 222, p. 110922, 2019.
- [10] M. E. Kazemi, L. Shanmugam, L. Yang, and J. Yang, "A review on the hybrid titanium composite laminates (htcls) with focuses on surface treatments, fabrications, and mechanical properties," *Composites Part A: Applied Science and Manufacturing*, vol. 128, p. 105679, 2020.
- [11] P. Boisse, J. Colmars, N. Hamila, N. Naouar, and Q. Steer, "Bending and wrinkling of composite fibre preforms and prepregs. a review and new developments in the draping simulations," *Composites Part B: Engineering*, vol. 141, pp. 234–249, 2018.
- [12] J.-Y. Kim, Y.-T. Hwang, J.-H. Baek, W.-Y. Song, and H.-S. Kim, "Study on inter-ply friction between woven and unidirectional prepregs and its effect on the composite forming process," *Composite Structures*, vol. 267, p. 113888, 2021.
- [13] R. Lokesh, V. Jagadesh, and S. Suresh, "Mechanical and low velocity impact behaviour of al based kevlar fabric reinforced epoxy laminate," *International Journal of Applied Engineering Research*, vol. 16, no. 8, pp. 660–669, 2021.
- [14] Y. Yang, R. Boom, B. Irion, D.-J. Van Heerden, P. Kuiper, and H. De Wit, "Recycling of composite materials," *Chemical Engineering and Processing: Process Intensification*, vol. 51, pp. 53–68, 2012.
- [15] R. Santiago, W. Cantwell, and M. Alves, "Impact on thermoplastic fibre-metal laminates: Experimental observations," *Composite structures*, vol. 159, pp. 800–817, 2017.
- [16] D. Mamalis, W. Obande, V. Koutsos, J. R. Blackford, C. M. Ó. Brádaigh, and D. Ray, "Novel thermoplastic fibre-metal laminates manufactured by vacuum resin infusion: the effect of surface treatments on interfacial bonding," *Materials & Design*, vol. 162, pp. 331–344, 2019.
- [17] Z. Ding, H. Wang, J. Luo, and N. Li, "A review on forming technologies of fibre metal laminates," *International Journal of Lightweight Materials and Manufacture*, vol. 4, no. 1, pp. 110–126, 2021.

- [18] T. Trzepieciński, S. M. Najm, M. Sbayti, H. Belhadjsalah, M. Szpunar, and H. G. Lemu, "New advances and future possibilities in forming technology of hybrid metal–polymer composites used in aerospace applications," *Journal of Composites Science*, vol. 5, no. 8, p. 217, 2021.
- [19] A. Sexton, W. Cantwell, and S. Kalyanasundaram, "Stretch forming studies on a fibre metal laminate based on a self-reinforcing polypropylene composite," *Composite Structures*, vol. 94, no. 2, pp. 431–437, 2012.
- [20] C. Russig, M. Bambach, G. Hirt, and N. Holtmann, "Shot peen forming of fibre metal laminates on the example of glare®," *International journal of material forming*, vol. 7, pp. 425–438, 2014.
- [21] A. Gisario and M. Barletta, "Laser forming of glass laminate aluminium reinforced epoxy (glare): On the role of mechanical, physical and chemical interactions in the multi-layers material," *Optics and Lasers in Engineering*, vol. 110, pp. 364–376, 2018.
- [22] S. Black, "fibre-metal laminates in the spotlight," *Composites World*, vol. 12, 2019.
- [23] K. Osakada, K. Mori, T. Altan, and P. Groche, "Mechanical servo press technology for metal forming," *CIRP annals*, vol. 60, no. 2, pp. 651–672, 2011.
- [24] A. C. Long, *Composites forming technologies*. Elsevier, 2014.
- [25] P. Harrison, R. Gomes, and N. Curado-Correia, "Press forming a 0/90 cross-ply advanced thermoplastic composite using the double-dome benchmark geometry," *Composites Part A: Applied Science and Manufacturing*, vol. 54, pp. 56–69, 2013.
- [26] L. Mosse, P. Compston, W. J. Cantwell, M. Cardew-Hall, and S. Kalyanasundaram, "The effect of process temperature on the formability of polypropylene based fibre–metal laminates," *Composites Part A: Applied Science and Manufacturing*, vol. 36, no. 8, pp. 1158–1166, 2005.
- [27] J. Dau, C. Lauter, U. Damerow, W. Homberg, and T. Tröster, "Multi-material systems for tailored automotive structural components," in *Proceedings of the 18th International Conference on Composite Materials, Jeju Island, Korea*, pp. 21–26, 2011.
- [28] E. Sherkatghanad, L. Lang, S. Liu, and Y. Wang, "Innovative approach to mass production of fibre metal laminate sheets," *Materials and manufacturing processes*, vol. 33, no. 5, pp. 552–563, 2018.
- [29] A. Saadatfard, M. Gerdooei, and A. Jalali Aghchai, "Drawing potential of fibre metal laminates in hydromechanical forming: a numerical and experimental study," *Journal of Sandwich Structures & Materials*, vol. 22, no. 5, pp. 1386–1403, 2020.
- [30] D. Chernikov, Y. Erisov, I. Petrov, S. Alexandrov, and L. Lang, "Research of different processes for forming fibre metal laminates," *International Journal of Automotive Technology*, vol. 20, pp. 89–93, 2019.

- [31] J. Dau, C. Lauter, U. Damerow, W. Homberg, and T. Tröster, "Multi-material systems for tailored automotive structural components," in *Proceedings of the 18th International Conference on Composite Materials, Jeju Island, Korea*, pp. 21–26, 2011.
- [32] R. Zafar, L. Lang, and R. Zhang, "Experimental and numerical evaluation of multi-layer sheet forming process parameters for light weight structures using innovative methodology," *International Journal of Material Forming*, vol. 9, no. 1, pp. 35–47, 2016.
- [33] S. Kalyanasundaram, S. DharMalingam, S. Venkatesan, and A. Sexton, "Effect of process parameters during forming of self reinforced-pp based fibre metal laminate," *Composite Structures*, vol. 97, pp. 332–337, 2013.
- [34] J. Nam, W. Cantwell, R. Das, A. Lowe, and S. Kalyanasundaram, "Deformation behaviour of steel/srpp fibre metal laminate characterised by evolution of surface strains," *Advances in aircraft and spacecraft science*, vol. 3, no. 1, p. 061, 2016.
- [35] V. Zal, H. M. Naeni, A. R. Bahramian, and J. Sinke, "Investigation of the effect of temperature and layup on the press forming of polyvinyl chloride-based composite laminates and fibre metal laminates," *The International Journal of Advanced Manufacturing Technology*, vol. 89, pp. 207–217, 2017.
- [36] M. Lee, S. Kim, O. Lim, and C. Kang, "The effect process parameters on epoxy flow behaviour and formability with cr340/cfrp composites by different laminating in deep drawing process," *Journal of Materials Processing Technology*, vol. 229, pp. 275–285, 2016.
- [37] S. Liu, L. Lang, E. Sherkatghanad, Y. Wang, and W. Xu, "Investigation into the fibre orientation effect on the formability of glare materials in the stamp forming process," *Applied Composite Materials*, vol. 25, pp. 255–267, 2018.
- [38] B. Bernd-Arno, H. Sven, G. Nenad, M.-C. Moritz, W. Tim, and N. André, "Forming and joining of carbon-fibre-reinforced thermoplastics and sheet metal in one step," *Procedia Engineering*, vol. 183, pp. 227–232, 2017.
- [39] Y. Guo, C. Zhai, F. Li, X. Zhu, F. Xu, and X. Wu, "Formability, defects and strengthening effect of steel/cfrp structures fabricated by using the differential temperature forming process," *Composite Structures*, vol. 216, pp. 32–38, 2019.
- [40] T. Mennecart, H. Werner, N. Ben Khalifa, and K. A. Weidenmann, "Developments and analyses of alternative processes for the manufacturing of fibre metal laminates," in *International Manufacturing Science and Engineering Conference*, vol. 51364, American Society of Mechanical Engineers, 2018.
- [41] S. Suttner and M. Merklein, "A new approach for the determination of the linear elastic modulus from uniaxial tensile tests of sheet metals," *Journal of Materials Processing Technology*, vol. 241, pp. 64–72, 2017.

- [42] Z. Marciniak and K. Kuczyński, "Limit strains in the processes of stretch-forming sheet metal," *International journal of mechanical sciences*, vol. 9, no. 9, pp. 609–620, 1967.
- [43] T. B. Stoughton, "A general forming limit criterion for sheet metal forming," *International Journal of Mechanical Sciences*, vol. 42, no. 1, pp. 1–27, 2000.
- [44] A. Hannon and P. Tiernan, "A review of planar biaxial tensile test systems for sheet metal," *Journal of materials processing technology*, vol. 198, no. 1-3, pp. 1–13, 2008.
- [45] Q. Chen, P. Boisse, C. H. Park, A. Saouab, and J. Bréard, "Intra/inter-ply shear behaviours of continuous fibre reinforced thermoplastic composites in thermoforming processes," *Composite structures*, vol. 93, no. 7, pp. 1692–1703, 2011.
- [46] Y. Zhang, F. Sun, Y. Wang, L. Chen, and N. Pan, "Study on intra/inter-ply shear deformation of three dimensional woven preforms for composite materials," *Materials & Design*, vol. 49, pp. 151–159, 2013.
- [47] K. Potter, "In-plane and out-of-plane deformation properties of unidirectional preimpregnated reinforcement," *Composites Part A: Applied Science and Manufacturing*, vol. 33, no. 11, pp. 1469–1477, 2002.
- [48] Y. Larberg and M. Åkermo, "In-plane deformation of multi-layered unidirectional thermoset prepreg—modelling and experimental verification," *Composites Part A: Applied Science and Manufacturing*, vol. 56, pp. 203–212, 2014.
- [49] J.-K. Kim and T.-X. Yu, "Forming and failure behaviour of coated, laminated and sandwiched sheet metals: a review," *Journal of Materials Processing Technology*, vol. 63, no. 1-3, pp. 33–42, 1997.
- [50] S. Thuillier, N. Le Maoût, and P.-Y. Manach, "Influence of ductile damage on the bending behaviour of aluminium alloy thin sheets," *Materials & Design*, vol. 32, no. 4, pp. 2049–2057, 2011.
- [51] A. Long and M. Clifford, "Composite forming mechanisms and materials characterisation," *Composites forming technologies*, pp. 1–21, 2007.
- [52] V. Zal, H. M. Naeini, J. Sinke, A. R. Bahramian, M. Abouhamzeh, and R. Benedictus, "A new procedure for finite element simulation of forming process of non-homogeneous composite laminates and fmls," *Composite Structures*, vol. 163, pp. 444–453, 2017.
- [53] Z. Liu, E. Simonetto, A. Ghiotti, and S. Bruschi, "Inter-ply friction behaviour in the temperature assisted forming of magnesium/glass fibre reinforced thermoplastic polymer laminates," *Composites Part A: Applied Science and Manufacturing*, p. 107635, 2023.
- [54] J. Barnes and F. Cogswell, "Transverse flow processes in continuous fibre-reinforced thermoplastic composites," *Composites*, vol. 20, no. 1, pp. 38–42, 1989.

- [55] S. Y. Kim, W. J. Choi, and S. Y. Park, "Spring-back characteristics of fibre metal laminate (glare) in brake forming process," *The International Journal of Advanced Manufacturing Technology*, vol. 32, pp. 445–451, 2007.
- [56] M. Fiorina, A. Seman, B. Castanié, K. Ali, C. Schwob, and L. Mezeix, "Spring-in prediction for carbon/epoxy aerospace composite structure," *Composite Structures*, vol. 168, pp. 739–745, 2017.
- [57] X. Wang and J. Cao, "On the prediction of side-wall wrinkling in sheet metal forming processes," *International Journal of Mechanical Sciences*, vol. 42, no. 12, pp. 2369–2394, 2000.
- [58] J. Cao, R. Akkerman, P. Boisse, J. Chen, H. Cheng, E. De Graaf, J. Gorczyca, P. Harrison, G. Hivet, J. Launay, *et al.*, "Characterization of mechanical behaviour of woven fabrics: Experimental methods and benchmark results," *Composites Part A: Applied Science and Manufacturing*, vol. 39, no. 6, pp. 1037–1053, 2008.
- [59] M. Khan, C. Pasco, N. Reynolds, and K. Kendall, "Shear deformability characteristics of a rapid-cure woven prepreg fabric," *International Journal of Material Forming*, vol. 14, pp. 133–142, 2021.
- [60] P. Boisse, N. Hamila, E. Vidal-Sallé, and F. Dumont, "Simulation of wrinkling during textile composite reinforcement forming. influence of tensile, in-plane shear and bending stiffnesses," *Composites Science and Technology*, vol. 71, no. 5, pp. 683–692, 2011.
- [61] G. Reyes and H. Kang, "Mechanical behaviour of lightweight thermoplastic fibre-metal laminates," *Journal of materials processing technology*, vol. 186, no. 1-3, pp. 284–290, 2007.
- [62] M. Ostapiuk, J. Bieniaś, and B. Surowska, "Analysis of the bending and failure of fibre metal laminates based on glass and carbon fibres," *Science and Engineering of Composite Materials*, vol. 25, no. 6, pp. 1095–1106, 2018.
- [63] J. Bieniaś, K. Dadej, and B. Surowska, "Interlaminar fracture toughness of glass and carbon reinforced multidirectional fibre metal laminates," *Engineering Fracture Mechanics*, vol. 175, pp. 127–145, 2017.
- [64] S. Khan, R. Alderliesten, and R. Benedictus, "Delamination growth in fibre metal laminates under variable amplitude loading," *Composites Science and Technology*, vol. 69, no. 15-16, pp. 2604–2615, 2009.
- [65] K. Jin, K. Chen, X. Luo, and J. Tao, "Fatigue crack growth and delamination mechanisms of ti/cfrp fibre metal laminates at high temperatures," *Fatigue & Fracture of Engineering Materials & Structures*, vol. 43, no. 6, pp. 1115–1125, 2020.
- [66] A. Rashidi, H. Montazerian, K. Yesilcimen, and A. Milani, "Experimental characterization of the inter-ply shear behaviour of dry and prepreg woven fabrics: Significance of mixed lubrication mode during thermoset composites processing," *Composites Part A: Applied Science and Manufacturing*, vol. 129, p. 105725, 2020.

- [67] S. Erland and T. Dodwell, "Quantifying inter-and intra-ply shear in the deformation of uncured composite laminates," *Advanced Manufacturing: Polymer & Composites Science*, vol. 7, no. 2, pp. 25–35, 2021.
- [68] L. Shichen, L. Lihui, and G. Shiwei, "An investigation into the formability and processes of glare materials using hydro-bulging test," *International Journal of Precision Engineering and Manufacturing*, vol. 20, pp. 121–128, 2019.

2

A DOUBLE-LAP SLIDING TEST METHOD FOR AN INTER-PLY FRICTION MODEL

Forming with pre-stacked and uncured epoxy-based metal-composite laminates offers improved deformability compared to full-cured hybrid laminates especially for the production of complex structural components. In this chapter, the inter-ply friction behaviour at the metal-prepreg interface of glass fibre reinforced aluminium laminate is investigated through a double-lap sliding test setup. The effect of sliding velocity, normal force, fibre orientation and resin viscosity coupled with temperature on static and kinetic friction coefficients are studied. The kinetic friction behavior in the transition region between mixed and hydrodynamic lubrication, shows a good agreement with the Stribeck-curve theory. While for the static friction, a modified Coulomb friction model is found to fit the experimental results. These models are translated into a phenomenological inter-ply friction model which is incorporated into Abaqus/Explicit as a user-defined friction subroutine for verification. The findings contribute to the development of the forming process with uncured metal-composite laminates.

This chapter has been published in: Liu S, Sinke J, Dransfeld C. An inter-ply friction model for thermoset based fibre metal laminate in a hot-pressing process. Composites Part B, 109400, 227, (2021).

2.1. INTRODUCTION

METAL-composite laminates are the type of lightweight composite materials made by alternating layers of fibre reinforced polymers and thin metal sheets. The hybrid structure achieves superior properties over its constituents, especially in fatigue resistance and corrosion [1]. For the epoxy-based metal-composite laminate such as glass fibre reinforced aluminium laminate (GLARE), the matrix obtains its properties through a cross-linking process, also referred to as curing. This cross-linking mechanism is irreversible and usually performed in autoclaves to apply the required temperatures and pressures [2]. However, the latest development in resin pre-treatment technology has made it possible to deform such hybrid laminate with epoxy prepregs, instead of autoclaving, offering relatively short cycle times while retaining the exceptional mechanical performance as the autoclaved laminate [3].

The forming process of epoxy-based metal-composite laminates as shown in Figure 1.8, aims at preforming an initial flat blank into a final 3D shape. The forming cycle involves preheating the pre-stacked laminate prior to the curing stage thereby decreasing the resin viscosity and increasing the ease of deformation, in particular inter-ply friction. Temperature and time are two critical factors that need to be carefully controlled as the initiation of resin cure would increase the stiffness of the prepreg and hamper the laminate from deforming. Preforming an initial flat blank requires the laminate that deforms following the desired shape in a predictable and repeatable way without the occurrence of fracture, wrinkles and other possible defects [4]. This method is achieved by allowing the individual layers to deform by intra-ply shear within the prepreg and inter-ply sliding in-between the metal sheets and prepreg layers. The latter mechanism is the focus of this chapter.

2.2. LITERATURE ON INTER-PLY FRICTION

MOST of the recent papers on the frictional properties of thermoset materials are limited to the unidirectional reinforcements and woven fabrics without metal sheet layers. These studies showed that processing parameters like temperature, sliding rate and normal force greatly affect the degree of sliding deformation within and in-between the layers [5–8]. Martin et al. [9] focused on the frictional resistance of woven thermoset prepregs and proposed that the friction coefficient depends on the prepreg system and temperature, and that prepreg with a lower viscosity and high amount of resin at the sliding surface exhibited lower frictional resistance. Dutta et al. [10] investigated the frictional properties of a unidirectional carbon/epoxy prepreg and found that fibre orientation greatly affects the friction coefficient at the prepreg-prepreg interfaces. The interfaces where 0° and 45° prepreg layers contact each other show the highest inter-ply friction while $0^\circ/0^\circ$ interfaces exhibit friction values similar or lower than $0^\circ/90^\circ$ interfaces. Therefore, resin rheology, fibre architecture and fibre orientation significantly influence the inter-ply friction coefficient for the thermoset polymers. In addition, the evaluations of tool-ply friction behaviours during composite forming are also crucial and the parameters like normal pressure, laminate temperature, tool temperature, atmosphere temperature and laminate orientation were found to affect friction coefficient between the metal tool and composite laminates [11], [12].

Generally, there exist two main methods in the simulation of the forming process for composite laminates. For the micromechanical approach: all the components of composite layers are modelled consisting of fibres and matrix. This method is supposed to be more realistic while it requires partitioning the model into small pieces, making the simulation complex and time-consuming [13]. The meso-level approach regards the composite layers as a homogeneous and continuum material which can be discretised into shell or solid elements. Usually the adhesive region between the adjacent layers is simulated by using a cohesive layer with zero thickness [14, 15]. This method is preferred to analyse damage problems like fracture and delamination by adopting a softening relationship between traction and separation based on cohesive law. However, the inter-ply sliding deformation is unable to be characterised using the cohesive zone modelling as the interfaces are loaded with high shear stresses. Also, the material parameters for cohesive elements are difficult to obtain and not suitable to fit in the applied processing conditions. Therefore, a frictional contact model applied at the interfaces can be a simple alternative method when considering relative motions of individual plies [16].

In previous frictional models for composite laminates, most researchers performing the forming simulations assume a constant friction coefficient at the tool-ply and ply-ply interfaces due to the lack of friction data [17, 18]. However, studies discovered that the friction coefficient is greatly affected by the reaction force of the tool as well as the formability and stress-strain relations on the laminate throughout the duration of the forming process. Fetfatsidis et al. [19] studied a hemisphere stamping simulation on woven fabric composites and found that the punch force is more than halved when using a friction coefficient of 0.1 versus the conventional 0.3. Mosse et al. [20] developed a finite element model for simulating the stamp forming process of thermoplastic based fibre metal laminate materials. He compared a friction coefficient of zero similar to stamping at high temperatures where the layers can slide over each other and a very high friction coefficient of 100, corresponding to fully coupled layers at low temperatures. The results indicated that the coupled layers result in higher strains accompanied with wrinkling in a critical corner region whereas the friction-less model had a more accurate representation of the experimental surface topology and strain features. The determination of friction phenomenon plays a significant role in establishing the frictional contact model for the finite element forming simulations.

2.3. THEORY OF FRICTION MODELS

THE friction models of two surfaces in contact generally consist of two mechanisms. If no fluid separates the interface, the friction is governed by the force normal to the dry surface which is usually described as Coulomb friction. The Coulomb coefficient of friction μ can be written as [21]:

$$\mu = F/N \quad (2.1)$$

where F is the pull-out force and N is the normal force. The equation is used by many scholars in determining the friction coefficient at the metal-polymer interfaces [22, 23]. However, Ajayi [24] studied the Coulomb friction coefficients for cotton and wool fabrics under two different surfaces at room temperature. He found that with the increasing number of test samples, the coefficient of Coulomb friction decreases due to the fabric

structures. The effective contact surface influences the friction and the increasing sliding velocity exhibited no consistent change in the friction coefficient. In addition, he noted that the relationship between normal force and friction force can be described as:

$$F = k \cdot N^n \quad (2.2)$$

where F is the friction force, N is the normal force, k and n are the friction constant and index which can be determined from experimental tests in a regression analysis.

Besides the Coulomb friction which occurs between dry surfaces, purely hydrodynamic friction exists when two surfaces in relative motion are completely separated by a fluid film. In this case the friction can be predicted in terms of the traction force acting on the film, ignoring the effect of surface roughness on the friction [25]. The hydrodynamic friction is independent of the normal force under steady load conditions, but depending on resin viscosity and shear rate as shown:

$$\tau = \eta \cdot \dot{\gamma} \quad (2.3)$$

where η is the matrix viscosity, $\dot{\gamma}$ and τ are the shear rate and shear stress, respectively. In addition, Wilks [26] designed a friction test that pulls a thin metal sheet from two pre-consolidated fibre-glass-polypropylene sheets where the normal force is applied by springs. He analysed that the shear stress is influenced by many processing parameters and established a friction model considering both Coulomb friction and hydrodynamic friction coefficients:

$$\tau = \mu \cdot P_N + \eta \cdot \dot{\gamma} \quad (2.4)$$

where μ is the coefficient of Coulomb friction, P_N is the normal pressure, η is the matrix viscosity and $\dot{\gamma}$ is the shear rate.

Clifford et al. [27] optimised the Wilks' friction model by adding a term for the effective contact ratio on Coulomb friction by investigating the tool-ply friction interactions. His analytical model considered the the Coulomb friction coupled with the polymer viscosity because of the variation in shear stress with shear rate and temperature,

$$\tau = \varphi \cdot \mu \cdot P_N + \eta \cdot \dot{\gamma} \quad (2.5)$$

where φ is the ratio of dry fibre regions in effective contact to the whole mould surfaces. The Clifford model showed good agreement with experimental results for shear stresses larger than 0.02 MPa.

Stribeck developed a theory to describe different types of friction mechanisms in relation to sliding velocity, bearing pressure and lubricant viscosity in tribology [28, 29]. He identified that at low sliding velocities, surface asperities coming into contact dominate and lead to high friction coefficients (called boundary lubrication), whereas at high velocities the friction is dominated by a hydrodynamic film resulting in low friction coefficients (called hydrodynamic friction). The so called Stribeck-curve which plots the relation of friction coefficient versus Hersey number as shown in Figure 2.1, exhibits the characteristic transition region between boundary, mixed and hydrodynamic lubrication. The Hersey number H , also referred as the Stribeck number, can be interpreted as a normalised sliding velocity and is a function of matrix viscosity η , sliding velocity v , and normal force N , where:

$$H = \frac{\eta \cdot v}{N} \quad (2.6)$$

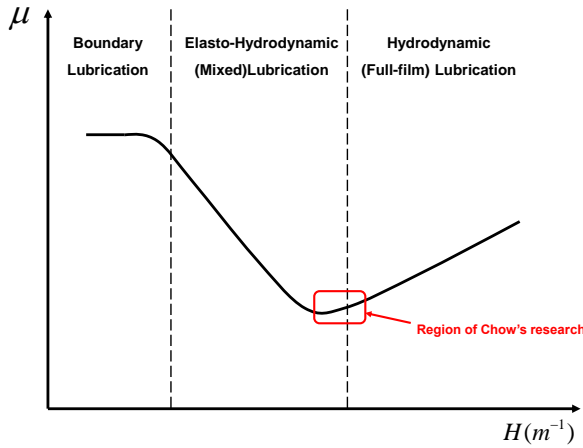


Figure 2.1: Stribeck curve on friction coefficient versus Hersey number, indicating the range of Chow's research [23]

Figure 2.1 demonstrates a theoretical Stribeck curve and shows the three lubrication regimes based on different types of friction (mechanisms). The first region is governed by boundary lubrication where the influence of the fluid film is negligible resulting in the friction similar to the Coulomb friction. The second part is an elasto-hydrodynamic mode friction, which is also referred as mixed lubrication. This mode would gradually transfer into a third hydrodynamic (full-film) region when the lubrication layer becomes thicker. The surfaces in this area are completely separated by a fluid film and the friction coefficient increases as the lubrication layer thickness (viscosity) increases. The curve provides a qualitative explanation of the mechanism affecting the friction coefficient for a range of processing parameters such as normal force, sliding rate, resin viscosity and temperature. This theory is used to study the friction at different composite laminate interfaces as well as the tool-ply interactions [8, 19, 30]. Chow [23] proposed an analytical model for the inter-ply friction on tool-ply surfaces for the glass-polypropylene fabrics. He predicted that the effective friction coefficient that can be used in numerical simulations under different processing values by incorporating the friction models of both Coulomb and hydrodynamic friction. The results illustrated that a corresponding relationship from the Stribeck curve is able to cover the transition of Coulomb and hydrodynamic friction under various test parameters.

A combination of the normal force and sliding velocity in Equation (2.6) can be adjusted to obtain the equal Hersey numbers at a constant viscosity. Consequently, the friction coefficients are expected to be equal in comparable situations with equal Hersey numbers. Since polymer viscosity is dependent on the processing history, a rheological model needs to be established for the calculation of Hersey numbers. At a given temperature, the viscosity for thermosets evolves as a function of the degree of cure. The empirical formula for temperature and degree of cure dependent viscosity model of the thermoset matrices can be expressed as [31, 32]:

$$\eta = \eta_0 \exp\left(\frac{\Delta E_\eta}{RT} + k \cdot \alpha_c\right) \quad (2.7)$$

where η_0 is the initial viscosity, ΔE_η is the viscous activation energy, α_c is the degree of cure, k is a constant, R is the universal gas constant and T is the absolute temperature in Kelvin. Once the test temperature and degree of cure for a certain epoxy thermoset is determined, the viscosity can be obtained using this rheological equation. The relationship between friction coefficient and Hersey number considering viscosity and temperature effects will be discussed further in the section 2.6.

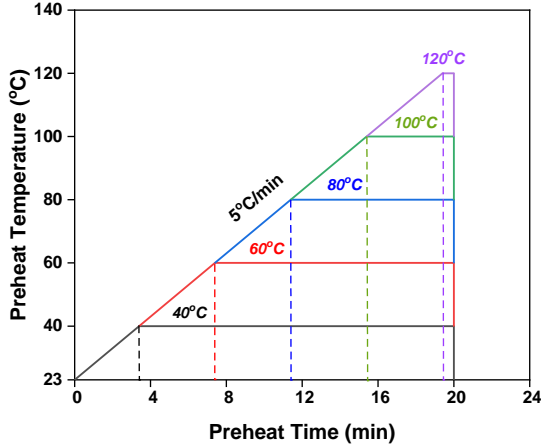


Figure 2.2: Preheat temperature and time cycles for the pre-stacked GLARE materials

2.4. INTER-PLY FRICTION EXPERIMENT

2.4.1. MATERIALS

THE material systems used in this chapter are the aerospace graded metal-composite laminates named as GLARE which are glass fibre reinforced aluminium laminates. Experimental samples consist of three 0.5-mm thick 2024-T3 aluminium sheets by GKN-Fokker and two composite layers of fibre reinforced unidirectional prepreg S2-glass/FM-94 epoxy provided by Solvay. Each composite layer consists of two prepreg plies and the nominal thickness is 0.18 mm for each ply. The unidirectional fibre oriented at 0° direction corresponds with the rolling direction of the aluminium sheet. Prior to assembling, the aluminium surfaces are pre-treated with chromic acid anodising and primed with BR 127 to inhibit corrosion [4] since the surface treatment has a huge impact on the friction. Conventional manufacturing process for GLARE materials is through a standard autoclave cycle with one-hour curing at a maximum temperature of 121°C and an autoclave pressure of 6 bar. In this chapter, the laminate samples are pre-heated following the cycles shown in Figure 2.2. The specimen undergoes an initial heating rate of $5^\circ\text{C}/\text{min}$ to the target temperature and subsequent holding to a total time of 20 minutes. The layup configuration and thickness of pre-stacked laminates are presented in Table 2.1.

2.4.2. SETUPS

CURRENT friction measuring methods consider the effects of normal force, pull-out velocity and temperature, while other factors which are critical in composite forming process such as resin property and fibre orientation have not been taken into account [21–23, 29]. Applying ASTM standard D 1894 as a basis, an inter-ply friction test apparatus and procedure that allowed for testing at various conditions, is designed for the measurement of the friction coefficient at the metal-prepreg interface based on a double lap specimen. The schematic diagram and dimension for the laminate sample is presented in Figure 2.3 and a normal force is applied on top and bottom aluminium sheets by a clamping loadcell (40 mm × 40 mm) using fine thread locking screws as shown in Figure 2.3(c). The force is measured by strain gauges in a wheatstone bridge, which are installed on the central region of the clamping loadcell. Figure 2.4(a) exhibits the calibration test of the normal force and the results shown in Figure 2.5 are used as the reference values for different test temperatures. The apparatus is used in a Zwick-20kN tensile /compression machine with a temperature chamber. The samples are put into the tensile machine and clamped by the loadcell in normal direction shown in Figure 2.4(b). The loadcell along the pull-out direction is fixed and the normal force can be adjusted to selected values through the rotating shaft. The temperature inside the chamber is preset and read by a thermocouple in contact with the aluminium sheet. Other variables such as fibre orientation and sliding velocity are altered by the layup design and manual input.

Table 2.1: Details of layup configuration and thickness of pre-stacked laminates

Structure	Stacking configuration	Total thickness	Schematic graph
GLARE 3/2	Al/[0°/0°]/Al/[0°/0°]/Al	2.2 mm	
	Al/[45°/45°]/Al/[45°/45°]/Al		
	Al/[90°/90°]/Al/[90°/90°]/Al		

The load-displacement relationships under different conditions are measured up to a pull-out displacement of 20 mm which make the inter-ply (0°/0° and 0°/90°) and intra-ply (45°/-45°) deformations significant. For the double-lap friction test in Figure 2.3(a), the middle aluminium sheet is clamped by both top and bottom aluminium sheets where the sliding occurs in four potential interfaces. Therefore, the experimental friction coefficient for the study is written as,

$$\mu = \frac{F}{2 \cdot N} \quad (2.8)$$

where F is the pull-out force obtained from the experiments and N is the set value of the normal force applied by the clamping loadcell. The friction coefficient calculated from Equation 2.8 is extracted from test data until the normal force begins to drop, and at least three samples are tested for each test configuration.

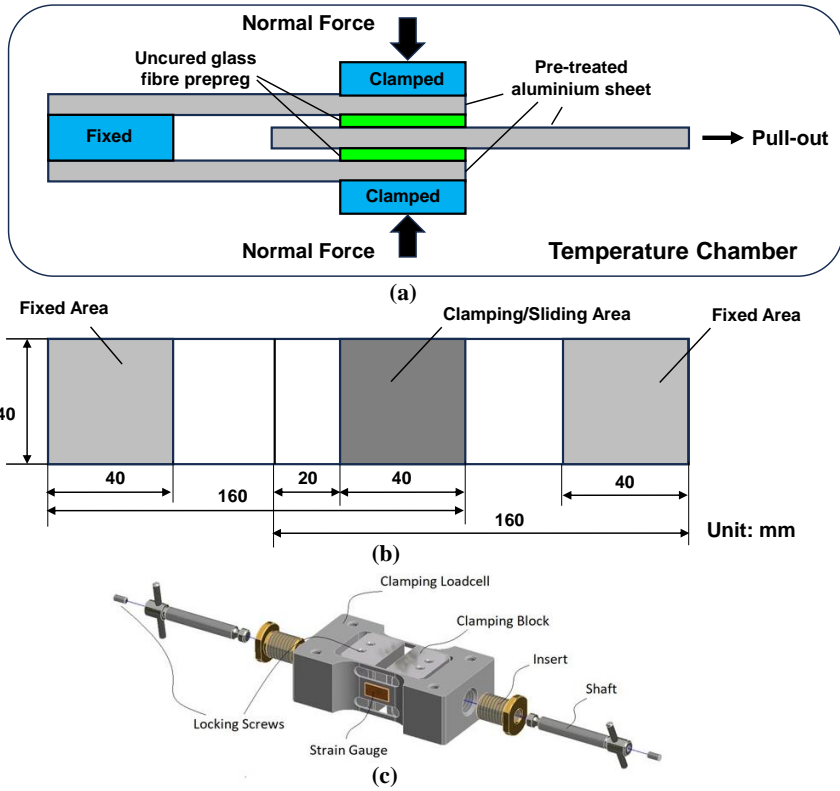


Figure 2.3: (a) Schematic graph and (b) Dimension for the friction test, (c) Details of the clamping loadcell

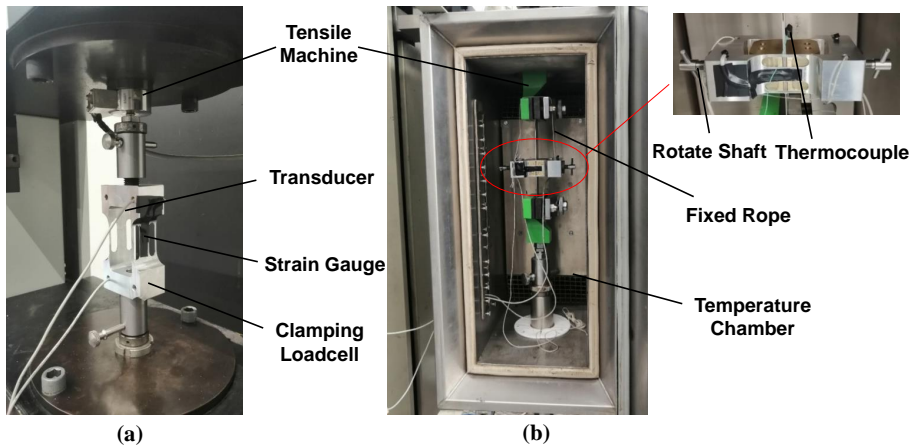


Figure 2.4: Experimental setup and apparatus: (a) Calibration test of normal force; (b) Inter-ply friction test

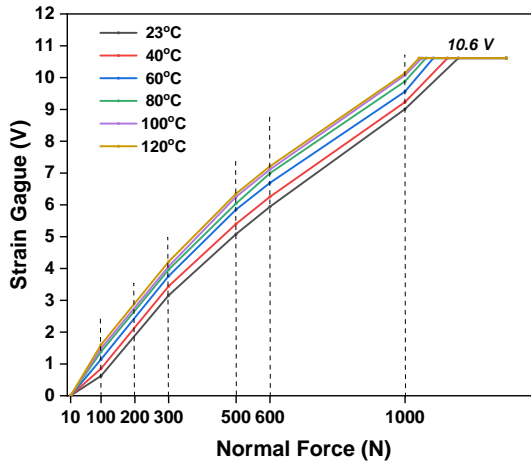


Figure 2.5: Normal force and strain voltage curve under various temperatures for the clamping loadcell

To investigate the effect of various parameters on the friction coefficient at the metal-prepreg interfaces, a set of value ranges are chosen for these parameters. The experiments are conducted varying one or two parameters at a time while keeping other parameters at their baseline value. Table 2.2 lists the parameters investigated for the friction test. These test parameters are chosen to illustrate whether the Stribeck-curve theory corresponds with the experimental results by fitting the relationship of the friction coefficient and Hersey number. It is assumed that equal Hersey numbers derived from the relations of normal force and sliding velocity lead to equal friction coefficients. Therefore, the same two test parameters are selected for each of the nine Hersey numbers (2.3) where the constant viscosity (η_0) for the experimental prepreg is assumed to be around 10^4 Pa·s at room temperature (23°C) [33].

Table 2.2: Test parameters used for inter-ply friction experiments

Parameter	Baseline value	Additional values investigated
Normal force (N)	500	100, 200, 300, 600, 1000
Sliding velocity (mm/min)	10	5, 15, 20, 30, 40
Fibre orientation (°)	0/0	45/45, 90/90
Preheat temperature (°C)	23	40, 60, 80, 100, 120

For fibre-reinforced epoxy FM-94 applied in the experiment, the viscosity is mainly influenced by the temperature and degree of cure. According to Equation 2.7, three modelling parameters should be determined and applied in the viscosity model. From the prior research and model fitting procedure [34–36] the rheokinetic model constants for FM-94 epoxy in Equation 2.7 are given in Table 2.4. Figure 2.6 reveals the predicted cure development of the FM-94 epoxy at different test temperatures including the degree of cure as a function of time and the viscosity evolution. In this chapter, inter-ply friction experiments on pre-stacked fibre metal laminate are conducted at the preheat temperature of 40, 60, 80, 100, 120°C and those temperatures are kept constant for the entire

experiment. Because the whole process consists of an initial heating ramp and subsequent holding at the preheat temperature (Figure 2.2). Viscosity values used in the friction model with a constant preheat time of 20 minutes are calculated by Equation 2.7 shown in Table 2.5. Incorporating the viscosity parameters into Hersey number (Equation 2.6), the relationship between the friction coefficient and Hersey number at various temperatures can be obtained to see if they fit the Stribeck curve.

Table 2.3: Test conditions for Hersey number studied at room temperature of 23°C ($\eta_0 \approx 10^4$ Pa-s)

Sample	Hersey number (m^{-1})	Sliding velocity (mm/min)	Normal force (N)
A-1	1.67E-03	5	500
A-2	1.67E-03	10	1000
B-1	2.78E-03	5	300
B-2	2.78E-03	10	600
C-1	3.33E-03	10	500
C-2	3.33E-03	20	1000
D-1	4.17E-03	5	200
D-2	4.17E-03	15	600
E-1	5.00E-03	15	500
E-2	5.00E-03	30	1000
F-1	6.67E-03	20	500
F-2	6.67E-03	40	1000
G-1	8.33E-03	5	100
G-2	8.33E-03	15	300
H-1	1.67E-02	10	100
H-2	1.67E-02	30	300
I-1	3.33E-02	20	100
I-2	3.33E-02	40	200

Table 2.4: The constants used in the viscosity model (Equation 2.7) for FM-94 epoxy [35, 36]

η_∞ (Pa-s)	ΔE_η (kJ/mol)	k
3.38E-03	36.67	10.44

Table 2.5: Computed viscosity used in the friction models with a constant preheat time of 20 minutes

Temperature (°C)	Degree of cure	Viscosity (Pa-s)
23	0	9997.8
40	0.001	4501.3
60	0.004	1993.1
80	0.008	981.5
100	0.011	518.3
120	0.016	299.2

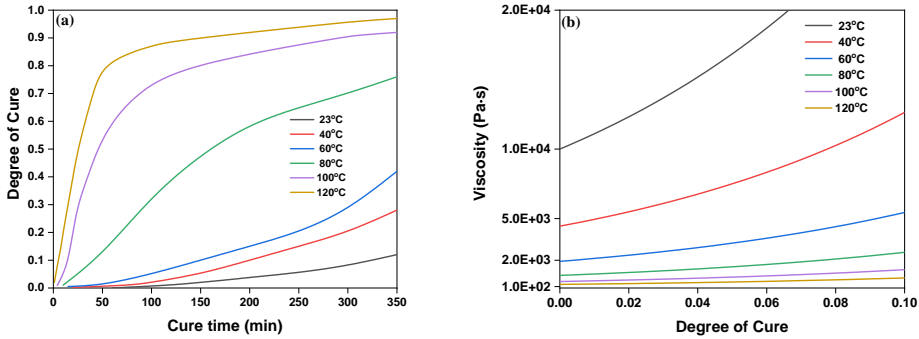


Figure 2.6: Predicted cure evolution of FM-94 epoxy at various temperatures: (a) Degree of cure; (b) Viscosity

2.5. RESULTS AND DISCUSSION

ALL the results for the pull-out force and displacement relationship follow the same general trend sketched in Figure 2.7. Firstly, the laminate samples undergo elastic deformation where the pull-out force increases sharply and reach a peak without movements at the metal-prepreg interfaces. This force corresponds to the static friction force required to initiate sliding between surfaces. After that, the load drops quickly and then reaches a nearly steady sliding corresponding to kinetic friction. This kind of stick-slide phenomenon can be analogous to the Stribeck-curve theory, where the interfaces overcome a boundary condition with high friction, break surface asperities and establish a lubrication layer that leads to the occurrence of kinetic sliding. In Figure 2.7, point A represents the initial static peak force, and the displacement is usually less than 0.5 mm. The displacement at point B for steady sliding is assumed to be 10 mm for all test configurations as the normal force gradually drops after that in the experiment. The pull-out forces at point A and B are used in Equation 2.8 to calculate the values for the static and kinetic friction coefficients, respectively. Based on the test results, the relationship on the friction coefficients and different sliding parameters can be obtained. Then, an initial fitting of the Stribeck curve for the inter-ply friction model is derived.

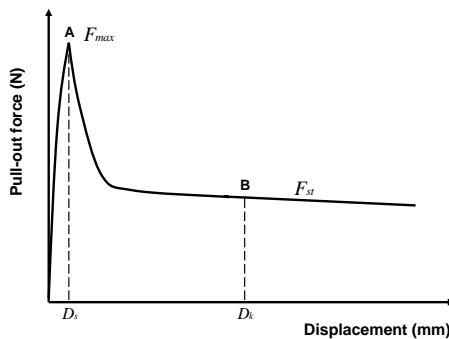


Figure 2.7: Schematic curve of pull-out force and displacement relation for the friction test

2.5.1. EFFECT OF NORMAL FORCE AND SLIDING VELOCITY

FIGURE 2.8 shows the experimental results of the static and kinetic friction coefficients and illustrates the influence of normal force on the inter-ply friction tested at various sliding velocities. For the test values in the figure, two factors, the fibre oriented at $0^\circ/0^\circ$ and the room temperature of 23°C , are kept at the baseline values. It can be seen that both the static and kinetic friction coefficients increase with the increasing sliding velocity and this relationship suggests that friction is characterised by Newtonian shearing of the epoxy matrix where shear stresses increase with the increasing shear rate. In contrast, the friction coefficient decreases with the increasing normal force and the kinetic friction drops before reaching a minimum value and plateau. One reason is that for low normal forces, interfaces between fibre reinforced prepreg and pre-treated aluminium sheet have a relatively rough surface contact with high asperities. Although higher frictional forces are required to pull the adjacent surfaces apart as the normal force increases, the oriented fibres as well as asperities at the contacting interfaces can be flattened out, resulting in a reduction of the roughness and consequently, the friction coefficients. The sketch of this phenomenon is mentioned in Figure 2.9 and upon increasing the normal force, further compaction of the laminate seems impossible because the frictional force would greatly increase and even damage may happen when the fibres in prepreg have direct contact with the aluminium surface.

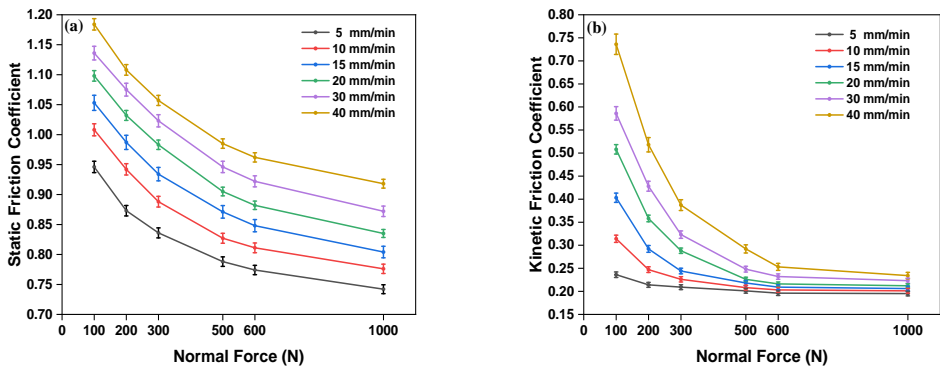


Figure 2.8: Friction coefficients as a function of normal force and sliding velocity at room temperature (23°C): (a) Static; (b) Kinetic

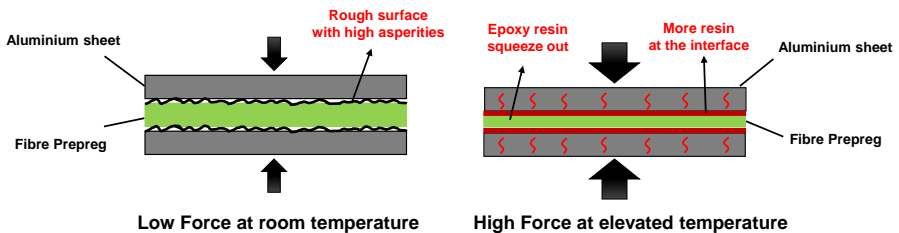


Figure 2.9: Sketch for illustrating the effect of normal force and temperature after the friction test

Cross-section micrographs of the sample perpendicular to the sliding direction after the friction test and subsequent curing (Figure 2.10(a)) are exhibited in Figure 2.11. The samples are tested with a normal force of 200 and 1000 N at the temperature of 80°C. Two fibre reinforced composite layers are separated by the three aluminium sheets shown in (striped) grey regions and the interfaces can be perfectly discerned. The distance measured on the micrographs reveals that a normal force of 1000 N leads to a higher degree of compaction compared with a lower normal force of 200 N. The nominal thickness for one composite layer is 360 μm. The average thickness after performing the friction test with a normal force of 200 N is 292.3 μm, while it is calculated to be 270.9 μm on average with a normal force of 1000 N. It can be concluded that the thickness decreases with the normal force increases and this reduction in thickness leads to a lower friction coefficient.

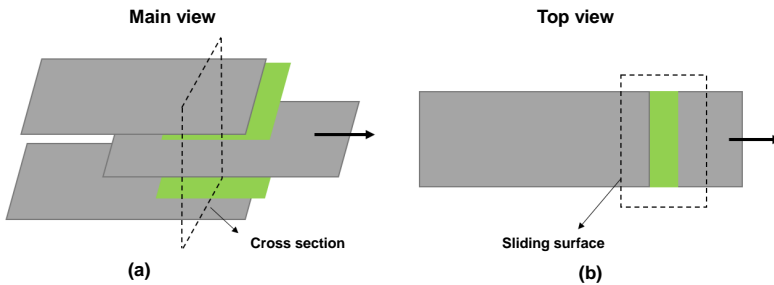


Figure 2.10: Sketch of the laminate sample after the friction test: (a) Cut-outs; (b) Sliding surfaces

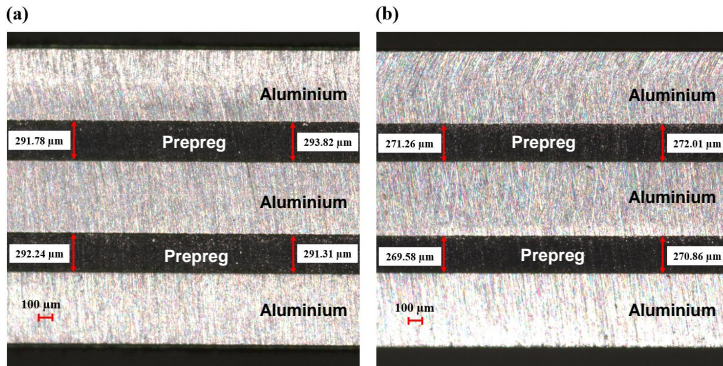


Figure 2.11: Cross-section micrographs after friction test performed with a normal force of (a): 200N and (b) 1000N at the temperature of 80°C – (×80)

The values of normal force and sliding velocity play an important role in determining the Hersey numbers in the Stribeck curve theory. Therefore, the relationships of Hersey number and friction coefficient at room temperature are plotted in Figure 2.12 with standard deviations. Upon fitting these test results, it is observed that the Hersey numbers studied at room temperature for kinetic friction coefficient look to fall into the hydrodynamic lubrication region in the Stribeck curve (Figure 2.1), since the lubrication re-

gion appears exponential with a positive slope (Figure 2.12(a)). Besides, it is shown that equal Hersey numbers (Table 2.3) have equal friction coefficients and the kinetic friction values gradually stabilise as the Hersey number gets smaller. For the static friction coefficient curve plotted in Figure 2.12(b), the trend follows a power law which does not correspond to the Stribeck curve and therefore cannot be explained with the known concept of fluid lubricated contacts.

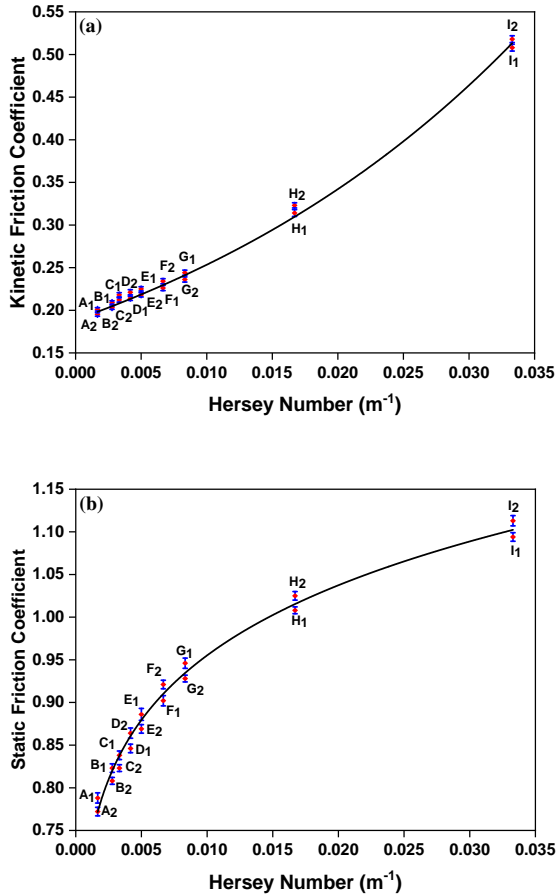


Figure 2.12: Hersey number versus test friction coefficient at room temperature: (a) Kinetic; (b) Static

2.5.2. EFFECT OF FIBRE ORIENTATION

ORIENTATION of the unidirectional fibres within the prepreg varies during the forming process, and the potential effect for different fibre orientation such as 0°/0°, 45°/45° and 90°/90° on friction is investigated. The results show that fibre orientation did not affect the coefficients of static friction. The reason is mainly due to the fact that the fibre orientation in the prepreg has a little impact on the fibre asperities and initial degree of

intimate contacts, which mostly decide the evolution of static friction. However, the kinetic friction behaves differently under various conditions of normal force and temperature. Figure 2.13 presents the two sliding effects in three different fibre orientations and the other variables are kept at their baseline values. It is shown that the kinetic friction coefficient decreases as the normal force or temperature increases. The fibre oriented at 45°/45° exhibits the highest kinetic friction coefficient while the 0°/0° layup interfaces show a lower friction coefficient compared with the 90°/90° interfaces under the same conditions. The difference implies that the presence of 45° and 90° plies increase interfacial shear stress when fibre orientation and aluminium rolling direction deviates. The effects of fibre orientation become more distinct with the increase of temperature, which shows that the interactions at metal-prepreg interfaces occur by the direct contact between the oriented fibres and aluminium surface at elevated temperatures.

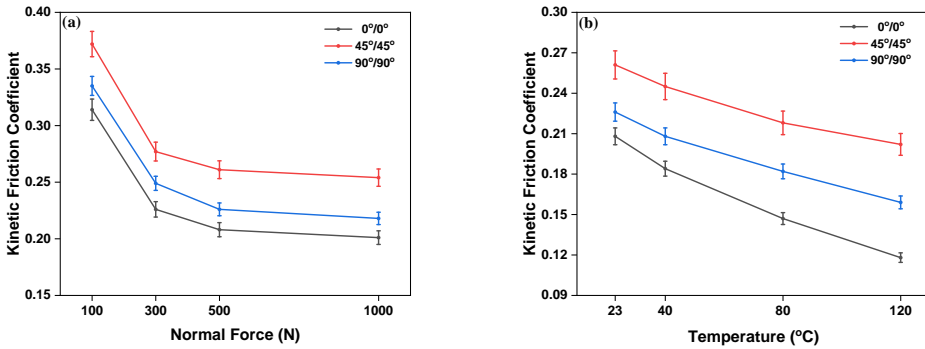


Figure 2.13: Kinetic friction coefficients of (a) different normal forces at room temperature of 23°C and (b) different temperatures at normal force of 500N

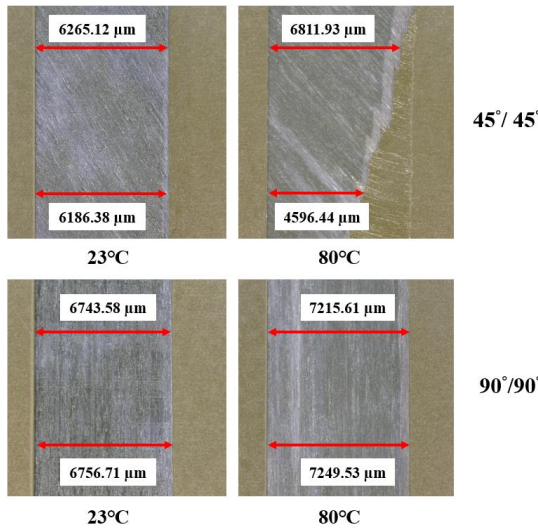


Figure 2.14: Sliding surfaces after the friction test performed with different fibre orientations – (×12)

The trend can be further explained through investigation of micrographs of the sliding surface and cut-outs. Sliding surfaces are performed by a digital microscope after subsequent curing to recognize the variations of sliding length in Figure 2.10(b). The fibre orientation of $45^\circ/45^\circ$ and $90^\circ/90^\circ$ at room temperature coupled with the temperature at 80°C after the inter-ply friction test are presented in Figure 2.14. A corresponding pull-out of fibre reinforced prepregs can be observed with the movement of middle aluminium sheet. At room temperature, the average sliding length for the prepreg of $45^\circ/45^\circ$ layup is 6.22 mm and the value increases to average 6.75 mm with the fibre orientation of $90^\circ/90^\circ$. The increase in prepreg sliding length means a lower frictional resistance at the interface. Even though the maximum displacement for both layups shows a positive elevation at high temperature, the laminate with $45^\circ/45^\circ$ interfaces exhibits a decrease in sliding length of prepreg on the bottom side. This phenomenon can be explained by the occurrence of intra-ply shear for $45^\circ/45^\circ$ interfaces while the layups of $0^\circ/0^\circ$ and $90^\circ/90^\circ$ only undergo inter-ply sliding during the friction test. The inter-ply sliding dominates the evolution of friction coefficient while intra-ply shear within the prepreg also contributes to friction. Therefore, the $45^\circ/45^\circ$ interfaces have the highest kinetic friction coefficient values compared with the $0^\circ/0^\circ$ and $90^\circ/90^\circ$ interfaces. The shearing phenomenon at elevated temperature demonstrates that decreasing viscosity has a positive influence on both inter-ply sliding and intra-ply shear behaviours. Figure 2.15 reveals that the cross-section thickness slightly drops from for $45^\circ/45^\circ$ interfaces to $90^\circ/90^\circ$ interfaces at the temperature of 80°C . This small difference of thickness shows that the fibre-orientation effect has a limited influence on the thickness reduction and friction coefficient. Although it affects the kinetic friction coefficient at various normal forces and temperatures, it is unable to determine the Hersey number in the Stribeck-curve theory or other friction models and no consistent law can be followed. Therefore, fibre orientation is not further considered for the development of the inter-ply friction model in the research.

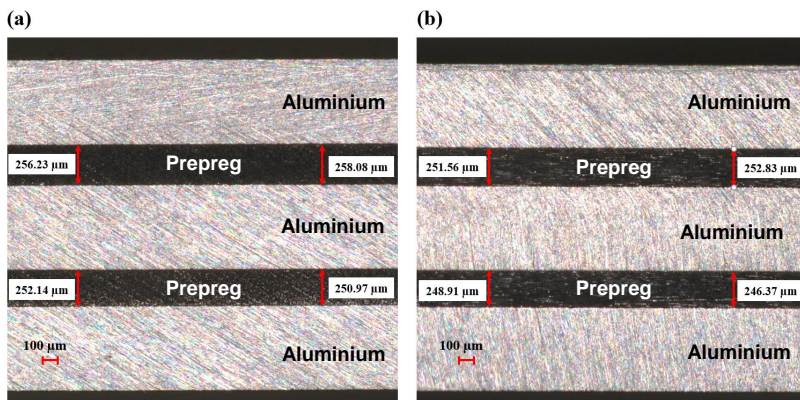


Figure 2.15: Cross-section micrographs after friction test performed with a fibre orientation of (a) $45^\circ/45^\circ$ and (b) $90^\circ/90^\circ$ at the temperature of 80°C and 500N – ($\times 80$)

2.5.3. EFFECT OF RESIN VISCOSITY AND TEMPERATURE

To investigate the influence of resin viscosity on friction coefficient, the combinations of the sliding velocity and normal force (v/N) are kept constant ranging from 0.01 to 0.1 mm/N·min shown in Figure 2.16. In this research, the resin viscosity decreases with the elevation of test temperature. Results reveal that the static and kinetic friction coefficients decrease as the test temperature increases from the room temperature of 23°C to the maximum temperature of 120°C. Rather than the quasi-linear reduction of static friction as the test temperature increases, the kinetic friction coefficient gradually converges at elevated temperatures. It can be concluded from the results that an increase of resin flow as viscosity decreases has a significant impact on the friction. The decreasing trend in the friction coefficient can be due to the resin squeezing out from the center of prepreg layer to the top and bottom interfaces. More resin at the interfaces creates resin film layers which increase the lubrication and reduce the friction coefficient as discussed in the Stribeck-curve theory. The illustrating sketch is also shown in Figure 2.9. However, the viscosity variations provide limited effects on the static friction state before the onset of sliding, and the decrease in friction coefficient may result from the temperature effect which alters the interface asperities. Therefore, the combined effect of sliding velocity and normal force has a small influence on the kinetic friction coefficient as the temperature rises.

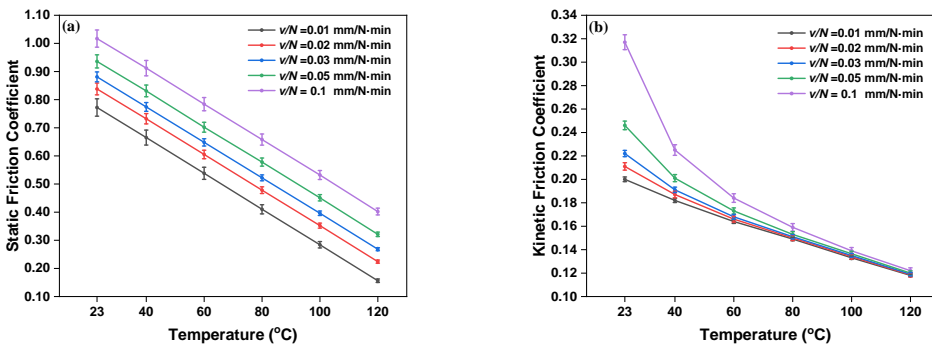


Figure 2.16: Experimental Friction coefficients under different temperatures: (a) Static; (b) Kinetic

Figure 2.17 shows the micrographs of the sliding surfaces at three different temperatures for $0^\circ/0^\circ$ interfaces at 500N and 10mm/min. A slight length increase for the sliding of prepreg layer shown on the surface top region are measured from 7.05 mm at 40°C to 7.62 mm at 120°C. This result helps to explain why the friction coefficient drops with increased resin flow by the elevation of test temperatures. However, it is also obvious to see the uneven ply boundary displacement on the surface bottom region for $0^\circ/0^\circ$ interfaces at the temperature of 120°C in Figure 2.17. There are two reasons which can explain the defects: One is that the polymer matrix tends to flow parallel to the fibre axis, which makes the transverse flow less likely to happen. Once the resin flow occurs in a direction off-axis the fibre orientation at high temperatures, the fibres are more likely to move with the resin. The other reason for the uneven ply boundary displacement can be caused by the direct contact in some regions between the oriented fibres and aluminium

sheet at high temperatures. When the normal force becomes very high or the degree of cure for the epoxy prepreg increases, the sliding interface would be damaged as the viscosity increases and results in higher friction coefficients. Further research on laminate cut-outs after performing the friction test (Figure 2.18) shows that the average thickness at the temperature of 40°C is 303.7 μm , while it is 251.9 μm average at the temperature of 120°C. The results imply that more resin flow at elevated temperature would lead to a distinct decrease in cross-section thickness.

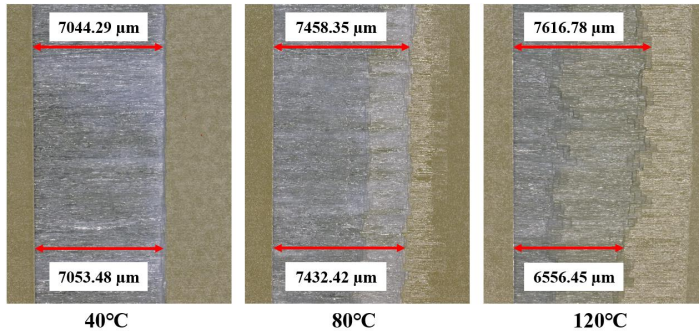


Figure 2.17: Sliding surfaces after the friction test performed with different temperatures for 0°/0° interfaces at 500N and 10mm/min – ($\times 12$)

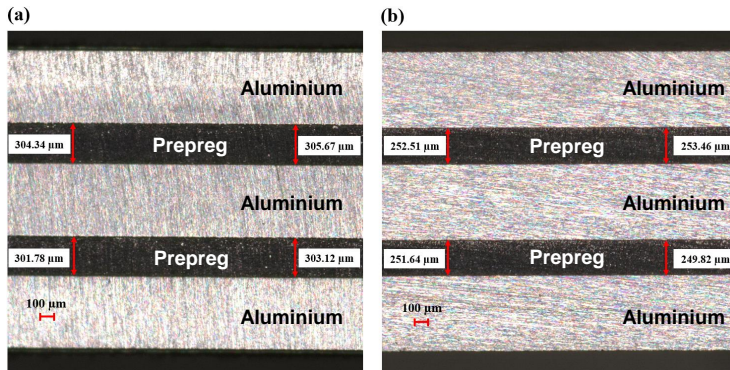


Figure 2.18: Cross-section micrographs after friction test performed with a temperature of (a) 40°C and (b) 120°C – ($\times 80$)

As stated in the theoretical section of this work, viscosity is another critical index on the Hersey number in the Stribeck-curve theory. A constant preheat time under various test temperatures is incorporated into the viscosity model. The relationships of friction coefficient and Hersey number at these test temperatures are made into a fitting curve shown in Figure 2.19. The result ignores the viscosity parameter in Hersey numbers for the static friction coefficient while a temperature compensation term [37, 38] for both friction coefficients is considered to incorporate into the inter-ply friction model.

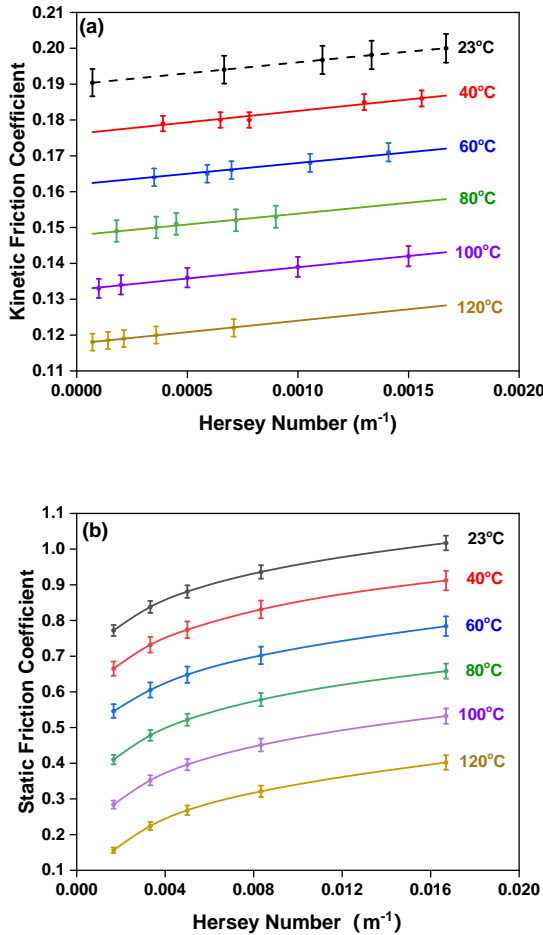


Figure 2.19: Effect of temperature on test friction coefficient and Hersey number: (a) Kinetic; (b) Static

2.6. DEVELOPMENT OF INTER-PLY FRICTION MODEL

THE inter-ply friction model for the kinetic friction can be derived by fitting a curve from the test results in Figure 2.12(a),

$$\mu_k = 0.22 \cdot e^{27.25H} - 0.03 \quad (2.9)$$

where μ_k is the coefficient of kinetic friction and H is the Hersey number.

It can be seen that an exponential fit represents the experimental data at room temperature and suggests that the range of studied values corresponds to the hydrodynamic lubrication domain in the Stribeck curve (Figure 2.1). However, the trend of the fitting curve only corresponds with the experimental results at room temperature when the effect of viscosity at different test temperatures is not considered. To account for the variations of temperature for the kinetic friction coefficient in the friction model, Gorczyca

et al. [37] proposed a temperature shift term, S_{kk} , which can be added to the model,

$$\mu_k = (0.22 \cdot e^{27.25H} - 0.03) - S_{kk} \quad (2.10)$$

where S_{kk} is the shift term to compensate for the temperature effect. Based on the result obtained from Figure 2.19(a), a linear fit can be matched to the test temperature versus kinetic friction data and the friction coefficient can be expressed as:

$$\mu_{kk} = -7.42 \times 10^{-4} \cdot T + 2.27 \times 10^{-1} \quad (2.11)$$

where μ_{kk} is the kinetic friction coefficient at the temperature T in °C. Then, the shift term for Equation 2.10 is written which represents the difference of the actual temperature and the baseline temperature (23°C),

$$S_{kk} = -7.42 \times 10^{-4} (T_B - T_A) \quad (2.12)$$

where T_A, T_B are the value of the actual temperature and baseline temperature in °C, respectively. When incorporating the result from Equation 2.12 into Equation 2.10 with the temperature difference $\Delta T = T_A - T_B$, the kinetic friction coefficient considering the investigated sliding effect is expressed as:

$$\mu_k = 0.22 \cdot e^{27.25 \cdot \frac{\eta v}{N}} - 7.42 \times 10^{-4} \cdot \Delta T - 0.03 \quad (2.13)$$

where η, v, N and ΔT are the processing parameters of resin viscosity, sliding velocity, normal force and temperature difference, respectively. From the Equation 2.13, it can be concluded that the kinetic friction plots in the transition region between mixed and hydrodynamic lubrication can be fit into the Stribeck curve.

However, the fitting curve for static friction coefficient versus Hersey number (Figure 2.12(b)) does not match with the Stribeck curve. The result in Figure 2.19(b) reveals that the viscosity parameter in the Hersey number has limited contribution to establish a static friction model, while the shift term should be applied to compensate for the temperature effect. Therefore, the static friction coefficient following a power-law fit at room temperature can be written as:

$$\mu_s = 5.02 \cdot \left(\frac{v}{N}\right)^{0.12} \quad (2.14)$$

where μ_s is the static friction coefficient, v is the sliding velocity and N is the applied normal force. To compensate for test temperature effect on the static friction, a static shift term is added to the model again [37]. This shift term S_{ss} also corresponds to a linear fit according to Figure 2.19(b) and the static friction coefficient at actual temperature, μ_{ss} , can be expressed as:

$$\mu_s = 5.02 \cdot \left(\frac{v}{N}\right)^{0.12} - S_{ss} \quad (2.15)$$

$$\mu_{ss} = -6.35 \times 10^{-3} \cdot T + 9.84 \times 10^{-1} \quad (2.16)$$

$$S_{ss} = -6.35 \times 10^{-3} \cdot (T_B - T_A) \quad (2.17)$$

where T_A, T_B are the value of the actual temperature and baseline temperature in °C, respectively. Then, the static friction coefficient considering the investigated sliding effect can be written as,

$$\mu_s = 5.02 \cdot \left(\frac{v}{N}\right)^{0.12} - 6.35 \times 10^{-3} \cdot \Delta T \quad (2.18)$$

Here, the static friction coefficient is determined as a function of sliding velocity v , normal force N and temperature difference ΔT . This static friction model could be fit into a modified Coulomb friction model by combining Equation 2.1 and Equation 2.2 where $\mu = k \cdot N^{n-1}$ with a friction index $n = 0.88$. The modified friction model considers temperature effects and the friction constant k is also influenced by sliding velocity. It is known from the model that the test temperature has the largest effect on static friction, followed by the applied normal force and the sliding velocity. As a result, an inter-ply friction model considering the static and kinetic friction coefficients under different sliding parameters can be applied in process simulation.

2.7. FINITE ELEMENT MODEL VALIDATION

THE commercially available finite element package Abaqus/Explicit allows for the implementation of user-defined frictional behaviour via a subroutine. A finite element model of the experimental friction test setup is run to validate the ability of the proposed friction model to replicate the response of the inter-ply friction test. The finite element model shown in Figure 2.20 includes two outer aluminium sheets fixed at one end and a middle aluminium sheet pulled out from the other end, together with two alternating glass fibre prepreg layers. A normal force is applied on the outer aluminium surfaces and the sizes as well as thicknesses are the same as the experimental setups. To simplify the setup and reduce computation time, the aluminium sheets and glass fibre prepreg are all created as four-node doubly curved conventional shell element with reduced integration (S4R) with the mesh size of 1 mm. Such laminate model is represented in the composite layup module where all layers and material parameters such as orientation, thickness, property and relative location can be defined.

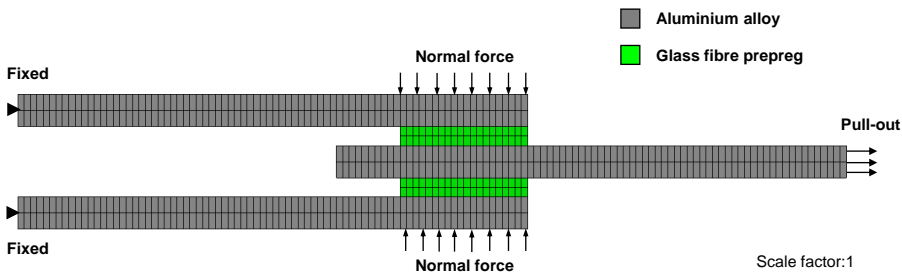


Figure 2.20: Finite element model of the inter-ply friction test of the pre-stacked laminates

A normal force corresponding to the inter-ply friction experiments is applied on the fixed top and bottom platens in first step of the analysis. In the subsequent steps, the applied force is held constant and a velocity is prescribed in the pull-out direction on the middle aluminium sheet for a maximum distance of 20 mm. A static-kinetic exponential decay equation (Equation 2.19) is used to model the transition from static to kinetic friction under different sliding effects,

$$\mu = \mu_k + (\mu_s - \mu_k) \cdot e^{-\beta \dot{\gamma}} \quad (2.19)$$

where μ_s is the static friction coefficient, μ_k is the kinetic friction coefficient, β is the decay constant and $\dot{\gamma}$ is the slip rate. The decay constant defines the transition rate from zero velocity to the final velocity, and a decay constant of 0.16 is calculated to best-fit the experimental data points which can be used in the finite element models. The friction coefficient versus displacement curves from Abaqus/Explicit friction-test and experimental validation are plotted in Figure 2.21 under some conditions. The model can capture a peak state as it is associated with the static friction and a steady sliding state for the kinetic friction. However, the static peak force and onset sliding displacement obtained from the model does not correspond exactly to the experimental results, and the model observes a steady kinetic friction at early stage of displacement while the experimental coefficient of friction continues to drop slightly. Because the kinetic friction coefficient is the dominating factor, the peak value is less important and can be fixed by a contact stiffness constant in the model. Therefore, the friction coefficient results indicate that the finite element model accurately accounts for the variations in sliding velocity, normal force and temperature to update the friction coefficient as a function of the test conditions. Through incorporating the inter-ply friction model into Abaqus/Explicit as a user-defined friction subroutine, an accurate press forming simulation of thermoset based fibre metal laminates can be established.

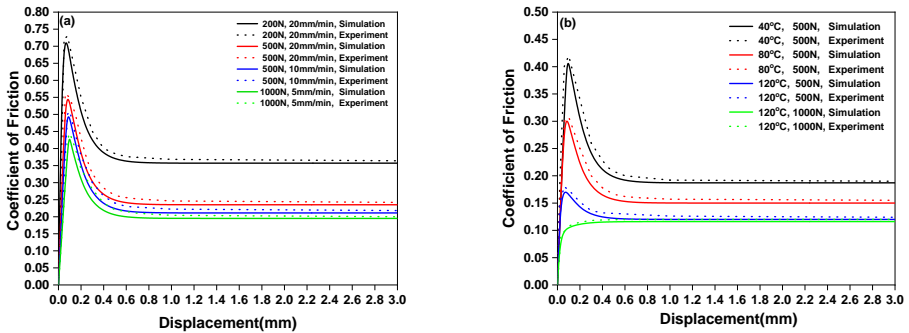


Figure 2.21: Comparison between numerical and experimental results for inter-ply friction of uncured hybrid laminates: (a) At room temperature of 23°C; (b) At sliding velocity of 10mm/min

2.8. CONCLUSIONS

THE inter-ply friction coefficient at the metal-prepreg interfaces for the glass-fibre reinforced aluminium laminate (GLARE) under different sliding parameters has been measured using a double-lap sliding test method. The influencing parameters are normal force, sliding velocity, fibre orientation, resin viscosity coupled with the temperature. Friction coefficient results are studied by the sliding displacement and cross-section thickness measurements. The sliding parameters which decrease the friction coefficients are obtained and an inter-ply friction model based on the test result is incorporated into Abaqus/Explicit as a user-defined friction subroutine. The main achievements are:

- (1) The static friction coefficient increases with the increase of sliding velocity and

decreases with the increase of normal force, while the kinetic friction coefficient drops with the increase of normal force at different sliding velocities before reaching a minimum value and plateau. Besides, the static friction coefficient drops quasi-linear with the increasing temperature. In contrast, the kinetic friction coefficient gradually converges at elevated temperature due to the decrease of resin viscosity. Combining the effect of the sliding velocity and normal force has a small influence on kinetic friction when the temperature becomes higher.

(2) The fibre orientation has limited impact on the coefficient of static friction while the fibre oriented at $45^\circ/45^\circ$ exhibits the highest kinetic friction coefficient and the $0^\circ/0^\circ$ interfaces show a lower friction coefficient compared with $90^\circ/90^\circ$ interfaces under the same conditions. Inter-ply sliding dominates the friction coefficient evolution while for $45^\circ/45^\circ$ interfaces, the intra-ply shear behavior within the prepreg affects the friction. In addition, the decreasing viscosity at elevated temperature has a significant influence on both inter-ply sliding and intra-ply shear behaviours.

(3) The kinetic friction for various combinations of sliding effects results in a relationship similar to the Stribeck curve with plots in the transition region between mixed and hydrodynamic lubrication. The static friction coefficient versus Hersey number does not match the trend in Stribeck-curve theory but obeys a modified Coulomb type of friction where resin viscosity has limited influence.

(4) A static-kinetic exponential decay equation in Abaqus/Explicit is applied to model the transition from the static to kinetic friction. The kinetic friction shows to be the dominating factor in the finite element model, and the friction coefficients obtained from the simulations correlate well with the experimental results.

REFERENCES

- [1] A. Asundi and A. Y. Choi, "fibre metal laminates: An advanced material for future aircraft," *Journal of Materials Processing Technology*, vol. 63, no. 1, pp. 384–394, 1997.
- [2] R. Wang, S. Zheng, and Y. Zheng, "Matrix materials," in *Polymer Matrix Composites and Technology*, Woodhead Publishing Series in Composites Science and Engineering, pp. 101–548, Woodhead Publishing, 2011.
- [3] M. Khan, N. Reynolds, G. Williams, and K. Kendall, "Processing of thermoset prepreps for high-volume applications and their numerical analysis using super-imposed finite elements," *Composite Structures*, vol. 131, pp. 917–926, 2015.
- [4] J. Sinke, "Manufacturing of glare parts and structures," *Applied composite materials*, vol. 10, pp. 293–305, 2003.
- [5] N. Ersoy, K. Potter, M. R. Wisnom, and M. J. Clegg, "An experimental method to study the frictional processes during composites manufacturing," *Composites Part A: Applied Science and Manufacturing*, vol. 36, no. 11, pp. 1536–1544, 2005.
- [6] W. Najjar, C. Pupin, X. Legrand, S. Boude, D. Soulat, and P. D. Santo, "Analysis of frictional behaviour of carbon dry woven reinforcement," *Journal of Reinforced Plastics and Composites*, vol. 33, no. 11, pp. 1037–1047, 2014.

- [7] S. Allaoui, C. Cellard, and G. Hivet, "Effect of inter-ply sliding on the quality of multilayer interlock dry fabric preforms," *Composites Part A: Applied Science and Manufacturing*, vol. 68, pp. 336–345, 2015.
- [8] C. Pasco, M. Khan, J. Gupta, and K. Kendall, "Experimental investigation on interply friction properties of thermoset prepreg systems," *Journal of Composite Materials*, vol. 53, no. 2, pp. 227–243, 2019.
- [9] C. Martin, J. Seferis, and M. Wilhelm, "Frictional resistance of thermoset prepregs and its influence on honeycomb composite processing," *Composites Part A: Applied Science and Manufacturing*, vol. 27, no. 10, pp. 943–951, 1996.
- [10] A. Dutta, M. Hagnell, and M. Åkermo, "Interply friction between unidirectional carbon/epoxy prepreg plies: Influence of fibre orientation," *Composites Part A: Applied Science and Manufacturing*, vol. 166, p. 107375, 2023.
- [11] R. Akkerman, M. Ubbink, B. Rooij, and R. Ten Thije, "Tool-ply friction in composite forming," in *10th ESAFORM conference on material forming, Zaragoza, Spain*, vol. 907, 2007.
- [12] L. Jeong-Min, K. Byung-Min, L. Chan-Joo, and K. Dae-Cheol, "A characterisation of tool-ply friction behaviors in thermoplastic composite," *Procedia Engineering*, vol. 207, pp. 90–94, 2017.
- [13] M. Smolnicki and P. Stabla, "Finite element method analysis of fibre-metal laminates considering different approaches to material model," *SN Applied Sciences*, vol. 1, no. 5, pp. 1–7, 2019.
- [14] P. Soltani, M. Keikhosravy, R. Oskouei, and C. Soutis, "Studying the tensile behaviour of glare laminates: A finite element modelling approach," *Applied Composite Materials*, vol. 18, no. 4, pp. 271–282, 2011.
- [15] V. Zal, H. Moslemi Naeini, J. Sinke, A. Bahramian, M. Abouhamzeh, and R. Benedictus, "A new procedure for finite element simulation of forming process of non-homogeneous composite laminates and fmls," *Composite Structures*, vol. 163, pp. 444–453, 2017.
- [16] P. Boisse, K. Buet, A. Gasser, and J. Launay, "Meso/macro-mechanical behaviour of textile reinforcements for thin composites," *Composites Science and Technology*, vol. 61, no. 3, pp. 395–401, 2001.
- [17] P. Boisse, N. Hamila, F. Helenon, and J. Cao, "Different approaches for woven composite reinforcement forming simulation," *International Journal of Material Forming*, vol. 1, no. 1, pp. 21–29, 2008.
- [18] D. Jauffrès, J. Sherwood, D. Morris, and J. Chen, "Discrete mesoscopic modeling for the simulation of woven-fabric reinforcement forming," *International Journal of Material Forming*, vol. 3, no. Suppl 2, pp. 1205–1216, 2010.

- [19] K. Fetfatsidis, D. Jauffrès, J. Sherwood, and J. Chen, "Characterization of the tool/fabric and fabric/fabric friction for woven-fabric composites during the thermostamping process," *International Journal of Material Forming*, vol. 6, no. 2, pp. 209–221, 2013.
- [20] L. Mosse, P. Compston, W. J. Cantwell, M. Cardew-Hall, and S. Kalyanasundaram, "The development of a finite element model for simulating the stamp forming of fibre-metal laminates," *Composite Structures*, vol. 75, no. 1, pp. 298–304, 2006.
- [21] ASTM-D1894, "Standard test method for static and kinetic coefficients of friction of plastic film and sheeting," *Annual Book of ASTM Standards*, pp. 1–8, 2001.
- [22] J. E. Maldonado, "Coefficient of friction measurements for plastics against metals as a function of normal force," *Annual Technical Conference - ANTEC, Conference Proceedings*, vol. 3, p. 3431 – 3433, 1998.
- [23] S. Chow, *Frictional interaction between blank holder and fabric in stamping of woven thermoplastic composites*. University of Massachusetts Lowell, 2002.
- [24] J. O. Ajayi, "Effect of fabric structure on frictional properties," *Textile Research Journal*, vol. 62, pp. 87–93, 1992.
- [25] G. Stachowiak and A. W. Batchelor, *Engineering tribology*. Butterworth-heinemann, 2013.
- [26] C. Wilks, "Characterization of the tool/ply interface during forming," *Nottingham: University of Nottingham*, 1999.
- [27] M. Clifford, A. Long, and P. deLuca, "Forming of engineering prepregs and reinforced thermoplastics," in *TMS annual meeting and exhibition, second global symposium on innovations in materials, processing and manufacturing: sheet materials: composite processing*, 2001.
- [28] E. Gelinck and D. J. Schipper, "Calculation of stribeck curves for line contacts," *Tribology International*, vol. 33, no. 3-4, pp. 175–181, 2000.
- [29] J. L. Gorczyca, J. A. Sherwood, L. Liu, and J. Chen, "Modeling of friction and shear in thermostamping of composites-part i," *Journal of Composite Materials*, vol. 38, no. 21, pp. 1911–1929, 2004.
- [30] Y. R. Larberg and M. Åkermo, "On the interply friction of different generations of carbon/epoxy prepreg systems," *Composites Part A: Applied Science and Manufacturing*, vol. 42, no. 9, pp. 1067–1074, 2011.
- [31] I. Baran, R. Akkerman, and J. H. Hattel, "Material characterization of a polyester resin system for the pultrusion process," *Composites Part B: Engineering*, vol. 64, pp. 194–201, 2014.
- [32] R. Geissberger, J. Maldonado, N. Bahamonde, A. Keller, C. Dransfeld, and K. Masania, "Rheological modelling of thermoset composite processing," *Composites Part B: Engineering*, vol. 124, pp. 182–189, 2017.

- [33] Solvay-Adhesive-Materials, “Technical datasheet for the fm-94 film adhesive,” <https://www.solvay.com/en/product/fm-94-product-documents>, 2017.
- [34] H. Li, Y. Xu, X. Hua, C. Liu, and J. Tao, “Bending failure mechanism and flexural properties of glare laminates with different stacking sequences,” *Composite Structures*, vol. 187, pp. 354–363, 2018.
- [35] M. Abouhamzeh, J. Sinke, K. Jansen, and R. Benedictus, “Kinetic and thermo-viscoelastic characterisation of the epoxy adhesive in glare,” *Composite Structures*, vol. 124, pp. 19–28, 2015.
- [36] M. Abouhamzeh, J. Sinke, K. Jansen, and R. Benedictus, “A new procedure for thermo-viscoelastic modelling of composites with general orthotropy and geometry,” *Composite Structures*, vol. 133, pp. 871–877, 2015.
- [37] J. L. Gorczyca-Cole, J. A. Sherwood, and J. Chen, “A friction model for thermostamping commingled glass–polypropylene woven fabrics,” *Composites Part A: applied science and manufacturing*, vol. 38, no. 2, pp. 393–406, 2007.
- [38] U. Sachs, R. Akkerman, K. Fetfatsidis, E. Vidal-Sallé, J. Schumacher, G. Ziegmann, S. Allaoui, G. Hivet, B. Maron, K. Vanclooster, *et al.*, “Characterization of the dynamic friction of woven fabrics: Experimental methods and benchmark results,” *Composites Part A: Applied Science and Manufacturing*, vol. 67, pp. 289–298, 2014.

3

A MODIFIED BIAS-EXTENSION TEST METHOD FOR INTRA-PLY SHEAR CHARACTERISATION

The bias-extension (BE) test is one of the test methods to characterise the intra-ply shear behaviour of continuous fibre reinforced composites including fabrics and unidirectional (UD) materials. For the determination of the major mechanical properties of metal sheets, often a uniaxial tensile test is used. Combination of these two methods for the in-plane shear deformation of uncured hybrid laminates is proposed comparing the method for cross-plyed unidirectional prepregs and woven fabric prepregs. The influences of material constituent, clamp displacement rate, preheat temperature and normal pressure on the intra-ply shear behaviour are investigated. The results indicate that the material constituents and friction depending on processing parameters play a critical role in the in-plane shear characterisation of the hybrid laminate. The shear angle measurement under four typical strains demonstrates that the support of metal layers improves the shear deformability by delaying the onset of fibre wrinkling. The modified intra-ply shear test contributes to a better understanding of the process design for the forming of metal-composite laminates.

This chapter has been published in: Liu S, Sinke J, Dransfeld C. A modified bias-extension test method for the characterisation of intra-ply shear deformability of hybrid metal-composite laminates. *Composite Structures*. 116964, **314**, (2023).

3.1. INTRODUCTION

THE metal-composite laminates consist of alternating thin sheets of metal alloys and layers of fibre reinforced polymers. A wide range of combinations are available based on the type of metal sheets, the architecture of fibres and resins, the number as well as thickness of layers, etc [1]. Advantages of such lightweight hybrid materials compared with the monolithic metal sheets are a better resistance to damage in case of impact, fatigue and corrosion [2]. However, one of the main difficulties of forming components made of metal-composite laminates, appears in its complex deformation mechanisms, which may result in tears, folds, wrinkles [3–5]. One promising method for the forming of such hybrid materials is through a press forming process especially designed for epoxy-based metal-composite laminates. The proposed process steps are shown in Figure 1.8 and involve preheating a laminate, forming of the uncured laminate, consolidation and (partial) curing in the same mould. Temperature and preheating time need to be carefully controlled to decrease the resin viscosity and thus increase the ease of deformation. This method could improve the laminate deformability based on the understanding of the deformation mechanisms for both material constituents. Here, the metal sheets are usually deformed into three-dimensional shapes by bending and in-plane plastic deformation [6, 7]. The deformation of fibre reinforced composites is achieved by inter-ply sliding in-between the layers and intra-ply shear within the prepreg layers [8–10]. Both mechanisms need to be combined in the proposed press forming process.

3.2. LITERATURE ON INTRA-PLY SHEAR

INTRA-PLY shear behaviour of the individual plies in composite laminates is recognised as the dominant mode of fibre deformation for shaping three-dimensional parts. This mechanism has been investigated by many researchers [11–15] especially for the woven fabrics which are shear dominated and deform as modelled by the pin-jointed net (PjN) theory. The PjN theory assumes that yarns are inextensible without any slippage at the cross-overs and free rotations are allowed for the fibre tows between warp and weft. The shear resistance gradually grows during deformation as the yarns rotate over each other. The deformation causes a sharp increase in shear force at a point and beyond which fibre wrinkling phenomena occur. This point, often called ‘locking angle’, depends largely on the properties of textile reinforcement, like type of fibre, type of weave, weave density, etc (Figure 3.1). Potter [16, 17] found some similarities on the shear behaviour between woven fabrics and cross-ply UD materials although the complete deformation is more complex for cross-ply UD materials than for woven fabrics due to the lack of physical interlocking constraints. He concluded that the shear deformation for cross-ply UD prepregs can be modelled by the same PjN assumption that was used for woven fabric prepregs and an improved forming capability can be obtained by controlling the linkage between the UD plies. However, there is no equivalent test standard to measure the shear angle of cross-ply UD prepreg and the limit of shear deformation can be either wrinkling or splitting within the fibre layers [18, 19].

The shear behaviour of dry fabrics or prepregs is typically characterised applying the well-known intra-ply shear tests with a picture frame (PF) test or a bias-extension (BE) test [20–23]. In the picture frame test, the fabric specimen is clamped with the yarns

aligned parallel and perpendicular to the four clamping bars. The shear deformation is developed by fixing one hinge of the frame while imposing a tensile load on the hinge at the opposite end of the frame. The main advantage of the PF method is the uniformly induced shear on the sample region which allows a direct measurement of the shear deformation. The limitation, however, is the sensitivity of misalignments in the direction of fibres and the accuracy needed when cutting the sample and clamping in the frame. Besides, the frame has been shown to cool the material immediately adjacent to the deforming sample during high-temperature testing, which may influence the results [20, 21].

At the start of a bias-extension (BE) test, the fibre orientations of the specimen are $\pm 45^\circ$ with respect to the tensile direction. The test sample is cut into a rectangular shape with the specimen length typically more than two times its width to obtain a suitable shear region. Normally, there are three distinct regions: 'pure shear', 'half shear' and 'undeformed'. The BE test shows mainly intra-ply sliding for dry fabrics or prepregs (both in fabrics/weaves and UD), but as they reach higher shear angles the PJN method may not be applicable anymore because of other deformation mechanisms involved [22, 23]. Rashidi et al. [24] proposed a slip-bias extension test to investigate the effect of slip conditions during the forming process of the woven fabric prepregs. They developed a modified shear stress formulation for the fast 3D simulations considering the effects of frictional interactions at different shear angles, normal pressures and asymmetric gripping conditions.

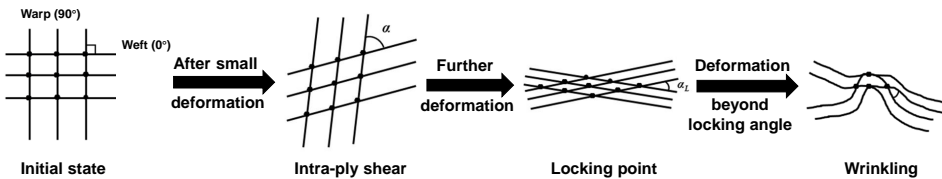


Figure 3.1: Typical intra-ply shear deformation behaviour of textile reinforcement materials

The PF and BE approaches can both be used to characterise the intra-ply shear behaviour of the unidirectional prepregs. The picture frame tests are usually not adopted for the UD prepregs because of the difficulty of tight clamping of specimens, the tendency of ply splitting and the adverse fibre tension under the effect of slight fibre misalignment [18]. Larberg et al. [25] proposed a bias-extension test on different cross-ply UD prepregs and found that intra-ply shear only dominates at small deformations while intra-ply and inter-ply friction together play an important role at large deformations. Besides, the research demonstrated that prepreg systems and temperature distributions were important factors affecting the degree of fibre rotation and the deformation modes as well as their limits. Brands et al. [26] conducted bias-extension experiments on the cross-ply laminates of thermoplastic UD tapes under various processing conditions and showed that the deformation is consistent with a PJN up to a shear angle of 25° . Haanappel and Akkerman [18] proposed a torsion bar test to characterise the shear mechanisms of unidirectional thermoplastic melts and developed a non-linear material model for carbon UD/PEEK under small strains. Wang et al. [27] conducted the intra-ply shear

characterisation of UD prepregs using a 10° off-axis BE test under various temperature distributions and test rates. The results validated that the shear stress and strain can be obtained using the off-axis BE test and the material response under these testing parameters provides robust models for composite manufacturing simulation.

The mechanical response of metal sheets is usually characterised through uniaxial tensile test where the material properties like yield and ultimate tensile strength, uniform and total elongation in a standard gauge length can be measured. Dog-bone shapes are primarily used for the tensile test samples to eliminate the effect of stress concentration in the clamping region and to ensure the highest probability that the sample fails in the standard gauge region [28]. A biaxial tensile test has becoming prevalent for evaluating the mechanical properties of metal sheets as the standard tensile test can only determine the performance in one direction while is not applicable to multi-directional forming processes such as deep-drawing [29]. Unlike the classical tensile tests, the in-plane shear behaviour of metal sheets is difficult to obtain through simple shear tests as the shear stress distribution is usually inhomogeneous and no intrinsic gauge length can be applied to define the local strain [30]. The shear tests of complex geometrical specimens are designed for some experimental setups while they are inconvenient for the dynamic testing [31, 32]. In addition, the in-plane torsion tests prove to be inappropriate for obtaining the shear behaviour of metal sheets due to their high plastic deformation and potential fracture at free edges [33].

As for the evaluation of the in-plane deformation for hybrid materials like the metal-composite laminates, most researchers prefer the same uniaxial tensile test for metal sheets [34–38]. The samples were consolidated following a standard curing cycle before the test and the shape of the specimen can either be rectangular or dog-bone. By the modification of metal surfaces and the adjustment of layup sequences or fibre orientations, the in-plane mechanical properties such as ultimate tensile strength can be greatly improved. Studies found that the in-plane deformability of metal-composite laminates mainly depends on the maximum failure strain and the interlaminar shear strength of composite layers. Due to the high bonding strength after consolidation and the limited fibre failure strain, the deformation of the hybrid laminates is constrained and the higher elastic-plastic deformability of metal sheets cannot be fully exploited. Therefore, the investigation on the role of metal sheet which affects the biaxial deformation of the uncured fibre prepreg becomes a meaningful topic. Also, there is an increasing interest for many researchers in the intra-ply shear behaviour of the uncured fibre prepreg inside the hybrid laminates during deformation. However, there are few related studies on discovering the shear properties of the uncured hybrid laminates due to the lack of efficient manufacturing and testing methods.

3.3. MATERIALS AND METHODS

3.3.1. MATERIAL CONSTITUENTS

THE hybrid material systems used in this research consist of two metal alloys and two types of fibre reinforced prepregs. For the metal materials, aluminium alloy 2024-T3 and AISI 304 stainless steel are selected for their different failure strains [39]. The aluminium alloy 2024-T3 is widely used in aircraft structures because of its high strength

and fatigue resistance, but the elongation at break is relatively low at around 15-18%. The AISI 304 stainless steel can withstand 45%-50% maximum tensile strain, which greatly increases the deformability of the entire hybrid laminates. The metal sheets are machined into a dog-bone shape with a specific dimension and a thickness of 0.5 mm. The woven and UD architectures for the fibre reinforced prepregs are based on the same epoxy resin and chosen for their different shear properties. Figure 3.2 displays the image of the two prepregs in undeformed state. The materials are commercially available from SHD composites (UK). The SHD-TW is a T-700 carbon reinforced prepreg with 3k tow size and Twill Weave (2×2) fabric having a thickness of 0.2 mm and fibre volume content of 58%, while SHD-UD is a T-700 carbon reinforced prepreg with the unidirectional reinforcement having a thickness of 0.15 mm and fibre volume content of 63%. The MTC510 epoxy system for both prepregs is designed to cure between 80°C and 120°C. The viscosity profile of MTC510 as a function of temperature at a ramp rate of 2°C/min as provided by the material supplier [40] is shown in Figure 3.3.

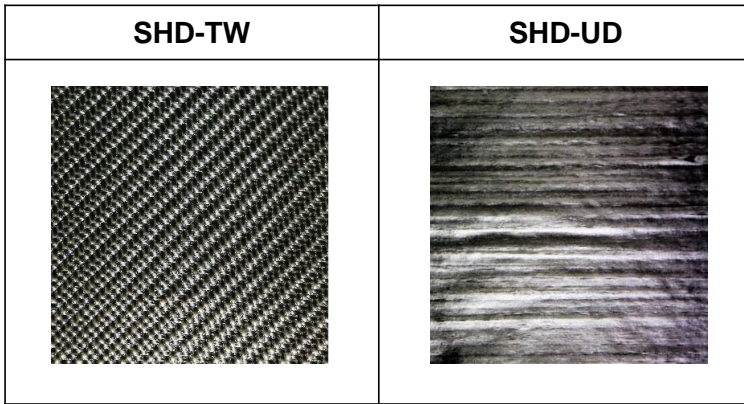


Figure 3.2: Two types of fibre reinforced prepregs used for the intra-ply shear tests

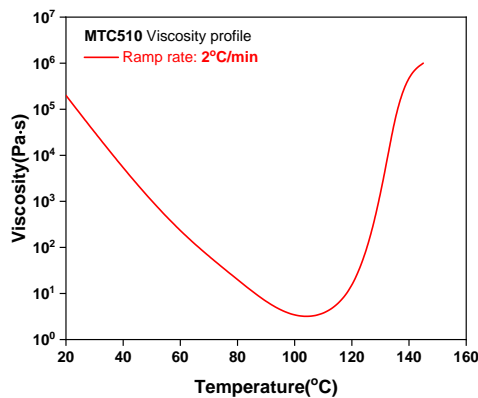


Figure 3.3: Viscosity profile for MTC510 matrix system used for SHD-TW and SHD-UD prepreg as a function of temperature

3.3.2. MODIFIED BIAS-EXTENSION TEST

THE uniaxial tensile test aims to obtain the tensile behaviour of the metal sheets while the bias-extension test is used to measure the in-plane intra-ply shear behaviour of fabrics or prepregs. A combination of these two test methods with dog-bone shaped metal sheets and rectangular shaped fibre prepregs, referred as a modified bias-extension test, is proposed to investigate how the support of metal sheet influences the shear properties of the prepreg layer under different conditions. The modified BE test with idealised shear regions is illustrated in Figure 3.4, with dimensions and schematics of the undeformed and deformed specimens according to the pin-joint net (PJN) theory. The geometry of fibre prepreg is rectangular where the sample length is 6.5 times the width to acquire a suitable state of shearing. The initial orientation of the fibre tows is at $\pm 45^\circ$ to the loading direction for both cross-plyed UD and woven fabric prepreg. In the modified bias-extension test, the PJN behaviour is assumed, predicting three shear zones within the specimen: A, B and C. Zone A is the pure shear region where the shear is uniform and a theoretical shear angle can be calculated through Equation 3.1 [22, 23],

$$\gamma = 90^\circ - 2 \cdot \arccos \frac{L + \delta}{\sqrt{2} \times L} \tag{3.1}$$

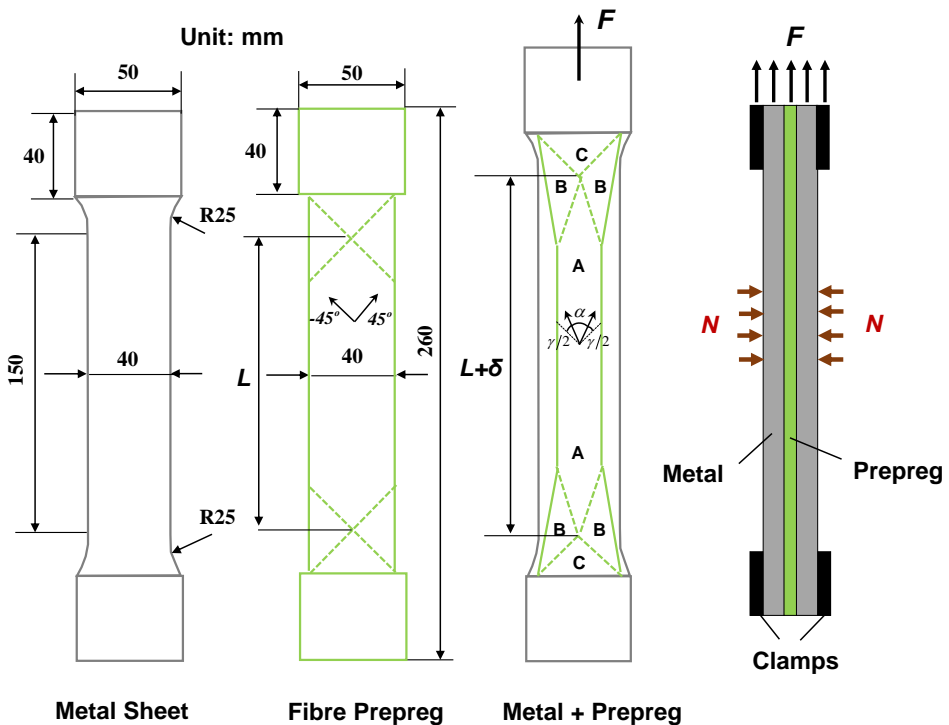


Figure 3.4: Schematic graph and dimension for the modified bias-extension test of metal-composite laminate

Here, L is the length of the pure shear region A, δ is the clamp displacement. The

shear angle in zone B is supposed to be half the value of zone A while zone C ideally has no effect on the overall deformation of the specimen. During deformation of the uncured laminate in the modified BE test, the strain in length direction for both materials is the same. In the transverse direction, however, the contraction of the metal sheet is (isotropy assumed) half of the lengthwise extension, while the contraction for the prepreg layer is equal to the lengthwise extension. This difference induces friction between the metal sheet and prepreg layer along both length and transverse direction. In addition, if a local pressure is applied on the central part of the pure shear region (40 mm \times 40 mm) as showed in Figure 3.4, the influence is twofold: possible wrinkling or wrinkling of the prepreg is suppressed, but also the intra-ply shear movement is hindered.

3.4. EXPERIMENTAL SETUPS

3.4.1. TEST CONDITIONS

THE modified bias-extension tests are performed on a Zwick-250kN tensile and compression machine equipped with a temperature chamber. The sample with the size and shape shown in Figure 3.4 is put into the tensile machine and clamped by the grips at two ends. Extensometers for measuring the tensile strains of metal sheets are used to determine the yield and elongation values at lower strains (<5%) of the specimen. The load-displacement curve for a given parameter combination can be obtained through the measurement system of the machine. The test temperature inside the chamber is preset at a ramp of 2°C/min and the real-time temperature is recorded by thermocouples. Other test parameters like clamp displacement rate and normal pressure can be altered by manual input and addition of an external tool. Figure 3.5 shows the experimental setups and apparatus for the modified BE tests used for three different pressure conditions. Next to the standard condition with no pressure applied on the forming region, the vacuum condition of 0.1 MPa and the autoclave condition of 0.6 MPa are conducted by a vacuum pump and a clamping loadcell, respectively [5], to put pressure on the forming regions.

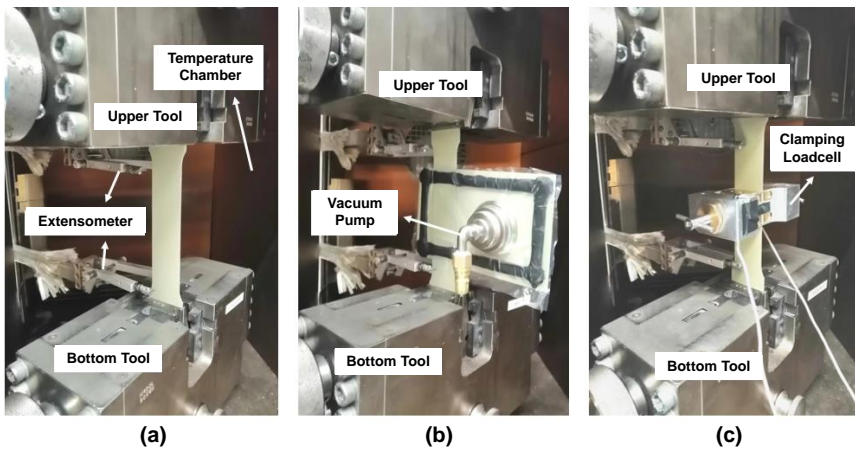


Figure 3.5: Experimental setups and apparatus for modified BE test used under various normal pressure conditions: (a) Standard condition; (b) Vacuum condition of 0.1 MPa; (c) Autoclave condition of 0.6 MPa

The material configurations and test conditions used for the modified bias-extension test are summarised in Table 3.1 and Table 3.2. The test for metal-composite laminate is performed with four combinations of material constituents and three different clamp displacement rates, three typical temperatures and three normal pressures. The tests are conducted varying one parameter at a time while keeping the other two parameters at their baseline value, and at least three samples are tested for each configuration. Two different fibre reinforced prepregs are characterised using the corresponding bias-extension test geometry under the same clamp displacement rate and preheat temperature conditions. These selected test conditions are based on the industrial conditions in material processing [4, 5] and are applied to investigate the influence of process parameters on the intra-ply shear performance, in particular the shear angle evolution during the modified BE test.

Table 3.1: Material configurations used for modified bias-extension test

Structure	Metal sheet	Fibre prepreg	Schematic graph
Hybrid laminate 2/1	Aluminium alloy Stainless steel	Cross-plyed UD Woven fabric	

Table 3.2: Test conditions used for modified bias-extension test

Test parameter	Baseline value	Additional values investigated
Clamp displacement rate (mm/min)	10	2, 20
Preheat temperature (°C)	23	50, 80
Normal pressure (MPa)	0	0.1, 0.6

3.4.2. SHEAR ANGLE MEASUREMENT

THE characterisation of the intra-ply shear behaviour of metal-composite laminates as well as their corresponding woven fabric and cross-plyed UD prepregs depend on an accurate shear angle measurement during the in-plane shear deformation. It has been expected that the prediction of shear angles in simulated bias-extension tests deviate from the experimentally measured shear angles during the course of shear deformation. Therefore, as the shear angle cannot directly be observed on the hybrid samples because of the metal sheets on the outside, it is critical to develop an experimental method which could measure the shear angle, particularly in the ‘pure shear region’ of the test specimens. For the pure fibre reinforced prepreg, the shear angle γ is obtained using a DIC (digital image correlation) measurement [23, 24]. The optical method is well suited for woven fabrics as the strain and fibre rotation on the specimen surface can be calibrated by the dual camera system in DIC. It is also applied for measuring the shear of cross-plyed UD prepreg as the strain and shear angle of the surface layer can be measured, assuming that the shear at the non-visible backside layer is symmetrical.

However, it is difficult to measure the intra-ply shear angles of the hybrid laminates because of the metal sheets covering the outer surfaces. One possible solution is to sep-

arate the layers after shear tests as the hybrid laminate is still uncured with low bonding performance. However, this method can only be performed at room temperature when no normal pressure is applied, since the degree of cure as well as the application of pressure may affect the fibre distributions and the surfaces. In order to visualise and evaluate the shear characterisation using the traditional measuring methodology, one side of metal sheet is removed from the sample after the tests. A second solution which is mainly applied in the study is the application of Alkaline Etching Method after curing [7, 41, 42]. The tested samples are first placed in a vacuum bag and transferred into an autoclave, and undergo a standard curing cycle with a maximum temperature of 120°C and a minimum cure time of an hour. After curing, the pure shear region ($40 \times 40 \text{ mm}^2$) is cut and one of the metal sheet layers is removed by etching using a 15% NaOH solution. To obtain a clear vision of fibre distributions, the dissolved specimens are ground and finally put on a digital microscope for the measurement of the shear angle. The latter method is rather robust since the movement of the fibres is minimal, and as the composite layers are cured and the outer metal layer is removed by etching, only rough grinding or other poor treatment may influence the fixed fibre shear angles. The entire testing sequence is shown in Figure 3.6 and the shear angles for various material constituents and processing parameters can be measured and compared from the samples.

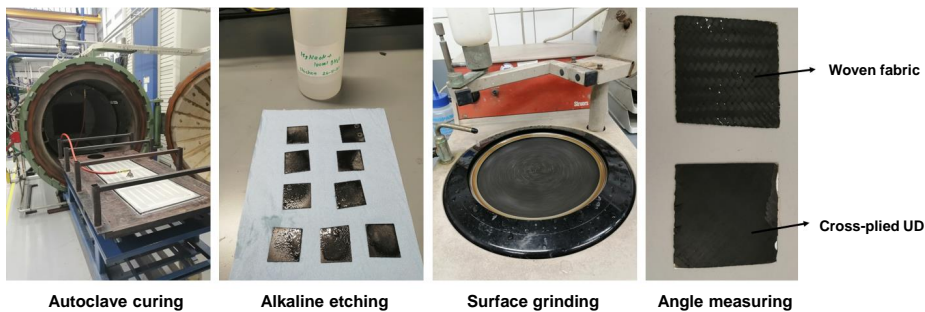


Figure 3.6: Whole process for the shear angle measurement of metal-composite laminates

3.5. RESULTS AND DISCUSSION

3.5.1. EFFECT OF FAILURE MODE

THE intra-ply shear behaviour for four metal-composite laminate combinations are analysed, and compared with their pure woven fabric and cross-plyed UD counterparts. The stress-strain curves for various material combinations under the condition of room temperature and 10mm/min clamp displacement rate are shown in Figure 3.7. It is noted that the main failure mode for both prepregs is fibre wrinkling even though the deformation mechanisms for woven fabric and cross-plyed UD fibres are different. However, the onset strain for wrinkling, which also relates to the locking angle, is different although the strain value is affected by test parameters such as clamp displacement rate and temperature as well as the difficulties for accurately define out-of-plane wrinkles in DIC. The two tangential slopes in the curve represent the shear modulus in the intra-ply shear and fibre wrinkling state. Therefore, the slope change occurs at

the shear-wrinkling transition point that defines the onset of fibre wrinkling. The result shows that the cross-plyed UD prepreg buckles earlier than the woven fabric prepreg under the same conditions. The reason is due to the fact that woven fabrics have bundles and the fibres are supported in the nodes, whereas the fibres in the UD material is not supported, which result in the earlier formation of the wrinkles. As the strain continues to increase after wrinkling, the final deformation limit for the cross-plyed UD prepreg is fibre splitting (>50%), which occurs when the shear force required for in-plane rotation is larger than the load transfer between the UD layers or within the fibre tows in a layer.

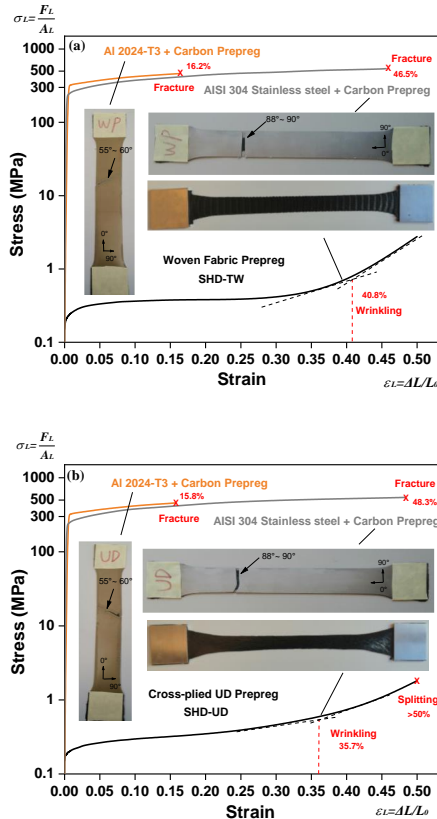


Figure 3.7: Stress and strain curves for different combination of hybrid as well as composite materials under the condition of room temperature and 10mm/min clamp displacement rate: (a) Based on woven fabric reinforced laminates; (b) Based on cross-plyed UD fibre reinforced laminates

The failure modes for the metal-composite laminates are shown in the Figure 3.7. The aluminium alloy 2024-T3 and AISI 304 stainless steel exhibits the failure strains of around 16% and 50%, respectively. The 45°/-45° hybrid materials with aluminium alloy 2024-T3 fracture along 55~60° direction corresponding to the direction of its maximum stress. When replacing the type of metal sheet for the hybrid materials to AISI 304 stainless steel, the laminate undergoes a fracture nearly perpendicular to the tensile stress

direction as plastic deformation grows in that region. Besides, the failure of aluminium-fibre reinforced laminate is introduced by the failure of the aluminium alloy 2024-T3 at the strain of around 16%. This is due to the fact the failure strain of the aluminum sheet is lower than the strain at which the fibre layers will buckle. While for the hybrid laminates with AISI 304 stainless steel, the failure of metal sheet with the combination of cross-ply UD prepreg and woven fabric prepreg undergo 48.3% strain and 46.5% on average, respectively. Since the onset strain of wrinkling for the two different prepregs is less than the above values, it can be deduced that the prepreg buckling occurs preceded metal failure for the stainless steel based hybrid laminates.

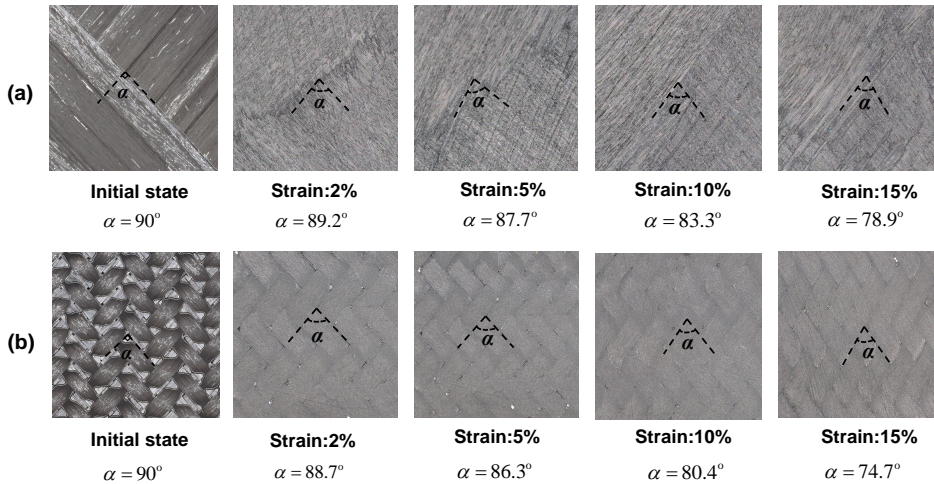


Figure 3.8: Microscopic measurements of the rotation angle (α) evolution for aluminium-fibre reinforced laminate under the condition of room temperature and 10mm/min clamp displacement rate: (a) Cross-ply UD structure; (b) Woven fabric structure

3.5.2. EFFECT OF MATERIAL CONSTITUENT

THE intra-ply shear angle in pure shear region after the modified bias-extension test is the most significant index for evaluating the intra-ply shear behaviour of metal-composite laminates. Figure 3.8 exhibits the intra-ply rotation angle evolution for the aluminium-fibre reinforced laminate at five typical strain stages under the condition of room temperature and 10mm/min clamp displacement rate using microscopic measurement as noted in Figure 3.6. The increase of strain decreases the rotation angle α between two initially perpendicular fibre tows, and thereby increasing the shear angle γ where $\gamma = 90^\circ - \alpha$. The result reveals that the hybrid woven fabric structure has a slightly larger decrease of rotation angle α , compared to the hybrid cross-ply UD structures. This is attributed to the different shear deformation mechanism of the two prepregs presented in Figure 3.9. Shearing of woven fabrics mainly involve in-plane rotation of the fibre tows at cross-over points of the weave especially under small strains and room temperature conditions. However, the kinematics of shear in cross-ply UD fibres are different from woven fabrics where the adjacent plies of the prepreg rotate and slide over each other and are only coupled through a viscous resin. Therefore, the shear

deformation for cross-ply UD fibres does not comply to the same PJN assumption that is used for woven fabrics as suggested by Potter [16, 17], and the higher inter-ply sliding ratio for cross-ply UD fibres results in a lower shear angle at the same strain.

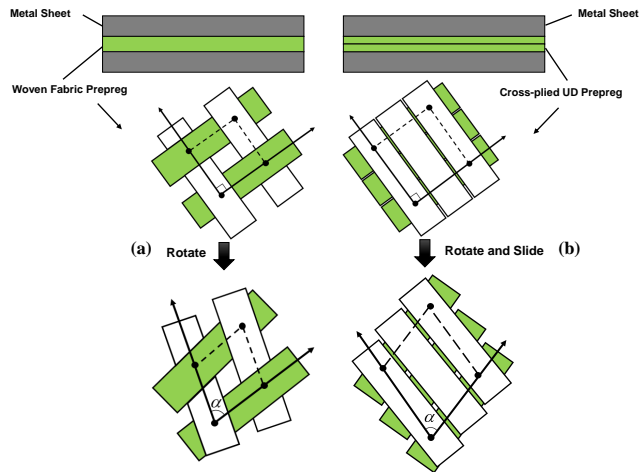


Figure 3.9: Shear deformation mechanism schematic of two different fibre prepregs:(a) Woven fabric; (b) Cross-ply UD fibres

Same trends are found when replacing the metal sheet from aluminium alloy to stainless steel and the value of shear angle γ witnesses a significant difference at higher shear strains. Figure 3.10 exhibits the average shear angle values for different combinations of the metal-composite laminates each at four shear strains within their respective strain ranges at room temperature and clamp displacement rate of 10mm/min. The results demonstrate that hybrid materials with woven fabric prepreg experience higher shear angles than hybrid materials with cross-ply UD prepreg at same shear strains. When the strain reaches 30% or even 45% , the measured shear angle for stainless steel-woven fabric reinforced laminate is almost twice the value for the same cross-ply UD type. The increasing gap of shear angles indicates that inter-ply sliding has a large influence at large strains for cross-ply UD prepregs. Even though both prepregs within the hybrid laminates have not reached their corresponding onset of wrinkling at 45% of strain, pure stretching instead of inter-tow rotation may occur for woven fabrics when the shear strain increases. This kind of stretching greatly decreases the deformability of the woven fabric reinforced stainless steel laminate and the inter-ply sliding of the UD prepregs explains why the stainless steel combined with cross-ply UD prepreg has larger failure strain. Besides, the four combinations which are all measured at 5% and 15% strain reveal that the stainless steel with both woven fabric prepreg and cross-ply UD prepreg exhibits somewhat lower shear angle when replacing the metal sheet to aluminium alloy. This can be observed in the stress-strain curve of the hybrid materials shown in Figure 3.7. At these two specific strains of 5% and 15%, the stress required to deform is higher for the aluminium alloy which increases the force for the fibre prepreg to shear. Therefore, the intra-ply shear angle is higher for aluminium-fibre reinforced laminate under the same strain although the difference is small.

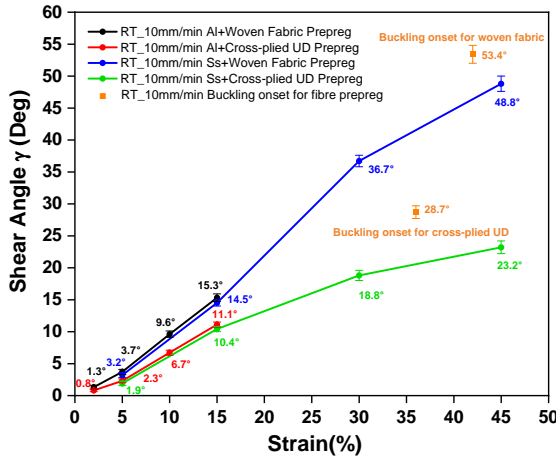


Figure 3.10: Shear angle and strain curves for different combinations of metal-composite laminates under the condition of room temperature and 10mm/min clamp displacement rate

3.5.3. EFFECT OF CLAMP DISPLACEMENT RATE

FIGURE 3.11 and 3.12 show the effect of clamp displacement rate for different combinations of material constituents compared with the theoretical PJN approach calculated by Equation 3.1. Shear angles for hybrid materials with aluminium alloy are measured at a lower strain range while the stainless steel-fibre reinforced laminates show a larger range of shear angles due to its higher failure strain. The figures reveal that the PJN assumptions seem to be valid only for woven fabric prepreg up to $20\sim 25^\circ$ which follows the result of Brands [26] and when the intra-ply shear angle reaches more than 25° , the theoretical and experimental values deviate from each other. For the cross-plyed UD prepreg, the shear angle deviates significantly under all ranges of shear strain because of the contribution of sliding at prepreg-prepreg interfaces as explained in Figure 3.9(b). However, the dominance of inter-ply sliding and the occurrence of pure stretching after the onset of wrinkling for the cross-plyed UD prepreg and woven fabric prepreg causes the stabilization of shear angles at large strains. Also, the results indicate that the shear angle increases with the increase of clamp displacement rate for different combinations of material constituents. This can be explained by the characterisation of viscous contribution of epoxy matrix where the shear stress increases with the increase of clamp displacement rate, and higher shear stress promotes more rotations of fibres to achieve the specified deformation. The result from Larberg [25] proves that the shear force increases with the increase of clamp displacement rate for cross-plyed UD prepreps and woven fabric prepreps [11, 14]. However, the effect of clamp displacement rate for the metal-composite laminate seems less sensitive compared to their corresponding prepreg. The reason can be attributed to the presence of a different force-transmitting mechanism and the increase of contact surfaces. For pure fibre reinforced prepreg like woven fabrics, the shear forces are transferred through fibre tows where very small variations in shear force lead to deformation of the prepreg. However, the shear forces for hybrid laminate are mainly transmitted from metal sheet to the woven fabric prepreg at the

metal-prepreg interfaces. The intrinsic slow force response of the metal sheet and the increased contact surfaces make it hard for the fibre tows to deform sensitively within the studied clamp displacement rate ranges as shown in Figure 3.13.

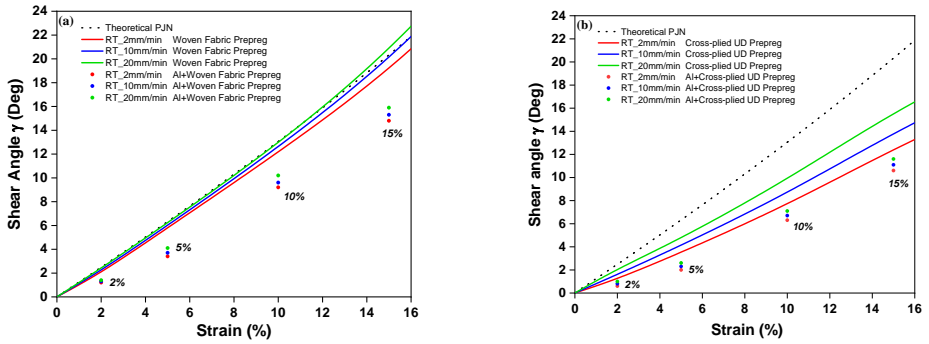


Figure 3.11: Shear angle and strain curves of aluminium-fibre reinforced laminate and its pure prepreg under different clamp displacement rates without normal pressure: (a) Woven fabric structure; (b) Cross-ply UD structure

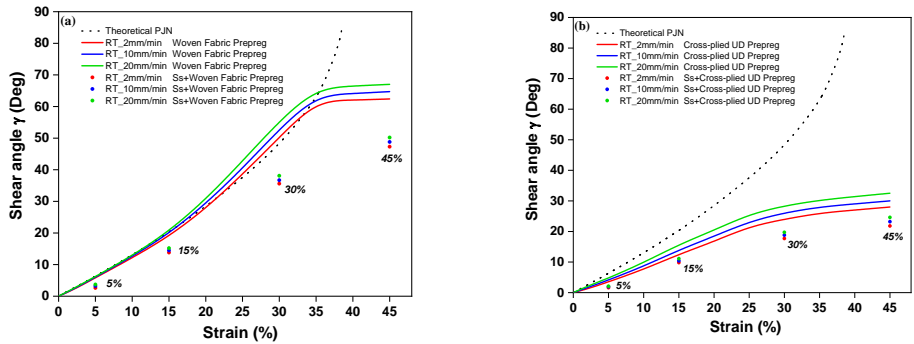


Figure 3.12: Shear angle and strain curves of stainless steel-fibre reinforced laminate and its pure prepreg under different clamp displacement rates without normal pressure: (a) Woven fabric structure; (b) Cross-ply UD structure

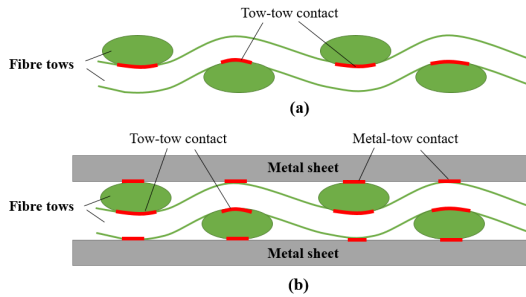


Figure 3.13: Schematic of the force transmitting and contact surfaces: (a) Woven fabric prepreg; (b) Metal-composite laminate

Another conclusion from the figures is that the shear angle values at specific strains for metal-composite laminates are lower than their corresponding prepregs. This indicates that the support of metal sheets reduces the shear deformation of fibre tows and thereby delays the onset of wrinkling. The decrease of shear angles for hybrid laminates is mainly due to the occurrence of friction at metal-prepreg interfaces and the different strain state for the metals and prepregs during shearing. Figure 3.14 shows the test specimens for the pure prepreg and a one-side metal-composite laminate at the shear strain of 30%. The initial width for all materials on the pure shear zone is 40 mm, but it changes as the elongation of the specimen increases. The width for the stainless steel drops to 36.7 mm, while for the attached cross-ply UD and woven fabric prepreg width drop to 31.8 mm and 28.9 mm, respectively. After comparing to their corresponding pure prepreg shear under the same condition, it is obvious to validate the fact that the outer metal sheet limits the fibre deformation by inducing the inter-ply friction. Meanwhile, the pure prepregs are free to move or deform through the thickness direction where they are greatly constrained for the hybrid structures. Moreover, another interesting phenomenon for woven fabric reinforced stainless steel laminate in Figure 3.14 is that the shear of woven fabric does not seem to follow the theoretical PJN approach, where the widths of the assumed 'half shear' and 'undeformed' regions (circled in the figure) are smaller than the 'pure shear' region. The smaller width results in a higher shear angle and can be attributed to the fact that the fibre tows are clamped close to the tabs where a tensile force can be transmitted, while the fibres in the middle of the specimen have freedom to move as both ends are not clamped. Therefore, due to the relatively low force transfer in the assumed 'pure shear' region of the woven fabric, the displacement of the prepreg become less in this region under the same friction conditions. Furthermore, the smaller width for woven fabric prepreg shown in the figure further validates that cross-ply UD fibres are even more 'free' than the woven fabrics.

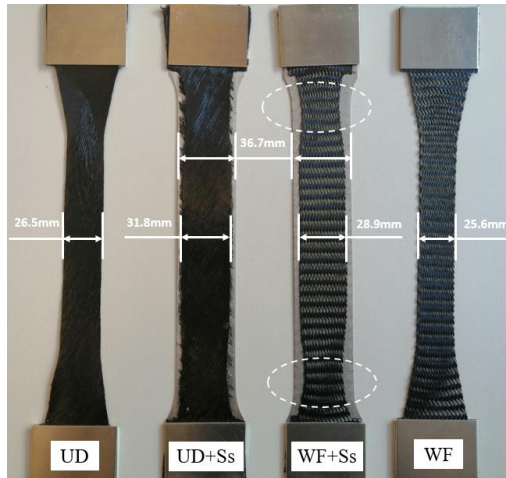


Figure 3.14: Picture of test-specimens to the shear strain of 30% at room temperature for different material combinations without normal pressure (UD-Cross-plyed unidirectional fibre prepreg, WF-Woven fabric prepreg, Ss-Stainless steel)

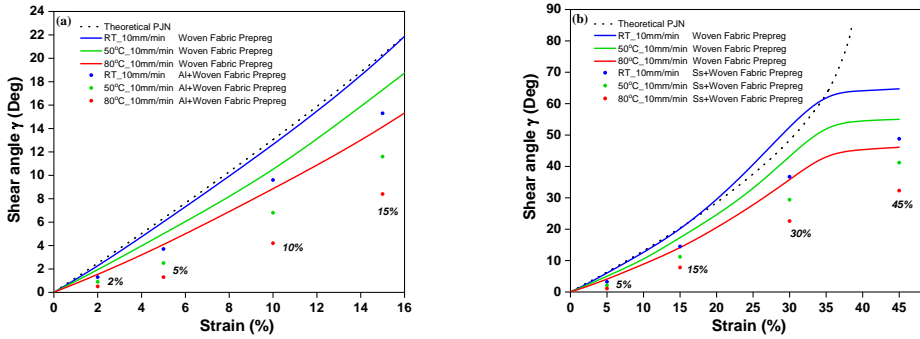


Figure 3.15: Shear angle and strain curves of woven fabric reinforced-metal laminate and its pure prepreg under different preheat temperatures without normal pressure: (a) Aluminium alloy structure; (b) Stainless steel structure

3.5.4. EFFECT OF PREHEAT TEMPERATURE

PREHEAT temperature is also one of the key factors which affects the intra-ply shear performance by altering the epoxy resin viscosity. In this research, the resin viscosity decreases with the increase of preheat temperature from room temperature (23°C) to the temperature of 80°C. The residual thermal effects are ignored as the degree of cure is low under these time and temperatures. Figure 3.15 shows the effect of preheat temperature on shear angles for woven fabric prepreg and its reinforced hybrid laminates compared to the theoretical PJN assumption calculated by Equation 3.1. The deviation of PJN behaviour for woven fabric prepreg gradually increases at higher temperature and is even larger for its reinforced hybrid laminate with aluminium alloy and stainless steel structure. The increased deviation suggests that the significant drop in resin viscosity at high temperatures triggers other deformation mechanisms than just pure shear. As the intra-ply shear angle decreases with the increase of preheat temperature for woven fabric reinforced metal laminates and their prepreg constituent, it can be concluded that an increased inter-tow slippage at higher temperature for the woven fabric prepreg affects the shear. This can also be found from Khan's research [15] that the elevated temperature testing of woven prepreg promotes inter-tow slippage and higher temperature leads to earlier deviation from PJN assumptions. As depicted in Figure 3.16(a) that the kinematic assumption of PJN theory is well maintained at room temperature for the woven fabric prepreg as the viscous resin acts like a pin at cross-over points and the inter-tow slippage is limited. When increasing the temperature, the decreasing resin viscosity lowers the stiffness of the material in shear deformation and inter-tow slippage tends to occur. To validate the existence of inter-tow slippage at high temperature, test specimens in actual shear response of 30% strain for woven fabric prepreg at room temperature (RT) and 80°C are presented on the right side of Figure 3.17. It is found that the width of the pure shear region at RT is relatively small compared to the width when tested at 80°C. A close-up view of the central shear region shows that the intra-ply rotation angle α is higher at higher temperature (80°C) and this indicates that inter-tow slippage becomes much easier with less viscous resin displacing out of the fibre tows and the overall re-

sistance towards intra-ply shear decreases. Besides, Figure 3.15 reveals that the values of shear angle at specific strains for hybrid laminates with woven fabric are lower and the effect of preheat temperature is more sensitive compared to the pure woven fabric prepreg. The support of metal sheet creates more friction at metal-prepreg interfaces which restricts the rotation of fibre tows, however, the elevation of temperature lowers such inter-ply friction and thus decreases the intra-ply shear angles.

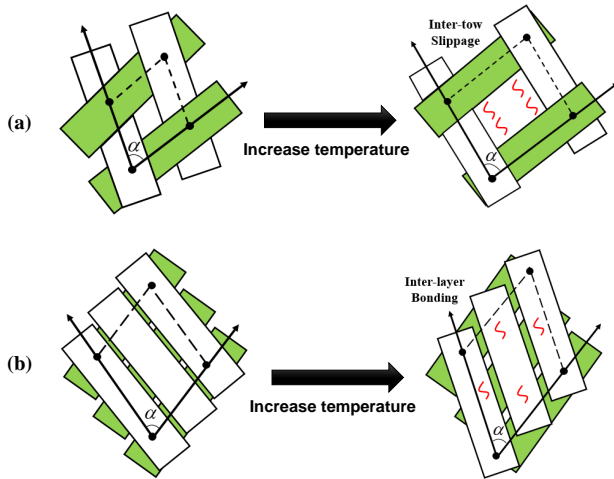


Figure 3.16: Shear deformation of two different prepregs at higher temperature:(a) Woven fabric; (b) Cross-plyed UD

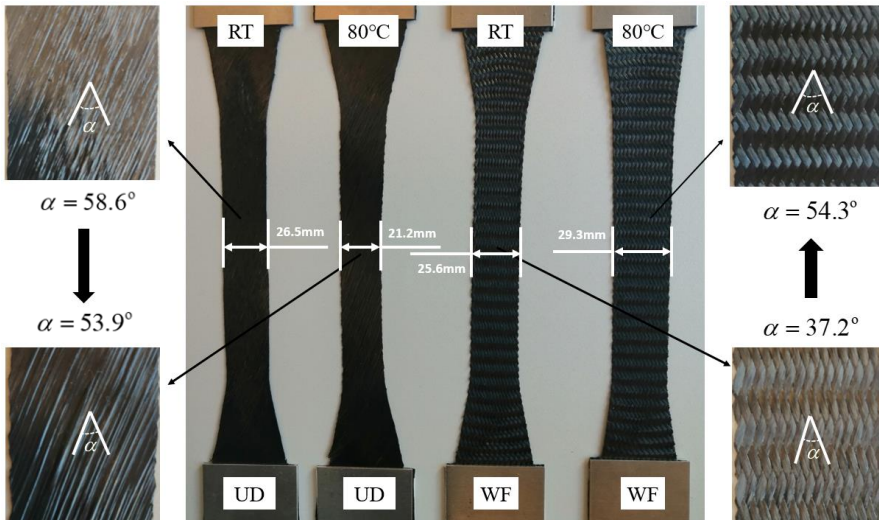


Figure 3.17: Picture of test-specimens to the shear strain of 30% at room temperature and 80°C for pure composite prepregs (UD-Cross-plyed unidirectional fibre prepreg, WF-Woven fabric prepreg)

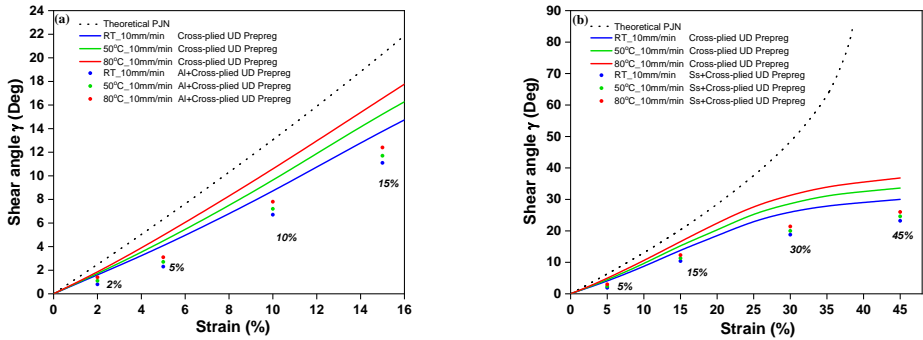


Figure 3.18: Shear angle and strain curves of cross-plyed UD reinforced-metal laminate and its pure prepreg under different preheat temperatures without normal pressure: (a) Aluminium alloy structure; (b) Stainless steel structure

The temperature trends are interestingly contrasting for the cross-plyed UD prepreg and its reinforced metal laminates under the same conditions. As shown in Figure 3.18, the PJN behaviours are invalid for all cross-plyed UD type of materials while the increase of preheat temperature makes it more closer to the theoretical PJN curve. The increase in shear angle as the temperature increases is mainly due to the different shear behaviour of UD materials compared to woven fabrics. As mentioned in the previous section, there are no physical links enabling the PJN kinematics for the cross-plyed UD layers at room temperature and rotation is allowed through the viscous resin. At higher temperature like 80°C, the viscosity of the resin decreases and reduces its capability as a lubricant between the plies, and thus providing more opportunities for the frictional interaction between the cross-plyed UD fibres. This kind of quasi-physical linking can act like the PJN approach, and increase the shear angle at higher temperature. The same observation is found in the literature [15] that maximum shear angles at elevated temperature are higher than those at RT as the viscous resin provides more contact between UD layers. The schematic graph in Figure 3.16(b) reveals that although the increasing temperature accelerates the slide at prepreg-prepreg interfaces, the dominance of inter-layer bonding increases the shear angle. The test specimens for cross-plyed UD prepreg shown in Figure 3.17 exhibit that the intra-ply rotation angle α decreases as the temperature increases. Meanwhile, it is measured that the specimen width is narrow for the cross-plyed UD prepreg at 80°C and a close-up view of the central shear region witnesses obvious fibre wrinkling due to the occurrence of higher shear angle α at this temperature. The shear angle for the cross-plyed UD fibre reinforced metal laminates follows the same trend as their pure cross-plyed UD prepreg, despite the lower value of intra-ply shear angle at specific strains. The reason can also be explained by the less fibre rotation because of the occurrence of friction at the metal-prepreg interfaces. However, the result from Figure 3.18 reveals that the effect of temperature is no longer sensitive for the cross-plyed UD fibre reinforced metal laminates as the decreasing friction at the metal-prepreg and prepreg-prepreg interfaces conflicts with the inter-ply bonding of UD fibres at high temperatures.

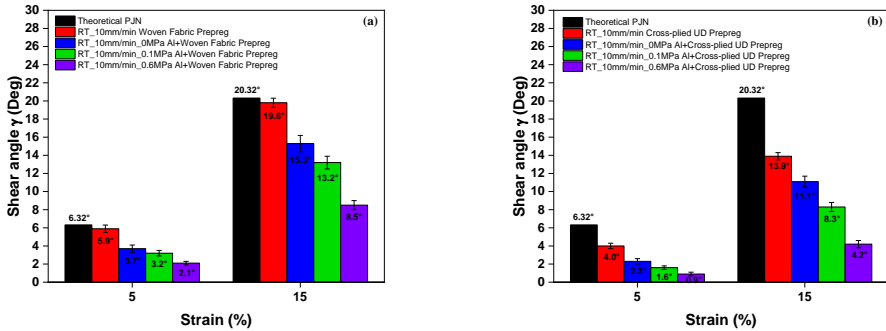


Figure 3.19: Shear angle values at two strains for aluminium alloy-fibre reinforced laminate and its pure prepreg under different normal pressures: (a) Woven fabric structure; (b) Cross-plyed UD structure

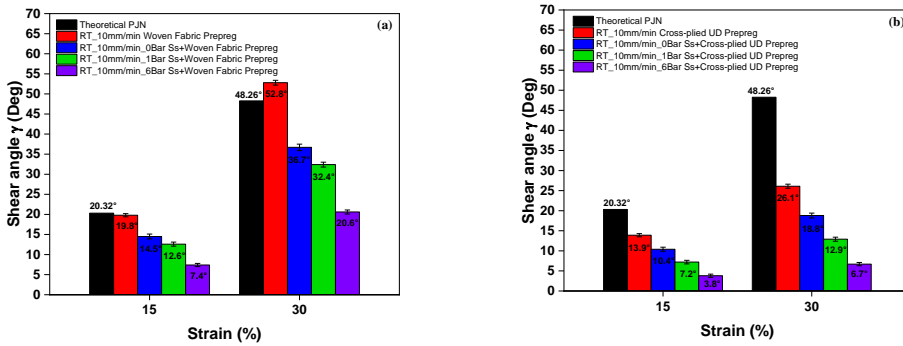


Figure 3.20: Shear angle values at two strains for stainless steel-fibre reinforced laminate and its pure prepreg under different normal pressures: (a) Woven fabric structure; (b) Cross-plyed UD structure

3.5.5. EFFECT OF NORMAL PRESSURE

NORMAL pressure is not taken into account for the shear of fibre reinforced prepregs through bias-extension test, while the influence of normal pressure is vital for the investigation of intra-ply shear characterisation of metal-composite laminates to obtain a situation which will be relevant for forming experiments. Figure 3.19 and 3.20 exhibit the values of shear angle at two different shear strains for the aluminium alloy and stainless steel based fibre reinforced laminates under different normal pressure conditions. The results are also compared with the theoretical P.J.N method and their pure fibre reinforced prepreg to understand how it affects the intra-ply shear behaviour. The result indicates that the support of metal sheet and normal pressure greatly decrease the shear angle of fibre reinforced prepregs for both woven fabric and cross-plyed UD types at the same strain. As mentioned in previous section that the outer metal sheet induces friction between the metal and prepreg layers, the increase of normal pressure further increases the friction and lowers the shear deformation of the prepreg layers. Furthermore, the hybrid metal-composite laminates with cross-plyed UD structure shown in Figure 3.19(b) and 3.20(b) are more sensitive to normal pressure at different levels of strain as com-

pared with hybrid woven fabric structures shown in Figure 3.19(a) and 3.20(a). The decrease of shear angle for woven fabric reinforced metal laminate is less than 15% and 45% under the normal pressure of 0.1 MPa and 0.6 MPa, while the shear angle reduction for the hybrid cross-ply UD structures is more than 30% and 60%, respectively. This demonstrates that the frictional response is much higher for the hybrid cross-ply UD structures as more resin squeezes out from the prepreg-prepreg interface to the metal-prepreg interface as the normal pressure increases. Besides, the UD material has smooth and flat contact surfaces with the metal, whereas the contact surface of the woven fabric is much more rough. Therefore, further compaction of the hybrid laminates seems impossible because the inter-ply friction would largely increase and damage may occur when the fibres have direct contact with the metal surface. The specimens shown in Figure 3.21 corroborate the explanation that the two cross-ply UD layers undergo higher friction resulting in a larger width coupled with the hard-to-move fibre tows. The unpressurised shear regions (Circled in the figure) undergo higher shear deformation than the specimen applied without normal pressure; in this situation the shear deformation is concentrated in these regions. The result makes it abundantly clear that the application of normal pressure has a huge effect on the shear properties of metal-composite laminates.

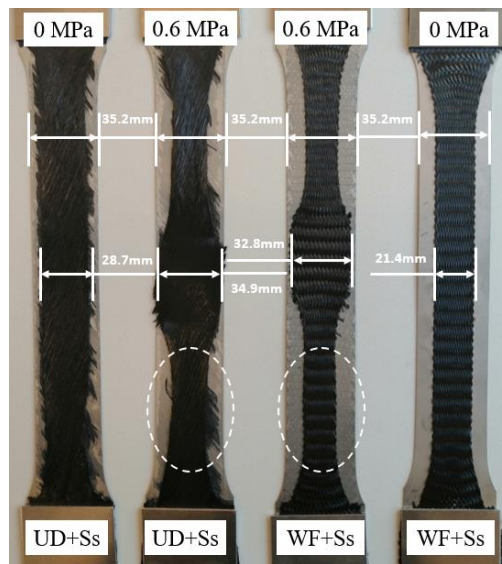


Figure 3.21: Picture of test-specimens to the shear strain of 45% at RT under two normal pressures for hybrid laminates (UD-Cross-plyed unidirectional fibre prepreg, WF-Woven fabric prepreg, Ss-Stainless steel)

3.6. CONCLUSIONS

THE intra-ply shear angle which is the evaluation parameter in the in-plane shear characterisation for the metal-composite laminate has been measured using a modified bias-extension test. Various combinations of material constituents as well as the influenced processing parameters such as clamp displacement rate, preheat temperature

and normal pressure are investigated and compared. The results indicate that the shear mechanism of woven fabrics and cross-ply UD fibres is different and intra-ply shear deformability of the hybrid materials is highly controlled by the viscosity state of epoxy resin and the application of external normal pressure. These parameters have huge effects on a number of output parameters like fibre shear stress, shear angle, inter-tow and inter-ply sliding. This chapter contributes to the material selection, process design and modelling for the forming of double-curved products by metal-composite laminates. It can be concluded that:

(1) The support of metal sheets generally decrease the shear angles in the modified BE test due to the differences in contraction between metal sheet and composite layers, and the variations in shear angles for hybrid laminates are mainly caused by the friction at the metal-prepreg interface. The intra-ply shear deformability of the fibre reinforced stainless steel laminate can be greatly improved as the failure strain increases 5~10% with the delay of fibre wrinkling.

(2) The effects of clamp displacement rate and preheat temperature on the shear angles of metal-composite laminate follow the trends of their corresponding prepregs. The shear angles increase with the increasing clamp displacement rate for all material combinations while the growth is less sensitive (<5%) at various shear strains especially for hybrid laminates. However, the effect of preheat temperature differs in two prepreg systems. The shear angles decrease with the increasing preheat temperature for pure woven fabrics and the reduction for woven fabric reinforced metal laminate is becoming larger (>20%). But the shear angle undergoes an increase as the temperature increases for cross-ply UD structures especially for the cross-ply UD reinforced metal laminates (<10%).

(3) The shear angles show a sharp decrease when applying the normal pressure on the central shear region. The decrease of shear angle for woven fabric reinforced metal laminate is 15% and 45% under the normal pressure of 0.1 MPa and 0.6 MPa, while the shear angle reduction for the hybrid cross-ply UD structures is 30% and 60%, respectively. The maximum value for the applied normal pressure is 6 bar as it may cause defects or even damages for the hybrid materials. Besides, it is better to apply the normal pressure on the entire shear region rather than the central region, which is more realistic for practical applications.

(4) The pure PJN approach is only valid for the woven fabric prepreg to a shear angle of up to 20~25° and the woven fabric reinforced metal laminates are more suitable to deform under low strain conditions. And for the hybrid material deforming under large strain conditions, cross-ply UD reinforced metal laminates are more favourable. Even though the size and edge effects of the metal sheet and fibre prepreg are not considered in the modified bias-extension test, this chapter provides good insights on the press forming of uncured hybrid laminates which is relevant for material selection and process optimization.

REFERENCES

- [1] T. Sinmazçelik, E. Avcu, M. Ö. Bora, and O. Çoban, "A review: Fibre metal laminates, background, bonding types and applied test methods," *Materials & Design*, vol. 32,

- no. 7, pp. 3671–3685, 2011.
- [2] D. Nardi, M. Abouhamzeh, R. Leonard, and J. Sinke, “Investigation of kink induced defect in aluminium sheets for glare manufacturing,” *Composites Part A: Applied Science and Manufacturing*, vol. 125, p. 105531, 2019.
- [3] M. A. Khan, N. Reynolds, G. Williams, and K. N. Kendall, “Processing of thermoset prepregs for high-volume applications and their numerical analysis using superimposed finite elements,” *Composite Structures*, vol. 131, pp. 917–926, 2015.
- [4] J. Sinke, “Feasibility of tailoring of press formed thermoplastic composite parts,” in *AIP Conference Proceedings*, vol. 1960, AIP Publishing, 2018.
- [5] S. Liu, J. Sinke, and C. Dransfeld, “An inter-ply friction model for thermoset based fibre metal laminate in a hot-pressing process,” *Composites Part B: Engineering*, vol. 227, p. 109400, 2021.
- [6] A. Kubit, T. Trzepieciniski, M. Kłonica, M. Hebda, and M. Pytel, “The influence of temperature gradient thermal shock cycles on the interlaminar shear strength of fibre metal laminate composite determined by the short beam test,” *Composites Part B: Engineering*, vol. 176, p. 107217, 2019.
- [7] M. Megahed, M. Abd El-baky, A. Alsaedy, and A. Alshorbagy, “An experimental investigation on the effect of incorporation of different nanofillers on the mechanical characterization of fiber metal laminate,” *Composites Part B: Engineering*, vol. 176, p. 107277, 2019.
- [8] Q. Chen, P. Boisse, C. H. Park, A. Saouab, and J. Bréard, “Intra/inter-ply shear behaviors of continuous fiber reinforced thermoplastic composites in thermoforming processes,” *Composite structures*, vol. 93, no. 7, pp. 1692–1703, 2011.
- [9] S. Erland and T. Dodwell, “Quantifying inter-and intra-ply shear in the deformation of uncured composite laminates,” *Advanced Manufacturing: Polymer & Composites Science*, vol. 7, no. 2, pp. 25–35, 2021.
- [10] T. Mattner, M. Wrensch, and D. Drummer, “Shear behavior of woven and non-crimp fabric based thermoplastic composites at near-processing conditions,” *Composites Part B: Engineering*, vol. 185, p. 107761, 2020.
- [11] J. Cao, R. Akkerman, P. Boisse, J. Chen, H. Cheng, E. De Graaf, J. Gorczyca, P. Harrison, G. Hivet, J. Launay, *et al.*, “Characterization of mechanical behavior of woven fabrics: Experimental methods and benchmark results,” *Composites Part A: Applied Science and Manufacturing*, vol. 39, no. 6, pp. 1037–1053, 2008.
- [12] H. Alshahrani, R. Mohan, and M. Hojjati, “Experimental investigation of in-plane shear deformation of out-of-autoclave prepreg,” *Int. J. Compos. Mater.*, vol. 5, no. 4, pp. 81–87, 2015.

- [13] P. Wang, X. Legrand, P. Boisse, N. Hamila, and D. Soulat, "Experimental and numerical analyses of manufacturing process of a composite square box part: Comparison between textile reinforcement forming and surface 3d weaving," *Composites Part B: Engineering*, vol. 78, pp. 26–34, 2015.
- [14] M. Khan, C. Pasco, N. Reynolds, and K. Kendall, "Shear deformability characteristics of a rapid-cure woven prepreg fabric," *International Journal of Material Forming*, vol. 14, pp. 133–142, 2021.
- [15] M. A. Khan, C. Pasco, N. Reynolds, and K. N. Kendall, "On the validity of bias-extension test method for the characterisation of in-plane shear properties of rapid-cure prepregs," *Composite Structures*, vol. 246, p. 112399, 2020.
- [16] K. Potter, "Bias extension measurements on cross-plyed unidirectional prepreg," *Composites Part A: Applied Science and Manufacturing*, vol. 33, no. 1, pp. 63–73, 2002.
- [17] K. Potter, "Beyond the pin-jointed net: maximising the deformability of aligned continuous fibre reinforcements," *Composites Part A: Applied Science and Manufacturing*, vol. 33, no. 5, pp. 677–686, 2002.
- [18] S. Haanappel and R. Akkerman, "Shear characterisation of uni-directional fibre reinforced thermoplastic melts by means of torsion," *Composites Part A: Applied science and manufacturing*, vol. 56, pp. 8–26, 2014.
- [19] Y. Larberg and M. Åkermo, "In-plane deformation of multi-layered unidirectional thermoset prepreg—modelling and experimental verification," *Composites Part A: Applied Science and Manufacturing*, vol. 56, pp. 203–212, 2014.
- [20] G. Lebrun, M. N. Bureau, and J. Denault, "Evaluation of bias-extension and picture-frame test methods for the measurement of intraply shear properties of pp/glass commingled fabrics," *Composite structures*, vol. 61, no. 4, pp. 341–352, 2003.
- [21] P. Harrison, M. J. Clifford, and A. Long, "Shear characterisation of viscous woven textile composites: a comparison between picture frame and bias extension experiments," *Composites science and technology*, vol. 64, no. 10-11, pp. 1453–1465, 2004.
- [22] I. Taha, Y. Abdin, and S. Ebeid, "Comparison of picture frame and bias-extension tests for the characterization of shear behaviour in natural fibre woven fabrics," *Fibers and Polymers*, vol. 14, pp. 338–344, 2013.
- [23] P. Boisse, N. Hamila, E. Guzman-Maldonado, A. Madeo, G. Hivet, and F. Dell'Isola, "The bias-extension test for the analysis of in-plane shear properties of textile composite reinforcements and prepregs: a review," *International Journal of Material Forming*, vol. 10, pp. 473–492, 2017.
- [24] A. Rashidi, H. Montazerian, and A. Milani, "Slip-bias extension test: A characterization tool for understanding and modeling the effect of clamping conditions in forming of woven fabrics," *Composite Structures*, vol. 260, p. 113529, 2021.

- [25] Y. R. Larberg, M. Åkermo, and M. Norrby, "On the in-plane deformability of cross-plyed unidirectional prepreg," *Journal of composite materials*, vol. 46, no. 8, pp. 929–939, 2012.
- [26] D. Brands, W. Grouve, S. Wijskamp, and R. Akkerman, "Intra-ply shear characterization of unidirectional fiber reinforced thermoplastic tape using the bias extension method," *ESAFORM MS02(Composites)*, 2021.
- [27] Y. Wang, M. K. Chea, J. P.-H. Belnoue, J. Kratz, D. S. Ivanov, and S. R. Hallett, "Experimental characterisation of the in-plane shear behaviour of ud thermoset prepreps under processing conditions," *Composites Part A: Applied Science and Manufacturing*, vol. 133, p. 105865, 2020.
- [28] ASTM-E8/E8M, "Standard test methods for tension testing of metallic materials," *Annual Book of ASTM Standards*, pp. 1–27, 2010.
- [29] A. Hannon and P. Tiernan, "A review of planar biaxial tensile test systems for sheet metal," *Journal of materials processing technology*, vol. 198, no. 1-3, pp. 1–13, 2008.
- [30] A. Abedini, J. Noder, C. Kohar, and C. Butcher, "Accounting for shear anisotropy and material frame rotation on the constitutive characterization of automotive alloys using simple shear tests," *Mechanics of Materials*, vol. 148, p. 103419, 2020.
- [31] J. Peirs, P. Verleysen, and J. Degrieck, "Novel technique for static and dynamic shear testing of ti6al4v sheet," *Experimental mechanics*, vol. 52, pp. 729–741, 2012.
- [32] T. Rahmaan, A. Abedini, C. Butcher, N. Pathak, and M. J. Worswick, "Investigation into the shear stress, localization and fracture behaviour of dp600 and aa5182-o sheet metal alloys under elevated strain rates," *International Journal of Impact Engineering*, vol. 108, pp. 303–321, 2017.
- [33] Q. Yin, C. Soyarslan, K. Isik, and A. E. Tekkaya, "A grooved in-plane torsion test for the investigation of shear fracture in sheet materials," *International Journal of Solids and Structures*, vol. 66, pp. 121–132, 2015.
- [34] B.-E. Lee, E.-T. Park, J. Kim, B.-S. Kang, and W.-J. Song, "Analytical evaluation on uniaxial tensile deformation behavior of fiber metal laminate based on srpp and its experimental confirmation," *Composites Part B: Engineering*, vol. 67, pp. 154–159, 2014.
- [35] A. P. Sharma, S. H. Khan, and V. Parameswaran, "Experimental and numerical investigation on the uni-axial tensile response and failure of fiber metal laminates," *Composites Part B: Engineering*, vol. 125, pp. 259–274, 2017.
- [36] M. S. Maryan, H. Ebrahimnezhad-Khaljiri, and R. Eslami-Farsani, "The experimental assessment of the various surface modifications on the tensile and fatigue behaviors of laminated aluminum/aramid fibers-epoxy composites," *International Journal of Fatigue*, vol. 154, p. 106560, 2022.

- [37] Y. Chen, Y. Wang, and H. Wang, "Research progress on interlaminar failure behavior of fiber metal laminates," *Advances in Polymer Technology*, vol. 2020, pp. 1–20, 2020.
- [38] A. Rajpurohit, S. Joannès, V. Singery, P. Sanial, and L. Laiarinandrasana, "Hybrid effect in in-plane loading of carbon/glass fibre based inter-and intraply hybrid composites," *Journal of Composites Science*, vol. 4, no. 1, p. 6, 2020.
- [39] H. Do Kweon, J. W. Kim, O. Song, and D. Oh, "Determination of true stress-strain curve of type 304 and 316 stainless steels using a typical tensile test and finite element analysis," *Nuclear Engineering and Technology*, vol. 53, no. 2, pp. 647–656, 2021.
- [40] SHD-Composite-Materials, "Technical datasheet for the mtc510 epoxy prepreg," <https://shdcomposites.com/admin/resources/mtc510-tds.pdf>, 2018.
- [41] D. Mamalis, W. Obande, V. Koutsos, J. R. Blackford, C. M. Ó. Brádaigh, and D. Ray, "Novel thermoplastic fibre-metal laminates manufactured by vacuum resin infusion: the effect of surface treatments on interfacial bonding," *Materials & Design*, vol. 162, pp. 331–344, 2019.
- [42] Y. Zhao, Y. Gu, T. Zhang, H. Li, B. Zhang, and Z. Zhang, "Characterization of intra-ply shear behaviors of unidirectional prepreps during hot diaphragm forming process," *Polymer Composites*, vol. 42, no. 2, pp. 1008–1020, 2021.

4

A CLAMPED-BEAM BENDING TEST METHOD FOR LAMINATE FLEXURAL BEHAVIOUR

In this chapter, flexural behaviour of uncured metal-CFRP laminates under clamped-beam bending conditions is investigated with various local pressures. The test method is designed to evaluate the effect of clamping on the ratio between stretching and drawing of the laminate deformation during a proposed press forming process. The variations of laminate structure including metal constituents, layup and fibre orientation, as well as processing temperature on the evolution of bending force, spring-back depth and length of laminate sliding are measured and compared. The results indicate that the increase of clamping pressure reduces the sliding, causing higher plastic strain in the metal layers and a lower spring-back. Moreover, the flexural behaviour of uncured hybrid laminates depends mainly on its constituents, where the maximum bending force is the largest for aluminium based materials with higher overall thickness. The fibre orientation and processing temperature affect the properties of CFRP material, while an increase of intra-ply shear within the prepregs and a decrease of inter-ply friction at the interfaces play a limited role. Furthermore, the numerical and experimental results show a good correlation at room temperature with various clamping pressures for the studied materials. This study contributes to a better understanding of the bendability during the press forming process for uncured metal-CFRP laminates.

4.1. INTRODUCTION

IN recent years, new lightweight materials with excellent mechanical properties have attracted the interest of many scholars in the field of aircraft manufacturing. Metal-composite laminates, also known as fibre metal laminates (FMLs), are one of those materials, made by alternating layers of thin metal alloy sheets and fibre reinforced polymers [1, 2]. The hybrid laminate combines the advantages of metallic materials and fibre reinforced matrix systems with its significant weight reduction, high specific strength and stiffness, as well as other excellent properties like better fatigue and corrosion resistance [3–5]. As a kind of hybrid material, the metal-composite laminate has multiple-interfaces consisting of the interfaces of fibre-metal sheet, fibre-matrix and the matrix-metal sheet. However, these interfaces are sensitive to delamination due to the external loading like bending and torsion. Therefore, the manufacturing process of metal-composite laminate is difficult as various forming and curing stages are required involving complex deformation and failure mechanisms [6–8].

In order to improve the manufacturability of such hybrid materials, an integral forming and curing cycle is proposed in Figure 1.8 which includes the stages of preheating before and curing of the laminates after a press forming process. Time and temperature are carefully controlled during the preheating stage, so that the inter-ply sliding at the metal-prepreg interfaces and the intra-ply shear within the prepregs are greatly enhanced as the resin viscosity decreases [9–12]. In addition, the still uncured laminate is formed and subsequently cured, thereby avoiding extra process steps like unloading and reloading in a separate curing system with lower pressure, which can be time-saving and cost-saving [13, 14]. Moreover, the advantages such as interlaminar bonding enhancement in such cycles are attractive especially for the small and medium sized components with special-shaped geometry [15, 16]. The press forming of such laminate geometries is a combination of bending, stretching and drawing which results in multiple in-plane and out-of-plane deformations. Therefore, the flexural properties of the individual layers and the ability to simultaneously bend at the metal-composite interfaces, is the topic of the research.

4.2. LITERATURE ON LAMINATE BENDING

BENDING is a manufacturing process that produces the V-shape, U-shape or channel shape parts along a straight axis in ductile materials, most commonly metal sheet. The bending over a non-straight axis is beyond the scope of the research although it is a common element in three-dimensional (3D) manufacturing. Among the test methods for the characterisation of material bending behaviour, three-point bending is the most frequently used flexural test which involves a specified test fixture on a universal testing machine. This method provides values for the flexural modulus, bending stress-strain responses of the material, etc [17–19]. The four-point bending test is similar to the three-point bending test while the main difference is that the centre section of the beam between the two inside load bearing points is under constant stress without shear. Advantages for both test methods consist of simple sample geometries and test fixtures, and the possibility to use as-fabricated materials. However, one of the disadvantages for four-point flexural test are the complex stress-strain distribution through the sample

[20]. The two methods for the evaluation of the bending properties are also applied for the fibre reinforced composite materials, although most studies regard the bending behaviour for such composites as unimportant due to the fact that the bending stiffness is small compared to the in-plane shear/tension stiffness. Also, many studies found that the bending stiffness of the fibre reinforced composites should be considered as it may play a critical role on the formation of wrinkling during forming [21–23].

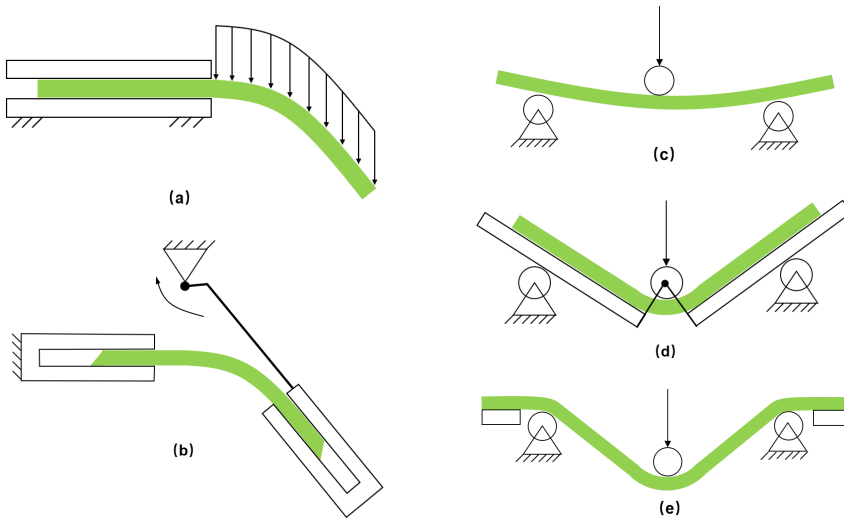


Figure 4.1: Setups for the characterisation of bending behaviour for fibre reinforced composites: (a) Cantilever test based, (b) Kawabata test based and (c)-(e) Vee-bending test based methods

Therefore, various test methods are developed for fibre reinforced composites, and the three main types of bending coupled with temperature for the carbon fibre reinforced polymer (CFRP) are shown in Figure 4.1. The cantilever test set up has one end fixed and the other end free, which results in a free radius after bending. Liang et al. [24] improved the cantilever test with an environmental chamber to study the effect of temperature on bending stiffness. However, the influence of weight itself cannot be avoided in this method and a “vertical” cantilever test would be a better solution to overcome the issues. The Kawabata test based approach, as presented in Figure 4.1(b), was designed to characterise the bending behaviour of the continuously fibre reinforced composites for either a UD or a woven reinforcement. The approach aims to test the bending moment by imposing a constant radius on the specimen through the rotation of a clamp [25]. Sachs et al. [26] proposed an improved test method including a standard rheometer and an environmental chamber to evaluate the rate-dependency as well as the temperature-dependent bending behaviour of UD tapes. The results mentioned that the test setup was highly suitable for the bending characterisation, especially for large curvature deformation. Moreover, the Vee-bending test method based on the three-point bending test setup for characterising the bending behaviour of CFRP fabricated with UD tapes was illustrated in Figure 4.1(c). This method was further improved by controlling the deformation of the specimen under two certain geometric supports [27], as presented in

Figure 4.1(d) and (e) where the latter device requires two clamps on top of the flanges in order to have complete equilibrium. In addition, even though the vee-bending mechanism used to characterise the out-of-plane bending properties was able to consider the influence of test speed and temperature, the fixtures tend to be unstable when the temperature is close to the melting point of the thermoplastic resin [28].

The literature studies focus not only on the bending behaviour of metal alloys and some types of fibre reinforced composites, but also on the combination of these two materials in particularly the cured hybrid laminates. In addition, the aim of these studies applying the bending test for metal-composite laminates is to evaluate and measure the interlaminar shear strength (ILSS) through the short-beam test methods. For example, Ostapiuk et al. [29] analysed the bending and failure behaviour of glass and carbon fibre reinforced metal-composite laminates. He noted that the maximum strain and stress of the fibres are directly related by the modulus, and besides, the thicknesses of metal layers as well as the fibre orientations are also critical factors to be considered. Liu et al. [30] studied the interlaminar failure behaviour of Glare-3/2-0.3 laminates with different span length-to-specimen thickness ratios (L/h) under short-beam three-point-bending loads. He found that the lay-up configuration of the glass/epoxy layers affects the load-deflection response, especially the failure loads and the corresponding failure modes. Li et al. [31] investigated the bending failure mechanisms and flexural properties of Glare laminates with various stacking sequences in a short-beam bending test. He mentioned that the bending modulus decreased with the increase of the number of layers from 3/2 to 6/5, while the variations of bending strength are opposite for unidirectional and cross-ply Glare laminates. Hu et al. [32] worked on the experimental and numerical characterisation of the flexural properties and failure behaviour of the Al/CFRP laminates through a series of three-point-bending test. He found that a lower bending modulus and strength can be obtained with the increase of metal volume fraction for the aluminium sheet, and the CFRP materials played a prominent role in the bending properties of Al/CFRP laminates.

Since most of the recent findings on the flexural behaviours and failure mechanisms of metal-composite laminates focus on short-beam three-point-bending test ($L/h < 10$) and on cured laminates where hybrid material undergoes full curing, the test approaches for the characterisation of the flexural properties for uncured epoxy-based hybrid laminates on a long-beam bending test ($L/h > 100$) has not been proposed. Besides, the application of local pressure tends to influence the ratio between stretching (Deform in horizontal direction) and drawing (Deform in vertical direction) of the laminates: where higher clamping pressures lead to more stretching and the bending stresses are superimposed with in-plane stresses due to such stretching. Therefore, the increasing plastic strain in the cross-section of the metal sheet is significant for laminate deformation during the press forming process. Moreover, the flexural behaviour under various material constituents and laminate structures, as well as the processing parameter conditions for metal-composite laminates forming with uncured prepregs remain to be discussed. Then, the numerical modelling method applied to verify the experimental results are also needed. Therefore, the study for the solution of the above scientific issues is becoming crucial for understanding the flexural behaviour of the uncured metal-composite laminates.

4.3. MATERIALS AND METHODS

4.3.1. MATERIAL PREPARATION

THE metal-composite laminates used in the research are composed of metal sheets of aluminium alloy 2024-T3 and stainless steel 304L, as well as the T300 carbon fibre-MTC510 unidirectional (UD) prepregs. The surfaces of the aluminium alloy are anodized by phosphoric acids and both metal materials with a thickness of 0.5mm are washed by acetone [1, 2]. As for the carbon fibre reinforced composite layers, two cross-ply UD prepregs of 0°/90° and 45°/-45° with a nominal total thickness of 0.3mm are chosen. The fibre volume fraction for each ply is 60% and the viscosity of the epoxy-based prepregs greatly decreases from room temperature (23°C) to the temperature of 110°C when increased at a ramp rate of 2°C/min [33]. The mechanical properties of the material constituents in laminates are shown in Table 4.1 and it is assumed that the properties of the metal sheets will not be affected under the studied temperature ranges [34, 35]. Two parameters of the elastic modulus, shear modulus and ultimate strength for the UD prepregs denote the properties in the fibre orientation of 0° and 90°, respectively. The rolling direction for the metal sheets and the fibre orientation of 0° for the fibre reinforced prepregs are parallel to the bending line of the laminate in the test.

Table 4.1: Mechanical properties of the material constituents in bending test [33–35]

Materials	Density (g/cm^3)	Elastic modulus (GPa)	Shear modulus (GPa)	Yield strength (MPa)	Poisson's ratio	Ultimate strength (MPa)	Elongation at break (%)
Aluminium alloy 2024-T3	2.7	71	28	320	0.33	480	16.2
Stainless steel 304L	8.0	200	77	210	0.30	574	45.6
UD carbon fibre prepreg -MTC510	1.5	119.3/8.2	3.6/2.0	-	0.34	2282/54	1.3

4.3.2. CONCEPT DESIGN

THE concept of clamped-beam bending test came from the design of an integral forming and curing cycle in the proposed press forming process as shown in Figure 1.8. The traditional three-point-bending method can consider the influence of material constituent, laminate structure, and preheat temperature on the flexural behaviour of uncured metal-CFRP laminates. However, the factor which is important for material flow and wrinkling control like forming pressure especially on the flange regions are not taken into account. Therefore, based on the three-point bending as well as fixed-beam bending method, a clamped-beam bending test is designed for the evaluation of the flexural behaviour of uncured metal-CFRP laminates under various conditions. The schematic graph and dimensions of the clamped-beam bending concept are shown in Figure 4.2. The hybrid laminate with a size of 300 mm × 50 mm is placed symmetrically on the supports and clamped by two blocks with a size of 50 mm × 50 mm. Then, the punch with a diameter of 10 mm moves vertically down the centreline of the laminate to a specified displacement. In order to achieve a uniform and symmetrical loading of the clamping

force, a double acting pneumatic cylinder ADN-50-10-A-P-S6 from FESTO is selected and the schematic graph of the pressure loading concept for the product is presented in Figure 4.3. The pneumatic cylinder performs in both extension and retraction strokes, and meets the need of the test conditions for high temperature and pressure. Based on the dimension and stroke of the pneumatic cylinder, a bending tool system is designed and manufactured as shown in Figure 4.4. The bending tool system contains four vertical columns and fixed guides, two lateral support blocks and pressure blocks, as well as two pneumatic cylinders and one ground plate. The maximum dimension for the whole system is 400 mm × 240 mm × 300 mm and the size for each component follows the concept in Figure 4.2. The radii for the two support blocks are 5 mm and the influence on the bending and unloading is neglected. The pressure block and upper profile are bolted and connected through the pneumatic cylinder, and the vertical column can have adjustable movement along the ground plate. Then, the laminate specimen can be placed horizontally on the support blocks and pressed by the two pressure blocks.

4

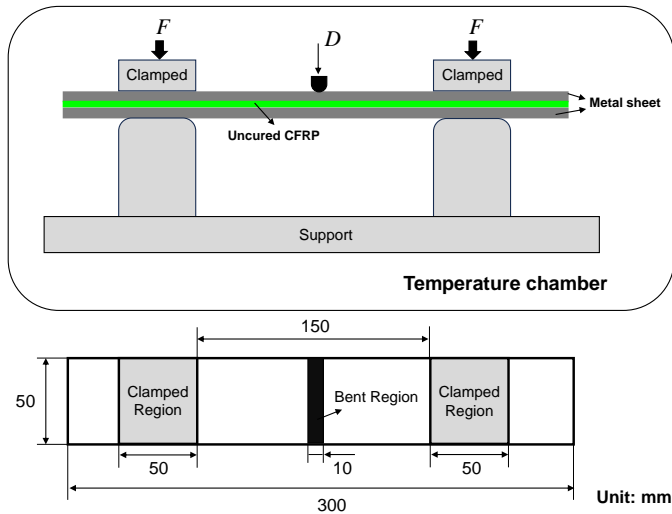


Figure 4.2: Schematic graph and specimen dimensions for the laminate clamped-beam bending concept

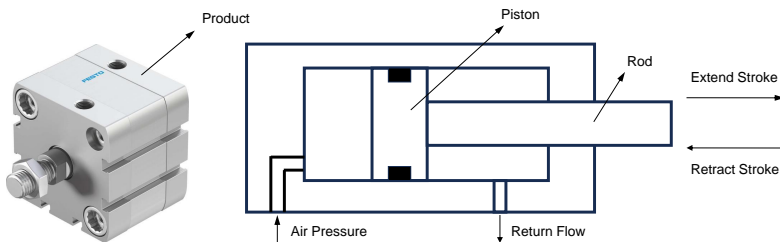


Figure 4.3: Double-acting pneumatic cylinder and the schematic graph of the pressure loading concept

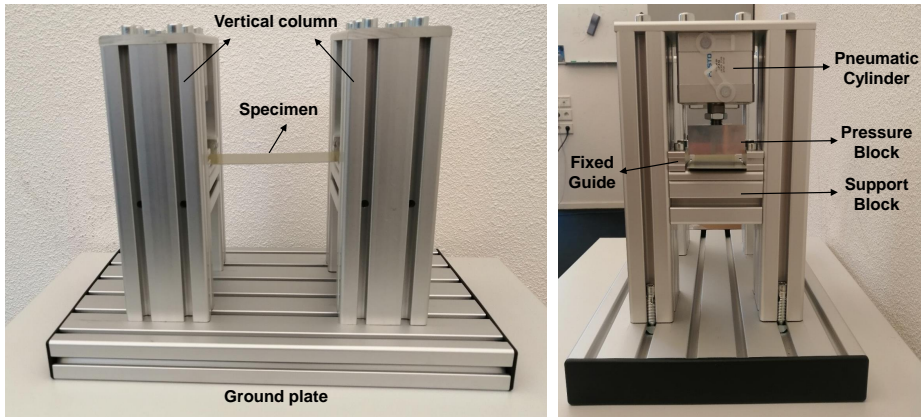


Figure 4.4: Bending tool system with two pneumatic cylinders for the clamped-beam bending concept

4.3.3. EXPERIMENTAL PROCEDURE

THE clamped-beam bending test method is performed on a Zwick-250kN tensile-compression machine equipped with a temperature chamber. The bending tool system with two pneumatic cylinders for the concept is installed and fixed on the lower table of the machine, while the bending punch is connected to the upper tool along the vertical centreline for the specimen as presented in Figure 4.5(a). The load-displacement curve for a given parameter combination can be obtained through the measuring system of the machine. Moreover, the processing temperature is preset by the temperature chamber system while the real-time temperature inside the chamber is recorded by the thermocouples. Other test parameters like punch speed of 10 mm/min and punch displacement of 40 mm are set as constants by the manual input in the machine system. To measure and control the pressure, a real-time pressure tank and manual pressure controller are used as shown in Figure 4.5(b) and (c). The maximum pressure from the tank is 9 bar, and the air pressure inlets as well as return flow outlets are converged in two separate channels and connected to the tank, respectively. Through the preset value on the controller, the pressure block is able to adjust the load.

Table 4.2: Material configurations and test parameters used for clamped-beam bending test

Structure	Material configuration			
Metal sheet	Aluminium 2024-T3	Stainless steel 304L		
Fibre prepreg (UD)	CFRP (T300 carbon-MTC510)			
Layup and orientation	2/1(0°/90°)	2/1(45°/-45°)	3/2(0°/90°)	3/2(45°/-45°)
Processing temperature (°C)	23(RT)	50	80	110
Clamping pressure (Bar)	0	1	3	6

The material configurations and test conditions used for the clamped-beam bending test of the uncured metal-CFRP laminates are summarized in Table 4.2. The tests are performed with Al/CFRP and Ss/CFRP laminates, as well as four combinations of layup and fibre orientation, four processing temperatures and four clamping pressures. In addition, the tests are conducted varying one parameter at a time while keeping the

other parameters at the baseline value, and at least three specimens are applied for each configuration. The baseline values for the bending are the layup and orientation of 2/1 and 0°/90°, processing at room temperature (23°C) and clamping pressure of 0 bar. The single-layer metal sheets are characterised using the same specimen geometry under the same conditions compared with the corresponding hybrid laminates. These selected test conditions are based on the industrial applications for the laminate press forming and are used to study the effect on the flexural behaviour, in particular the bending force evolution during the clamped-beam bending process.

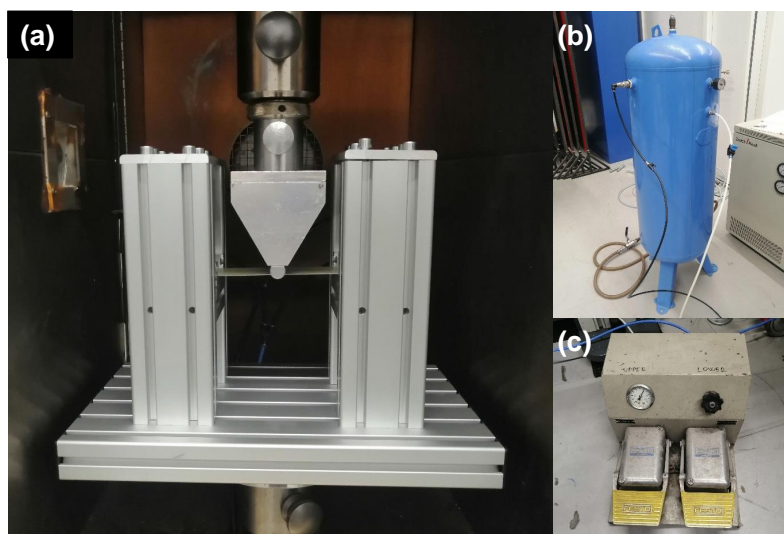


Figure 4.5: Experimental procedure and apparatus of the laminate bending: (a) Clamped-beam bending setup; (b) Real-time pressure gauge tank; (c) Manual pressure controller

4.4. FINITE ELEMENT MODEL

THE application of a finite element model made it efficient to analyse the proposed clamped-beam bending process and support the results from the actual experimental tests. In the study, finite element analysis software Abaqus is used to simulate the bending procedure of the uncured metal-CFRP laminates by using the stress-strain distributions of the metal sheet and the unique anisotropic properties of the carbon fibre reinforced prepreg (CFRP). Figure 4.6 exhibits the simulation model established for the research and all the materials as well as tool geometries followed the concept of the experimental setups. The elastic-plastic properties of the metal sheets and the elastic constants for the uncured CFRP lamina as shown in Figure 4.7 and Table 4.1 are imported into the material property module in the Abaqus software. In the finite element model, all tools including the bending punch, upper and lower supports are modelled as discrete rigid shell elements with a mesh size of 2 mm. Metal sheets and the uncured CFRP material are all created as four-node doubly curved conventional shell elements with reduced integration (S4R) in a same mesh size of 2mm. The laminate structure in the FE model is represented in the composite layup module where all layers and their pa-

rameters such as orientation, thickness, property and relative location are defined and assembled into the bending simulation. As for the interactions and boundary conditions in the model, the value of clamping force and punch displacement can be set, and the contacts between the fixed tools and uncured metal-CFRP laminates are set as penalty friction in a constant value of 0.15. The interaction at the metal-prepreg interfaces is defined as friction contact which consists of the mechanical elastic and viscous flow. A static-kinetic exponential decay model in Abaqus is applied to simulate the transition of friction and the value can be obtained from a previous study [11]. In order to characterise and validate the flexural behaviour of the test materials, the load-displacement response in the Static/Standard step, and the spring-back depth as well as the length reduction coupled with plastic deformation in the Dynamic/Explicit step are analysed and compared with the experimental results [32, 36].

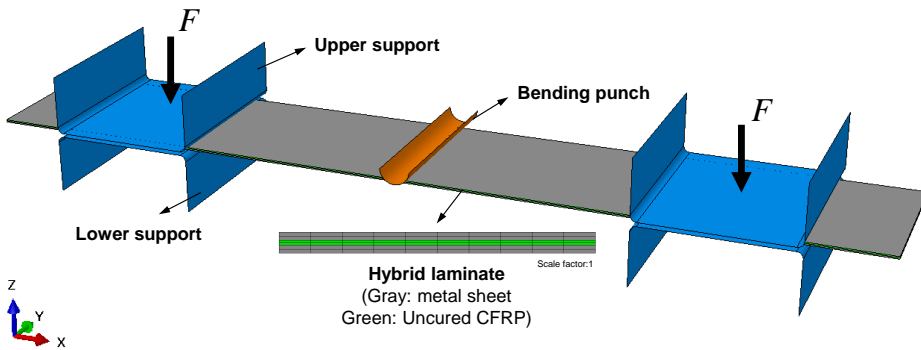


Figure 4.6: Finite element model of the clamped-beam bending test for the uncured metal-CFRP laminates

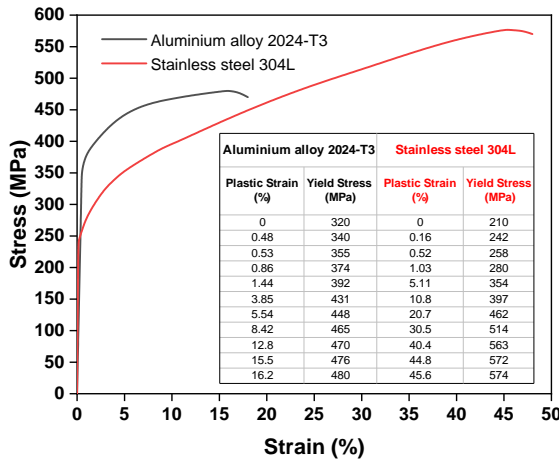


Figure 4.7: Stress-strain curve of the metal sheets applied for the clamped-beam bending test simulations

4.5. RESULTS AND DISCUSSION

4.5.1. BENDING LOAD-DISPLACEMENT RESPONSE

EFFECT OF METAL CONSTITUENT

DURING the clamped-beam bending process, the load-displacement response is one of the most quantitative results to characterise the flexural behaviour of the test materials. The experimental results coupled with the finite element simulation results on the bending load-displacement response without clamping at room temperature are shown in Figure 4.8. At the initial stage of bending, the increase of bending force in the simulation model is a bit larger when compared to the test conditions for the bent materials. This is mainly because of the delayed response of the testing machine at the initial contact between the punch and specimen. However, with the increasing punch displacement, the bending force gradually grows to be consistent at the displacement of 40mm. Therefore, the values of the maximum bending force can be regarded as an appropriate evaluation indicating that the test method and finite element model show a good agreement at the end of bending. For the effect of the metal constituent, the maximum bending force for the single-layer aluminium alloy 2024-T3 and Al/CFRP laminate is larger compared with the single-layer stainless steel 304L and the corresponding Ss/CFRP laminate under the same configurations and conditions. Furthermore, the bending force levels off earlier for the stainless steel based materials during the bending process. This can be explained by the stress-strain curve of these two metal sheets in Figure 4.7, which indicates that the aluminium alloy has a higher yield stress than the stainless steel and higher stress causes the higher reaction forces of the punch. However, due to the lower yield stress of the stainless steel, the material would enter the plastic stage earlier which results in the slow growth of the stress as well as bending force.

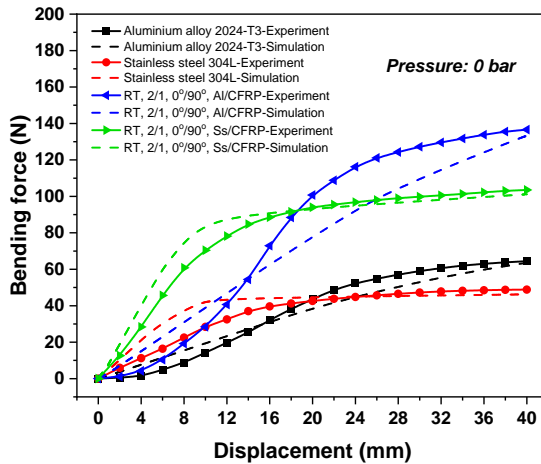


Figure 4.8: Experimental and numerical results on the bending force evolution of the metal sheet and the corresponding metal-CFRP laminate at room temperature (RT) with the clamping pressure of 0 bar

Moreover, it can be obtained from Figure 4.8 that the maximum bending force of the uncured metal-CFRP laminate is higher than the sum force of two single-layer metal

sheets under the same test conditions. One reason is that the uncured hybrid laminates are deformed independently from each other, the required bending moments are sum of bending all these sheets. Other explanations can be obtained from the differences of the stress distribution through the thickness direction after bending as shown in Figure 4.9. The bending deformation of the metal sheet is simplified as a material exhibiting elastic-ideal plastic behaviour without hardening. For a single-layer metal sheet, the stress distribution is symmetrical along the neutral layer where the metal surfaces 1&2 undergo the maximum tensile stress and compressive stress, respectively. In the outer surfaces, the stress will be capped at the maximum stress σ_m where the vertical lines denote the plastic deformation regions. The outer surfaces 1&4 for a hybrid laminate with the 2/1 layup experience the same stress state as the metal sheet, while the metal sheets and fibre prepreg deform independently from each other when the hybrid laminate is bent with an uncured fibre prepreg in the middle. The inner surfaces (2&3) of the metal sheet could slip over the prepreg layer and the sliding resistance depends on the friction at the metal-prepreg interfaces. Therefore, the stress at the outer metal surface for the uncured hybrid laminate σ_h is higher than the stress for the single-layer metal sheet σ_m due to the inter-ply friction. Moreover, it is noted that the maximum bending force for Al/CFRP and Ss/CFRP laminate with a 2/1 layup is slightly over twice the value than their corresponding single-layer metal sheet. The finding shows that the bending properties of the hybrid laminates depend mainly on the properties of metal sheets while the uncured CFRP material plays a limited role.

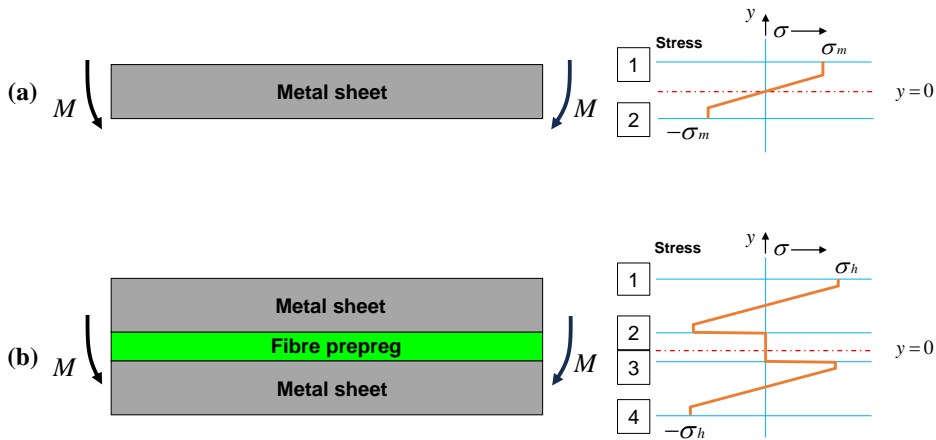


Figure 4.9: Schematic graph of the stress distribution after bending process for different test materials: (a) Single-layer metal sheet; (b) uncured metal-composite laminate with 2/1 layups

EFFECT OF CLAMPING PRESSURE

THE application of clamping pressure is one of the focus points in the research and the investigation of clamping effects on the flexural behaviour of uncured laminates becomes significant. Figure 4.10(a) and (b) exhibit the experimental bending force and displacement curve of the single-layer aluminium sheet and the Al/CFRP laminate under

different clamping pressures, respectively. The uncured Al/CFRP laminates are tested at room temperature (23°C) with a layup of 2/1 and fibre orientation of 0°/90°. For the bending of the single-layer aluminium alloy shown in Figure 4.10(a), the bending force gradually increases with the punch movement and the increase of clamping pressure from 0 bar to 3 bar increases the bending force with displacement of the punch. When replacing the single-layer metal sheet with an Al/CFRP laminate with a specific configuration, the bending force increases until it reaches the maximum value at the end of the bending test as well. The result validates that clamping pressure plays a significant role in the bending force of both metal sheet and the hybrid laminates. However, although all the test materials experience growth in bending force with the increase of punch displacement, the trends of increase are different when applying different clamping pressures. When there is no clamping pressure on the clamped regions, the bending force grows significantly at the initial stage of bending and gradually goes towards a nearly constant value until the end of the bending test. As the pressure increases, the increase in bending force becomes more distinct and the stage where the force tends to level off earlier in the bending process. One of the explanations is that the increase of clamping pressure restricts the material flow in longitudinal direction, which requires greater bending force to achieve the same amount of deformation. It can also be explained through the increase of plastic strain at the same amount of displacement with the increasing clamping pressure. As shown in Figure 4.7 that a higher force (stress) induces more plastic strain and an earlier start of plastic deformation. It can be observed from the bent specimens of the aluminium alloy 2024-T3 in Figure 4.10(a) that the single-layer aluminium sheet under the clamping pressure of 3 bar undergoes larger plastic deformation and becomes more pronounced compared to the bent aluminium sheet without clamping pressure. The effect of clamping pressure on the bending force for the hybrid laminate is even greater since the force scale runs from 0 to 600 N as shown in Figure 4.10(b). The reason is due to the increase of bent layers and frictional force at the tool-metal and metal-prepreg interfaces which hinder the sliding, making the stress σ_m and σ_h greater than the bent material without clamping pressure. More details on the effect of clamping pressure on material plastic deformation will be discussed.

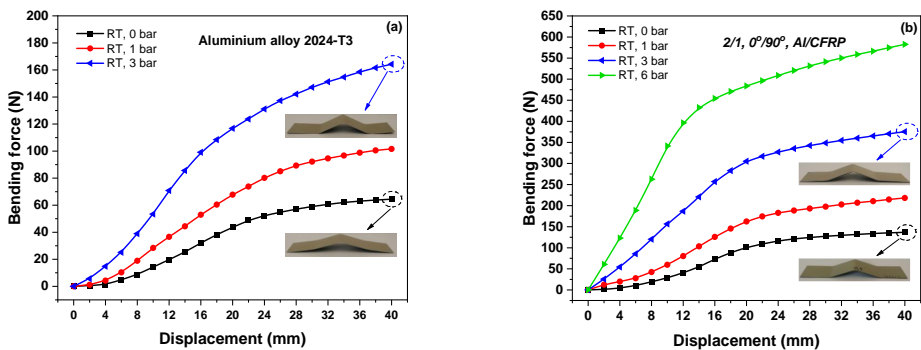


Figure 4.10: Experimental bending force and displacement curves under various clamping pressures for clamped-beam bending test: (a) Single-layer aluminium alloy 2024-T3; (b) 2/1, 0°/90° Al/CFRP at room temperature of 23°C

EFFECT OF LAYUP AND FIBRE ORIENTATION

IN order to investigate the effect of laminate layup on the bending force, the Ss/CFRP laminates of 2/1 and 3/2 layups at room temperature (23°C) with the fibre orientation of 0°/90°, as well as the single-layer stainless steel are compared. Experimental results on the bending force evolution of the three materials under the clamping pressures of 0 bar and 3 bar are shown in Figure 4.11. It is obvious that the increase of laminate layup from a single-layer metal sheet to a 3/2 hybrid laminate contributes to the increase of bending force. The increasing number of layers dominates the growth of bending force which follows the conclusions of the three-point bending and the fixed-beam bending studies from literature [37, 38]. Besides, it is obtained from the results that the bending force is determined by the metal sheets whereas the composite layers hardly contributes since the uncured laminates act independently. The bent specimens of the Ss/CFRP laminates under two clamping pressure conditions are more pronounced and has an increased remaining bent depth after unloading when compared to the single-layer stainless steel. More details on the spring-back effect will be discussed in section "Spring-back depth". For the effect of fibre orientation, the cross-ply unidirectional CFRP materials of 0°/90° and 45°/-45° for the metal-CFRP laminates of a 2/1 layup are compared. Figure 4.12 exhibits the test results of the maximum bending force for four different laminate structures under three clamping pressures at room temperature (23°C). It can be observed from the figure that the hybrid materials with a fibre orientation of 45°/-45° have slightly smaller bending force due to the intra-ply shear at the maximum displacement than the metal-CFRP laminates with the fibre orientation of 0°/90° under the same conditions.

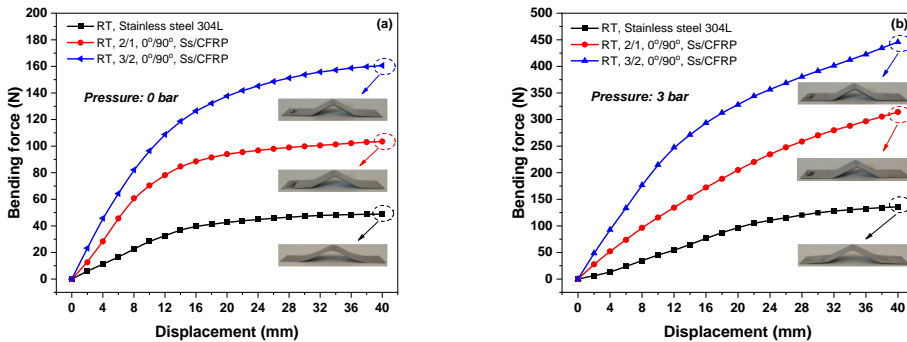


Figure 4.11: Experimental bending force and displacement curves of the single-layer stainless steel and its corresponding hybrid laminates at room temperature (23°C) for clamped-beam bending with two clamping pressures: (a) 0 bar; (b) 3 bar

Figure 4.13 describes the two deformation mechanisms during the bending process for the CFRP materials in the hybrid laminates. Bending of cross-ply unidirectional (UD) structure with a fibre orientation of 0°/90° mainly involves slide at the prepreg-prepreg interface. Assuming that the gaps between each fibre tow at the initial state are a constant value t , and the gaps after bending along a new axis of L' and W' between the fibre tow are t_1 and t_2 , respectively. It is noted that the $L-W$ and $L'-W'$ coordinate system are kept as vertical during bending and the relationship between the tow-gap is $t_2 < t < t_1$. However, the kinematics of the cross-ply unidirectional (UD) structure with

a fibre orientation of $45^\circ/-45^\circ$ are different where the adjacent plies of the fibre prepreg rotate and slide over each other and are coupled through a viscous resin. The vertical coordinate system $U - V$ gradually changes into a new coordinate system $U' - V'$ with a rotation angle α . Although the gaps of fibre tow after bending still follow the relationship of $t'_2 < t < t'_1$, the relationship between the gaps of fibre tow for the $45^\circ/-45^\circ$ and $0^\circ/90^\circ$ structures is $t_1 > t'_1 > t, t > t'_2 > t_2$ due to the existence of prepreg rotations at the same deformation. Therefore, the different deformation mechanisms for the hybrid materials with a fibre orientation of $45^\circ/-45^\circ$ and $0^\circ/90^\circ$ may affect the values of the maximum bending force during bending.

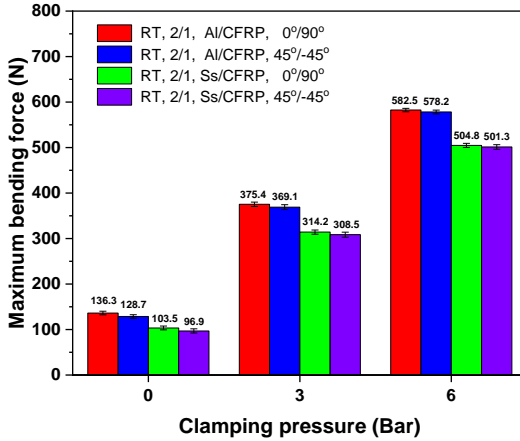


Figure 4.12: Experimental results for the maximum bending force of different laminate structures under three clamping pressures

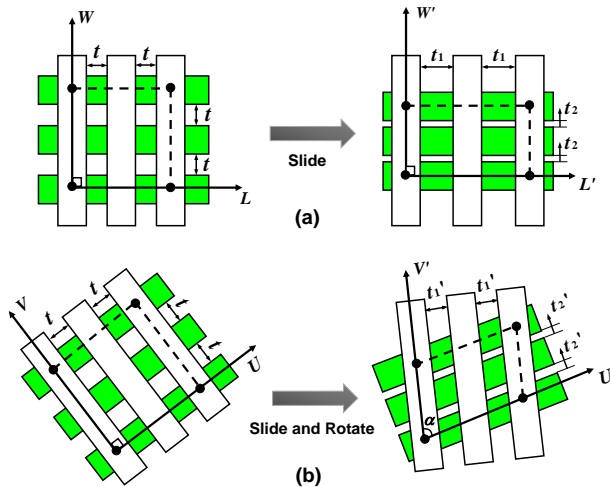


Figure 4.13: Schematic graph of the deformation mechanisms during bending for two typical fibre orientations of cross-ply UD prepregs: (a) $0^\circ/90^\circ$; (b) $45^\circ/-45^\circ$

EFFECT OF PROCESSING TEMPERATURE

THE processing temperature is also a crucial factor affecting the bending force since the elastic modulus of the uncured CFRP materials, as well as the frictional force at the metal-prepreg interfaces and prepreg-prepreg interfaces are temperature-dependent. Figure 4.14 exhibits the experimental results of the maximum bending forces at four different processing temperatures under the clamping pressure of 0 bar and 3 bar. The two curves reveal that the maximum bending force decreases with increase of temperature, while the magnitude of decrease is different for the uncured 2/1 hybrid laminates with a fibre orientation of 45°/-45° and 0°/90°. When the pressure applied on the clamped regions is zero, the maximum bending force for Al/CFRP and Ss/CFRP laminates with the 45°/-45° structure at the processing temperature of 110°C is higher than their corresponding laminates with the 0°/90° structure. At room temperature, the result is the other way around. There are two reasons which helps to explain the bending force reduction. Firstly, due to the resin viscosity decrease with the temperature increases, the softening of CFRP material decreases the overall elastic modulus and thus, lower the bending force. Then, the frictional force at the interfaces of each layer decreases significantly as the temperature increases, which further reduces the maximum bending force for the uncured laminates. This can be referred to Figure 4.9(b) where the stress σ_h for laminate bending decreases since the sliding at the metal-prepreg interfaces is easier. However, the hybrid structures with 45-degree layers at least offers a higher contribution on the bending moment than the 90-degree layers, which seem contrary to the trend of force reduction.

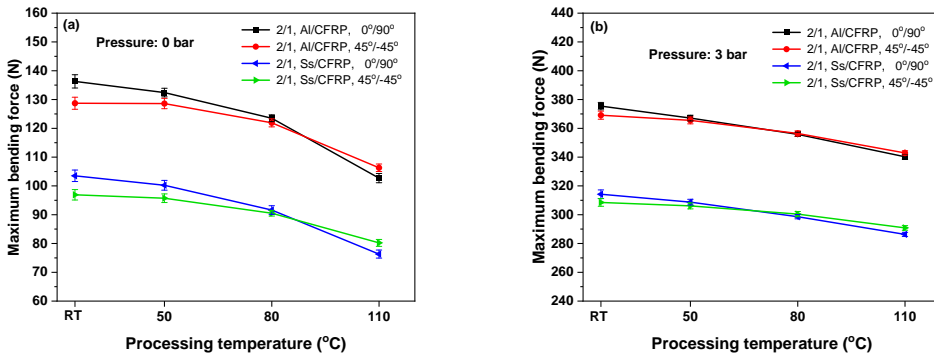


Figure 4.14: Experimental results on the maximum bending force and a displacement of 40mm for various processing temperature and pressure conditions for the hybrid laminate of 2/1 layouts: (a) 0 bar; (b) 3 bar

The previous study [12] also found that the temperature effect dominates the in-plane shear force for the cross-ply UD reinforced metal laminates with 45°/-45° structures. Once the increased bending moment and shear force accumulate to a certain value, the 45°/-45° structures need a greater maximum bending force at a certain temperature for the 45°/-45° structures than the 0°/90° structures which only experience the inter-ply sliding during bending. Besides, the increase of clamping pressure hinders the sliding of the uncured metal-CFRP laminates, which further increases the shear force at

the same displacement for $45^\circ/-45^\circ$ structures. This reveals that the maximum bending force becomes larger for low temperature and high pressure conditions. The microscopic measurement for the rotation angle α on the central regions of the 2/1 Al/CFRP laminates with the fibre orientation of $45^\circ/-45^\circ$ are applied [12] and the results under various bending conditions are shown in Figure 4.15. The results for the angle measurement prove that the increase of clamping pressure and temperature helps to decrease the rotation angle α .

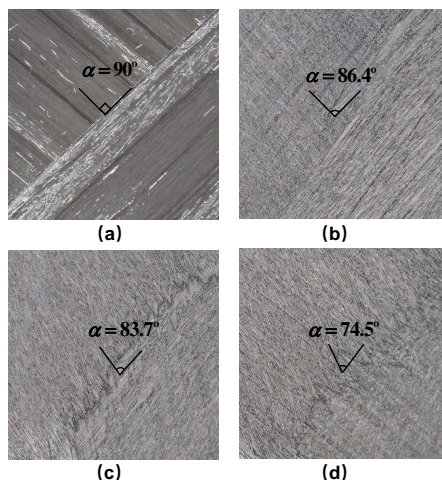


Figure 4.15: Microscopic measurements of the rotation angle on the centre region of the 2/1, Al/CFRP laminate with the fibre orientation of $45^\circ/-45^\circ$ under various bending conditions: (a) Initial state; (b) RT, 0 bar; (c) 80°C , 0 bar; (d) 80°C , 3 bar

4.5.2. LAMINATE BENDABILITY CHARACTERISATION

SPRING-BACK DEPTH

THE evolution of spring-back after the clamped-beam bending process can also be used for the characterisation of the flexural behaviour of the test materials. The experimental and numerical simulation methods are applied to study the differences of the bent materials before and after spring-back as exhibited in Figure 4.16. The values of spring-back depth for various material configurations at room temperature without clamping pressure are shown in Figure 4.17. The spring-back depth D' is measured by the differences of the bending depth before and after spring-back ($D' = D_0 - D_1$). The effect of fibre orientation and processing temperature on the spring-back depth for the uncured metal-CFRP laminates are not investigated as the effects can be ignored. The test and simulation results reveal that the aluminium based materials experience more spring-back than stainless steel based materials and the increase of laminate layup would reduce the spring-back depth. This can also be explained from the stress-strain curve presented in Figure 4.7, where the higher elastic modulus and lower yield strength of the stainless steel result in a lower elastic response compared with the aluminium alloy when the metal sheet reaches the same amount of deformation. Furthermore, the increase of laminate layup also plays a significant role in the spring-back reduction

where the bending radius of the outer sheet of the uncured laminates is larger than the single-layer sheet, which have a huge impact on the strain distribution of that layer and its elastic response. Therefore, the spring-back depth of the metal-CFRP laminates are lower than their corresponding single-layer metal sheets. The numerical colourmaps of the vertical displacement (U_3) before and after spring-back for various material configurations at room temperature without clamping pressure are shown in Figure 4.18. It is observed that the vertical displacement and shapes after unloading for the single-layer metal sheets and hybrid laminates are different. As the thickness of a single-layer metal sheet is small, the bent materials at centre and flange regions undergo opposite displacement after unloading without clamping pressure on the flange regions. However, the increase of layup and bending radius gradually hinders the vertical movement and the materials become flat on the flange regions.

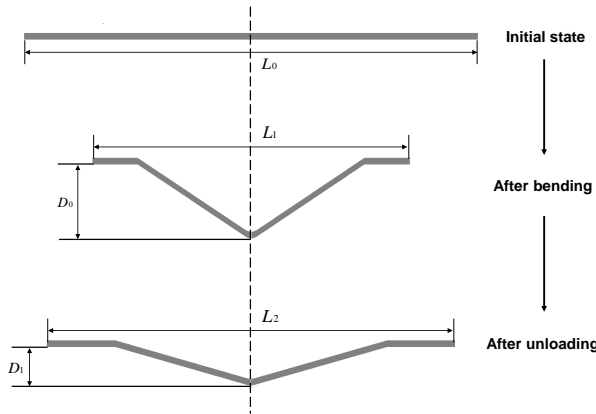


Figure 4.16: Schematic graph and dimension of three different stages during the laminate bending process

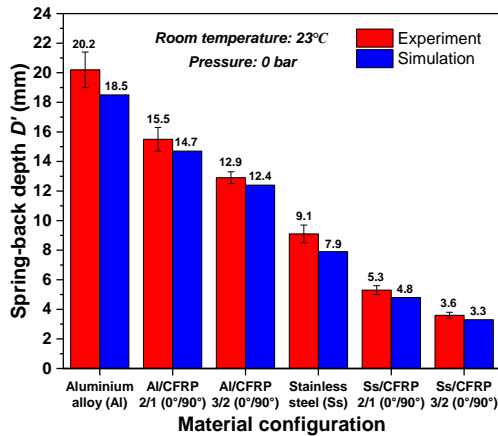


Figure 4.17: Experimental and numerical comparisons on the spring-back depth for different material configurations

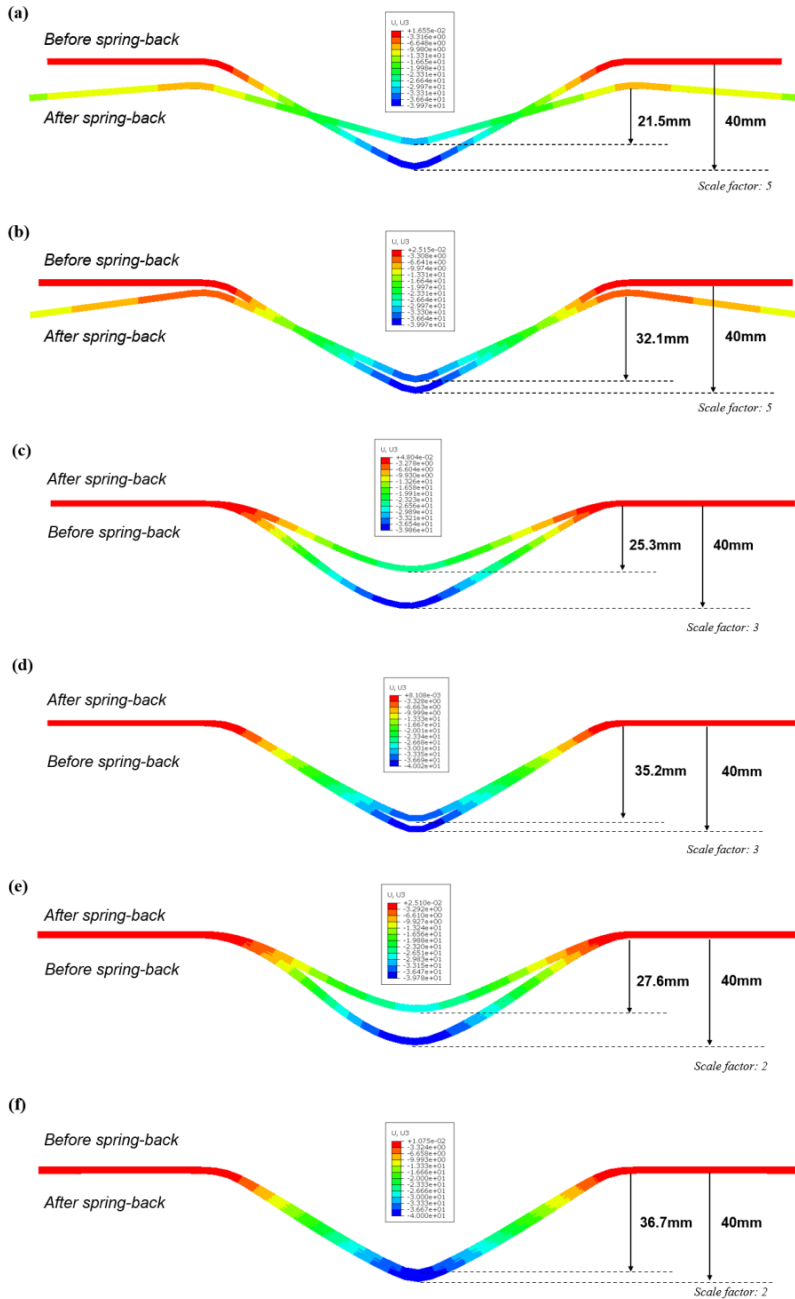


Figure 4.18: Numerical results of the vertical displacement (U_3) before and after spring-back of bending for different materials under the conditions of no clamping pressure and room temperature (23°C): (a) Single-layer aluminium alloy 2024-T3; (b) Single-layer stainless steel 304L; (c) 2/1, 0°/90°, Al/CFRP; (d) 2/1, 0°/90°, Ss/CFRP; (e) 3/2, 0°/90°, Al/CFRP; (f) 3/2, 0°/90°, Ss/CFRP

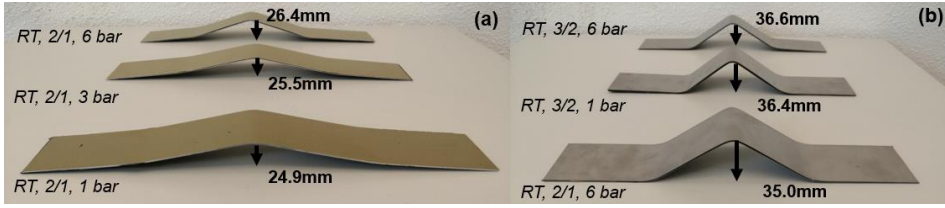


Figure 4.19: Test specimens after spring-back for different laminate configurations and test conditions at room temperature: (a) 2/1, 0°/90°, Al/CFRP laminates; (b) 0°/90°, Ss/CFRP laminates

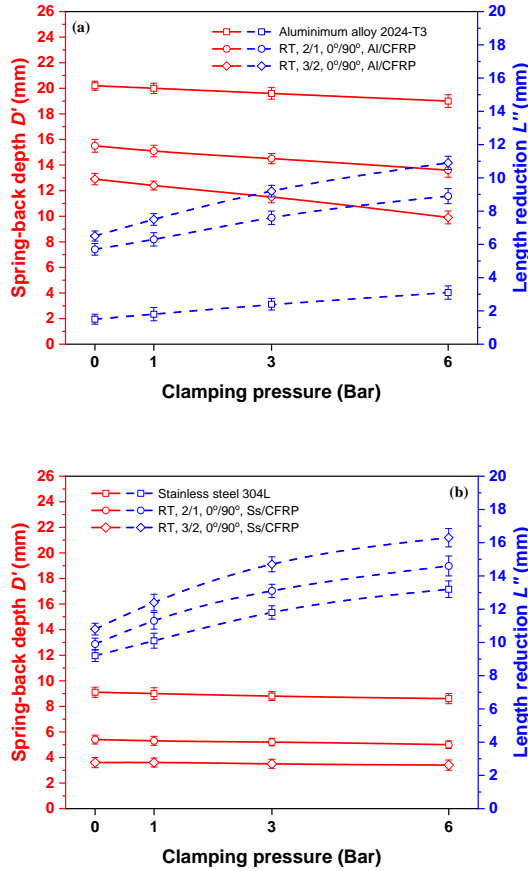


Figure 4.20: Experimental results on the spring-back depth and length reduction after unloading under various pressure conditions: (a) Aluminium alloy based materials; (b) Stainless steel based materials

The experimental tests on the depth of laminate spring-back are also performed under different clamping pressure conditions. Figure 4.19 exhibits the test specimens after spring-back for different laminate configurations and test conditions at room temperature, and the spring-back depth D' for the aluminium-based and stainless steel-based

materials under various pressure conditions are shown in Figure 4.20(a) and (b). All the curves on the evolution of spring-back depth show that the increase of clamping pressure contributes to the reduction of spring-back. The results are visible in Figure 4.19 where the introduction of an increasing tension force in the laminates decreases the out-of-plane spring-back. However, it can be seen from the curves that the decreasing trend of spring-back is different for the Al/CFRP and Ss/CFRP laminates with the increase of clamping pressure. The Al/CFRP laminates show more obvious spring-back decrease when the pressure increases especially for the 3/2 layups, while the effect of clamping pressure on the spring-back reduction for the Ss/CFRP laminates is limited. Although the spring-back depth for the Ss/CFRP laminate itself is small, the influence of laminate layup dominates the spring-back process when the bending punch is unloaded.

4

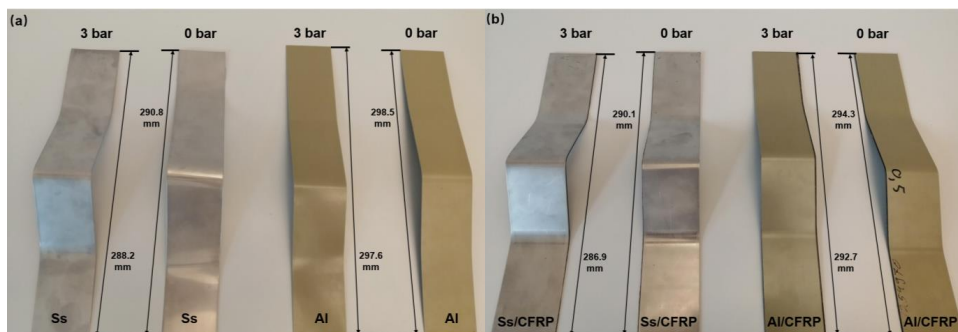


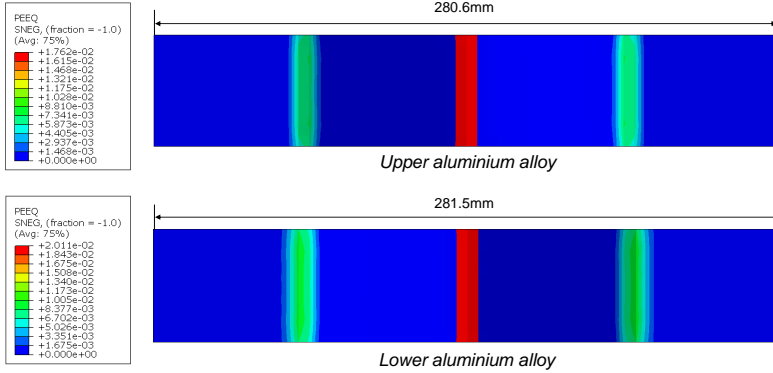
Figure 4.21: Test specimens under two clamping pressure conditions at room temperature for different materials after spring-back: (a) Single-layer metal sheets; (b) 2/1, 0°/90°, hybrid metal-CFRP laminates

LENGTH REDUCTION

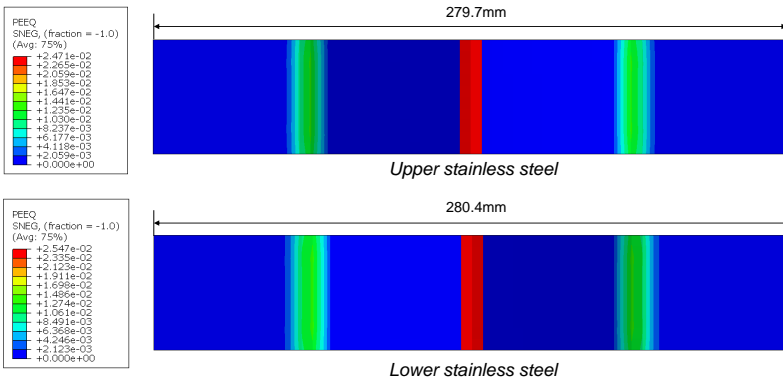
DUE to the application of clamping pressure on the local flange regions of the specimen, the length reduction along the longitudinal direction is also an index for the characterisation of the flexural behaviour. Therefore, the study of the clamping pressure effect on the length variations before and after unloading is proposed, and the factors affecting the properties of CFRP material such as fibre orientation, processing temperature are not studied as the variations on the bent length is quite small. The length reduction after unloading L'' is defined and calculated by the differences of the initial longitudinal length and the bent length after unloading ($L'' = L_0 - L_2$) which is described in Figure 4.16. The initial longitudinal length is 300 mm and the bent lengths after unloading for the test materials under two clamping pressure conditions at room temperature are shown in Figure 4.21. It is seen that all the materials undergo the length reduction after bending and unloading under the pressure conditions. The increasing clamping pressure causes more stretch of the materials and increases the plastic deformation in the bend zone, which increases the length reduction after unloading. The curves on length reduction L'' under various pressure conditions as shown in Figure 4.20(a) and (b) reveal that the aluminium-based materials have smaller length reduction compared to the stainless steel-based materials especially for the single-layer metal sheet. The reason is mainly because of the higher elastic response after unloading for the aluminium

sheet where the bent length is closer to the initial length. Besides, the result shows that the increase of laminate layup leads to an increase on the length reduction for the bent laminates and the sliding resistance become more significant under higher clamping pressure conditions.

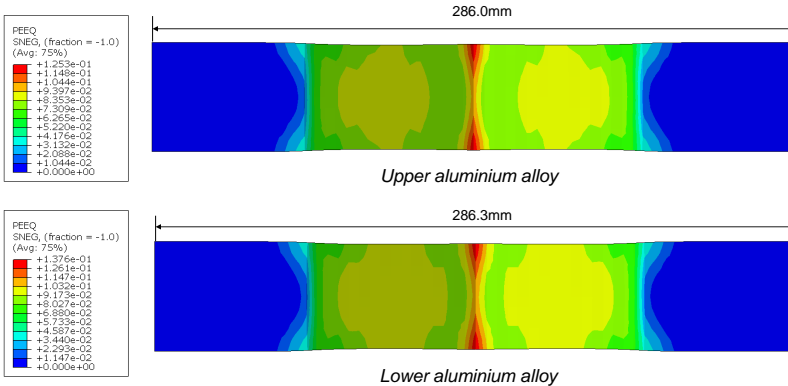
(a) RT, 2/1 Al/CFRP laminate, Clamping pressure: 0 Bar



(b) RT, 2/1 Ss/CFRP laminate, Clamping pressure: 0 Bar



(c) RT, 2/1 Al/CFRP laminate, Clamping pressure: 6 Bar



(d) RT, 2/1 Ss/CFRP laminate, Clamping pressure: 6 Bar

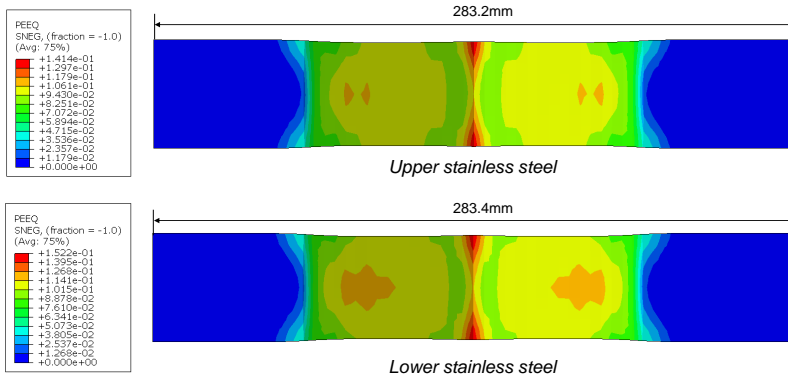


Figure 4.22: Numerical results on the equivalent plastic strain at room temperature (23°C) for hybrid laminates after the bending process

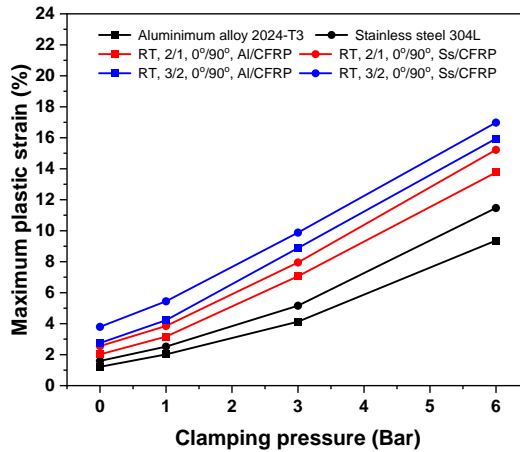


Figure 4.23: Numerical results on the relationship of maximum plastic strain and clamping pressure for different materials

PLASTIC STRAIN

In order to quantify the influence of clamping pressure on the flexural behaviour of the uncured metal-CFRP laminates in the test, the evolution of plastic deformation is investigated. The numerical colourmaps of the equivalent plastic strain for hybrid laminates before unloading are presented in Figure 4.22. The bent length before unloading and the equivalent plastic strain are smaller for the upper metal surfaces than the lower metal surfaces in the metal/CFRP laminate of 2/1 layout under two pressure conditions. The reason can be referred to the sliding at the metal-prepreg interfaces and the stress distribution diagram as shown in Figure 4.9(b). When the clamping pressure is 0 bar, the maximum equivalent plastic strain for the Al/CFRP and Ss/CFRP laminate is about 2.01% and 2.55%. However, the equivalent plastic strain distribution is different when

the pressure changes to 6 bar where the strain increases on the unsupported areas of the bent laminates. The maximum equivalent plastic strain occurs on the edge regions along the centreline and the value increases to 13.76% and 15.22%, respectively. Based on the numerical results on the equivalent plastic strain values, the influence of clamping pressure on the plastic deformation at room temperature can be obtained in Figure 4.23. It can be observed that the maximum plastic strain for all the materials increases with the increase of clamping pressure and the growth become more distinct with the increase of laminate layup. The stainless steel-based materials undergo more plastic deformation than the aluminium-based materials under the same conditions. The result demonstrates that higher clamping pressure which results in more plastic deformation in the bend zone helps to improve the deformability of the uncured metal-CFRP laminates.

4.6. CONCLUSIONS

THE flexural behaviour of the uncured metal-CFRP laminates is experimentally and numerically characterised by the analysis of load-displacement response, spring-back depth, length reduction and plastic strain in the clamped-beam bending process. The method is proposed under the condition of various clamping pressures on the local regions of the specimen and the factors affecting the flexural behaviour, including the material constituent, laminate layup and fibre orientation, processing temperature and clamping pressure are analysed in details. The relevant conclusions are:

(1) The application of clamping pressure has a significant impact on the flexural behaviour of the bent materials. With the increasing clamping pressure, the force required to bend increases significantly, the depth of spring-back gradually reduces and the resistance of sliding increases. It contributes to the result of higher material plastic deformation in the metal layers of the uncured metal-CFRP laminates.

(2) The flexural behaviour of the uncured metal-CFRP laminates mainly depends on the type of the metal constituents and layups of the hybrid laminates. The aluminium-based materials with a lower elastic modulus and a higher yield strength exhibits a greater maximum bending force and a higher spring-back after bending and unloading, while the stainless steel based materials undergo more plastic deformation and larger length reduction under the same material configurations and test conditions. Also, the increase of laminate layup increases the bending force while decreases the spring-back.

(3) The factors affecting the properties of CFRP material such as the fibre orientation and processing temperature play a limited role and this type of bending for the uncured metal-CFRP laminates is dominated by metal sheet. The hybrid laminates with a fibre orientation of $45^\circ/-45^\circ$ have a slightly smaller maximum bending force than the same hybrid materials with a fibre orientation of $0^\circ/90^\circ$ at room temperature. The result differs in high clamping pressure and high temperature conditions with a somewhat larger intra-ply shear force and inter-ply frictional force for the uncured CFRP material.

(4) The numerical simulation results show a good agreement with the experimental results at room temperature (23°C) with various clamping pressure for uncured metal-CFRP laminates. More work on the finite element model validations should be done to evaluate the results under different processing temperature conditions.

REFERENCES

- [1] A. Asundi and A. Y. Choi, "Fiber metal laminates: an advanced material for future aircraft," *Journal of Materials processing technology*, vol. 63, no. 1-3, pp. 384–394, 1997.
- [2] J. Sinke, "Manufacturing of glare parts and structures," *Applied composite materials*, vol. 10, pp. 293–305, 2003.
- [3] T. Sinmazçelik, E. Avcu, M. Ö. Bora, and O. Çoban, "A review: Fibre metal laminates, background, bonding types and applied test methods," *Materials & Design*, vol. 32, no. 7, pp. 3671–3685, 2011.
- [4] D. Nardi, M. Abouhamzeh, R. Leonard, and J. Sinke, "Investigation of kink induced defect in aluminium sheets for glare manufacturing," *Composites Part A: Applied Science and Manufacturing*, vol. 125, p. 105531, 2019.
- [5] K. Kavitha, R. Vijayan, and T. Sathishkumar, "Fibre-metal laminates: A review of re-inforcement and formability characteristics," *Materials Today: Proceedings*, vol. 22, pp. 601–605, 2020.
- [6] L. Mosse, P. Compston, W. J. Cantwell, M. Cardew-Hall, and S. Kalyanasundaram, "The development of a finite element model for simulating the stamp forming of fibre–metal laminates," *Composite Structures*, vol. 75, no. 1-4, pp. 298–304, 2006.
- [7] Z. Ding, H. Wang, J. Luo, and N. Li, "A review on forming technologies of fibre metal laminates," *International Journal of Lightweight Materials and Manufacture*, vol. 4, no. 1, pp. 110–126, 2021.
- [8] T. Heggemann and W. Homberg, "Deep drawing of fiber metal laminates for automotive lightweight structures," *Composite Structures*, vol. 216, pp. 53–57, 2019.
- [9] Q. Chen, P. Boisse, C. H. Park, A. Saouab, and J. Bréard, "Intra/inter-ply shear behaviors of continuous fiber reinforced thermoplastic composites in thermoforming processes," *Composite structures*, vol. 93, no. 7, pp. 1692–1703, 2011.
- [10] S. Erland and T. Dodwell, "Quantifying inter-and intra-ply shear in the deformation of uncured composite laminates," *Advanced Manufacturing: Polymer & Composites Science*, vol. 7, no. 2, pp. 25–35, 2021.
- [11] S. Liu, J. Sinke, and C. Dransfeld, "An inter-ply friction model for thermoset based fibre metal laminate in a hot-pressing process," *Composites Part B: Engineering*, vol. 227, p. 109400, 2021.
- [12] S. Liu, J. Sinke, and C. Dransfeld, "A modified bias-extension test method for the characterisation of intra-ply shear deformability of hybrid metal-composite laminates," *Composite Structures*, vol. 314, p. 116964, 2023.
- [13] S. Liu, L. Lang, E. Sherkatghanad, Y. Wang, and W. Xu, "Investigation into the fiber orientation effect on the formability of glare materials in the stamp forming process," *Applied Composite Materials*, vol. 25, pp. 255–267, 2018.

- [14] L. Shichen, L. Lihui, and G. Shiwei, "An investigation into the formability and processes of glare materials using hydro-bulging test," *International Journal of Precision Engineering and Manufacturing*, vol. 20, pp. 121–128, 2019.
- [15] C. Liu, D. Du, H. Li, Y. Hu, Y. Xu, J. Tian, G. Tao, and J. Tao, "Interlaminar failure behavior of glare laminates under short-beam three-point-bending load," *Composites Part B: Engineering*, vol. 97, pp. 361–367, 2016.
- [16] C. Bellini, V. Di Cocco, F. Iacoviello, and L. Sorrentino, "Performance evaluation of cfrp/al fibre metal laminates with different structural characteristics," *Composite Structures*, vol. 225, p. 111117, 2019.
- [17] K. Zhao and J. Lee, "Finite element analysis of the three-point bending of sheet metals," *Journal of Materials Processing Technology*, vol. 122, no. 1, pp. 6–11, 2002.
- [18] N. Seemuang, S. Panich, and T. Slatter, "Bendability evaluation of sheet metals in three-point bending test by using acoustic emission features," *The Journal of Applied Science*, vol. 16, no. 2, pp. 15–22, 2017.
- [19] A. Farrokhhabadi, S. A. Taghizadeh, H. Madadi, H. Norouzi, and A. Ataei, "Experimental and numerical analysis of novel multi-layer sandwich panels under three point bending load," *Composite Structures*, vol. 250, p. 112631, 2020.
- [20] F. Mujika, "On the difference between flexural moduli obtained by three-point and four-point bending tests," *Polymer testing*, vol. 25, no. 2, pp. 214–220, 2006.
- [21] P. Wang, N. Hamila, and P. Boisse, "Thermoforming simulation of multilayer composites with continuous fibres and thermoplastic matrix," *Composites Part B: Engineering*, vol. 52, pp. 127–136, 2013.
- [22] S. Haanappel, R. H. ten Thije, U. Sachs, B. Rietman, and R. Akkerman, "Formability analyses of uni-directional and textile reinforced thermoplastics," *Composites Part A: Applied science and manufacturing*, vol. 56, pp. 80–92, 2014.
- [23] P. Boisse, J. Colmars, N. Hamila, N. Naouar, and Q. Steer, "Bending and wrinkling of composite fiber preforms and prepregs. a review and new developments in the draping simulations," *Composites Part B: Engineering*, vol. 141, pp. 234–249, 2018.
- [24] B. Liang, P. Chaudet, and P. Boisse, "Curvature determination in the bending test of continuous fibre reinforcements," *Strain*, vol. 53, no. 1, p. e12213, 2017.
- [25] D. Dörr, F. J. Schirmaier, F. Henning, and L. Kärger, "A viscoelastic approach for modeling bending behavior in finite element forming simulation of continuously fiber reinforced composites," *Composites Part A: Applied science and manufacturing*, vol. 94, pp. 113–123, 2017.
- [26] U. Sachs and R. Akkerman, "Viscoelastic bending model for continuous fiber-reinforced thermoplastic composites in melt," *Composites Part A: Applied Science and Manufacturing*, vol. 100, pp. 333–341, 2017.

- [27] A. Margossian, S. Bel, and R. Hinterhoelzl, "Bending characterisation of a molten unidirectional carbon fibre reinforced thermoplastic composite using a dynamic mechanical analysis system," *Composites Part A: Applied science and manufacturing*, vol. 77, pp. 154–163, 2015.
- [28] S. Ropers, M. Kardos, and T. A. Osswald, "A thermo-viscoelastic approach for the characterization and modeling of the bending behavior of thermoplastic composites," *Composites Part A: Applied Science and Manufacturing*, vol. 90, pp. 22–32, 2016.
- [29] M. Ostapiuk, J. Bieniaś, and B. Surowska, "Analysis of the bending and failure of fiber metal laminates based on glass and carbon fibers," *Science and Engineering of Composite Materials*, vol. 25, no. 6, pp. 1095–1106, 2018.
- [30] C. Liu, D. Du, H. Li, Y. Hu, Y. Xu, J. Tian, G. Tao, and J. Tao, "Interlaminar failure behavior of glare laminates under short-beam three-point-bending load," *Composites Part B: Engineering*, vol. 97, pp. 361–367, 2016.
- [31] H. Li, Y. Xu, X. Hua, C. Liu, and J. Tao, "Bending failure mechanism and flexural properties of glare laminates with different stacking sequences," *Composite Structures*, vol. 187, pp. 354–363, 2018.
- [32] C. Hu, L. Sang, K. Jiang, J. Xing, and W. Hou, "Experimental and numerical characterization of flexural properties and failure behavior of cfrp/al laminates," *Composite Structures*, vol. 281, p. 115036, 2022.
- [33] SHD-Composite-Materials, "Technical datasheet for the mtc510 epoxy prepreg," <https://shdcomposites.com/admin/resources/mtc510-tds.pdf>, 2018.
- [34] R. K. Desu, H. N. Krishnamurthy, A. Balu, A. K. Gupta, and S. K. Singh, "Mechanical properties of austenitic stainless steel 304l and 316l at elevated temperatures," *Journal of Materials Research and Technology*, vol. 5, no. 1, pp. 13–20, 2016.
- [35] A. L. Santos, R. Z. Nakazato, S. Schmeer, and E. C. Botelho, "Influence of anodization of aluminum 2024 t3 for application in aluminum/cf/epoxy laminate," *Composites Part B: Engineering*, vol. 184, p. 107718, 2020.
- [36] S. Keipour and M. Gerdooei, "Springback behavior of fiber metal laminates in hat-shaped draw bending process: experimental and numerical evaluation," *The International Journal of Advanced Manufacturing Technology*, vol. 100, pp. 1755–1765, 2019.
- [37] J.-B. Sauvage, M. Aufray, J.-P. Jeandrou, P. Chalandon, D. Poquillon, and M. Nardin, "Using the 3-point bending method to study failure initiation in epoxide-aluminum joints," *International Journal of Adhesion and Adhesives*, vol. 75, pp. 181–189, 2017.
- [38] T. Sharma and A. Tyagi, "Review of mechanical modelling of fixed-fixed beams in rf mems switches," in *2013 Third International Conference on Advanced Computing and Communication Technologies (ACCT)*, pp. 211–214, IEEE, 2013.

5

A CURE-DEPENDENT SPRING-BACK INVESTIGATION IN A PRESS FORMING CYCLE

This chapter focuses on the spring-back as a function of the degree of cure on single-curved metal-composite laminates. The manufacturing through a press forming process involves different (curing) stages and can reduce the spring-back with the proper combination of forming and curing. The cure-dependent spring-back is measured and analysed as a function of material constituents, fibre directions, laminate layups, and the process parameters including temperature, time and pressure. . The results indicate that the spring-back ratio after full-cured process is relatively small and mainly depends on the mechanical properties of the metal sheet in laminates. However, temperature and time have a significant effect on the spring-back of partially-cured laminates and the same type of fibre prepreg combined with two different metal sheets have similar trends of spring-back reduction. Moreover, the study found that the hybrid laminates with aluminium sheet delaminate at low pressure after full-cured, while the delamination disappears as the pressure increases. The characterisation on cure-dependency of the spring-back offers an opportunity to control the spring-back of these laminates and contributes to a better understanding of creating more accurate products .

5.1. INTRODUCTION

METAL composite laminates are high-performance lightweight materials consisting of thin metal sheets and fibre reinforced prepreg layers by alternatively stacking, curing under proper temperature and pressure [1, 2]. These hybrid materials combine the advantages of metal sheet and fibre reinforced polymer such as high specific strength and stiffness, and properties like high fatigue and impact resistance, as well as the better corrosion and fire resistance, etc [3–6]. However, the manufacturing of such hybrid laminates is difficult as various forming and curing stages are required coupling with the complex deformation and failure mechanisms [7–9]. In order to improve the manufacturability of the hybrid laminates, an integral forming and curing cycle is proposed in Figure 1.8. The most critical stages in the process are preheating and curing of the laminates before and after press forming. The time and temperature needs to be controlled in the preheating stage, so that the inter-ply sliding at the metal-prepreg interfaces and the intra-ply shear within the prepregs are greatly enhanced when the resin viscosity decreases [10–13]. The hybrid laminate is formed and cured in a subsequent stage, avoiding loading and unloading of the part and an extra curing system, which can be time-saving and cost-saving [14]. However, there arises several scientific questions on how the state of curing affects the accuracy of the final part and whether the pressure applied during curing assists in reducing or eliminating the spring-back, which plays a role in the accuracy of the related tool geometry as well.

5

5.2. LITERATURE ON SPRING-BACK

THE concept of spring-back comes as a consequence of the elastic strain or energy recovery during unloading and the residual stresses are the counterpart of spring-back. In the conventional sheet metal forming process, the occurrence of spring-back is common and inevitable in each stage where the metal material undergoes plastic deformations. The parameters affecting the spring-back behaviour of metal sheets are mainly related to the stresses generated during the loading and unloading process and can be divided into three groups: material, tool and geometry. The properties of the metal sheet such as the size and thickness, elastic modulus, yield strength and hardening coefficient, affect the spring-back. For example, the material with a higher yield strength will have a higher ratio of elastic-plastic strain for equivalent elastic moduli, while the metal sheet with a higher elastic modulus shows less spring-back than a material with a lower elastic modulus for equivalent yield strengths [15–17]. As for the geometry related parameters, the punch height and radius, die opening and radius, the tool-metal friction are all critical variables affecting the spring-back [18–20]. Gawade et al. [19] found that the metal sheet has a minimum radius/thickness ratio and the spring-back gradually increases with the increase in such R/t ratio due to the strains decrease in the bend line. Besides, the reduction in friction between the metal sheet and forming tools increases the spring-back and decreases the bend force. Other critical factors affecting the spring-back of metal sheet are the process parameters like the forming and cooling rate, etc. Melwin et al. [21] found that the spring-back decreases with an increase in cooling rate for a hot stamping steel and the increase in cooling rate results in spring-forward owing to the formation of an increased volume fraction of martensite.

The spring-back behaviour of the fibre reinforced polymers also originates from three different mechanisms: chemical mechanism, thermo-mechanical mechanism as well as the interactions between the tool and the composite laminate [22–32]. The properties of the fibre materials remain essentially constant, while the thermoset resin properties change dramatically during the cure cycle as it polymerizes and crosslinks transitioning from a viscous to rubbery and finally glassy state. Therefore, the resin morphology results in a volume change, which causes the accumulation of internal stress. With the increase of such internal stress which induces changes in curvature in plates, the spring-in phenomenon due to this chemical shrinkage cannot be ignored [22]. The thermo-mechanical mechanism is mainly because of the physical and mechanical differences between the dry fibres and the polymeric matrix. The CTE of the polymer-matrix materials is usually much higher than that of the fibres. This results in residual stresses existing on a micro-mechanical level for the unidirectional materials during processing. These residual stresses affect the stress-strain behaviour and influence the spring-back. Brauner et al. [26, 27] developed a simulation tool for the analysis of residual stresses related to the resin transfer moulding process, and a visco-elastic material model was derived integrating a dependency of the time-temperature-polymerisation and fibre volume content on the stress relaxation behaviour. In addition, the mechanical properties of the resin depend on the degree of cure which can be used to evaluate the development of spring-back. Uriya et al. [28] studied the spring-back behaviour of a carbon fibre-reinforced plastic sheet after cold and warm V-bending test and found a large decrease in spring-back when the forming temperature and degree of cure increases. Also, Pereira et al. [29] showed that a polymer with a lower degree of cure has a lower modulus of elasticity than a fully-cured polymer and the degree of cure associated with the cooling rates influences the spring-back. The third mechanism of spring-back is due to the contact effects between the metallic tool and the composite part. The parameters like tool material, surface condition (friction), cure cycle and pressure are shown to have a significant effect on the spring-back [30–32].

The mechanisms and factors affecting the spring-back behaviour of metal sheet and fibre reinforced polymer apply to the hybrid metal-composite laminates as well [33–41]. The amount of spring-back in such laminates depends on the material parameters like the material constituents, the laminate layup and thickness, as well as the fibre orientations. Keipour et al. [35] performed an experimental and numerical study of the spring-back in a hat-shaped bending test of a 2/1 fibre metal laminate and found that the thickness of composite core had limited effect on spring-back when the elastic modulus of the core is lower than the metal skin. However, Isikatas et al. [36] found that the amount of spring-back in a hybrid 2/1 laminate decreases with the increase of the thickness of the composite core when combining the aluminum 5754-H22 sheet and carbon fibre-reinforced plastics by adhesive. Moreover, many scholars found that the spring-back differs in the processing parameters during the manufacturing processes. Kim et al. [39] considered a brake forming process for fabricating the fibre metal laminate stringers and examined the spring-back under different processing conditions. They discovered that the spring-back ratio increases linearly with the increase of the punch radius while the spring-back ratio increases rather slowly with the increasing punch speed at room temperature. Also, the increase of forming force from 500N to 5000N in

the matching dies with a heat-up temperature of 100°C results in a significant decrease on spring-back. Vahid et al. [40] focused on the spring-back behaviour of the PVC-based metal-composite laminates when press forming a U-shaped product and concluded that the amorphous PVC matrix results in a larger spring-back at lower forming temperature, while higher forming temperature reduces the PVC elasticity significantly and overcomes the elastic spring-back. Safari et al. [42] conducted an experimental assessment of the creep forming properties of fibre metal laminates and studied the effect of temperature and time on spring-back. The result validated that the spring-back of the creep-formed laminates decreases with an increase in either time or temperature due to the decrease of elastic strain and the increase of creep strain. Besides, they believed that through multi-objective parameter optimisation during the forming process of the metal-composite laminates, the minimum spring-back can be achieved. Therefore, due to the high spring-back of the cured hybrid laminate, the in-situ curing of the curved shape after forming process of uncured laminate gains the interests. However, the role of individual metal sheet and prepreg layers in an uncured laminate during forming is unknown. Also, how the degree of cure and the forming pressure affect the interaction at the metal-composite interfaces remains to be discussed. Besides, there is a lack of studies on quantifying the laminate spring-back as a function of degree of cure and the experimental methods for the selection of appropriate material constituent and processing parameters for laminate forming with uncured prepregs have not been proposed.

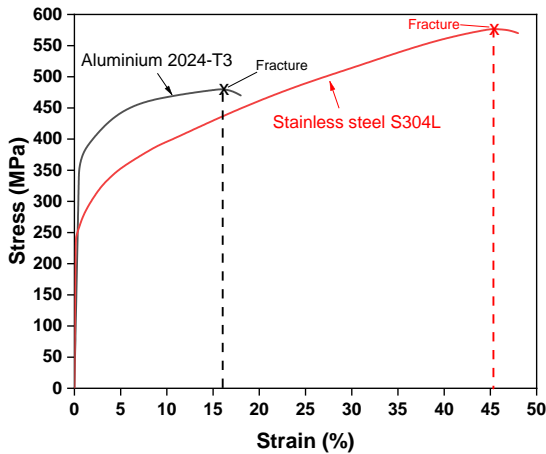


Figure 5.1: Stress-strain curve until fracture of two different metal sheets used for the spring-back analysis

5.3. MATERIALS AND METHODS

5.3.1. MATERIAL CONSTITUENTS

THE raw materials used for the laminate preparation are metal sheets of aluminium alloy 2024-T3 and stainless steel 304L, as well as two different fibre reinforced prepregs. The surfaces of aluminium sheet are anodized by phosphoric acid and both metal materials with a thickness of 0.5mm are washed by acetone [1, 2]. The stress-strain curves

which exhibit the elastic-plastic performance of two metal alloys used in the test are shown in Figure 5.1 and these curves can illustrate the effect of material behaviour on spring-back. As for the fibre-reinforced prepreg systems, an unidirectional S2 glass fibre-FM94 epoxy prepreg with a nominal thickness of 0.18 mm as well as a T300 carbon-MTC510 UD prepreg with a nominal thickness of 0.15 mm are selected. The fibre volume fraction for both prepregs is 60% and the thermoset polymers are cured at the temperature of 120°C and pressure of 6 bar which follows a standard curing cycle [42, 43]. The mechanical properties of the material constituents in hybrid laminates are exhibited in Table 5.1 and the behaviour of metal sheet cannot be affected under the studied temperature ranges. Two values of the elastic modulus and ultimate strength for UD prepregs represent the properties in fibre orientation of 0° and 90°, respectively. For all tests, the rolling direction for the metal sheet and the fibre orientation of 0° for the fibre reinforced prepreg are parallel to the bending line of the laminate.

Table 5.1: Mechanical properties of the material constituents in spring-back analysis [42, 43]

Materials	Density (g/cm^3)	Elastic modulus (GPa)	Shear modulus (GPa)	Poisson's ratio	Yield strength (MPa)	Ultimate strength (MPa)	Shear strength (MPa)	Elongation at break (%)
Aluminium alloy 2024-T3	2.7	71	28	0.33	320	480	283	16.2
Stainless steel 304L	8.0	200	77	0.30	210	574	378	45.6
UD glass fibre prepreg -FM94	2.6	54.0/9.4	5.5/2.6	0.33	-	1870/50	38.5	3.8
UD carbon fibre prepreg -MTC510	1.5	119.3/8.2	3.6/2.0	0.34	-	2282/54	99.0	1.3

5.3.2. RHEOLOGICAL ANALYSIS

THE FM94 and MTC510 are two epoxy systems allowing compatibility for metal sheet bonding of the metal-composite laminate. For press forming process of the prepared and uncured blanks, the degree of cure and the resin viscosity of the epoxy play a critical role in the relative sliding between the interlayers and the occurrence of possible defects like fibre buckling. In order to obtain the relationship between the degree of cure and resin viscosity, Differential Scanning Calorimetry (DSC) and rheometer analysis can be used for the characterisation of cure kinetics and rheokinetics, respectively [44]. For the DSC, the heat flow is the internal heat, H , generated per unit mass and per unit time during the cross-link reaction and is represented as:

$$\frac{dH}{dt} = H_{tot} \cdot \frac{d\alpha}{dt} \quad (5.1)$$

H_{tot} is the total heat of reaction after full cure of the epoxy and α is the degree of cure. The cure rate and total heat of the reaction can be determined by iso-conversion DSC measurements where the resin is heated at a constant heating rate and the energy input is measured versus the cure time [45]. For the calculation of cure rates, the Kamal-Sourour reaction ratio equation [46] is proposed and fitted as follows:

$$\frac{d\alpha}{dt} = k_0 \cdot e^{(-E_A/RT)} \cdot \alpha^m \cdot (1 - \alpha)^n \quad (5.2)$$

where R is the universal gas constant and T is the cure temperature in Kelvin, E_A is the activation energy, k_0 is a coefficient and m, n are two fitting constants. The degree of cure α of the epoxy at any time t is calculated by the integration of the instant cure rate as:

$$\alpha(t) = \int_0^t \frac{d\alpha}{dt} dt \quad (5.3)$$

By applying the kinetic model in Equation 5.2 and fitting parameters obtained from Table 5.2, the degree of cure of the epoxy can be predicted for isothermal cure for specific temperatures of the FM94 and MTC510 epoxy as exhibited in Figure 5.2 [45–47]. Besides, the viscosity of the epoxy evolves as a function of temperature and time: $\eta = f(T, t)$, or degree of cure and temperature: $\eta = g(T, \alpha)$. The rheological behaviour of the FM94 and MTC510 epoxy at a ramp of 2°C/min as provided by the material suppliers [42, 43] are presented in Figure 5.3.

Table 5.2: Cure kinetic parameters for epoxy FM94 and MTC510 [45–47]

Parameter	FM94	MTC510
K_0 (1/s)	3.52+E06	5.64+E06
E_A (J/mole)	6.75E+04	6.21E+04
m (-)	0.558	0.314
n (-)	2.508	1.216
H_{tot} (J/g)	134.9	321.8

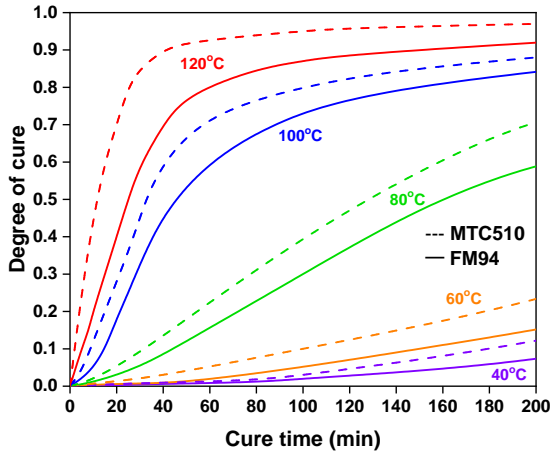


Figure 5.2: Predicted degree of cure evolution of the epoxy under specific temperatures: Solid line-FM94 and Dashed line-MTC510

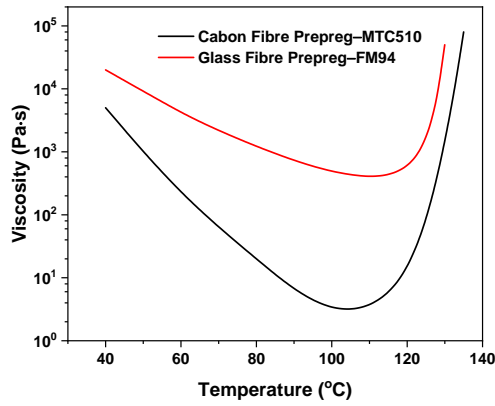


Figure 5.3: Rheological data of the FM94 and MTC510 epoxy at the ramp of 2°C/min

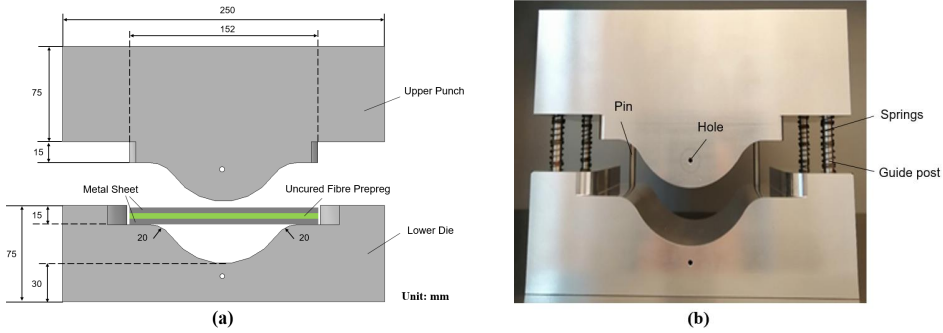


Figure 5.4: Single-curved mould design for the laminate press forming process: (a) mould dimension; (b) mould manufacture

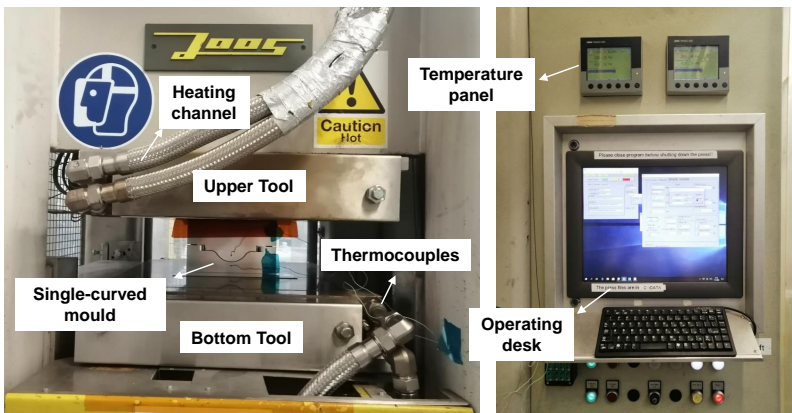


Figure 5.5: Experimental setup and apparatus for the hybrid laminate press forming process

5.3.3. EXPERIMENTAL SETUP

THE press forming process which can be an alternative method of forming for the metal-composite laminate is performed on a 1000kN heated flat Joos Press machine. In order to investigate the influence of spring-back without the forming defects like metal wrinkling or fibre buckling, a single-curved mould with the size of 250×120×150 mm is designed and manufactured, as shown in Figure 5.4. Four spring-wrapped guide posts are made to control the movement of the upper mould and ensure that the tool returns to its original position when the pressure is released. The specimen with an initial dimension of 150×40 mm is placed into the mould and positioned by two long vertical pins on the back. The experimental setup and apparatus for the laminate press forming process is shown in Figure 5.5. The heating temperature transferred from the upper and lower tool of the press to the forming mould is set by the heated platens and the real-time temperature in the mould is recorded by the thermocouples in holes in the upper and lower tools, and displayed on the temperature panel. The experimental forming cycle includes a temperature rise from room temperature to the set forming temperature at a rate of 2°C/min and the forming pressure increases to the set value in one step. Then, after maintaining a closed mould for a certain period of time, the temperature is decreased to the room temperature (23°C) at a cooling rate of 4°C/min. For the setup, it is possible to adjust the process parameters of forming temperature, holding time and forming pressure as they may affect the spring-back.

Table 5.3: Material configurations used for press forming process

Structure	Material configuration		
Metal sheet	Aluminium 2024-T3	Stainless steel 304L	
Fibre prepreg (UD)	S2 glass-FM94	T300 carbon-MTC510	
Laminate layup	2/1	3/2	4/3
Fibre orientation	0°/0°	0°/90°	90°/90°

Table 5.4: Test conditions used for laminate press forming process

Test parameter	Baseline value	Additional values investigated
Temperature (°C)	80	40, 60, 100, 120
Holding time (min)	20	0, 10, 30, 120
pressure (bar)	6	0, 0.1, 10, 20

Table 5.3 presents the material configurations used for the press forming process and Table 5.4 shows the test conditions for the experiments. The test varies one parameter at a time while keeping the other parameters at their baseline values. For each configuration under these test conditions, at least three specimens are tested. Among all the investigated test conditions, the hybrid laminates are regarded as complete cured when the forming temperature reaches 120°C with a holding time of 120 minutes and forming pressure of 6 bar. However, the tests performed below these temperature and time conditions are considered as partially-cured. As the temperature and time characterise the evolution of degree of cure, the value obtained from the rheological analysis is used to investigate the influence of degree of cure on spring-back. The computed degree of cure

for the prepregs under the selected temperature and time are summarised in Table 5.5. The laminate is assumed to be full-cured once the degree of cure exceeds 0.9 and the cure is assumed not to begin when the degree of cure is less than 0.01. The Schematic graph of the laminate forming process is presented in Figure 5.6 where the spring-back behaviour is compared for partially-cured and full-cured conditions.

Table 5.5: Computed degree of cure used for various holding time and temperature

Temperature	Degree of cure	Carbon Fibre Prepreg-MTC510			Glass Fibre Prepreg-MTC510		
		10min	20min	30min	10min	20min	30min
40°C		0.002	0.005	0.009	0.001	0.002	0.005
60°C		0.008	0.012	0.020	0.003	0.006	0.013
80°C		0.016	0.047	0.096	0.011	0.029	0.058
100°C		0.121	0.285	0.467	0.052	0.184	0.363
120°C		0.452	0.706	0.854	0.208	0.415	0.589

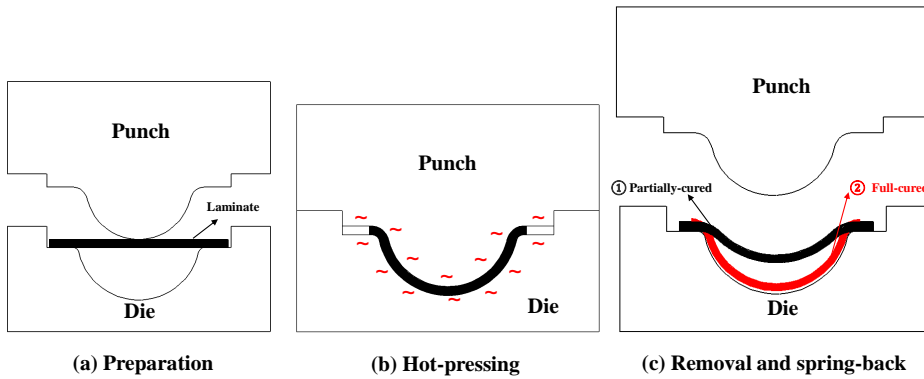


Figure 5.6: Schematic graph of the laminate forming process on cure-dependent spring-back

5.3.4. SPRING-BACK CHARACTERISATION

DURING the traditional sheet metal forming process, the spring-back before and after unloading is mainly characterised by the spring-back angle $\Delta\theta$ and the spring-back radius ΔR . As exhibited in Figure 5.7, the forming angle of the metal sheet is θ_0 , and the corresponding forming radius is R_0 . After spring-back, the value changes to θ_1 and R_1 , respectively. Then, the spring-back angle and radius are defined by Equation 5.4 and 5.5:

$$\Delta\theta = \theta_0 - \theta_1 \quad (5.4)$$

$$\Delta R = R_1 - R_0 \quad (5.5)$$

Here, R_0 and R_1 are both the radius of the neutral layer where the strain is assumed to be zero. During the spring-back period, it is assumed that the in-plane sections remain planar and the strain due to bending is proportional to the distance from the neutral layer. In addition, the through-the-thickness stress is ignored and no change occurs in sheet thickness ($t_0 = t_1$). Based on these assumptions, the relationship of forming angle

and radius can be written as [36, 48]:

$$\theta_0 \cdot R_0 = \theta_1 \cdot R_1 \quad (5.6)$$

Then, the spring-back ratio K which can be defined as the variation of spring-back angle divided by the initial forming angle is expressed as:

$$K = \frac{\Delta\theta}{\theta_0} = 1 - \frac{\theta_1}{\theta_0} = 1 - \frac{R_0}{R_1} \quad (5.7)$$

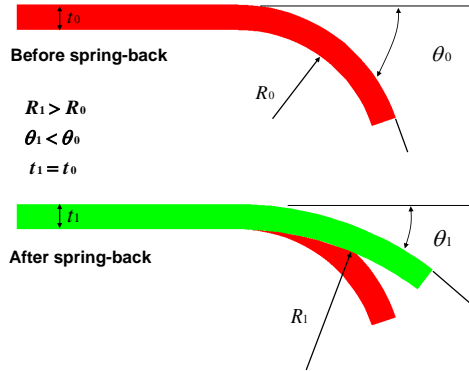


Figure 5.7: Definition of the spring-back angle and radius for the metal sheet forming process

For the press forming of the single-curved laminate in this work, the geometrical analysis of the spring-back ratio after removal of the forming loads is shown in Figure 5.8. The transition zone and fillet regions of the laminate exhibits non-cylindrical shape after spring-back which may affect the measurement of the forming depth and thus, influence the calculation of the spring-back radius. Therefore, a length L which is symmetrical to the vertical centreline is introduced to evaluate the spring-back behaviour. The geometric relations are expressed as follows:

$$(R_i - D_i)^2 + (L/2)^2 = R_i^2 \quad (5.8)$$

$$R_i = \frac{L^2 + 4D_i^2}{8D_i}, i = 1, 2 \quad (5.9)$$

where R and D are the radius and depth based on the length L , $i = 1, 2$ denotes the partially-cured and full-cured situations, respectively. Here, the curvature under the measure length is assumed to be a constant value. Besides, the maximum depth D_0 is 30 mm and the radius of the initial shape before spring-back R_0 is 50 mm. The dimensions can be substituted into Equation 5.9 and combined with Equation 5.7 to obtain the spring-back ratio:

$$K_i = 1 - \frac{8D_i \cdot R_0}{L^2 + 4D_i^2}, i = 1, 2 \quad (5.10)$$

Therefore, the spring-back ratio under different curing conditions can be calculated once the depth based on the length L is determined.

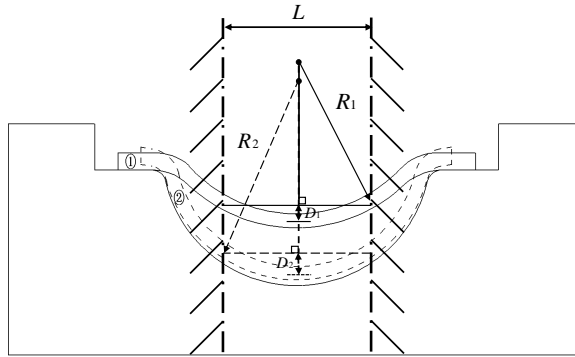


Figure 5.8: Geometric analysis of the laminate spring-back radius after removal of the forming loads

5.4. RESULTS AND DISCUSSION

5.4.1. EFFECT OF MEASURE LENGTH

FOR the press forming process of single-curved semi-cylindrical parts with flange areas, the non-cylindrical shapes after spring-back affect the evaluation of the spring-back behaviour. In order to accurately obtain the value of forming radius associated with the spring-back ratio, various lengths are applied in combination with their related forming depth. The single-curved parts and their corresponding profiles after spring-back under various material combinations are shown in Figure 5.9. The aluminium alloy (Al) and stainless steel (Ss) are the single-layer metal sheets, while the Al/GFRP and Ss/CFRP laminate with the layup of 2/1 and fibre orientation of $0^\circ/0^\circ$ which is parallel to the bend line are the hybrid materials under the full-cured conditions. The spring-back profiles are sketched and placed into an identical coordinate system to measure the forming depths under different lengths. Figure 5.10(a) exhibits the variations of the measured forming depth at five typical lengths as presented in Figure 5.9. The figure reveals that the final forming depth after spring-back increases with the increase of length while the depth varies for different material combinations. The forming radius can be calculated through the geometric relation in Equation 5.9 and the radius as a function of the measured length is shown in Figure 5.10(b). As for the investigated hybrid laminates, there is not much difference in the calculated forming radius when the measured length is smaller than 80mm. However, the forming radius increases as the length increases to 90mm and 100mm. The increase of radius becomes more significant at smaller values for the metal sheet especially for the single-layer aluminium 2024-T3. The results can be explained from the single-curved profiles in Figure 5.9, since the larger lengths include the transition zone and fillet regions, which falsely influence the value of the final radius. Besides, the smaller forming depth exhibits more spring-back and allows more regions to be in the flange. Therefore, the shape after spring-back becomes non-cylindrical and the forming radius changes significantly. Based on the radius curves as function of the length for the different materials, the forming radius at the measure length of 60mm is considered to be the most practical radius value to apply for the characterisation of spring-back in the study.

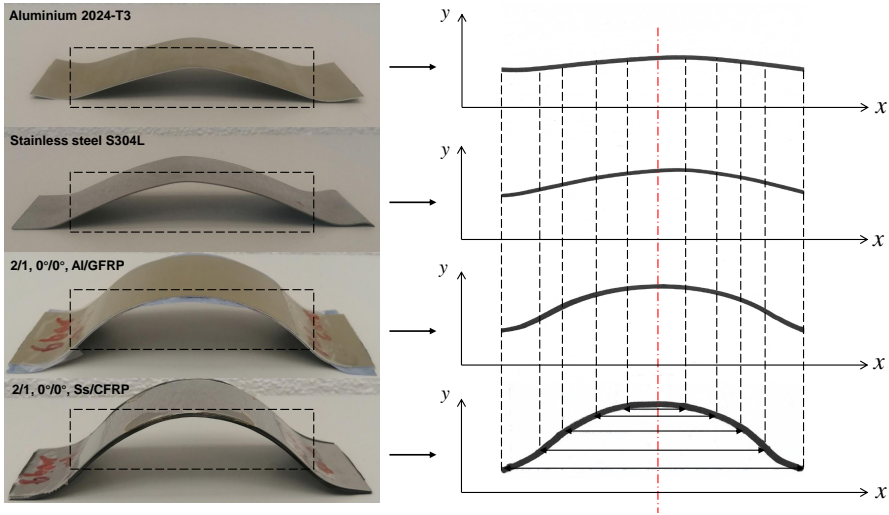


Figure 5.9: Single-curved parts and their profiles after spring-back for various material combinations

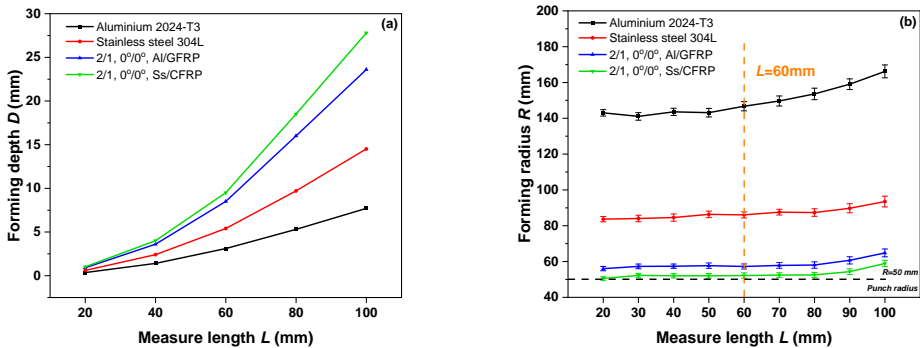


Figure 5.10: Two spring-back parameters under various measure lengths for different material combinations: (a) Forming depth; (b) Forming radius

5.4.2. EFFECT OF LAMINATE DESIGN

THE design of the metal-composite laminates consists of several material constituents, laminate layup and fibre orientation. After spring-back of the full-cured hybrid laminates, four different material combinations with the layup of 2/1 and fibre orientation of $0^\circ/0^\circ$ are shown in Figure 5.11. It can be seen from the graph that the stainless steel with carbon fibre reinforced prepreg (Ss/CFRP) has the largest forming depth at a length of 60mm and the forming depth for the combination of aluminium alloy sheet and glass fibre reinforced prepreg (Al/GFRP) is the smallest. Since the initial forming radius of the single-curved shape is 50mm, a higher forming depth after removal of the forming loads means a smaller spring-back ratio as the calculated forming radius is more close to the initial forming radius. Therefore, the result reveals that the material constituents play a significant role in the spring-back of the metal-composite laminates. The smaller spring-

back ratio of the hybrid laminates with stainless steel illustrates that the overall spring-back behaviour is mainly affected by the elastic-plastic deformation of the metal sheet. This can be explained from the stress-strain curve shown in Figure 5.1, where higher elastic modulus and lower yield strength of the stainless steel result in a lower elastic response compared to the aluminium alloy as the metal sheet reaches the same amount of deformation. Besides, the full-cured laminates with carbon fibre prepreg have a small decrease on the spring-back when compared with the metal-glass fibre reinforced hybrid laminates due to the higher elastic modulus for the carbon fibre prepreg. Moreover, the result shown in Figure 5.10 demonstrates that the presence of the prepreg system in hybrid laminate contributes significantly to the spring-back reduction when the laminate is full-cured. The calculated forming radiuses of the single-layer aluminium alloy and stainless steel after spring-back under the same conditions are 146.7 mm and 86.0 mm, and the spring-back ratios are 0.66 and 0.42, respectively.

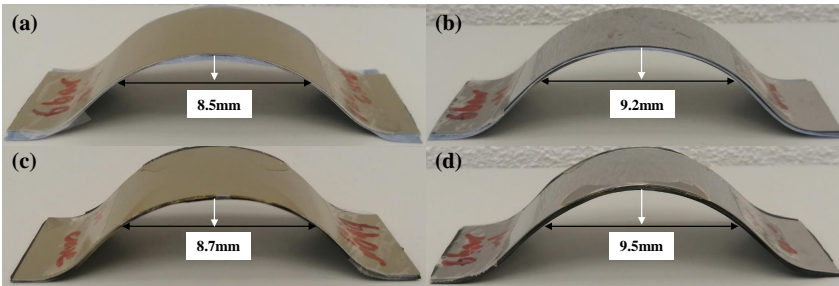


Figure 5.11: Single-curved part after full-cured process with different metal-composite combinations: (a) Al/GFRP; (b) Ss/GFRP; (c) Al/CFRP; (d) Ss/CFRP

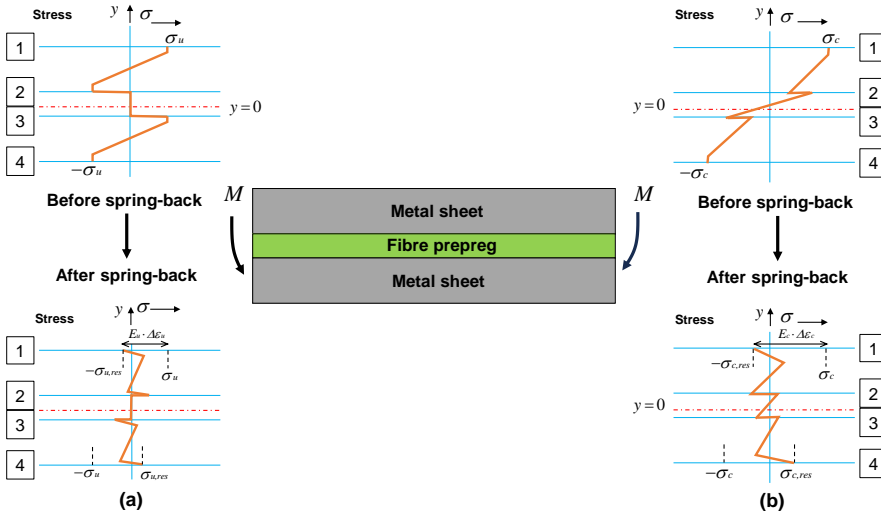


Figure 5.12: Schematic diagram of stress distribution after bending for metal-composite laminates: (a) Bent with an uncured prepreg and subsequently cured; (b) Bent with a full-cured prepreg

The substantial spring-back reduction for metal-composite laminates indicates that the spring-back is not only affected by the type of metal sheet since the aluminium alloy shows more spring-back than the stainless steel, but also by the design of the laminate. As the schematic diagram of the laminate stress distribution before and after spring-back exhibited in Figure 5.12, the bending deformation for metal sheet considers a material exhibiting elastic-ideal plastic behaviour without hardening. For the uncured hybrid laminate, the stress distribution for the metal sheet is symmetrical along its neutral layer, where the metal surfaces 1&2 (3&4) undergo the maximum tensile stress and compressive stress, respectively. In the outer metal surfaces, the stress will be capped at the maximum value where the vertical lines denote the plastic deformation regions. When a 2/1 laminate is bent with an uncured fibre prepreg in the middle (Figure 5.12(a)), the metal sheets can spring-back (more or less) independently from each other after unloading. The inner surfaces (2&3) of the metal sheet slip over the uncured fibre prepreg and this prepreg does not offer any resistance to this sliding. However, when a 2/1 laminate is bent with a full-cured prepreg and then unloaded, the metal layers are not able to spring-back independently anymore. In order to spring-back, the metal sheets should be unloaded elastically according to the stress distribution as sketched in Figure 5.12(b). Also, the two metal sheets are fixed after curing and the intermediate prepreg layer does not allow easy slip anymore, no spring-back occurs once the prepreg is full rigid. As a result, the spring-back can be greatly reduced and a larger residual stress remains at the metal-prepreg interface. Due to the increase of second moment of area I from the state of uncured to full-cured, the unloading flexural stiffness E_c with a full-cured laminate is larger than the unloading flexural stiffness E_u with an uncured laminate. Therefore, with the gradual increase of the residual stress during curing process, the internal stress $\sigma_{c,res}$ which related to the elastic strain recovery increases until the state of full-cured.

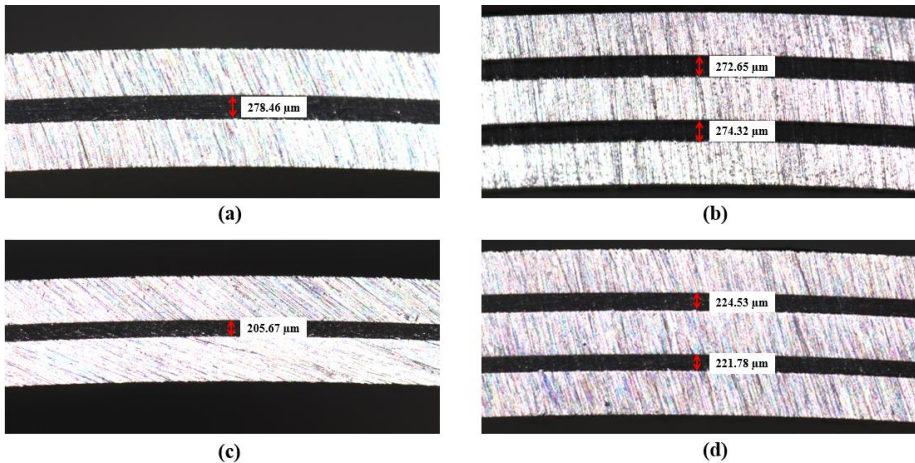


Figure 5.13: Cross-sectional micrographs of the central region in hybrid laminates after full-cured : (a) Al/GFRP with the layup of 2/1 and fibre orientation of $0^\circ/0^\circ$; (b) Al/GFRP with the layup of 3/2 and fibre orientation of $0^\circ/0^\circ$; (c) Al/CFRP with the layup of 2/1 and fibre orientation of $0^\circ/0^\circ$; (d) Al/GFRP with the layup of 3/2 and fibre orientation of $90^\circ/90^\circ$.

Since the study focuses on the out-of-plane spring-back where the dominate parameters are the elastic energy versus total energy, the energy for elastic deformation is reduced after full-cured which slows down the process of spring-back. In order to study the influence of the prepreg system on the spring-back after full-cure, cross-sectional micrographs on the central region of the laminate from the extracted profile (Figure 5.9) are shown in Figure 5.13. The various laminate structures after spring-back are presented and the prepreg layers are divided by the metal layers in the (striped) grey areas. The nominal thickness for carbon fibre prepreg and glass fibre prepreg layer are $300\mu\text{m}$ and $360\mu\text{m}$, and the average thickness of the prepreg layer drops to $205.67\mu\text{m}$ and $278.46\mu\text{m}$, respectively, as shown in Figure 5.13 (a) and (c). This demonstrates that the gradual curing process causes the matrix transverse flow and squeeze-out, which decreases the laminate thickness after curing.

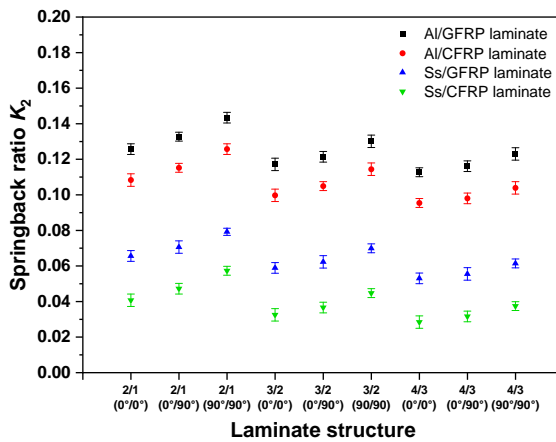


Figure 5.14: Spring-back ratio K_2 under different layup and fibre orientation conditions for hybrid laminates

The laminate layup and fibre orientation affects the overall thickness and the elastic modulus of the metal-composite laminates, which are also factors affecting the spring-back. Figure 5.14 exhibits the variations of the spring-back ratio after full-cured K_2 under various combinations of laminate layups and fibre orientations for the metal-composite laminates. The spring-back ratios after full-cured of aluminium-based fibre metal laminates are between 0.09 and 0.15, while the ratios of spring-back are less than 0.08 when replacing the aluminium sheet to stainless steel in hybrid laminates. This further shows that the properties of the metal sheet influence the spring-back after full-cure of the laminates. Besides, it is found from the figure that the increase of laminate layups leads to a moderate decrease on the spring-back ratio K_2 under the same fibre orientation condition. This is mainly because of the increase of overall thickness and the increase of residual stress during the press forming process. When the laminate changes from 2/1 structure to 3/2 structure under the same fibre orientation and pressure conditions as shown in Figure 5.13(a) and (b), the prepreg thickness witnesses a slight decrease due to the stress redistribution with the increase of metal sheets. Although the prepreg thickness for each layer decreases, the overall thickness increases with the increasing number

of layers. Therefore, as the radius/thickness ratio (R_0/t_h) affects the evolution of spring-back, the result follows the conclusion from the spring-back literature of the metal sheet [15–17] where the increased thickness reduces the ratios of spring-back. Moreover, the increase of prepreg layers promotes the increase of residual stresses which hinder the spring-back due to the increase of significant inelastic deformation. However, for metal-composite laminates with the same layups, the change of fibre orientation from $0^\circ/0^\circ$ to $90^\circ/90^\circ$ results in an increase on the spring-back after full-cured and there are mainly two reasons which can explain this phenomenon. First, the elastic modulus of the fibre prepreg relevant to the spring-back is much lower than that of the metal sheet when the fibre orientation changes from 0° to 90° and consequently, the lower axial residual stress in the composite layer has a less effect on the elastic unloading moment. In addition, the epoxy in the prepreg with a fibre orientation of $90^\circ/90^\circ$ is more prone to squeeze away from the curvature during curing process, which largely reduces the prepreg thickness as well as the overall thickness. The cross-sectional micrographs shown in Figure 5.13(b)(d) validates the thickness reduction where the average prepreg thicknesses in 3/2 Al/GFRP laminate with a fibre orientation of $0^\circ/0^\circ$ and $90^\circ/90^\circ$ are $273.49\mu\text{m}$ and $223.16\mu\text{m}$, respectively. Therefore, the results of the fibre orientation further illustrates that the hybrid laminates with lower elastic modulus and lower thickness result in a larger spring-back ratio after full-cured.

5.4.3. EFFECT OF DEGREE OF CURE

DURING the press forming process, forming temperature and holding time are two major parameters affecting the degree of cure and thereby the laminate spring-back and part quality. Therefore, various temperatures and times are set in the press forming process to investigate the spring-back of the hybrid laminates after a partial cure cycle. Figure 5.15 exhibits the formed single-curved parts at three temperatures at the holding time of 20 minutes for the Al/GFRP and Ss/CFRP laminate with a 2/1 layup and fibre orientation of $0^\circ/0^\circ$. Both hybrid materials exhibit an increase in forming depths with the increasing temperature for the measured length of 60mm while the tendency of increase is different. The forming depth of the Al/GFRP laminate increases slightly when the temperature increases from 40°C to 80°C , while the increase is significant when the forming temperature reaches 120°C . However, the forming depth for Ss/CFRP laminate undergoes a steady growth with these three temperatures. The observations illustrate that the increase of temperature results in the decrease of the partially-cured spring-back and the spring-back reduction is mainly due to the increase of elastic modulus resulting from increased crosslinking of the polymer network. Because the elastic modulus is higher, it requires larger residual stresses to cause the same amount of strain. Assuming that the spring-back of the metal sheet is consistent among the studied temperature range, the residual stresses generated by the glass fibre prepreg for Al/GFRP laminate before 80°C is too small to restrict the high spring-back behaviour of the aluminium sheet. However, when the forming temperature continues to rise, the substantial growth of the degree of cure (Figure 5.2) causes a higher residual stress and friction in-between the layers, which greatly reduces the spring-back. For Ss/CFRP laminate, the spring-back of stainless steel itself is lower and the residual stress generated by the carbon fibre prepreg also plays a role on the elastic recovery of the laminate. Besides, the cross-section micro-

graphs of the central region in the 2/1, 0°/0°, Al/CFRP laminate under these temperatures and 20-minute holding time shown in Figure 5.16 reveal that the average thickness of the prepreg decreases significantly from 273.94 μm to 212.63 μm as the temperature increases from 40°C to 120°C due to the epoxy squeeze flow and compaction along the width direction. The result illustrates that the decrease of prepreg thickness for hybrid laminates has a little effect on the partially-cured spring-back since the generation of residual stress dominates the spring-back formation and lower the spring-back ratio.

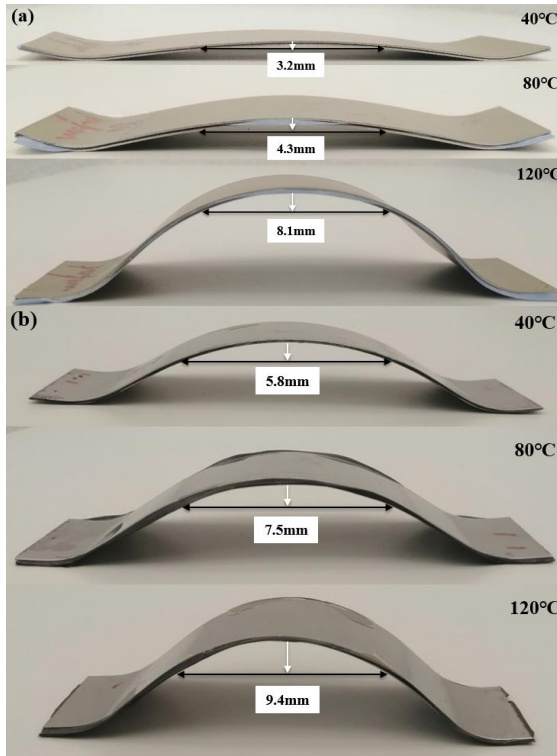


Figure 5.15: Single-curved parts after spring-back for two metal-composite combinations under various temperatures at the holding time of 20 min: (a) 2/1, 0°/0°, Al/GFRP; (b) 2/1, 0°/0°, Ss/CFRP

The residual stress generated during the press forming process depends on the reaction time of the epoxy as well. Therefore, different holding times are proposed to study the spring-back after partially-cured. Figure 5.17 presents the spring-back ratio K_1 of the Al/GFRP and Ss/CFRP laminates with the same 2/1 layout and fibre orientation of 0°/0° under various time and temperature conditions. When the holding time is zero, which denotes the instantaneous unloading as the pressure and temperature reach the set values, the spring-back ratio remains consistent within the temperature range, and the Al/GFRP laminates even have layer separations at elevated temperature. As the time gradually increases, both hybrid laminates have a spring-back decreasing trend where higher holding time contributes to the decrease of spring-back. The trend can be explained by the evolution of degree of cure and strength of adhesion. When the epoxy

system has no reaction time and zero degree of cure, the increase of forming temperature reduces the resin viscosity which decreases the strength of adhesion in-between the layers. The failure of layer separation occurs in the Al/GFRP laminate due to the higher spring-back behaviour of the aluminium alloy, while adhesion still occurs in the Ss/CFRP laminate even though the degree of adhesion is low at the temperature above 100°C. Once the holding time increases, the degree of cure and degree of adhesion increases, which hinder the release of elastic energy that has been accumulated in the laminate. In this case, there will be more interactions between the metal sheets and prepreg layers, and resulting in less spring-back and higher residual stress. Figure 5.18 exhibits the evolution of the cure-dependent spring-back ratio K as a function of the degree of cure α which is translated from the temperature and time for the metal-composite laminates. Here, the degree of cure for the spring-back after full-cured are set to be 0.9 and 0.95 for GFRP and CFRP materials, respectively and the computed values are obtained from Table 5.5. The figure reveals that hybrid laminates with the same prepreg system have similar trends of spring-back decreasing as the degree of cure increases. The spring-back ratios for the hybrid laminates drops significantly at the initial stage of curing, while the decrease becomes steady for metal/CFRP laminates at the degree of cure close to 0.1 and the degree of cure close to 0.4 for the metal/GFRP laminates. This indicates that metal sheets have limited influence on the partially-cured spring-back of the hybrid materials and the spring-back difference is mostly dependent on the thermo-chemical evolution of mechanical properties of the epoxy in prepregs.

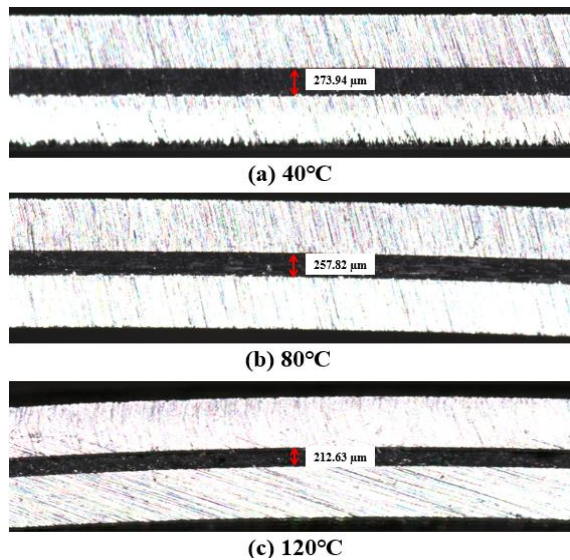


Figure 5.16: Cross-section micrographs of the central region in 2/1, 0°/0°, Al/CFRP laminate under three temperature conditions

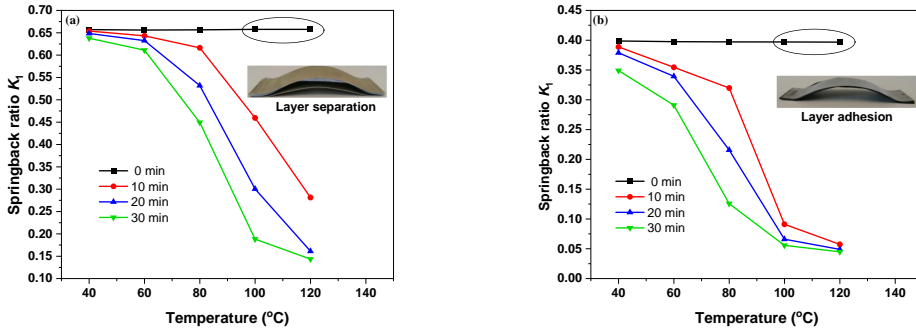


Figure 5.17: Spring-back ratio K_1 under various temperature and time conditions after partially-cured process: (a) 2/1, 0°/0°, Al/GFRP; (b) 2/1, 0°/0°, Ss/CFRP

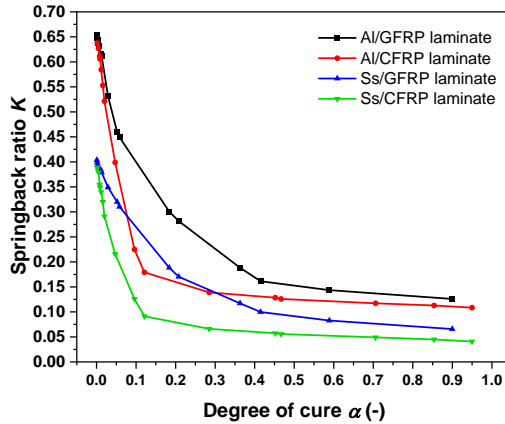


Figure 5.18: Evolution of spring-back ratio K as a function of degree of cure α for metal-composite laminates

5.4.4. EFFECT OF FORMING PRESSURE

THE results of the cure-dependent spring-back characterisation are all obtained under the forming pressure of 6 bar. However, the effect of forming pressure may also play a role on the spring-back behaviour of metal sheet and fibre prepreg. Figure 5.19 displays the spring-back ratio K_2 after full-cured under different pressure conditions for hybrid laminates with a 2/1 layout and fibre orientation of 0°/0°. It shows that the aluminium based metal-composite combinations separate under low pressure conditions after curing, while this separation disappears with the increasing pressure. The hybrid laminate with stainless steel does not separate at low pressure and the spring-back ratio after full-cured follows the trend where the value remains nearly constant at high pressure conditions. The trend shows that only low forming pressure affects the final shape of the formed part and the increase of pressure above a certain level will not further improve the spring-back of the hybrid laminate at full-cured state. Even though the overall thickness of the laminate decreases once the pressure increases which would somehow

promotes the spring-back, the increasing bending force between the metal sheet and prepreg layer results in the decrease of spring-back and higher residual stresses. The relative low degree of adhesion and friction under low pressure conditions is unable to compensate for the high elastic response of the aluminium alloy, which leads to the separation after full-cured process. However, when the degree of cure and adhesion at the metal-prepreg interfaces reaches the maximum value for full-bonding, further increase of the pressure under curing conditions has a limited effect on the spring-back. Therefore, the effect of forming pressure is negligible when the pressure increases beyond 6 bar during the press forming process of metal-composite laminates.

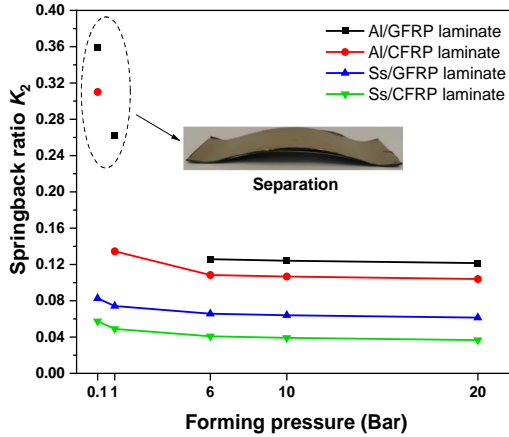


Figure 5.19: Spring-back ratio K_2 after full-cured under different forming pressures for hybrid laminates

5.5. CONCLUSIONS

THE cure-dependent spring-back of metal-composite laminate is experimentally characterised during the press forming process of a single-curved semi-cylindrical part. The spring-back ratios at the partially-cured and full-cured conditions are compared and the factors affecting the spring-back, including the material constituent, fibre orientation, laminate layup, holding time, forming temperature and pressure, are analysed in detail. The relevant conclusions are:

(1) The irregular shape of a single-curved semi-cylindrical part with flange regions affects the evaluation of the spring-back behaviour for different material combinations. The forming radius at a measured length of 60mm is considered to be the practical value for the characterisation of spring-back in this study.

(2) The cure-dependent spring-back and residual stress are counterparts. When the spring-back reduces due to the higher degree of cure, the residual stress increases and vice versa. They are both the result of the accumulated elastic energy and thermal effects in the laminate.

(3) The spring-back of metal-composite laminates are mainly driven by the elastic modulus and yield strength of the metal constituent; the low elastic modulus as well as high yield strength as for the aluminium 2024-T3 shows more spring-back. The pres-

ence of prepreg system in the hybrid materials contributes significantly to the decrease of spring-back especially for over 40% when the laminate is full-cured. The increase of laminate layups results in a moderate decrease of 1% on the full-cured spring-back, while the change of fibre orientation from $0^\circ/0^\circ$ to $90^\circ/90^\circ$ for the hybrid laminate witnesses a significant increase of 1% to 2% on the spring-back after full-cured.

(4) The spring-back of the metal-composite laminates after partially-cured depends on the forming temperature and holding time during the hot-pressing process. The increase of degree of cure and degree of adhesion results in spring-back reduction of 50% for aluminium based hybrid laminates and 30% for stainless steel based hybrid laminates. Also, the decrease becomes steady for metal/CFRP laminates at the degree of cure of 0.1 and the degree of cure of 0.4 for the metal/GFRP laminates. The high spring-back characteristics of the aluminium alloy induces the failure of layer separation at low degree of cure levels.

(5) The selection of forming pressure also influences the spring-back behaviour of the hybrid laminates. The aluminium based metal-composite laminate separate under low pressure conditions of less than 1kN after curing, while the separation disappears with the increase of pressure. However, further increase of forming pressure has a limited effect on the spring-back after full-cured and the pressure of 6 bar is regarded as a proper pressure for the press forming of metal-composite laminates.

REFERENCES

- [1] J. Sinke, "Manufacturing of glare parts and structures," *Applied composite materials*, vol. 10, pp. 293–305, 2003.
- [2] T. Sinmazçelik, E. Avcu, M. Ö. Bora, and O. Çoban, "A review: Fibre metal laminates, background, bonding types and applied test methods," *Materials & Design*, vol. 32, no. 7, pp. 3671–3685, 2011.
- [3] D. Nardi, M. Abouhamzeh, R. Leonard, and J. Sinke, "Investigation of kink induced defect in aluminium sheets for glare manufacturing," *Composites Part A: Applied Science and Manufacturing*, vol. 125, p. 105531, 2019.
- [4] Y. Guo, C. Zhai, F. Li, X. Zhu, F. Xu, and X. Wu, "Formability, defects and strengthening effect of steel/cfrp structures fabricated by using the differential temperature forming process," *Composite Structures*, vol. 216, pp. 32–38, 2019.
- [5] K. Kavitha, R. Vijayan, and T. Sathishkumar, "Fibre-metal laminates: A review of reinforcement and formability characteristics," *Materials Today: Proceedings*, vol. 22, pp. 601–605, 2020.
- [6] L. Mosse, P. Compston, W. J. Cantwell, M. Cardew-Hall, and S. Kalyanasundaram, "The development of a finite element model for simulating the stamp forming of fibre-metal laminates," *Composite Structures*, vol. 75, no. 1-4, pp. 298–304, 2006.
- [7] S. Roth, M. Stoll, K. Weidenmann, S. Coutandin, and J. Fleischer, "A new process route for the manufacturing of highly formed fiber-metal-laminates with elastomer

- interlayers (fmeI),” *The International Journal of Advanced Manufacturing Technology*, vol. 104, pp. 1293–1301, 2019.
- [8] Z. Ding, H. Wang, J. Luo, and N. Li, “A review on forming technologies of fibre metal laminates,” *International Journal of Lightweight Materials and Manufacture*, vol. 4, no. 1, pp. 110–126, 2021.
- [9] T. Heggemann and W. Homberg, “Deep drawing of fiber metal laminates for automotive lightweight structures,” *Composite Structures*, vol. 216, pp. 53–57, 2019.
- [10] S. Liu, J. Sinke, and C. Dransfeld, “An inter-ply friction model for thermoset based fibre metal laminate in a hot-pressing process,” *Composites Part B: Engineering*, vol. 227, p. 109400, 2021.
- [11] Q. Chen, P. Boisse, C. H. Park, A. Saouab, and J. Bréard, “Intra/inter-ply shear behaviors of continuous fiber reinforced thermoplastic composites in thermoforming processes,” *Composite structures*, vol. 93, no. 7, pp. 1692–1703, 2011.
- [12] A. Rashidi, H. Montazerian, K. Yesilcimen, and A. Milani, “Experimental characterization of the inter-ply shear behavior of dry and prepreg woven fabrics: Significance of mixed lubrication mode during thermoset composites processing,” *Composites Part A: Applied Science and Manufacturing*, vol. 129, p. 105725, 2020.
- [13] S. Erland and T. Dodwell, “Quantifying inter-and intra-ply shear in the deformation of uncured composite laminates,” *Advanced Manufacturing: Polymer & Composites Science*, vol. 7, no. 2, pp. 25–35, 2021.
- [14] L. Shichen, L. Lihui, and G. Shiwei, “An investigation into the formability and processes of glare materials using hydro-bulging test,” *International Journal of Precision Engineering and Manufacturing*, vol. 20, pp. 121–128, 2019.
- [15] F. J. Gardiner, “The spring back of metals,” *Transactions of the American Society of Mechanical Engineers*, vol. 79, no. 1, pp. 1–7, 1957.
- [16] M. Yang, Y. Akiyama, and T. Sasaki, “Evaluation of change in material properties due to plastic deformation,” *Journal of Materials Processing Technology*, vol. 151, no. 1-3, pp. 232–236, 2004.
- [17] S. Saravanan, M. Saravanan, and D. Jeyasimman, “Study on effects of spring back on sheet metal bending using simulation methods,” *International journal of mechanical and production*, vol. 8, pp. 923–932, 2018.
- [18] S. Chikalthankar, G. Belurkar, and V. Nandedkar, “Factors affecting on springback in sheet metal bending: a review,” *International Journal of Engineering and Advanced Technology*, vol. 3, no. 4, pp. 247–251, 2014.
- [19] G. Sharad and V. Nandedkar, “Spring-back in sheet metal bending - a review,” *Journal of Mechanical and Civil Engineering*, pp. 53–56, 2015.

- [20] R. K. Lal, V. K. Choubey, J. Dwivedi, and S. Kumar, "Study of factors affecting spring-back in sheet metal forming and deep drawing process," *Materials Today: Proceedings*, vol. 5, no. 2, pp. 4353–4358, 2018.
- [21] M. Sajjan, M. Amirthalingam, and U. Chakkingal, "A novel method for the spring-back analysis of a hot stamping steel," *Journal of Materials Research and Technology*, vol. 11, pp. 227–234, 2021.
- [22] M. Wisnom, M. Gigliotti, N. Ersoy, M. Campbell, and K. Potter, "Mechanisms generating residual stresses and distortion during manufacture of polymer–matrix composite structures," *Composites Part A: Applied Science and Manufacturing*, vol. 37, no. 4, pp. 522–529, 2006.
- [23] M. Fiorina, A. Seman, B. Castanié, K. Ali, C. Schwob, and L. Mezeix, "Spring-in prediction for carbon/epoxy aerospace composite structure," *Composite Structures*, vol. 168, pp. 739–745, 2017.
- [24] L. Mezeix, A. Seman, M. Nasir, Y. Aminanda, A. Rivai, B. Castanié, P. Olivier, and K. Ali, "Spring-back simulation of unidirectional carbon/epoxy flat laminate composite manufactured through autoclave process," *Composite structures*, vol. 124, pp. 196–205, 2015.
- [25] M. Abouhamzeh, J. Sinke, and R. Benedictus, "Prediction models for distortions and residual stresses in thermoset polymer laminates: an overview," *Journal of Manufacturing and Materials Processing*, vol. 3, no. 4, p. 87, 2019.
- [26] C. Brauner, S. Bauer, and A. S. Herrmann, "Analysing process-induced deformation and stresses using a simulated manufacturing process for composite multispar flaps," *Journal of Composite Materials*, vol. 49, no. 4, pp. 387–402, 2015.
- [27] C. Brauner, T. Frerich, and A. S. Herrmann, "Cure-dependent thermomechanical modelling of the stress relaxation behaviour of composite materials during manufacturing," *Journal of Composite Materials*, vol. 51, no. 7, pp. 877–898, 2017.
- [28] Y. Uriya and J. Yanagimoto, "Suitable structure of thermosetting cfrp sheet for cold/warm forming," *International Journal of Material Forming*, vol. 9, pp. 243–252, 2016.
- [29] G. C. Pereira, P. LeBoulluec, W.-T. Lu, M. Yoshida, A. P. Alves, and A. F. Avila, "Spring-back behavior on l-shaped composite structures: A statistical analysis of angular recovery as a function of time and residual cure," *Composites Part A: Applied Science and Manufacturing*, vol. 124, p. 105491, 2019.
- [30] K. E. Tarsha-Kurdi and P. Olivier, "Thermoviscoelastic analysis of residual curing stresses and the influence of autoclave pressure on these stresses in carbon/epoxy laminates," *Composites science and technology*, vol. 62, no. 4, pp. 559–565, 2002.
- [31] G. Twigg, A. Poursartip, and G. Fernlund, "Tool-part interaction in composites processing. part i: experimental investigation and analytical model," *Composites Part A: Applied Science and Manufacturing*, vol. 35, no. 1, pp. 121–133, 2004.

- [32] O. G. Kravchenko, S. G. Kravchenko, and R. B. Pipes, "Cure history dependence of residual deformation in a thermosetting laminate," *Composites Part A: Applied Science and Manufacturing*, vol. 99, pp. 186–197, 2017.
- [33] Y. Guo, Z. Chen, F. Li, X. Xu, J. Chen, Y. Ren, and Y. Wang, "Study on formability and failure modes of steel/cfrp based fmls consisting of carbon fiber reinforced polymer prepreg and steel sheet," *Composite Structures*, vol. 281, p. 114980, 2022.
- [34] M. Parsa, M. Ettehad, *et al.*, "Experimental and finite element study on the spring back of double curved aluminum/polypropylene/aluminum sandwich sheet," *Materials & Design*, vol. 31, no. 9, pp. 4174–4183, 2010.
- [35] S. Keipour and M. Gerdooei, "Springback behavior of fiber metal laminates in hat-shaped draw bending process: experimental and numerical evaluation," *The International Journal of Advanced Manufacturing Technology*, vol. 100, pp. 1755–1765, 2019.
- [36] A. Isiktas and V. Taskin, "Springback behavior of fiber metal laminates with carbon fiber-reinforced core in v-bending process," *Arabian journal for science and engineering*, vol. 45, no. 11, pp. 9357–9366, 2020.
- [37] M. Hahn, N. Ben Khalifa, C. Weddeling, and A. Shabaninejad, "Springback behavior of carbon-fiber-reinforced plastic laminates with metal cover layers in v-die bending," *Journal of Manufacturing Science and Engineering*, vol. 138, no. 12, p. 121016, 2016.
- [38] J. Wang, J. Li, C. Fu, G. Zhang, W. Zhu, X. Li, and J. Yanagimoto, "Study on influencing factors of bending springback for metal fiber laminates," *Composite Structures*, vol. 261, p. 113558, 2021.
- [39] S. Y. Kim, W. J. Choi, and S. Y. Park, "Spring-back characteristics of fiber metal laminate (glare) in brake forming process," *The International Journal of Advanced Manufacturing Technology*, vol. 32, pp. 445–451, 2007.
- [40] V. Zal, H. M. Naeini, A. R. Bahramian, and J. Sinke, "Investigation of the effect of temperature and layup on the press forming of polyvinyl chloride-based composite laminates and fiber metal laminates," *The International Journal of Advanced Manufacturing Technology*, vol. 89, pp. 207–217, 2017.
- [41] M. Safari, M. Salamat-Talab, A. Abdollahzade, A. Akhavan-Safar, and L. da Silva, "Experimental investigation, statistical modeling and multi-objective optimization of creep age forming of fiber metal laminates," *Proceedings of the Institution of Mechanical Engineers, Part L: Journal of Materials: Design and Applications*, vol. 234, no. 11, pp. 1389–1398, 2020.
- [42] Solvay-Adhesive-Materials, "Technical datasheet for the fm-94 film adhesive," <https://www.solvay.com/en/product/fm-94-product-documents>, 2017.
- [43] SHD-Composite-Materials, "Technical datasheet for the mtc510 epoxy prepreg," <https://shdcomposites.com/admin/resources/mtc510-tds.pdf>, 2018.

- [44] R. Hardis, J. L. Jessop, F. E. Peters, and M. R. Kessler, "Cure kinetics characterization and monitoring of an epoxy resin using dsc, raman spectroscopy, and dea," *Composites Part A: Applied Science and Manufacturing*, vol. 49, pp. 100–108, 2013.
- [45] M. Abouhamzeh, J. Sinke, K. Jansen, and R. Benedictus, "Kinetic and thermo-viscoelastic characterisation of the epoxy adhesive in glare," *Composite Structures*, vol. 124, pp. 19–28, 2015.
- [46] S. Sourour and M. Kamal, "Differential scanning calorimetry of epoxy cure: isothermal cure kinetics," *Thermochimica Acta*, vol. 14, no. 1-2, pp. 41–59, 1976.
- [47] A. Dimopoulos, A. A. Skordos, and I. K. Partridge, "Cure kinetics, glass transition temperature development, and dielectric spectroscopy of a low temperature cure epoxy/amine system," *Journal of applied polymer science*, vol. 124, no. 3, pp. 1899–1905, 2012.
- [48] J. Liu and W. Xue, "Unconstrained bending and springback behaviors of aluminum-polymer sandwich sheets," *The International Journal of Advanced Manufacturing Technology*, vol. 91, pp. 1517–1529, 2017.

6

A NUMERICAL STUDY ON SIMULTANEOUS DEFORMATION FOR A DOME PART

This chapter focuses on the simultaneous deformation of uncured metal-composite laminates under the press forming process of a double-curved dome part. The study is designed to evaluate the effect of material type, fibre orientation, inter-ply friction as well as clamping force by the use of a finite element modelling method. The result shows that the main failure mode for aluminium-based hybrid materials is metal cracking while prepreg buckling dominates the failure of stainless steel-based hybrid materials. The increase of clamping force contributes to the deformation of fibre reinforced prepreg layer and decrease the risk of prepreg buckling, but the simultaneous increase of plastic deformation tends to induce the failure of metal cracking. The change of fibre orientation from 0°/90° to 45°/-45° affects the intra-ply shear strain and the variation of friction coefficient at metal-prepreg interface affects the inter-ply sliding displacement during the forming process. This study provides a numerical method on the material selection and process parameter optimisation where the compatible deformation of the individual layers can be achieved through its own mechanisms.

6.1. INTRODUCTION

METAL-composite laminates, which are also known as fibre metal laminates (FMLs), are the composite materials made by alternating thin sheets of metal alloys and layers of fibre reinforced polymers [1, 2]. This hybrid combination leads to a material which has excellent specific strength, higher stiffness, and superior fatigue resistance with respect to the monolithic metal sheets and better impact strength and damage tolerance compared to pure composites [3, 4]. Traditional method for the manufacturing of metal-composite laminates is through layup techniques followed by autoclave curing, which is suitable for the product with a relatively simple shape, having large radius like aircraft fuselages [5]. As for the forming of small and medium sized parts with relatively small radii and complex shapes, the concept of press forming is proposed where the hybrid laminates are pressed using dies and shaped by the deforming force [6]. However, there are some limitations for the press forming process of hybrid laminates especially for epoxy-based hybrid materials because of the needs for various forming and curing stages and for the complex and different deformation mechanisms. Therefore, this study proposes a press forming cycle involving a laminate preparing and preheating stage, forming of uncured laminate, consolidation or (partial) curing in a same mould as well as the cooling and removal of the part as shown in Figure 1.8. This research contributes to a better formability of metal-composite laminates based on the understanding of different deformation mechanisms for both layers as well as the optimisation of processing parameters in the press forming cycle.

6.2. LITERATURE ON SIMULTANEOUS DEFORMATION

THE forming of metal sheet into the desired shape involves the elastic-plastic deformation of the material by bending, stretching and drawing. Typically, the deformation induces in-plane strain ratios from pure shear to biaxial stretch and the failure strain for the metal alloy materials is in the range of 10% to 50% [7, 8]. Therefore, the deformability of the metal sheet is mainly determined by the composition and temperature condition of the metal alloy and the failure mode is dominated by the metal cracking during the forming process [9]. The wrinkling occurs for metal sheet which is caused by the increase of compressive stress, but an increasing thickness and clamping force contributes to the delay of wrinkling/buckling [10]. For the deformability of composite materials, fibre reinforcements and prepregs are particularly prone to wrinkling due to the fibre architecture and the possible slippage in-between the fibre tows [11, 12]. The wrinkling of woven fabrics is related to intra-ply shear in studies on the “shear locking angle”, which is the maximum angle between warp and weft yarns [13]. Furthermore, the wrinkling of unidirectional (UD) fibre prepregs occurs due to the large differences in rigidity between the fibre orientation and its transverse direction. Therefore, the wrinkles are related to the fibre bridging of the ply and the ply-ply friction during forming [14]. Larberg [15] found that the stacking sequence of UD-prepreg laminates has a significant effect on the wrinkle development when forming a spar geometry. He explained that the combination of 0° and 45° layers reduces the material deformability by shearing. Akermo et al. [16] discovered that the friction improves the forming behaviour of cross-ply UD prepregs by serving as a connection between the plies, but may also introduce wrinkles

if not properly controlled.

The numerical modelling of metal-composite laminates can be approached mainly in three ways at the micro-level, the meso-level and the macro-level. As for the micro-level approach, the model consists of fibres and matrix. This is the most complex but realistic approach as it requires partitioning the model into different parts [17]. The meso-level method regards the laminate as a system of independent layers with specific homogenized mechanical properties. This approach results in an effective modelling for all type of hybrid laminates as it requires relatively limited number of elements. Although there are simplifications where the issue of boundary conditions for the layers are skipped, it would not affect the laminate performance unless delamination or other failure phenomena occur [18, 19]. The macro-level approach describes the entire hybrid laminate as a homogenized material with anisotropic properties. This approach can be described as a simple generalization since only a few engineering constants are needed. The biggest problem for this method is to obtain the data of the homogenized material substituting the hybrid laminate. One of the possible solutions is the application of Classical Laminate Theory which enables the description of their behaviour under external loads according to the engineering constants, representing membrane, bending and coupling behaviour, or by the uniaxial tensile test of the specimen in order to obtain the mechanical properties in the theory [20, 21]. Moreover, process simulation of the press forming of fibre metal laminates requires an accurate mathematical description of the main deformation mechanisms like intra-ply shear, inter-ply sliding as well as bending [22]. None of these mechanisms is negligible or dominant, as the laminate deformability is supposed to be a result of a delicate balance among them [23, 24]. Therefore, more advanced material constitutive models and boundary conditions of each deformation mechanisms are required to improve the predictive quality for manufacturing. The aim of this chapter is to apply a numerical method on investigating the failure modes during the simultaneous deformation of the double-cured part and optimising the process parameter to achieve a non-defect forming though the uncured hybrid laminates.

6.3. MATERIALS AND METHOD

6.3.1. MATERIALS

THE hybrid laminates involved in the research are the metal sheets of aluminium alloy 2024-T3 (Al) and stainless steel 304L (Ss), as well as the fibre reinforced preregs of S2-glass/FM-94 (GFRP) and T300-carbon/MTC510 (CFRP). The metal-composite materials consist of two layers of 0.5-mm thick metal sheet and one layer of fibre preregs which are known as a 2/1 layup. Each fibre layer includes two cross-plyed unidirectional (UD) preregs with a total thickness of 0.3mm. The UD fibre ply oriented at 0° corresponds with the rolling direction of metal sheet and the fibre orientation applied in the hybrid laminates is 0°/90° and 45°/-45°. The mechanical properties of the materials in uncured hybrid laminates are shown in Table 6.1 and it is assumed that the behaviour of the metal sheet will not be affected under the studied temperature ranges. Two parameters of elastic modulus and ultimate strength for the UD reinforced fibre preregs represent the properties in the fibre orientation of 0° and 90°, respectively [25, 26].

Table 6.1: Mechanical properties of the material in the forming simulation [25, 26]

Materials	Density (g/cm^3)	Elastic modulus (GPa)	Shear modulus (GPa)	Poisson's ratio	Yield strength (MPa)	Ultimate strength (MPa)	Shear strength (MPa)	Elongation at break (%)
Aluminium alloy 2024-T3	2.7	71	28	0.33	320	480	283	16.2
Stainless steel 304L	8.0	200	77	0.30	210	574	378	45.6
UD glass fibre prepreg -FM94	2.6	54.0/9.4	5.5/2.6	0.33	-	1870/50	38.5	3.8
UD carbon fibre prepreg -MTC510	1.5	119.3/8.2	3.6/2.0	0.34	-	2282/54	99.0	1.3

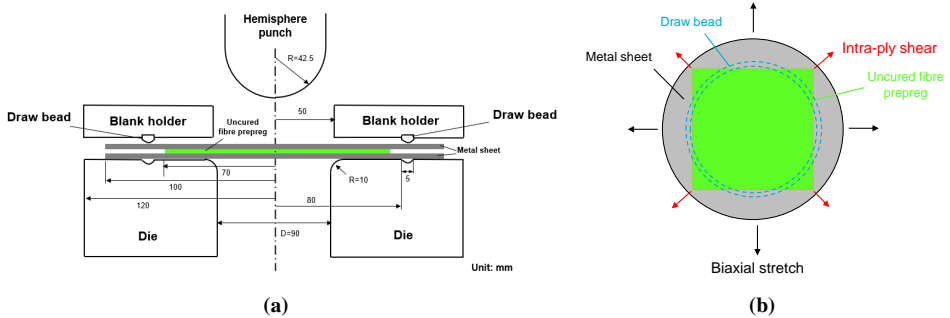


Figure 6.1: (a) Schematic graph of the double-curved dome forming tool design and dimensions; (b) Deformation mechanisms and initial shapes of the individual metal sheet and uncured fibre prepreg

Table 6.2: Test parameters used for the hybrid laminate press forming concept

Test parameter	Baseline value	Additional values investigated
Clamping force (N)	0	0.1, 1, 2
Inter-ply friction (μ)	1 (RT)	∞ (Tie), 0.5, 0.2

6.3.2. CONCEPT DESIGN

THE concept of simultaneous deformation of metal and composite layers for uncured metal-composite laminates came from the design of an integral forming and curing cycle in the proposed press forming process as exhibited in Figure 1.8. In order to investigate the three-dimensional (3D) deformations of the individual layers and the metal-prepreg interfaces, a double-curved dome forming tool with draw bead is designed in the schematic graph as shown in Figure 6.1(a). The hybrid laminate with a circle shape of 70mm radius for metal sheet layer and a square shape of 100 mm \times 100mm for fibre prepreg layer is placed symmetrically on the die surface and clamped by a blank holder. As the schematic graph presented in Figure 6.1(b) indicates, the metal sheet and fibre prepreg deform independently through bias-stretch and intra-ply shear respectively, and the different blank shape designs aim for the study of the compatibility of the deforma-

tions of the individual layers. Furthermore, the draw bead with the depth of 1mm and length of 5mm is proposed to constrain the material flow as well as to achieve a part without cracks and wrinkles. The punch with a radius of 42.5mm moves vertically down the centreline of the laminate to a predefined displacement. In addition to the different material types studied in the study, the effects of clamping force and inter-ply friction are compared as well. Table 6.2 presents the test parameters used for the forming simulation and the model will vary one parameter at a time while keeping the other parameters at the baseline value. To simplify the press forming temperature condition, the friction coefficient (μ) of 1 is regarded as the forming condition of room temperature (RT). Then, the frictional contacts where $\mu = \infty$ (Tie), 0.5, 0.2 are created as the state of full-cured, medium-friction as well as low-friction, respectively.

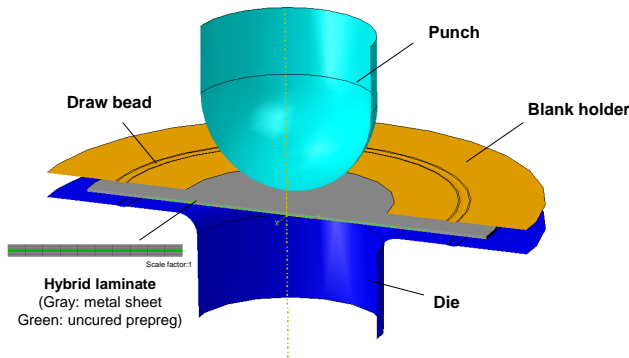


Figure 6.2: Finite element model of the press forming process for uncured hybrid laminates

6.3.3. FINITE ELEMENT MODEL

THE application of finite element model (FEM) is an efficient method to analyse the simultaneous deformation of uncured hybrid laminates and provide a guidance for actual experimental testing. Here, the finite element analysis software Abaqus/Explicit is used to simulate the press forming process of the uncured laminates by the meso-level approach using the stress-strain distributions of the metal sheet and the unique anisotropic properties of the fibre reinforced prepreg. Figure 6.2 exhibits the simulation model established for the study including the hybrid material and tool geometries. The elastic-plastic properties of the metal sheets and the elastic constants for the uncured prepreg lamina as shown in Table 6.1 are imported into the material property module in Abaqus. The failure criteria of the metal sheet and composite layer apply the Ductile and Hashin failure, respectively. In the finite element model, all tools including the punch, die and blank holder are modelled as discrete rigid shell elements with a mesh size of 2 mm. Metal sheets and the uncured fibre prepreg are created as four-node doubly curved conventional shell element with reduced integration (S4R) in the same mesh size. The laminate structure in the simulation model is represented in the composite layup module where all layers and their parameters such as orientation, thickness, property and relative location are defined and assembled into the forming simulation. As for the interactions and boundary conditions in the model, the value of clamping force and punch

displacement can be set, and the contacts between the fixed tools and the uncured laminates are set as penalty friction in a constant value of 0.15. Each of the metal sheets and composite layers is an own shell element with contact formulation for inter-ply friction as shown in Table 6.2. These friction coefficients can be simplified for different temperature conditions during the forming process.

6.4. RESULTS AND DISCUSSION

6.4.1. EFFECT OF MATERIAL COMPOSITION

DURING the laminate press forming process, the metal and composite type both play a significant role in the deformability and failure modes of the hybrid materials. Figure 6.3 shows the numerical result of the vertical displacement (U3) before failure for Al/GFRP laminate at room temperature and zero clamping force. The metal cracking which dealt by element deletion when the element exceeds the forming limits is the main failure mode as shown in the figure. It is observed that the lower aluminium sheet cracks first at the displacement of 25.08mm and the failure occurs at the centre regions of the metal material. The GFRP material, which is not shown in the figure, stays in contact with the outer metal layers and has no failure at such displacement. Also, the type of fibre prepreg has limited effect on the metal cracking and maximum depth for the aluminium-based hybrid laminates as the prepreg changes from GFRP to CFRP. The reason is due to the fact that the aluminium alloy has lower failure strain than the stainless steel while the fibre prepreg in the middle has not experienced large intra-ply shear strains nor failure at the same depth. When replacing the metal type from aluminium alloy to stainless steel, the failure mode for hybrid materials is totally different. The CFRP and GFRP material in the stainless steel-based hybrid laminate undergo prepreg buckling while the outer metal layers have no failure of metal cracking as exhibited in Figure 6.4. In this case, the numerical result on the vertical displacement (U3) before failure under room temperature and zero clamping force condition for the Ss/CFRP and Ss/GFRP laminates are 39.81mm and 44.64mm, respectively. The prepreg buckling is caused by the layer overlaps due to the increase of intra-ply shear strain which exceeds the locking angle. The locking strain for the GFRP is higher than the CFRP under the same condition which results in a larger failure depth during the forming process.

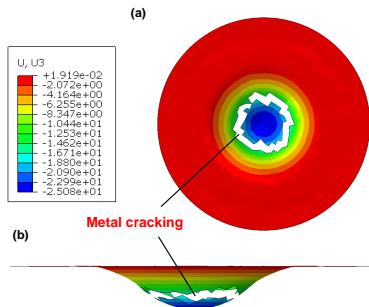


Figure 6.3: Numerical simulation on vertical displacement (U3,mm) before failure at room temperature and zero clamping force for Al/GFRP laminate: (a) XY plane-Al; (b) XZ plane-Al

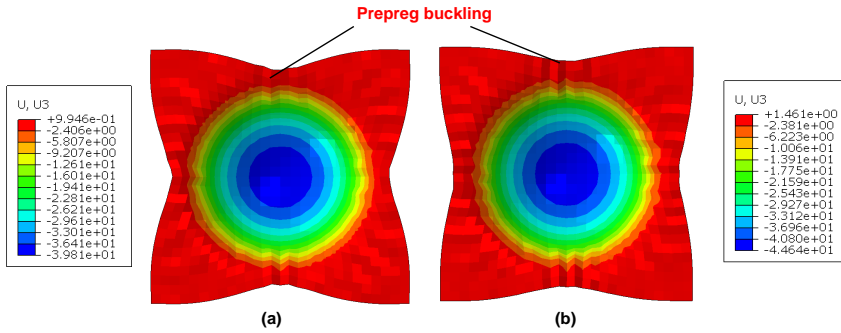


Figure 6.4: Numerical simulation on vertical displacement (U_3 , mm) before failure at room temperature and zero clamping force for stainless steel (Ss)-based hybrid materials: (a) CFRP layer; (b) GFRP layer

6.4.2. EFFECT OF CLAMPING FORCE

FIGURE 6.5 shows the simulation results on maximum draw depth and its corresponding failure mode under four clamping force conditions at room temperature. For the aluminium-based hybrid laminates with both CFRP and GFRP materials, the increase of clamping force tends to decrease the maximum draw depths even though the influence is limited. The reason is mainly due to the increase in biaxial stress which induces earlier cracking of the aluminium sheet. Besides, the main failure mode for such laminates is metal cracking and the prepreg layer witnesses no prepreg buckling. However, the larger draw depth with less clamping force does not mean a better formability for Al/CFRP and Al/GFRP laminates as the metal wrinkling occurs at the flange regions. For the stainless steel-based hybrid laminates, the failure mode is complex under various clamping forces. The increase of clamping force from 0 kN to 1 kN increases the maximum draw depth and the failure of metal cracking occurs coupled with prepreg buckling. As the clamping force reaches 2 kN, the metal cracking is dominated with lower failure depth while the phenomenon of prepreg buckling does not exist anymore. This indicates that the increase of clamping force delays the prepreg buckling. A more detailed graph on the different failure modes for Ss/CFRP laminates under 1 kN and 2 kN is exhibited in Figure 6.6. It is obvious to see that higher clamping force lowers the maximum failure depth and metal cracking occurs at the inner radius regions. The firm clamping on the four-square corners for CFRP reduces the occurrence of prepreg buckling by inducing tension forces in the prepreg layers through friction between draw bead-metal and blank holder-metal interfaces. In order to investigate the friction effects, the comparison between two clamping forces against the initial and final prepreg shapes for Ss/CFRP laminates at room temperature and draw depth of 40 mm is presented in Figure 6.7. When the clamping force is 0 kN, the CFRP is easier to flow into the central region which increase the possibility of prepreg buckling. However, the four-square corners of CFRP have nearly no movement when the clamping force is 2 kN. Since the clamping force only applies on the four-square corners of the CFRP layer, the effect on the deformability of the $0^\circ/90^\circ$ CFRP at four central edge regions is limited as the relative displacement is measured to be almost the same. Therefore, the clamping force at 1 kN can be regarded as an optimised parameter for a better deformability.

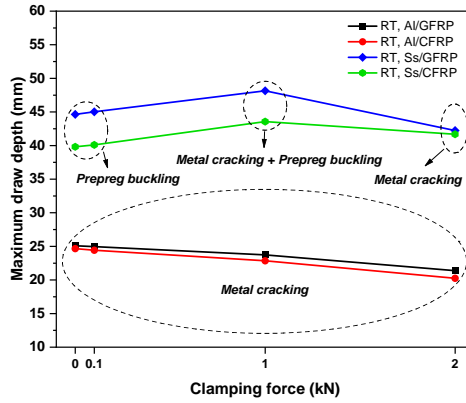


Figure 6.5: Numerical simulation on maximum draw depths and failure modes at room temperature under different clamping force for metal-composite laminates

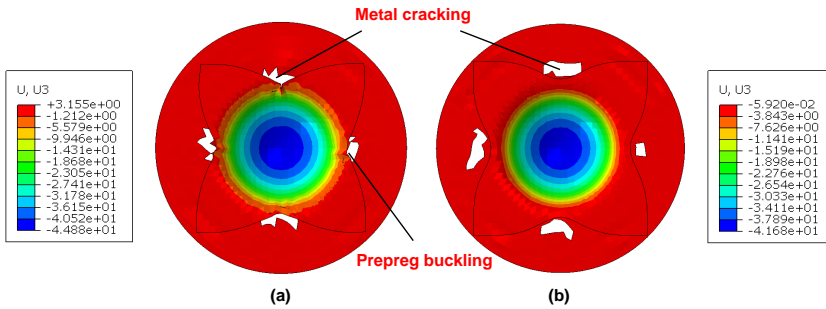


Figure 6.6: Numerical simulation on vertical displacement (U_3 ,mm) at the maximum value at room temperature for Ss/CFRP laminates under two clamping forces: (a) 1kN; (b) 2kN

6.4.3. EFFECT OF FIBRE ORIENTATION

To analyse the intra-ply shear mechanisms of the middle prepreg layer, the distributions of shear strain under two clamping force and two fibre orientation conditions are evaluated at a certain draw depth of 40mm at room temperature. Figure 6.8 shows that the deformation during forming for the cross-plyed UD CFRPs which oriented at $45^\circ/-45^\circ$ and $0^\circ/90^\circ$ is different. The maximum shear strain occurs at diagonal location along the 45-degree direction for the $0^\circ/90^\circ$ layups, while the $45^\circ/-45^\circ$ layups undergo the maximum shear strain at central area along the horizontal and vertical direction. With the increase of clamping force, the evolution of shear strain seems to have opposite trend. Although the increasing clamping contributes to the deformation of both layups, the CFRP with $0^\circ/90^\circ$ layout can exert its deformability in a better mechanism. As the length and width increases at the maximum shear strain regions for $45^\circ/-45^\circ$ layout, the compression force it induces tend to have the failure of prepreg buckling. Therefore, the CFRP material which oriented at $45^\circ/-45^\circ$ is not suitable for forming the dome part under the same condition as the prepreg requires intra-ply shear for deformation.

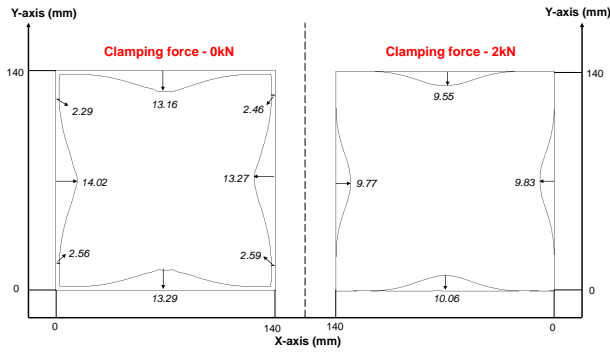


Figure 6.7: Comparison between two clamping forces against the initial and final prepreg shapes from the numerical simulation for Ss/CFRP laminates (Draw depth=40mm)

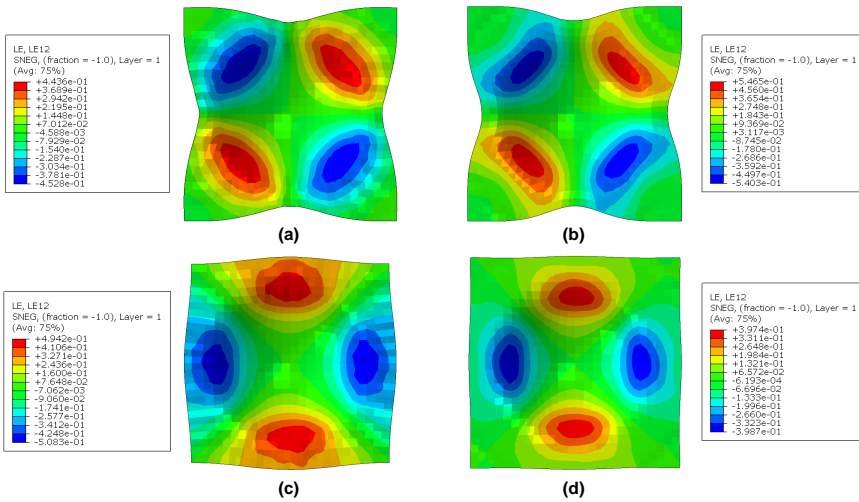


Figure 6.8: Numerical comparison on the shear strain distributions of the prepreg layer for Ss/CFRP laminates at room temperature (Draw depth=40mm): (a) 0kN, 0°/90°; (b) 2kN, 0°/90°; (c) 0kN, 45°/-45°; (d) 2kN, 45°/-45°

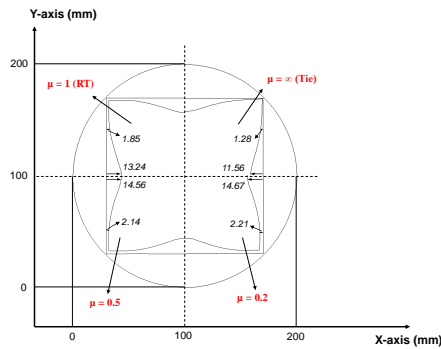


Figure 6.9: Comparison between different inter-ply frictions against the initial and final laminate shapes from the numerical simulation for Ss/CFRP laminates under the clamping force of 1kN (Draw depth=40mm)

6.4.4. EFFECT OF INTER-PLY FRICTION

THE importance of inter-ply friction can be underlined by conducting a “tie” ($\mu = \infty$) simulation and simulations with different frictional coefficients. Figure 6.9 shows the laminate shapes before and after forming at the draw depth of 40mm from the numerical simulation for Ss/CFRP laminates. The effect of friction on the inter-ply sliding is analysed by looking at the position of the edge of the prepreg layer. When the metal-prepreg interface is constrained which denotes a cured laminate, the maximum horizontal displacement for CFRP is 11.56mm and the horizontal gap at the centre location is small. With the decrease of inter-ply friction, the corresponding horizontal displacement and gap increases. This means that higher friction induces a limited sliding which constrain the deformation and delay the buckling of the CFRP material. However, the high friction and low friction condition seems to have distinct influence on the failure mode. Figure 6.10 presents the numerical results at the maximum vertical displacement for Ss/CFRP laminates under the clamping force of 1kN. It is seen that the metal-prepreg interfaces with a tie constraint witness a higher failure depth with metal cracking, while the failure of prepreg buckling is dominated when the inter-ply friction coefficient is 0.2. Therefore, the result demonstrates that a proper selection of inter-ply friction coefficient may help to increase the uncured laminate formability without the failure of either metal cracking or prepreg buckling.

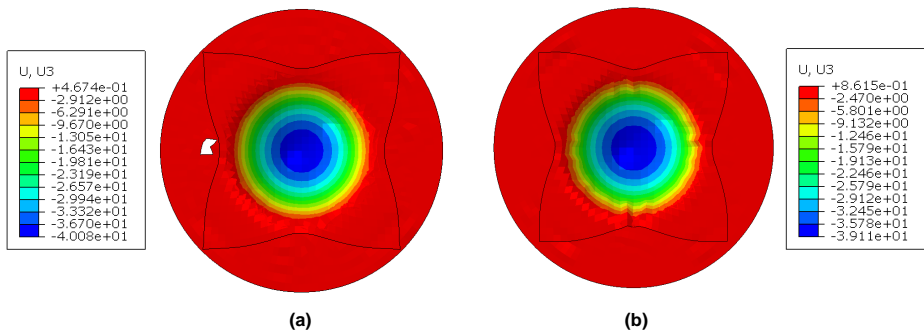


Figure 6.10: Numerical simulation on vertical displacement (U_3 , mm) before failure for Ss/CFRP laminates under the clamping force of 1kN and two inter-ply friction coefficients: (a) $\mu = \infty$; (b) $\mu = 0.2$

6.4.5. DISCUSSION OF OTHER EFFECTS

APART from the above mentioned effects on the numerical study for the press forming of uncured metal-composite laminates, there are multiple other influencing factors need to be considered. A few of them will be discussed briefly in this section.

First, the application of a draw bead aims to control the material flow of both metal sheets and prepreg layers by applying a dedicated clamping force. Therefore, the size and location of the draw bead are critical in such research. Since the ring-shaped draw bead covers all sections of the circular metal blanks, the larger bead or a higher blank holder pressure results in more restriction of the metal flow, which cause earlier cracking during forming. However, in these cases the defect of metal wrinkling is postponed if the draw bead and blank holder are properly applied. For the effects of the draw bead on the

uncured prepreg: the larger the size on the four-square corner regions that is clamped, the more pronounced the intra-ply shear of the prepreg layers, which is beneficial for prepreg deformation. The same effect can be achieved by increasing the pressure .

Second, the blank diameter and blank thickness for the metal sheet affect the laminate deformability as well which is proven by studies on deep-drawing process [6, 14]. From those studies it is clear that the blank diameter has an optimum for a given material and thickness. Increasing the diameter shifts the balance between drawing and stretching towards stretching, while decreasing the diameter shifts the balance towards drawing. A decreasing thickness results in more primary and secondary wrinkling problems. For the uncured prepreg the size effects are less dominant.

Third, another parameter that affects the results is the friction between the layers during forming. An increased temperature lowers the resin viscosity and friction coefficient at the metal-prepreg interfaces, while the increase of fibre shear angles as the temperature increases for cross-ply UD prepregs (Chapter 3) will further accelerate the occurrence of prepreg buckling. Therefore, the proper heating of the uncured laminates under a medium temperature and friction condition is beneficial to form a high-quality dome part without the failure of metal cracking and prepreg buckling at the same time. In this respect the type of resin and the fibre architecture also play their roles.

The last item to be mentioned is the product shape. In this numerical study only a circular blank was investigated to be deformed in a dome-shape. When other shapes, like e.g. box shapes, are investigated, the strategy to induce the two deformation mechanisms (biaxial stretching for metals, intra-ply shear for prepregs) requires new blank designs for both metal sheets and prepreg layers. In addition, the tool design, including the position of draw beads and size and shape of blank holder, needs to be considered. All these items are recommended to be explored in future research.

6.5. CONCLUSION

THE simultaneous deformation of the uncured metal-composite laminates is numerically investigated under different material composition, fibre orientation, inter-ply friction as well as clamping force conditions. The proposed method applies a initial circle and square shape for metal sheet and uncured fibre prepreg, respectively. The main conclusions are:

(1) The failure mode of the uncured hybrid laminates depends on the type of metal composition. The aluminium-based materials with a lower fracture strain exhibit a lower maximum forming depth with aluminium cracking. While for the stainless steel-based materials, the prepreg buckling dominates the laminate failure with a higher maximum forming depth. In addition, the Ss/GFRP undergoes a higher forming depth than the Ss/CFRP under the same condition, but the effect of fibre reinforced prepreg layer on aluminium-based materials is limited.

(2) The increase of clamping force contributes to the deformation of fibre reinforced prepreg and decrease the risk of prepreg buckling, while the increase of biaxial stress as well as the hinder of sliding and material flow tend to induce metal cracking for the stainless steel-based materials. A medium clamping force of 1kN is regarded as a compromise forming parameter since the effect of clamping on metal sheet and fibre prepreg is opposite.

(3) The fibre orientation plays a significant role in the intra-ply shear strain and the fibre prepreg oriented at $45^\circ/-45^\circ$ is not suitable for the forming of dome part compared with the $0^\circ/90^\circ$ layups. Besides, a proper heating of the uncured hybrid laminates under a medium temperature and friction condition increase the laminate deformability without the failure of either metal cracking or prepreg buckling.

(4) The application of draw bead results in the constrain of the material flow of metal sheet and fibre prepreg when applying pressure. The effects of tool design, blank diameter and thickness of the metal sheet in hybrid laminates during press forming need to be discussed.

REFERENCES

- [1] A. Asundi and A. Y. Choi, "Fiber metal laminates: an advanced material for future aircraft," *Journal of Materials processing technology*, vol. 63, no. 1-3, pp. 384–394, 1997.
- [2] L. B. Vogelesang and A. Vlot, "Development of fibre metal laminates for advanced aerospace structures," *Journal of materials processing technology*, vol. 103, no. 1, pp. 1–5, 2000.
- [3] E. C. Botelho, R. A. Silva, L. C. Pardini, and M. C. Rezende, "A review on the development and properties of continuous fiber/epoxy/aluminum hybrid composites for aircraft structures," *Materials Research*, vol. 9, pp. 247–256, 2006.
- [4] T. Sinmazçelik, E. Avcu, M. Ö. Bora, and O. Çoban, "A review: Fibre metal laminates, background, bonding types and applied test methods," *Materials & Design*, vol. 32, no. 7, pp. 3671–3685, 2011.
- [5] J. Sinke, "Manufacturing of glare parts and structures," *Applied composite materials*, vol. 10, pp. 293–305, 2003.
- [6] K. Osakada, K. Mori, T. Altan, and P. Groche, "Mechanical servo press technology for metal forming," *CIRP annals*, vol. 60, no. 2, pp. 651–672, 2011.
- [7] X. Wang and J. Cao, "On the prediction of side-wall wrinkling in sheet metal forming processes," *International Journal of Mechanical Sciences*, vol. 42, no. 12, pp. 2369–2394, 2000.
- [8] S. Suttner and M. Merklein, "A new approach for the determination of the linear elastic modulus from uniaxial tensile tests of sheet metals," *Journal of Materials Processing Technology*, vol. 241, pp. 64–72, 2017.
- [9] H. Blala, L. Lang, S. Khan, L. Li, S. Sijia, A. Guelailia, S. A. Slimane, and S. Alexandrov, "Forming challenges of small and complex fiber metal laminate parts in aerospace applications—a review," *The International Journal of Advanced Manufacturing Technology*, vol. 126, no. 5-6, pp. 2509–2543, 2023.
- [10] Y. Chen, Y. Yang, Z. Wang, H. Wang, J. Li, and L. Hua, "Accurate simulation on the forming and failure processes of fiber metal laminates: A review," *International Journal of Lightweight Materials and Manufacture*, 2023.

- [11] Q. Chen, P. Boisse, C. H. Park, A. Saouab, and J. Bréard, “Intra/inter-ply shear behaviors of continuous fiber reinforced thermoplastic composites in thermoforming processes,” *Composite structures*, vol. 93, no. 7, pp. 1692–1703, 2011.
- [12] P. Hallander, J. Sjölander, and M. Åkermo, “Forming induced wrinkling of composite laminates with mixed ply material properties; an experimental study,” *Composites Part A: Applied Science and Manufacturing*, vol. 78, pp. 234–245, 2015.
- [13] E. Guzman-Maldonado, P. Wang, N. Hamila, and P. Boisse, “Experimental and numerical analysis of wrinkling during forming of multi-layered textile composites,” *Composite Structures*, vol. 208, pp. 213–223, 2019.
- [14] M. Irani, M. Kuhtz, M. Zapf, M. Ullmann, A. Hornig, M. Gude, and U. Prahl, “Investigation of the deformation behaviour and resulting ply thicknesses of multilayered fibre–metal laminates,” *Journal of Composites Science*, vol. 5, no. 7, p. 176, 2021.
- [15] Y. Larberg and M. Åkermo, “In-plane deformation of multi-layered unidirectional thermoset prepreg—modelling and experimental verification,” *Composites Part A: Applied Science and Manufacturing*, vol. 56, pp. 203–212, 2014.
- [16] M. Åkermo, Y. Larberg, J. Sjölander, and P. Hallnager, “Influence of interply friction on the forming of stacked prepreg,” in *The 19th International Conference on Composite Materials (ICCM19), July 28 to August 2, 2013 in Montreal, Canada*, pp. 919–928, Curran Associates, Inc., 2013.
- [17] P. Linde, J. Pleitner, H. de Boer, and C. Carmone, “Modelling and simulation of fibre metal laminates,” in *ABAQUS Users’ conference*, vol. 421, 2004.
- [18] P. Soltani, M. Keikhosravy, R. Oskouei, and C. Soutis, “Studying the tensile behaviour of glare laminates: a finite element modelling approach,” *Applied Composite Materials*, vol. 18, pp. 271–282, 2011.
- [19] V. Zal, H. M. Naeni, J. Sinke, A. R. Bahramian, M. Abouhamzeh, and R. Benedictus, “A new procedure for finite element simulation of forming process of non-homogeneous composite laminates and fmls,” *Composite Structures*, vol. 163, pp. 444–453, 2017.
- [20] P. Boisse, K. Buet, A. Gasser, and J. Launay, “Meso/macro-mechanical behaviour of textile reinforcements for thin composites,” *Composites Science and Technology*, vol. 61, no. 3, pp. 395–401, 2001.
- [21] M. Smolnicki and P. Stabla, “Finite element method analysis of fibre-metal laminates considering different approaches to material model,” *SN Applied Sciences*, vol. 1, no. 5, p. 467, 2019.
- [22] S. P. Haanappel, *Forming of UD fibre reinforced thermoplastics*. University of Twente, 2013.

- [23] U. Sachs, R. Akkerman, K. Fetfatsidis, E. Vidal-Sallé, J. Schumacher, G. Ziegmann, S. Allaoui, G. Hivet, B. Maron, K. Vanclooster, *et al.*, “Characterization of the dynamic friction of woven fabrics: Experimental methods and benchmark results,” *Composites Part A: Applied Science and Manufacturing*, vol. 67, pp. 289–298, 2014.
- [24] S. Liu, J. Sinke, and C. Dransfeld, “An inter-ply friction model for thermoset based fibre metal laminate in a hot-pressing process,” *Composites Part B: Engineering*, vol. 227, p. 109400, 2021.
- [25] Solvay-Adhesive-Materials, “Technical datasheet for the fm-94 film adhesive,” <https://www.solvay.com/en/product/fm-94-product-documents>, 2017.
- [26] SHD-Composite-Materials, “Technical datasheet for the mtc510 epoxy prepreg,” <https://shdcomposites.com/admin/resources/mtc510-tds.pdf>, 2018.

7

CONCLUSIONS AND RECOMMENDATIONS

This chapter highlights the answers of the proposed research questions and main conclusions generated in the previous chapters of this work. Recommendations are also provided to shed light onto possible research paths in the future.

7.1. MAIN CONCLUSIONS

WITH the increasing use of composite materials like metal-composite laminates in structural component application in the aerospace industries, the manufacturing of such hybrid laminates becomes a topic. This thesis aims to assess the formability of uncured metal-composite laminates by investigating the deformation mechanisms, defects and failures during a press forming cycle with the integration of preheating, forming and curing. The proposed process enables the formation of rather complex shaped products made of stacks of uncured hybrid laminates. However, transformation from an uncured stack of layers to a cured and 3D-shaped product cannot be described and developed in its entirety. Hence, multiple deformation mechanisms during the process such as inter-ply friction, intra-ply shear, flexural bending are investigated independently, enabling quantitative, predictive and defect-free forming of uncured metal-composite laminates (Chapter 2-4). In addition, the tool design is important for the press forming since it needs to support these different, sometimes opposing deformation mechanisms. In addition, the defect of cure-dependent spring-back, the failure of metal cracking, prepreg buckling have been considered for (simulation of) the simultaneous deformation for uncured laminates (Chapter 5-6). The main conclusions and findings are related to the items shown in (Figure 7.1).

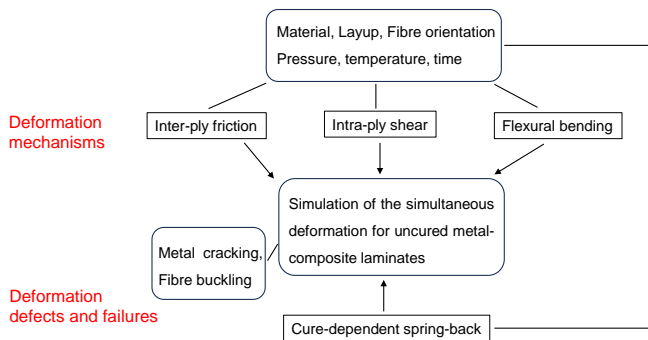


Figure 7.1: Summary on the main topics of the thesis

7.1.1. CHARACTERISATION OF DEFORMATION MECHANISMS AND DEFECTS

This addresses RQ1- 'How to analyse and characterise the mechanisms and defects in non-coherent deformations'.

For the deformation of an uncured stack of metal sheets and prepreg layers, a number of deformation mechanisms need to be activated including the inter-ply sliding (at the metal-prepreg interfaces), the intra-ply shear (within the prepreg layers), the flexural bending of the complete stack and in-plane plastic deformation of the metal layers. Due to the introduction of elastic deformation, spring-back should be accounted for.

- The inter-ply sliding behaviour has been investigated by a double-lap sliding test. Based on the results the static friction can be modelled using a Coulomb type of friction, and the kinetic friction complies with the transition of the mixed and hydrodynamic lubrication as described by the Stribeck-curve. When modelled for Abaqus/Explicit, the

inter-ply friction behaviour will be described by a static-kinetic exponential decay equation (Chapter 2).

- The intra-ply shear behaviour has been tested using a modified bias-extension test. During testing, it has been illustrated that the support of metal sheets in uncured hybrid laminates decreases the shear angles and delays the fibre wrinkling in the prepreg layers. Therefore, the forming limits of the uncured prepregs can be extended. (Chapter 3).

- The flexural bending has been experimentally and numerically characterised using a clamped-beam bending test. Based on the results the higher plastic deformation in the metal layers results in a significant increase of bending force and a reduction in the spring-back depth after unloading. Therefore, the forming limits of the metal sheet can be improved. (Chapter 4)

- Spring-back and residual stress are phenomena related to the elastic energy which are included during the press forming process and act as antagonists. The proposed forming process, including the (partial) cure cycle, definitely has a positive effect on the reduction of spring-back. When the degree of cure (and the strength of the adhesion) is increased, the more effective the composite layers are to restrict spring-back. As a consequence the residual stresses will increase, although these often are an order of magnitude smaller than the stresses applied during operation of the product. (Chapter 5)

7.1.2. ROLES ON INDIVIDUAL LAYERS OF METAL SHEET AND FIBRE PREPREG

This addresses RQ2- 'What roles have the individual layers of metal sheet and uncured fibre prepreg play during forming'.

The press forming of uncured metal-composite laminates includes three major roles of the different constituents: the deformation of the metal sheets, the deformation of the composite layers, and the sliding of the layers with respect to each other.

- The deformation of the metal sheets has a large similarity with the deformations encountered in common press forming techniques. Major deviations are the small thickness of these sheets and the applied high temperature during press forming, even though this does not have a significant influence on the forming limits. The forming limits are mainly determined by the basic metal properties which has been demonstrated with the results of Aluminium and Stainless Steel based laminates. The Stainless Steel, which has a much better formability, is therefore more suitable for the proposed process or shapes.

- The deformation of the composite layers differs in the shear mechanisms of woven fabric prepregs and cross-ply UD fibre prepregs. The sliding and shear within the prepregs for the cross-ply UD fibre prepregs in hybrid laminates postpone the occurrence of prepreg buckling and extends the forming limits. The types of prepreg layer including the glass fibre reinforced prepreg (GFRP) and carbon fibre reinforced prepreg (CFRP) as well as the fibre orientations play limited role in the deformability of the composite layers.

- The deformation of the uncured stack of layers also need accommodation of inter-ply sliding. The effect of inter-ply sliding largely depends on the properties of the prepreg layer and the applied pressure during forming. Lower friction at the metal-prepreg interfaces promotes the deformation of individual layers into their own mechanisms and contribute to the increase of deformability.

7.1.3. INFLUENCING FACTORS ON UNCURED LAMINATE DEFORMATION

This addresses RQ3- 'Which factors influence the simultaneous deformation of uncured laminates and how do they correlate'.

In order to improve the formability during this proposed press forming process in comparison with the forming of cured laminates, the following parameters are relevant: temperature, time and pressure/force.

- The temperature is the critical factor influencing the deformation mechanisms and defects during forming. For the inter-ply sliding, both the static and kinetic friction coefficients drop with increasing temperature (Chapter 2). For the intra-ply shear, the effect of temperature differs in two different prepregs. The fibre shear angle decreases with the increasing temperature for woven fabric based metal-composite laminates while the fibre shear angle undergoes an increase for cross-ply UD reinforced metal laminates (Chapter 3). However, the temperature affecting the properties of fibre prepreg play a limited role on the flexural bending (Chapter 4). The increase of temperature at a certain amount of time also results in the spring-back reduction after the integration of forming and curing for the hybrid laminates (Chapter 5).

- Time is also relevant in the preheating stage of the process. The preheating time to forming temperature should not be too large, otherwise the curing will already start. The increase of degree of cure and the strength of adhesion as the time increases will help the decrease of spring-back and achieve the forming with high accuracy (Chapter 5).

- The pressure/force is another important factor influencing the deformation mechanisms and defects during forming. In the inter-ply sliding study in Chapter 2, it can be noted that the static friction coefficient decreases with the increase of normal force, while the kinetic friction coefficient drops with the increase of normal force. In the intra-ply shear study in Chapter 3, it is mentioned that the fibre shear angles show a sharp decrease when applying the normal pressure on the central shear region. In the flexural bending study in Chapter 4, the application of clamping pressure has a significant impact on the flexural behaviour of the bent materials. With the increasing clamping pressure, the force required to bend increases significantly, the depth of spring-back gradually reduces and the resistance of sliding increases. The selection of forming pressure also affects the spring-back of the hybrid laminates as shown in Chapter 5. The aluminium-based metal-composite laminate separates under low pressure conditions after curing, while the separation disappears with the increase of pressure. The simultaneous study in Chapter 6 indicates that increase of clamping force contributes to the deformation of uncured fibre prepreg and delays the prepreg buckling, while the increase of plastic deformation as well as the hinder of sliding and material flow tend to induce metal cracking for the uncured hybrid materials.

These three major parameters have a strong correlation to each other. First, the temperature influences the viscosity of the resin. At high temperature this viscosity is low and enables easy inter-ply sliding and intra-ply shear deformations. However, in combination with time, the temperature also accelerates the curing of the resin, represented by the degree of cure. Therefore, the process window is limited.

The temperature and pressure also have a correlation at the consolidation stage where lower temperature and pressure cause the insufficient bonding of the metal sheet and fibre prepreg, thus influence the quality and accuracy of the final product. However, high

temperature and pressure will cause damage to the epoxy-based prepregs.

Even though the stage of cool down has limited influence on the quality of the epoxy-based hybrid laminates. Proper time and pressure will prevent the premature relaxation, which is beneficial for a non-defect product.

7.2. RECOMMENDATIONS FOR FUTURE WORK

THE present thesis proposes a press forming process for the manufacturing of uncured metal-composite laminates to form a defect-free component and the deformation mechanisms as well as defects are investigated to improve the deformability. However, more efforts are required to put the press forming of such hybrid laminates into actual industrial application. The main recommendations regarding future work are presented as follows:

(1) To obtain an accurate numerical simulation results, the metal sheets and fibre prepregs with matched deformation mechanisms can be developed. The friction at the metal-prepreg interfaces can be tailored through different material combinations and process conditions. The intra-ply shear behaviour can be used for both woven fabrics and cross-ply UD fibres. For a higher fidelity model description, a full coupled rheokinetic model with heat transfer can be a better solution to represent the entire process, even to capture residual stresses and strains.

(2) The simultaneous deformation of metal and uncured composite layers is shown to be feasible by applying a finite element simulation method. However, there is a lot can be added including the shapes, materials, layups, etc. The numerical validation is expected to be more efficient as it helps to inspect defects and achieves the process optimisation. However, the experimental testing is also crucial to compare with the numerical result and conversely, optimise and modify the model. Then, the quality inspection for the formed component are also topics need to be discussed. To meet the requirements, a combination of scanning electron microscope (SEM) and ultrasonic C-scan for the detection of laminate surface and cross-section can be used.

(3) The tool designs need to be further investigation including the more advanced tools on the clamping loadcell in the studies of inter-ply friction and intra-ply shear. Also, the tools for the formation of the dome are relatively simple and easy to predict the deformation. It becomes curious to see how the creation of local pressure steer the metal sheets and composite layers to activate their individual and different deformation mechanisms when more complex shape products are made.

(4) The thermoplastic based metal-composite laminates are extremely interesting for automotive industry and have the potential for (partial) recycling. Therefore, the investigation on the proposed press forming applied for thermoplastic based metal-composite laminates is recommended.

ACKNOWLEDGEMENTS

Many years ago when I started my bachelor, I cannot imagine that one day I can obtain the PhD degree in a prestigious university abroad. But now looking back to the last four to five years of my PhD research, it is been a really wonderful journey and this thesis is only a byproduct that tells my experience and growth in the Netherlands. The journey would not have been possible without the help of my colleagues, friends and family and the people who always support me, and I am appreciated to express my deepest gratitude to them.

First of all, I would like to thank my co-promotor and daily supervisor Ir Jos Sinke. Thanks for helping me develop the research framework, for guiding me to make progress step by step, for encouraging me to keep trying and never be afraid to make mistakes. I still remember the day when we had the first online interview and your kindness gave me so much confidence and motivation. Thanks for trusting me and giving me the freedom to explore and make my own decisions during the study. You taught me how to be critical, how to work independently and how to deal with some difficulties especially in the lab. Thanks for being so patient during the reviewing process of my draft papers, I finally find the suitable recipe and master the right skill for writing scientific papers. Most importantly, thanks for being there for me when I need it no matter for the research or personal life, and for sharing me with your own experience. I hope I could work with more people like you in the future and I really could not have done it without you.

Secondly, I would like to express my thanks to my promotor Prof. Clemens Dransfeld. You recruit me to the AMT Group and I really enjoy talking with you every time we met in the coffee table, and of course, during the research meetings. I am really appreciated that you gave me a lot of fun ideas and provide me the help I need during my experiments. You always encourage me and being patient with my progress when I present the updates of my work. I have always loved our discussions in the office and your valuable advice over the last year really helped me a lot. I also learned a lot from the way you review my paper and the style you work with others. I would always recognise your smile that gives me so much love and comfort.

In the meantime, I would like to thank our secretaries, Gemma, Marianne, Shanta and Annejet. Thank you for helping me with the paperwork on my visa and extension. Thanks for all the support during my PhD study including Go/No-Go meeting, yearly progress meetings and the thesis defence. Thank you for your patience helping me deal with the life issues when I am not good at Dutch. My PhD life cannot be more smoothly without your help.

As I spent more than four years conducting experiments in the DASML and DEMO, I would like to thank Berthil, Marlies, Durga, Alexander, Dave, Chantal, Victor and Fred for their help in material preparation and mechanical testing. Thank you Ed, Rob and Peter for helping me with the machining of test samples and tools. Special thanks to Victor and Fred in the composite lab for helping me with the mould design and laminate

layup. Besides, I would like to thank Dave in the mechanical lab for helping me with the experimental setup, tool design as well as the sample measurement.

To all my colleagues from the ASM group, Amin, Onur, Muhamad, Satya, Huub, Davide, Billy, Silvia, Giovanna, Natalia, Ujala, Deniz, Chizoba, Caroline, Jimmy, Bram, Yanos, Camila, Julie, Kunal, Daniel, Bilim, Baris Caglar and Baris Kumru, and of course Jos and Clemens. Thanks for the nice drinks and foods, discussions, meetings and gathering. I really enjoy the three coaching sessions we had and special thanks to Clemens for providing us the opportunities.

To my NB0.22 office mates: Deniz, Ujala, Chizoba and Jimmy. I really enjoy talking with you and thank you all the support, and nice and interesting discussions both on research and life. Special thanks to Chizoba and your family, thanks for inviting me to your home for your birthday and your baby's events. I really enjoy the food you made and the surroundings you had. Your family and friends make me feel at home and wish you and your family all the best.

To the other foreign colleagues and friends I have met in the ASM department as well as in the faculty of aerospace engineering: Rinze, Sofia, Rene, Irene, Calvin, John-Alan, Otto, Saullo, Pedro, Ozan, Morteza, Sasan, Stratos, Eva, Romina, Chantal and everyone I have forgotten to mention. Thank you for the nice talks, lunches, discussions and help during my PhD study.

To my Chinese friends and colleagues, Ran, Xiang, Nan, Xi Li, Nan Yue, Yuzhe, Jingjing, Xiaodong, Dong Quan, Huaguan, Hongwei, Lubin, Yuqian, Wenjie, Zhiyuan, Weikang, Ruipeng, Xiaopeng and everyone I have forgotten to mention. Thank you for the nice talks, discussions and parties. Special thanks to Xiaopeng for many nice lunches, talks and discussions both my studies and daily life. You really helped me a lot during my PhD and wish you all the best in the future.

In the end, I would like to thank my parents and my brother, for their constant love, encouragement and faith in me. Then, I would like to express my gratitude to my girlfriend. Thanks for your support and what you have done for me during all the difficult time. With you by my side, this journey has been much more meaningful and beautiful. This thesis might mark the end of a chapter in my life but many more await to be written in our lifelong story.

CURRICULUM VITÆ

Shichen LIU



04-Aug-1994

Born in Ji'an, China.

EDUCATION

Oct.2019 - Sept.2024

Ph.D, Faculty of Aerospace Engineering
Delft University of Technology, Delft, the Netherlands

Sept.2016 - Jan.2019

MSc, School of Mechanical Engineering & Automation
Beihang University, Beijing, China

Sept.2012 - Jun.2016

BSc, School of Aeronautical Manufacturing Engineering
Nanchang Hangkong University, Nanchang, China

LIST OF PUBLICATIONS

JOURNAL PAPERS

4. **Shichen Liu**, Jos Sinke, Clemens Dransfeld, *A clamped-beam bending test method for the flexural behaviour of uncured metal-CFRP laminates*, Under review.
3. **Shichen Liu**, Jos Sinke, Clemens Dransfeld, *Experimental characterisation of cure-dependent spring-back behaviour of metal-composite laminates in a hot-pressing process*, Under review.
2. **Shichen Liu**, Jos Sinke, Clemens Dransfeld, *A modified bias-extension test method for the characterisation of intra-ply shear deformability of hybrid metal-composite laminates*, [Composite Structures](#) **314**, 116964 (2023).
1. **Shichen Liu**, Jos Sinke, Clemens Dransfeld, *An inter-ply friction model for thermoset based fibre metal laminate in a hot-pressing process*, [Composites Part B](#), **227**, 109400 (2021).

CONFERENCE PAPERS

2. **Shichen Liu**, Jos Sinke, Clemens Dransfeld, *Hot-pressing of uncured metal-composite laminates: A numerical study on simultaneous deformation*, in [Proceedings of the 21th European Conference on Composite Materials: For Academic And Industry, ECCM21 \(2024\)](#).
1. **Shichen Liu**, Jos Sinke, Clemens Dransfeld, *Experimental and numerical validation of an inter-ply friction model for thermoset based fibre metal laminate under hot-pressing conditions*, in [Proceedings of the 20th European Conference on Composite Materials: Composites Meet Sustainability, ECCM20 \(2022\)](#).